Luciana Grazziotin Rossato

The cardiotoxicity of mitoxantrone: a mechanistic approach using *in vitro* and *in vivo* models

Tese do 3º Ciclo de Estudos conducente ao grau de Doutor em Ciências Farmacêuticas – Toxicologia, submetida à Faculdade de Farmácia da Universidade do Porto, Portugal. Trabalho realizado sob supervisão do Professor Doutor Fernando Remião, e co-supervisão de Doutora Vera Marisa Freitas Costa e Doutor Carlos Palmeira.

NOVEMBRO/2013.

U. PORTO

FACULDADE DE FARMÁCIA
UNIVERSIDADE DO PORTO

É AUTORIZADA A REPRODUÇÃO INTEGRAL DESTA TESE APENAS PARA EFEITOS DE INVESTIGAÇÃO, MEDIANTE DECLARAÇÃO ESCRITA DO INTERESSADO, QUE A TAL SE COMPROMETE.

“Quem quer passar além do Bojador
Tem que passar além da dor.
Deus ao mar o perigo e o abismo deu,
Mas nele é que espelhou o céu.”

Fernando Pessoa

DECLARAÇÃO

Ao abrigo do nº 2 do artigo 8º do Decreto-Lei nº 388/70, declara-se que fazem parte desta tese os seguintes trabalhos publicados. Para esses trabalhos, o autor da tese contribuiu maioritariamente na execução das experiências laboratoriais, interpretação dos resultados e preparação dos manuscritos.

PUBLICAÇÕES

Artigos em revistas de circulação internacional com arbitragem científica incluídos nesta tese:

Rossato, L. G., Costa, V. M., De Pinho, P. G., Freitas, V., Viloune, L., Bastos, M.L., Palmeira, C., Remião, F. (2013) The metabolic profile of mitoxantrone and its relation with mitoxantrone-induced cardiotoxicity. Arch Toxicol 87 (10):1809-20.

Rossato, L. G., Costa, V. M., Villas-Boas, V., Bastos, M.L., Rolo, A., Palmeira, C., Remião, F. (2013) Therapeutic concentrations of mitoxantrone elicit energetic imbalance in H9c2 cells as an earlier event. Cardiovasc Toxicol *In Press.* DOI: 10.1007/s12012-013-9224-0

Rossato, L. G., Costa, V. M., Dallegrave, E., Arbo, M., Silva, R., Ferreira, R., Amado, F., Dinis-Oliveira, R.J., Duarte, J.A., Bastos, M.L., Palmeira, C., Remião F. (2013) Mitochondrial cumulative damage induced by mitoxantrone: late onset cardiac energetic impairment. Cardiovasc Toxicol *In Press.* DOI: 10.1007/s12012-013-9230-2.

Rossato, L., Costa, V., Dallegrave, E., Arbo, M., Dinis-Oliveira, R.J., Silva, A., Duarte, J.A., Bastos, M.L., Palmeira, C., Remião, F. (2013) Cumulative mitoxantrone-induced haematologic and hepatic adverse effects in a sub-chronic *in vivo* model. Basic Clin Pharmacol Toxicol *In Press.* DOI: 10.1111/bcpt.12143

DIVULGAÇÃO DOS RESULTADOS

Comunicação oral em eventos científicos:

Rossato, L.G., Costa, V.M., Dallegrave, E., Bastos, M.L., Dinis-Oliveira, R.J., Duarte, J.A., Palmeira, C. M., Remião, F. (2012) A comparative study of early and late toxic effects of mitoxantrone in rats. XLII Reunião da Sociedade Portuguesa de Farmacologia, Lisboa, Portugal.

Rossato, L.G., Costa, V.M., Firmo, E., Bastos, M.L., Palmeira, C., Remião, F. (2011) Therapeutic concentrations of mitoxantrone elicit cytotoxic effects on H9c2 cells. 47th Congress of the European Societies of Toxicology (EUROTOX), Paris, França.

Comunicação na forma de pôster em eventos científicos:

Rossato, L.G., Costa, V.M., Dallegrave, E., Bastos, M.L., Dinis-Oliveira, R., Duarte, J.A., Palmeira, C., Remião, F. (2012) Mitoxantrone: A comparative study of early and late toxic effects in rats. 48th Congress of the European Societies of Toxicology (EUROTOX), Estocolmo, Suécia.

Rossato, L.G., Costa, V.M., Firmo, E., Bastos, M.L., Palmeira, C.M., Remião, F. (2011) Therapeutic concentrations of mitoxantrone elicit cytotoxic effects on H9c2 cells. XX Porto Cancer Meeting, Porto, Portugal.

Remião, F., Rossato, L.G., Dallegrave, E., Arbo, M., Silva, R., Ferreira, R., Amado, F., Dinis-Oliveira, R.J., Duarte, J.A., Bastos, M.L., Palmeira, C., Costa, V. (2013) Mitochondrial impairment after mitoxantrone multi-administration to male Wistar rats. 49th Congress of European Societies of Toxicology (EUROTOX), Interlaken, Suiça.

Resumos publicados em anais de eventos:

Remião, F., Rossato, L.G., Dallegrave, E., Arbo, M., Silva, R., Ferreira, R., Amado, F., Dinis-Oliveira, R.J., Duarte, J.A., Bastos, M.L., Palmeira, C., Costa, V. (2013) Mitochondrial impairment after mitoxantrone multi-administration to male Wistar rats. Toxicol Lett. v. 221, p.S171.

Rossato, L.G., Costa, V.M., Dallegrave, E., Bastos, M.L., Dinis-Oliveira, R., Duarte, J.A., Palmeira, C., Remião, F. (2012) Mitoxantrone: A comparative study of early and late toxic effects in rats. Toxicol Lett. , v.211, p.S76.

Rossato, L.G., Costa, V.M., Dallegrave, E., Bastos, M.L., Dinis-Oliveira, R.J., Duarte, J.A., Palmeira, C. M., Remião, F. (2012) A comparative study of early and late toxic effects of mitoxantrone in rats. Livro de Resumos da XLII Reunião da Sociedade Portuguesa de Farmacologia, Lisboa, Portugal.

Rossato, L.G., Costa, V.M., Firmo, E., Bastos, M.L., Palmeira, C., Remião, F. (2011) Therapeutic concentrations of mitoxantrone elicit cytotoxic effects on H9c2 cells. Toxicol Lett. v.205, p.S56 - S56.

Rossato, L.G., Costa, V.M., Firmo, E., Bastos, M.L., Palmeira, C.M., Remião, F. (2011) Therapeutic concentrations of mitoxantrone elicit cytotoxic effects on H9c2 cells In: XX Porto Cancer Meeting, Porto, Portugal. Livro de Resumos do XX Porto Cancer Meeting - Drug resistance in cancer: from biology to molecular targets and drugs - Poster 29.

AGRADECIMENTOS

Um título de Doutoramento não se constrói sozinha. Este trabalho é fruto do empenho de muitas pessoas que dedicaram o seu tempo em orientar os meus estudos e que, através deste esforço, me permitiram encontrar o meu próprio caminho.

Primeiramente, gostaria de agradecer à Doutora Maria de Lourdes Bastos, porque só cheguei a Portugal porque um dia ouvi-a falar. E desde este dia, passou a ser uma referência científica muito forte para mim. Fico muito feliz por ter sido tão bem recebida em vosso país, laboratório e também em vossa casa, e pelo laço de amizade que construímos.

Gostaria de agradecer a paciência, a sensibilidade e a atenção do meu orientador, Doutor Fernando Remião, e também por ter apostado pela segunda vez em mim quando convidou-me para embarcar neste Doutoramento sob sua supervisão.

À minha orientadora, Doutora Vera Marisa Costa, agradeço por estar sempre disponível, pelo olhar criterioso e pelo rigor científico que sempre pautou esta orientação. Jamais esquecerei a atenção que sempre dedicou a este trabalho, desde a construção do projeto até as fases finais de sua concretização.

Ao meu co-orientador, Doutor Carlos Palmeira, agradeço por ter me aberto as portas de seu Laboratório, por arranjar um tempo para me ensinar pessoalmente o isolamento de mitocôndrias e pelo otimismo contagiante. Aproveito para agradecer também o auxílio da Doutora Anabela Rolo e a simpatia de todos os membros do Centro de Neurociências e Biologia Celular de Coimbra. Sempre me senti muito bem recebida em Coimbra.

À Doutora Helena Carmo, agradeço pela simpatia e delicadeza com que sempre me tratou e ao Doutor Félix Carvalho agradeço por contagiar-nos com o seu entusiasmo pela ciência.

À Engenheira Maria Elisa agradeço pela preocupação, por me ouvir e tantas vezes me falar. Por não medir esforços para que eu me sentisse em casa e por organizar os meus aniversários com várias delícias da culinária portuguesa. Todas estas pequenas coisas significaram imenso!

Gostaria de agradecer também a todos os colaboradores que estiveram de alguma forma envolvidos neste trabalho, nomeadamente à Doutora Paula Guedes, Doutor Victor de Freitas, Doutora Rita Ferreira, Doutor Francisco Amado, Doutora Alice Silva, Doutor

José Duarte e Doutor Ricardo Dinis Oliveira, por viabilizarem algumas etapas deste trabalho. Estendo o meu agradecimento também as vossas equipas.

À Doutora Eliane Dallegrave, agradeço por tudo que me ensinou e continua a me ensinar e pela amizade.

À Renata Silva gostaria de expressar meu sincero agradecimento por sempre ter partilhado o seu conhecimento, por ser uma excelente colega de trabalho e uma grande amiga. Desejo profundamente que consigamos manter nossa amizade.

Agradeço também todos os amigos portugueses que conheci ao longo deste período: Helena e Tiago, as melhores heranças do mestrado; Helena Pontes, a primeira a me convidar para passear ao fim de semana; Daniel, cuja dedicação e competência admiro muito e que muito me ajudou com as formatações desta tese e aos amigos da Faculdade de Desporto por todos os bons momentos. Todos os meus colegas de laboratório e pessoas que fizeram parte do meu dia a dia laboratorial (Dona Julia, Catia, Margarida, Doutora Sonia, Marcia, Rita, Laure, Eduarda, Tiago, João, Diana, Filipa, Juliana), o meu mais sincero obrigada!

À Aninha, Teresa e Vania gostaria de dizer que fiquei muito feliz em conhecer vocês! Hoje as considero minhas grandes amigas e devo dizer que a convivência com vocês me faz muita falta!

Ao Marcelo agradeço pela parceria, pelas conversas engraçadas, e por ter se revelado um grande amigo.

À minha família, que me ensinou a ser um ser humano antes de ser um profissional, gostaria de dizer que a distância de vocês foi o que mais pesou durante todo este tempo. Obrigada por apoiarem a minha ausência geográfica em tantos momentos que eu não queria ter estado ausente e por continuarem entendendo as minhas ausências nas fases finais desta tese. Espero que agora os tempos de exílio científico voluntário não sejam tão grandes!

Ao Artur agradeço pela compreensão, apoio e pela oportunidade de partilhar um projeto muito maior que este: a nossa vida a dois.

Agradeço também aos meus amigos, por terem me recebido novamente de volta e por me fazerem sentir que o tempo não passou. À Universidade de Passo Fundo e a todos os meus novos colegas e alunos, agradeço pela receptividade e por todas as oportunidades que me possibilitam continuar a fazer o que tanto gosto.

Durante 4 anos vivenciei o modo de vida português. Participei de momentos alegres e outros nem tanto... Desculpem-me se algumas vezes nossas diferenças culturais nos afastaram e por todas as vezes que fui “brasileiramente invasiva”, sem querer sê-lo. O importante é que acredito que encontramos um caminho de amizade e respeito. Com o ponto final desta tese encerra-se também o vínculo formal que tenho com Portugal. Porém, os vínculos afetivos que construímos, estou certa que permanecem. Muito obrigada por tudo!

This work was supported by the Fundacão para a Ciência e Tecnologia (FCT) — project (EXPL/DTP-FTO/0290/2012) — QREN initiative with EU/FEDER financing through COMPETE − Operational Programme for Competitiveness Factors (FCOMP-01-0124-FEDER-027749), and Pest C/EQB/LA0006/2011. Luciana Grazziotin Rossato also acknowledges FCT for their PhD Grant (SFRH/BD/63473/2009).

FCT
Fundação para a Ciência e a Tecnologia
MINISTÉRIO DA CIÊNCIA, TECNOLOGIA E ENSINO SUPERIOR

ABSTRACT

Mitoxantrone (MTX) is a chemotherapeutic agent that emerged as an alternative to anthracycline therapy. However, the use of MTX is also related to late cardiotoxicity whose mechanisms remain largely unknown. Thus, the present thesis aims to highlight the underlying mechanisms involved in the MTX-induced cardiotoxicity, namely the effects related to mitochondria and metabolism, using *in vivo* and *in vitro* models. The *in vitro* models employed in the present work were hepatic S9 fractions and mitochondria, both isolated from Wistar male adult rats and H9c2 culture cells. The Wistar rat was the *in vivo* model used.

MTX (concentrations from 10nM to 100μM) elicited a time- and concentration-dependent cytotoxicity in H2c9 cells. Two therapeutic concentrations (100nM and 1μM) and three time-points were selected (24, 48, and 96h) for further studies. Both MTX concentrations caused a significant increase in caspase-3 activity at 24h. Significant decreases were observed in the total and reduced glutathione levels only in MTX 100nM at 96h, however neither alterations in oxidized glutathione, nor increases in malondialdehyde levels were observed in any time or concentrations tested. On the other hand, changes in the intracellular ATP levels, mitochondrial membrane potential, and intracellular calcium levels were observed in both concentrations and all time-points tested. Noteworthy, for the first time, decreased levels of ATP-synthase expression and activity and increases in the reactive species generation were observed at 96h in both MTX working concentrations. However, neither the radical scavenger N-acetylcysteine nor the mitochondrial function enhancer *L*-carnitine prevented MTX cytotoxicity.

As evidenced by the *in vitro* study in H9c2, MTX causes cytotoxicity in therapeutic concentrations, then, the following approaches aimed to disclosure the principal mechanisms of MTX-induced toxicity, mainly focusing on MTX metabolism and MTX-induced mitochondrionopathy. The metabolic studies started with the use of hepatic S9 fractions isolated from rats incubated for 4h with MTX (100μM), whose products were analyzed through liquid chromatography coupled with mass spectrometry. After a 4h incubation, the MTX content was 35% lower and five metabolites were identified: an acetoxy ester derivative never described before, two glutathione conjugates, the MTX monocarboxylic acid derivative, and the MTX naphtoquinoxaline. Noteworthy, the presence of MTX and of the naphtoquinoxaline metabolite was also evidenced *in vivo* in liver and heart after 7.5mg/kg MTX-administration in rats. Then, the potential cytotoxic effects of MTX and MTX plus metabolites were evaluated in the H9c2 cells after 24h incubation with MTX alone and MTX after S9 metabolization. The cytotoxicity caused by

MTX plus metabolites was higher than that observed in the H9c2 cells incubated with non-metabolized MTX group. Moreover, the co-incubation of MTX with CYP450 and CYP2E1 inhibitors partially prevented the cytotoxicity observed in the MTX groups incubated with H9c2 cells, highlighting that the metabolism of MTX is relevant for its undesirable effects. However, increases in caspase-3 activity caused by MTX incubation were not prevented by co-incubation with CYP450 or CYP2E1 inhibitors in this cell model.

To evaluate the cardiac mitochondrial toxicity of MTX, male Wistar rats were treated with three cycles of 2.5mg/kg MTX at day 0, 10, and 20. One treated group was euthanized on day 22 (MTX22) to evaluate early MTX cardiac toxic effects while the other was euthanized on day 48 (MTX48), to allow the evaluation of MTX late effects. MTX treatment caused a reduction in relative body weight gain in both treated groups with no significant changes in water and food intake. Increased cardiac relative mass was observed in MTX22 group and microscopic changes suggestive of dilated cardiomyopathy were evident in both treated groups. Considering mitochondrial effects, it was shown, for the first time that MTX induced an increase in the activity of both complex IV and complex V in MTX22 group, while the decrease in the complex V activity was accompanied by the reduction of ATP content in the MTX48 rats. Despite the MTX-induced cardiotoxicity evidenced in our study, we also observed hematotoxicity and direct hepatotoxicity upon this MTX administration regimen.

In summary, this thesis highlights the relevance of CYP450- and CYP2E1-mediated metabolism to the MTX-induced cytotoxicity. Moreover, it was shown that energetic crisis observed after MTX incubation/administration acts as a possible key factor in the cell injury. MTX presents the potential to cause mitochondrionopathy as demonstrated both by *in vivo* and *in vitro* approaches.

Keywords: Mitoxantrone. Metabolism. Cardiotoxicity. Mitochondrionopathy.

RESUMO

A mitoxantrona (MTX) é um agente antineoplásico que foi sintetizado com o intuito de ser uma alternativa à terapia com antraciclinas. Contudo, o uso clínico da MTX também tem sido associado ao desenvolvimento de cardiotoxicidade tardia, a exemplo do que é observado na terapia com antraciclinas. Os mecanismos envolvidos na cardiotoxicidade descrita não foram ainda devidamente elucidados. Assim, os estudos desenvolvidos no âmbito desta tese tiveram como objetivo esclarecer os principais mecanismos associados à cardiotoxicidade induzida pela MTX, nomeadamente no que diz respeito à influência do seu metabolismo e os efeitos adversos cardíacos ao nível mitocondrial, recorrendo a modelos *in vivo* e *in vitro*. Os modelos *in vitro* utilizados nestes trabalhos foram as frações S9 hepáticas e mitocôndrias, ambas isoladas de ratos Wistar adultos e a linha celular imortalizada H9c2. O rato Wistar foi o modelo *in vivo* utilizado.

As células H9c2 foram incubadas com diferentes concentrações de MTX (10nM a 100µM) por 24, 48, 72, ou 96h, observando-se uma citotoxicidade dependente da concentração e do tempo de incubação. Selecionou-se para os estudos subsequentes duas concentrações de MTX consideradas clinicamente relevantes (100nM e 1µM) e três tempos de incubação (24, 48, e 96h). Ambas as concentrações de MTX causaram aumentos significativos na atividade da caspase-3 após 24h de incubação. Após 96h, observou-se ainda uma redução significativa nos níveis intracelulares de glutationa total e reduzida, mas apenas com a concentração de 100nM de MTX. Contudo, não foram observadas alterações nos níveis de glutationa oxidada ou nos níveis de malondialdeído em nenhuma concentração e tempo de incubação testados. Por outro lado, observou-se alterações nos níveis intracelulares de ATP, assim como o aumento do potencial de membrana mitocondrial e dos níveis intracelulares de cálcio em todos os tempos avaliados. Observou-se, ainda, pela primeira vez, que a MTX nas concentrações selecionadas e após 96h de incubação, originou uma diminuição da expressão e da atividade da ATP sintetase, acompanhada pelo aumento na formação de espécies reativas. Contudo, nem a co-incubação com N-acetilcisteína (um captador de espécies reativas) ou com a *L*-carnitina (um potenciador da função mitocondrial) preveniu a citotoxicidade induzida pela MTX nestas células.

Os estudos metabólicos foram realizados incubando MTX (100µM) com frações S9 isoladas de fígado de ratos Wistar adultos. Ao fim de 4h de incubação, os produtos do metabolismo da MTX foram extraídos e analisados utilizando cromatografia em fase líquida acoplada com detetor de massa. Após 4h de incubação com as frações S9 hepáticas, o conteúdo de MTX foi 35% inferior à quantidade inicialmente adicionada ao sistema. Além disso, cinco metabolitos foram identificados: um acetoxi éster nunca antes descrito, dois conjugados com glutationa, um derivado do ácido monocarboxílico e o derivado naftoquinoxalínico da MTX. De realçar que a presença da MTX e do seu derivado naftoquinoxalínico também foi detetada *in vivo* nos fígados e corações de ratos tratados com 7.5mg/kg de MTX. De seguida, os efeitos citotóxicos da MTX sem qualquer metabolismo e da MTX após biotransformação obtida através destas incubações foram avaliados através da incubação por 24h com as células H9c2. A citotoxicidade causada pela MTX em presença de seus metabolitos foi significativamente maior que a observada nas células incubadas apenas com MTX. A co-incubação de MTX com os inibidores do metabolismo mediado pela CYP450 e CYP2E1 preveniu parcialmente a citotoxicidade, provando que o metabolismo da MTX é relevante para os seus efeitos tóxicos. Contudo, o aumento na atividade da caspase-3 observada após 24h de incubação com a MTX (100nM e 1μM) não foi prevenido pela co-incubação com os inibidores da CYP450 ou CYP2E1.

Para avaliar a toxicidade cardíaca mitocondrial *in vivo* exercida pela MTX, utilizamos como modelo animal ratos machos Wistar tratados com três ciclos de MTX (2.5mg/kg) nos dias 0, 10 e 20. Um dos grupos tratados com MTX foi eutanasiado no dia 22 (MTX22) para avaliar os efeitos cardiotóxicos da MTX logo após o seu último ciclo. O outro grupo foi eutanasiado no dia 48 (MTX48) a fim de avaliar os efeitos cardiotóxicos tardios causados pelo fármaco. O tratamento com MTX causou uma redução no aumento de massa corporal relativa nos dois grupos que receberam MTX, alteração que não foi acompanhada por mudanças nos consumos de água e ração. Observou-se, também, um aumento na massa relativa dos corações no grupo MTX48 e alterações microscópicas compatíveis com cardiomiopatia dilatada nos dois grupos. A administração de MTX causou um aumento na atividade dos complexos IV e V mitocondriais no grupo MTX22 e uma diminuição na atividade do complexo V mitocondrial, acompanhada pela redução nos níveis cardíacos de ATP no grupo MTX48. Foi ainda possível observar efeitos tóxicos hematológicos e uma possível hepatotoxicidade direta causada pela administração de MTX neste modelo animal e condições experimentais.

Em conclusão, este estudo contribuiu para demonstrar a relevância do metabolismo mediado pela CYP450 e CYP2E1 para os efeitos cardiotóxicos relacionados com a MTX. Além disso, observou-se que um dos principais mecanismos de cardiotoxicidade da MTX envolve o estabelecimento de uma falha energética, conforme demonstrado através dos efeitos tóxicos mitocondriais observados nos modelos *in vivo* e *in vitro* utilizados.

Palavras-chave: Mitoxantrona. Metabolismo. Cardiotoxicidade. Toxicidade mitocondrial.

TABLE OF CONTENTS

LIST OF FIGURES .... **xxiii**
LIST OF TABLES .... **xxv**
ABBREVIATIONS USED IN THE TEXT .... **xxvii**
OUTLINE OF THE THESIS .... **xxxi**
PART I **1**
General introduction **1**
I.1. Historic context **3**
I.2. MTX chemical aspects **4**
I.3. Therapeutic uses **4**
I.4. Pharmacological action mechanisms **6**
I.5. Pharmacokinetics **7**
  I.5.1. Absorption and distribution 7
  I.5.2. Metabolism 8
  I.5.3. Elimination 12
I.6. Adverse effects **13**
  I.6.1. MTX-induced cardiotoxicity 13
  I.6.2. MTX-induced hepatotoxicity 16
  I.6.3. MTX-induced hematotoxicity 17
Objectives **21**
II. General objective **23**
II.1. Specific objectives **23**

PART II **25**
Material and Methods **25**
III.1. Brief considerations on the experimental models and concentrations used in the studies **27**
  III.1.1. *In vitro* models 27
  III.1.1.1. Hepatic S9 fractions isolated from adult male Wistar rat 27
  III.1.1.2. H9c2 cell line 28
  III.1.1.3. Cardiac mitochondria isolated from male Wistar rat 30
  III.1.2. *In vivo* model 31
  III.1.3. MTX concentrations and doses 33
III.2. Methods **34**

III.2.2. Evaluation of the metabolic profile of MTX using hepatic S9 fractions by LC-DAD/ESI-MS 34
III.2.3. Cytotoxicity assays 34
III.2.3.1. LDH leakage Assay 35
III.2.3.2. MTT reduction assay 35
III.2.4. Caspase-3 activity assay 35
III.2.5. Evaluation of oxidative stress 36
III.2.5.1. Evaluation of reactive species generation 36
III.2.5.2. Measurement of intracellular total glutathione (GSHt), GSH, and oxidized glutathione (GSSG) levels 36
III.2.5.3. Evaluation of lipid peroxidation 36
III.2.6. Evaluation of the energetic function 37
III.2.6.1. Measurement of ATP levels 37
III.2.6.2. Evaluation of the ATP synthase expression 37
III.2.6.3. Evaluation of the ATP synthase activity 37
III.2.6.4. Blue native polyacrylamide gel electrophoresis (BN-PAGE) separation of cardiac mitochondria membrane complexes of MTX-treated rats 37
III.2.6.5. In-gel activity of mitochondrial complexes IV and V after MTX treatment 37
III.2.6.6. Cardiac mitochondrial DNA quantitation in MTX treated rats 38
III.2.7. Evaluation of the mitochondrial membrane potential after *in vivo* and *in vitro* treatment with MTX 38
III.2.8. Flow cytometry analysis 38
III.2.9. Heart and liver preparation for light and transmission electron microscopy 38
III.2.10. Plasma biochemical analysis 39
III.2.11. Hematological analysis 39
III.2.12. Total protein quantification 39
III.2.13. Statistical analysis 39
Results 41
Manuscript I 43
Manuscript II 57
Manuscript III 73
Manuscript IV 87

PART III 99
Discussion and Conclusions 99
IV.1. Metabolic profile of MTX: *in vitro* and *in vivo* studies 101

IV.2. Influence of MTX metabolism on its (cardio)toxicity 106

IV.2.1. Cytoxicity as a consequence of metabolic activation 109

IV.2.2. MTX-induced oxidative stress and its (cardio)toxicity.................................112

IV.3. Calcium regulation, mitochondrial membrane potential and cell death......117

IV.4. MTX-induced cell death 120

IV.5. Energetic imbalance as a protagonist of MTX-induced cardiotoxicity........124

IV.6. MTX-induced mitochondrial toxicity 126

IV.7. Types of cardiomyopathies 130

IV.8. Intersubject variability in the *in vivo* study 133

IV.9. MTX-induced hepatotoxicity 134

IV.10. MTX-induced hematotoxicity 136

IV.11. Conclusions and future perspectives 138

PART IV 141

References 141

LIST OF FIGURES

Figure 1: Chemical structure of MTX. The chromophore ring is highlighted in red. 3

Figure 2: Chemical structure of 8,11-dihydroxy-4-(2-hydroxyethyl)-6-[[2-[(2-hydroxyethyl)amino]ethyl]amino]-1,2,3,4,7,12-hexahydronaphto-[2-3]-quinoxaline-7-12-dione or naphtoquinoxaline, the main bioactive metabolite of MTX. 12

Figure 3: Phase contrast micrographs of H9c2 cells. A) at low densities; B) at confluence (79). 29

Figure 4: Graphic representation of the *in vivo* experiment design performed in Manuscript III and IV. 32

Figure 5: Proposed chemical structure of the metabolites corresponding to the five chromatographic peaks obtained by LC/DAD-ESI/MS analysis. Compounds were obtained after 4h incubation of MTX (100µM) with hepatic S9 fractions isolated from adult male rats pre-treated with phenobarbital (0.2% in drinking water for one week prior isolation). Hepatic S9 fractions (4mg/ml) were supplemented with NADPH (1mM) and GSH (4mM)...102

Figure 6: Chemical representation of nucleophilic attack sites in the MTX molecule. The position 6 of MTX is the site of the intramolecular attack of the nucleophilic side chain resulting in the formation of the naphtoquinoxaline metabolite. The external nucleophilic attack is favored at position 2 and 3 of MTX molecule. 104

Figure 7: Schematic representation of one-electron and two-electron reduction of anthraquinones. The one-electron reduction involves the formation of semi-quinone radicals that can enter into redox cycling. Two-electron reduction generates hydroquinones, which can be detoxified or suffer auto-oxidation (two consecutive one-electron reductions). Adapted from (36,130). 110

Figure 8: Mechanisms of elimination and maintenance of calcium cytosolic levels. (A) Calcium ATPase-mediated pumping into the extracellular space, (B) ion-gradient driven transport into the extracellular space by the sodium/calcium exchanger, (C) ion-gradient driven transport into mitochondria by calcium uniporter, and (D) ATPase-mediated transport into the endoplasmic reticulum. Adapted from (148)...........118

Figure 9: Schematic representation of the energetic-dependent cascade of events leading to diverse apoptotic pathways. Each pathway activates its own procaspase, which will converge to caspase-3 activation (with the exception of granzyme A via that is caspase-independent). Caspase-3 activation results in other procaspases activation (procaspase 6 and 7) and, finally, leads to morphological and biochemical features of apoptosis. Adapted from (148,157). 122

Figure 10: Schematic representation of PCr mobilization. PCr is an energetic reserve that, through CK catalyzed-reaction, produces creatine and ATP. 125

LIST OF TABLES

Table 1: MTX usual adult dose regimen protocols 5

Table 2: Compilation of studies performed to elucidate the metabolic profile of MTX using different models. 10

Table 3: MTX conventional dose for FDA approved therapeutic indications in humans. 33

Table 4: Diagram representing the chronogram of energetic/mitochondrial changes observed in the H9c2 cells after incubation with MTX. (yes = presence of the effect, n.o = not observed [absence of the effect], n.d= not determined). The results were obtained after comparison with control cells. 128

ABBREVIATIONS USED IN THE TEXT

ABCG2 – ATP-binding cassette G2

ALT – alanine transaminase

Apaf-1 – apoptotic protease activating factor-1

AST – aspartate transaminase

ATP – adenosine 5′-triphosphate

BCRP – breast cancer resistance protein

BN-PAGE– blue native polyacrylamide gel electrophoresis

CK – creatine kinase

DAD – diode array detector

DAS – diallyl sulfide

DCFH-DA – dichlorodihydrofluorescein diacetate

DISC – death-inducing signaling complex

DHR – dihydrhodamine 123

DNA – deoxyribonucleic acid

DTNB – 5,5-dithio-bis(2-nitrobenzoic) acid

ESI – electrospray ionization interface

FDA – Food and Drug Administration

GGT – δ-glutamyltranspeptidase

GSH – reduced glutathione

GSHt – total glutathione

GSSG – oxidized glutathione

h – hour

Hb – hemoglobin

HCT – hematocrit

HPLC – high performance liquid chromatography

i.p. – intraperitoneal

i.v. – intravenous

LC_{50} – mean lethal concentration

LD_{50} – mean lethal dose

LDH – lactate dehydrogenase

LVEF – left ventricular ejection fraction

MCV – mean cell volume

MCH – mean cell hemoglobin

MCHC – mean cell hemoglobin concentration

min – minute

MPT – mitochondrial permeability transition pore

MPV – mean platelet volume

MS – mass spectrum

MTP – metyrapone

MTT – 3-(4,5-dimethylthiazol-2-yl)-2,5-diphenyltetrazolium bromide

MTX – mitoxantrone

NAC – N-acetylcysteine

PCr – phosphocreatine

PCT – plateletcrit

PDW – platelet distribution width

Pi – inorganic phosphate

PLT – platelet

RBC – red blood cell

RNA – ribonucleic acid

RDW – red cell distribution width

TBA – thiobarbituric acid

TBARS – thiobarbituric acid reactive substances

TMRM – tetramethylrhodamine

TPP^+ – tetraphenylphosphonium

UV – ultraviolet

VIS – visible

WBC – white blood cell

OUTLINE OF THE THESIS

The present thesis is divided into four main sections:

- **Part I: General introduction**

  In this section, a review on the existing literature about mitoxantrone is presented, in order to provide a good basis for understanding the objectives and the obtained results of the experimental studies. The general introduction is subdivided in two subchapters. The description of the main objectives is included in the second subchapter.

- **Part II: Experimental section**

  This section is subdivided into two subchapters: one regarding the material and methodologies employed in the studies presented in this thesis and the other concerning the manuscripts published in the scope of the present thesis.

- **Part III: Discussion and Conclusions**

  In this section, the integration of the results obtained in all the studies of this thesis is performed. The discussion of their potential relevance and their connection with existing scientific reports is also addressed here. Moreover, part III includes the main conclusions taken from the work performed in this thesis.

- **Part IV: References**

  In this final part, all the references of the literature that were used in the introduction, material and methods, and discussion sections are listed.

PART I

General introduction

I.1. Historic context

Mitoxantrone (MTX) is a chemotherapeutic agent that belongs to the anthracenedione chemical group (Figure 1). This chemical group comprises naturally occurring quinones present in plants or animals that due to their intense color were used as dyes since ancient times (1). Despite the lack of antitumor activity of many naturally occurring quinones, the anthracycline antibiotics doxorubicin and daunorubicin, which contain the anthracenedione ring framework in their tetracyclic chromophore part are ranked as one of the most effective anti-cancer drugs ever developed (1–4). However, due to the serious toxicity presented and difficulties experienced in the synthesis of anthracycline, molecules with only the anthracenedione group seemed to be a good alternative to be explored as anticancer drugs (1). In fact, structural variations conducted in the laboratory resulted in active *bis*-substituted aminoanthracenedione derivatives with significant antitumor activity such as ametantrone (1,5). Trying to increase the antitumor activity of these compounds, structural variations resulted in the MTX molecule in 1979 (1,6–8).

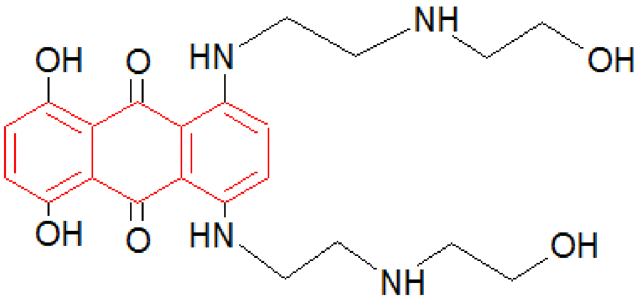

Figure 1: Chemical structure of MTX. The chromophore ring is highlighted in red.

The chemical synthesis of MTX involves the reaction of leuco-1,4,5,8-tetrahydroxyanthraquinone with 2-[(2-aminoethyl)amino]ethanol. The product of this reaction is further aromatized with chloranil (9). Nowadays, MTX is a medicine supplied as a dark-blue solution in vials, containing 2mg/ml (Novantrone® or mitoxantrone dihydrochloride).

I.2. MTX chemical aspects

MTX is a crystalline, hygroscopic blue powder with melting point of 160-162ºC or 203-205ºC (for the dihydrochloride form) (9). It is sparingly soluble (from 30 to 100 parts of solvent for one part of solute) in water, slightly soluble (from 100 to 1,000 parts of solvent for one part of solute) in methanol, and practically insoluble (more than 10,000 parts of solvent for one part of solute) in organic solvents such as acetone, acetonitrile, and chloroform (9,10).

In aqueous solution, MTX presents a relevant adsorption to materials such as glass and filters (1). Moreover, MTX reacts with sodium metabisulfite and EDTA (10). Solutions containing MTX are stabilized by the addition of 0.5% ascorbic acid (10). Additionally, MTX is stable in spiked whole blood for 3-6 hours (h) if samples are kept on ice and in plasma samples for at least 24h (10,11). After reconstitution with 0.9% sodium chloride or 5% dextrose, MTX is stable for at least 48h (1).

I.3. Therapeutic uses

MTX is a Food and Drug Administration (FDA) approved chemotherapeutic agent in the treatment of malignances such as myelogenous acute leukemia and prostate cancer and in the treatment of multiple sclerosis (secondary progressive, progressive relapsing, or worsening relapsing-remitting) to reduce neurologic disability and/or frequency of clinical relapses (2,12,13). Furthermore, MTX is also used in the treatment of acute lymphoid leukemia and as an initial approach in adults for the treatment of acute non-lymphocytic leukemia (which can include myelogenous, promyelocytic, monocytic and erythroid acute leukemia), bone marrow transplant, breast cancer, head and neck cancer, liver carcinoma, malignant lymphoma, non-Hodgkin’s lymphoma, ovarian cancer, and solid tumors (12).

In general, MTX chemotherapy protocol in humans consists on the administration of MTX for 30 minutes (min) via continuous infusion (1,9). The usual doses and dosing regimen for MTX indications are summarized on Table 1. It is important to note that the chemotherapy schedule might be individually adjusted taking into account the disease progression and the clinical condition of the patient, especially when the optimal dose and timing is not defined, as it occurs in the non-FDA labeled indications (12). In these situations, many intravenous (i.v.) administration regimens and intervals are described in the literature, namely a single dose every 28 days, 24h infusion, continuous infusion over five or 21 days, three times a day, five times a day, weekly and even high dose regimen for refractory lymphoma employing 90mg/m^2 MTX were already described (1,14). Moreover, the safety and effectiveness parameters of most MTX uses in pediatric patients are not well established, but in such patients presenting solid tumor configuration, the recommended dose is 5 to 8mg/m^2/week i.v. or an alternative dosing regimen of 18 to 20mg/m^2 i.v. every three to four weeks (12).

Table 1: MTX usual adult dose regimen protocols.

Disease	Dose regimen protocol	References
Acute myeloid leukemia	Induction phase: 12mg/m^2/day i.v. on days one to three in combination with cytarabine (100mg/m^2/day) as continuous i.v. 24h infusion on days one to seven; if leukemia persists, a second induction course of 12mg/m^2/day i.v. for two days in combination with cytarabine (100mg/m^2) daily as continuous i.v. 24h infusion on days one to five may be given; 12mg/m^2/day i.v. over 30min on days one, three, and five with cytarabine (25mg/m^2) once as an i.v. bolus followed by 100mg/m^2/day as a continuous i.v. infusion for 10 days and etoposide (100mg/m^2) i.v. over 1h on days one to five Consolidation phase: 12mg/m^2/day i.v. on days one and two in combination with cytarabine (100 mg/m^2/day) as continuous 24h i.v. infusion on days one to five; 12mg/m^2/day i.v. over 30min for three days (on days four to six) with cytarabine (500mg/m^2) i.v. over 2h every 12h on days one to six	(12)
Multiple sclerosis	12mg/m^2 i.v. every three months	(12,15)
Prostate cancer	12 to 14mg/m^2 i.v. every 21 days	(2,12)
Metastatic breast cancer and non-Hodgking's lymphoma, hepatoma	Monotherapy: First dose of 14mg/m^2 i.v. This administration might be repeated after 21 days if blood counts return to normal/acceptable values. Patients presenting myelosupression at the beginning of treatment may receive a lower dose of 2mg/m^2. Combined therapy: 10 to 12mg/m^2 as the initial dose.	(16)

In acute myeloid leukemia, the induction phase is the first course of treatment and it aims to induce total remission, which is characterized by the absence of blasts in the peripheral blood and the presence of ≤ 5% blasts in bone marrow smears (17). After reaching this stage, the consolidation phase aims to maintain the total remission. Thus, in the referred acute myeloid leukemia treatment, the antimetabolic agent cytarabine is commonly associated to MTX, as described in the Table 1. Another drug associated to MTX to deal with cancer relapse or refractory to conventional primary chemotherapy is etoposide (16). Recently, a prospective multicenter phase two trial assessed a novel regimen protocol for T-cell prolymphocytic leukemia based on induction by fludarabine (25mg/m^2/day, i.v., on days one through three), MTX (8mg/m^2/day, i.v., on day one), and cyclophosphamide (200mg/m^2/day on days one and three, repeated on day 28), up to four cycles, followed by alemtuzumab in the consolidation phase (30mg i.v. three times weekly for a maximum of 12 weeks) (18).

It is also important to point that, due to the toxicity profile of MTX, its dose regimen is limited to the maximum cumulative dose of 140mg/m^2 (2). Due to the apparent increased susceptibility of multiple sclerosis patients to cardiotoxicity, some authors state that maximum cumulative dosage in multiple sclerosis patients might be defined as 100mg/m^2 (19,20). Furthermore, MTX administration is not recommended in patients with a baseline neutrophil count of less than 1500 cells/mm^3 (unless the patient is receiving MTX for the treatment of acute nonlymphocytic leukemia) (12). Moreover, in patients with hepatic impairment, the dosage adjustment is necessary and in patients with multiple sclerosis presenting this condition, MTX use is not indicated (12). All these aspects are discussed in more detail in the next sections.

I.4. Pharmacological action mechanisms

MTX is a deoxyribonucleic acid (DNA) intercalating agent that causes single and double breaks in the DNA by the stabilization of a complex formed between DNA and topoisomerase II (1,2,21). The planar electron-rich chromophore group of MTX (Figure 1) is essential for its ability to intercalate in the DNA strains (21). This interaction is completed by electrostatic interactions of MTX side chains with the anionic exterior of the DNA (1,21). As a consequence, MTX inhibits the DNA replication, the ribonucleic acid (RNA) transcription, and also promotes the cell cycle arrest (1,22). Moreover, epigenetic effects of MTX were evidenced using purified isolated histones. The incubation with MTX (0.1-100μM) demonstrated the high affinity of MTX to histone H1 and core histone proteins, suggesting an additional target of this drug (23).

Due to its immunosuppressive capacity, MTX is also employed to suppress active inflammation preventing myelin and axonal damage observed in multiple sclerosis (15). MTX induces short- and long-term immunosuppressive effects leading to the induction of apoptosis in antigen-presenting cells and the induction of cell lysis, which results in reduced levels of blood leukocytes and inhibition of the proliferation of all types of immune cells (15,24). MTX inhibits lymphocytes (T cells and B cells) activity and suppresses the expression of pro-inflammatory molecules such as prostaglandin, C-reactive protein, cytokines (TNF-α, IL-1β, IL-6, IL-12, and IL-23), and lipopolysaccharide induction of nitric oxide production by astrocyte (1,15,25). The clinical effects of MTX in multiple sclerosis are suggested to last up to one year after the end of treatment (15,24). As a consequence, a reduction in the neurological disability and/or the frequency of clinical relapses is expected (2).

I.5. Pharmacokinetics

I.5.1. Absorption and distribution

The i.v. route is the preferential via of MTX administration (1,26). Intravenously administered MTX rapidly disappears from plasma due to the distribution to highly perfused organs in humans and laboratory animals (1,26). The MTX distribution half-life is about 15min (1,26) and studies are consistent to report very high volumes of distribution associated to MTX therapy (1,2,14,26). Thus, in humans, the best fit for the plasma-concentration curve is reached in a 3-compartment model (1). In patients with refractory lymphoma, after 30min i.v. infusion (15mg/m^2 or 90mg/m^2), the mean maximum MTX plasma concentrations were about 1.5 and 12μM, respectively. The volume of distribution at steady state (486 ± 254L/m^2) was shown to be independent of the dose (14). Firstly, the concentration in peripheral cells is higher than plasmatic levels (1,14). In cancer patients, 35 days after a single i.v. dose of 12mg/m^2 C^{14}-labeled MTX, the wide distribution volume of MTX was corroborated (26). The tissues that present higher MTX content were the liver (1140ng/g wet tissue), soon followed by pancreas (1040ng/g wet tissue), thyroid (958ng/g wet tissue), spleen (733ng/g wet tissue), heart (716ng/g wet tissue), stomach (555ng/g wet tissue), lymph node (432ng/g wet tissue), kidney (312ng/g wet tissue), lung (276ng/g wet tissue), small intestine (173ng/g wet tissue), and bone marrow (78ng/g wet tissue) (26). From the best of our knowledge, there are no data regarding pharmacokinetic parameters of MTX orally administered in humans because it is not intended for use as an oral medication (26).

In animal models, when administered intramuscularly, significant amounts of MTX remain at the muscular tissue used in the administration. For example, in dogs, 16.2% of the intramuscular administrated MTX dose (0.37mg/kg) persisted at the injection site for ten days (26). In mice, the single intramuscular administration of MTX at doses 0.3mg/kg and 3mg/kg resulted in the intramuscular retention of 17.6% and 8.9% of MTX, respectively, for at least 24h (26). Besides being an erratic pathway for MTX administration, the intramuscular via should be avoided because there is increased risk of extravasation with consequent tissue necrosis when MTX is injected into a muscle, subcutaneously, or into spinal cord (2,15). Thus, in humans, this via is irrelevant.

I.5.2. Metabolism

MTX metabolism has been evaluated through *in vivo* and *in vitro* studies. It was already described in human, pig, and rat (27). Regarding *in vitro* protocols, studies using exogenously added isolated enzymes, such as NADPH cytochrome P450 reductase (28,29), peroxidase enzyme systems (27,30), primary cultures of hepatocytes isolated from rats, rabbits, and humans (31), microsomes, and cytosol fractions isolated from rat liver (32) were performed.

The metabolism of MTX involves phase I, phase II, and phase III reactions. MTX main metabolic products are the naphtoquinoxaline metabolite (Figure 2) and its respective oxidation products, MTX mono- and dicarboxilic derivatives, and MTX conjugated with reduced glutathione (GSH) and glucuronic acid. Regarding the interspecies variability, mono- and dicarboxylic acid derivatives of MTX are major products of human and rabbit hepatic metabolism, while in rats they are residual (27,31).

Concerning phase I reactions, the oxidoreductive metabolism of MTX is mediated by the microsomal system and/or peroxidase enzymes such as human neutrophil myeloperoxidase (33,34). Chemically, the position of the hydroxyethylamino group on the chromophore ring produces steric hindrance, impairing the one-electron reductase-mediated metabolism of MTX (35). Thus, MTX possess a lower one-electron reduction potential compared to others analogues (35). Hence, since the one-electron reduction of MTX is not facilitated, the preferential pathway of MTX metabolism is the two-electron reduction (33,36,37), which generates more stable products when compared to the semi-quinone radicals produced by one-electron reduction (33).

As already mentioned, oxidative metabolism of MTX is of great interest since its byproducts seem to be involved in the MTX cytotoxic action (33,36,37). This hypothesis is supported by the observation that MTX has particular effectiveness in tumors with high contents of peroxidases and that the cellular sensitivity to MTX damage is proportional to cell metabolic skills (27,30,37). Additionally, the inhibitory effect of MTX (5μM) on cell growth in hepatoma cells (HepG2) was prevented after the blockage of cytochrome P450 metabolism by the co-incubation with metyrapone (MTP) (0.5mM) (33). In another study, the inhibition of cytochrome P450 metabolism with the same inhibitor (MTP 1mM) in the same cell line (HepG2) and in rat isolated hepatocytes resulted in the total loss of MTX-induced cytotoxicity, even with high doses of MTX (200 to 400μM incubated for 4 and 9h), leading the authors to assume that, without suffering metabolism, MTX has a negligible toxic effect in those models (37). Accordingly, in a human breast cancer cell model, the co-incubation of MTP (0.5mM) also prevented the cytotoxicity observed with MTX (5 to 200μM) (36).

Still regarding oxidative metabolism of MTX, it was suggested that epoxide hydrolase might contribute to MTX detoxification since its inhibition leads to increased MTX cytotoxicity. Thus, it suggests that at least one toxic relevant metabolite of MTX is an epoxide (33).

The main studies aiming to elucidate the chemical structures of MTX metabolites are summarized on Table 2. Until now, the most pharmacological relevant MTX oxidation product is the naphtoquinoxaline metabolite (Figure 2), which presents cytotoxic features (37,38).This metabolite was already identified in human, rat, and pig after MTX administration (27).

Table 2: Compilation of studies performed to elucidate the metabolic profile of MTX using different models.

Model	**Doses and regimen of administration**	**Analytical protocol**	**Metabolites**	**Reference**
Human breast cancer patients, male Wistar rat, and Gottinger minipig urine	Humans: MTX (12mg/m^2) to patients with breast cancer. It was also administered cyclophosphamide (600mg) in the same day of MTX administration Urine was collected over 24h Rat (350g): ^{14}C- labeled MTX (9.7mg/kg) was injected in the tail vein Pig (25kg): ^{13}C- labeled MTX (6.2 and 6.5mg/kg) was injected as bolus via the vena cava catheter	Isolation of the metabolite through preparative high performance liquid chromatography (HPLC) and further characterization by tandem mass spectrometry and ultraviolet (UV)-visible (VIS) spectroscopy	Humans: naphtoquinoxaline metabolite, mono- and dicarboxilic derivatives Rat: naphtoquinoxaline metabolite Pig: naphtoquinoxaline metabolite	(27)
Primary cultured hepatocytes isolated from humans, rabbit, and rat	^{14}C- labeled MTX (1 to 20µM) incubated during 48h with isolated hepatocytes	Extracellular medium analysis through HPLC/UV	Humans: mono- and dicarboxylic derivatives. Polar non-identified derivative as a minority product Rabbit: mono and dicarboxylic derivatives. Polar non-identified derivative as a minority product Rat: polar non-identified derivative, trace amounts of mono- and dicarboxylic derivatives	(31)
Hepatic microsomes (1mg/ml) or cytosol (4mg/ml) isolated from male Wistar rats	MTX (1mM) in the presence/absence of NADPH (1mM), GSH (4mM), and UDP-glucuronic acid (1mM). Incubations were carried out at 37ºC, up to 2h	Aliquots of samples collected in different time points were analyzed through HPLC/UV	MTX conjugates with GSH and glucuronic acid	(32)

Table 2 **(cont.)** Compilation of studies performed to elucidate the metabolic profile of MTX using different models.

Model	Doses and regimen of administration	Analytical protocol	Metabolites	Reference
Enzymatic system	Incubation of MTX (30mg) with horseradish peroxidase (2mg) and hydrogen peroxide 3% (74µl) in the presence of GSH (25mg)	Isolation and purification of the metabolite through HPLC and characterized through ^{1}H- and ^{13}C- NMR, and mass spectrum (MS)	MTX conjugated with one and two molecules of GSH	(27)
Enzymatic system	MTX (34µM) incubated with horseradish, lignin, and lacto peroxidase (2µM)	Identification of metabolite structures through LC/MS analysis	Naphtoquinoxaline metabolite, naphtoquinoxaline mono- and dicarboxylic derivatives and three non colored degradation products	(30)

Phase II metabolism enzymes are protagonists in the MTX detoxification process, namely the conjugation with GSH and glucuronic acid (1,27,32,37).

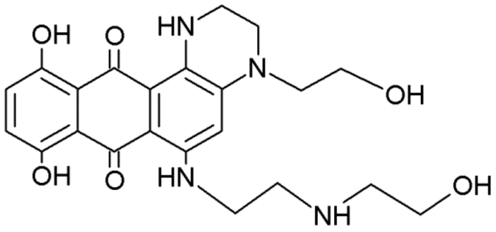

Figure 2: Chemical structure of 8,11-dihydroxy-4-(2-hydroxyethyl)-6-[[2-[(2-hydroxyethyl)amino]ethyl]amino]-1,2,3,4,7,12-hexahydronaphto-[2-3]-quinoxaline-7-12-dione or naphtoquinoxaline, the main bioactive metabolite of MTX.

Efflux transporters are often recognized as phase III metabolism (39,40). MTX is substrate of the adenosine 5′-triphosphate (ATP)-binding cassette G2 (ABCG2) transporter or breast cancer resistance protein (BCRP), which works as a multidrug resistance pump (41). Furthermore, a study using a BCRP and P-glycoprotein inhibitor (GF-120918 10mg/kg, administered via jugular vein cannula) co-administered to rats receiving MTX (2mg/kg, administered via jugular vein cannula) demonstrates that BCRP or P-glycoprotein, or both, elicit an important role in the MTX biliary excretion (42). In fact, MTX is described as a substrate of BCRP, although, its transport via P-glycoprotein occurs in a minor extent (42). It is an important observation as in cancer treatment, the drug extrusion is associated to the resistance to MTX therapy, thus, currently several studies are focused on the development of new formulations/vehicles or functionalized nanoparticles to overcome drug resistance (43).

I.5.3. Elimination

The redistribution of the MTX sequestered in the tissues back to the plasma and its elimination from the body is a slow process (26). Indeed, the long-term pharmacological and even toxicological effects attributed to MTX might be related to its long cellular residence time and its strong affinity for cellular macromolecules and membranes (35,44). The majority of excretion studies are designed measuring the radioactivity in the urine and feces after MTX labeled administration instead of identifying the metabolites chemical structures (1). In humans and laboratory animals, biliary excretion is the main elimination route of unchanged MTX and its conjugated metabolites, although, less amounts can be found in urine (1,26,37,42,45).

I.6. Adverse effects

As an aggressive chemotherapy drug, MTX treatment has been associated to several undesirable effects, such as myelosupression, nausea, vomiting, diarrhea, mucositis, and hepatotoxicity (1,9,12,46). Myelosupression manifests as severe neutropenia, and sometimes the administration of colony stimulating factors such as filgrastim or sargramostim is recommended. Blood transfusion may be needed in patients presenting severe thrombocytopenia, anemia, or hemorrhage (12). MTX is classified as a drug with low emetic risk (47). However, the management of MTX-induced nausea and vomiting is done with dexamethasone and metoclopramide (47). MTX has a high extravasation risk, being a vesicant agent (2). If extravasation occurs, the infusion must be discontinued and the affected area should be elevated (12).

The most concerning MTX adverse effect is the late cardiotoxicity due to its life-threatening risk (2,13), followed by the hematotoxicity and hepatotoxicity, due to their high frequency (2,9,12). Due to their relevance, since they can limit the therapy, these MTX-related toxicities will be addressed separately in independent sub-sections.

The mean lethal dose (LD_{50}) of MTX in experimental animals was set at 5mg/kg in rats, 10mg/kg in mice, and 10mg/m^2 in beagle dogs (9,48). As already stated, besides the symptoms commonly related to chemotherapy, namely nausea, fatigue, diarrhea, alopecia, anorexia, and mucositis, the toxic effects associated with MTX treatment include hematotoxicity (2,9), significant hepatotoxicity (9,49), and serious and (sometimes irreversible) cardiotoxicity (2,9,20,46).

I.6.1. MTX-induced cardiotoxicity

MTX was produced with the goal to overcome the cardiotoxicity observed with anthracyclines such as doxorubicin, the prototype of the group. However, MTX has been also reported as cardiotoxic in humans, affecting up to 18% of treated patients (2,13,50,51).

The majority of MTX-induced cardiotoxicity manifests as congestive cardiac failure characterized by the reduction left ventricular ejection fraction (LVEF) (13). Other cardiac disturbances such as tachycardia, dysrhythmias, and chest pain were also reported as MTX cardiac side effects (12). In cancer treatment, risk factors for the development of

MTX-related cardiotoxicity include previous treatment with anthracyclines, mediastinal radiotherapy, pre-existing cardiovascular disease, and cumulative doses superior to 140mg/m^2 (2,13). Additionally, patients presenting LVEF < 50% cannot receive MTX (13,52). Thus, monitoring the cardiac function is recommended after a cumulative dose of 80mg/m^2 (2). A reduction of about 10% in the LVEF baseline associated with an absolute LVEF value less than 50% should be viewed with concern and cessation of MTX therapy is recommended (13,52,53). The main limitation of this approach is its low sensitivity to detect cardiotoxicity at early stage. Monitoring based only in the LVEF values do not allow preventive strategies since it detects myocardial damage only when a functional impairment has already occurred (53). Hence, measurement of cardiac troponin has proven to help the early identification of patients susceptible to develop myocardial dysfunction and cardiac events (53).

Despite the most common manifestation of MTX-induced cardiotoxicity is decrease in LVEF, less frequent symptoms are disturbances of heart rhythm (12,54). The 2h incubation of isolated guinea pig ventricular myocytes with MTX (30μM) induced a time-dependent prolongation of action potential duration occasionally accompanied by early after depolarization (55), which can contribute to the proarrhythmic effect attributed to MTX. Additionally, in the same study, it was demonstrated that the same MTX working concentration (30μM) caused the depression of both inward rectifier potassium current and delayed rectifier potassium current (which can induce torsades de pointes), the blockage of 93% the muscarinic-gated receptor potassium current evoked by 1μM carbamylcholine incubation, while it did not affect the L-type calcium channels (55).

Regarding human reports, a female patient, 55 years old, presenting a relapse of acute myelogenous leukemia was admitted to reinduction therapy with MTX (10mg/m^2, i.v.) and etoposide (100mg/m^2, i.v.), daily, for five doses. About 22min after her fifth dose, the patient presented chest tightness and bradycardia, which was reverted with the discontinuation of the drug. She was rechallenged twice in a monitored setting and the symptoms recurred (54). It is important to point out that this patient was subjected to a previous regimen of chemotherapy months before, namely an induction chemotherapy (cytarabine, etoposide, and idarubicin in a cumulative dose of 36mg/m^2) followed by the consolidation phase with high dose of cytarabine. Furthermore, other medications that the patient received in that moment included acyclovir, ciprofloxacin, allopurinol, granisetron, potassium chloride, magnesium sulfate, and lorazepam. Thus, possibly, the previous anthracycline therapy contributed to the cardiotoxic reaction observed in this patient (54).

Patients with multiple sclerosis seem more susceptible to cardiac adverse effects due to the higher frequency of low baseline LVEF observed in untreated patients compared to individuals without multiple sclerosis (13,46). In these patients, the cardiotoxicity occurs at a median of 7.2 cycles of MTX (12mg/m^2, every three months, cumulative dose of 86.4mg/m^2) (19), but it can occur before. In a prospective study, 28 multiple sclerosis patients treated with MTX were subjected to a LVEF evaluation before receiving the fourth cycle of MTX. The results revealed that, at that moment, five patients (17.8%) already underwent a significant decline in their baseline LVEF (13). It suggests that MTX-cardiotoxicity could be evident at lower doses and earlier in multiple sclerosis patients (46) and thus, such patients treated with MTX should be followed warily. The monitoring of cardiac function includes a baseline echocardiogram followed by echocardiograms at one and two years and even every cycle of MTX (19). Conservative authors claim that the maximum cumulative dosage in such patients might be defined as 100mg/m^2 (19,20). Therefore, in multiple sclerosis, the use of MTX is recommended only in cases of very aggressive multiple sclerosis, presenting increased disability, frequent and severe relapses, and many active inflammatory lesions (20).

In multiple sclerosis, MTX treatment frequently induces clinical asymptomatic reduction of baseline LVEF, which is counteracted, returning to normal values, after MTX end of therapy (19,20,56,57). In a review of clinical data from 18 multiple sclerosis patients who received MTX dosage (12 patients received 12mg/m^2; two patients received 10mg/m^2, two patients started with 15mg/m^2 and were kept with cycles of 8mg/m^2, two patients started with 15mg/m^2 and were gradually lowered to 12 and 8mg/m^2) and interval cycles (12 patients followed the conventional three months interval, two patients alternated three and two months courses, one patient performed three cycles with three months interval, three cycles of four months and the last three cycles of two months intervals, and the last three patients followed a one month interval course) depending on the clinical response and side-effects. Cardiac LVEF decrease was observed in all MTX treated patients, but only two cases presented severe LVEF decrease (LVEF<55%, considered below the normal values). These patients received only two drug infusions and were advised to discontinue the therapy although they were clinically asymptomatic. Following this procedure their LVEF returned to normal values (56).

In a retrospective review of 128 patients with multiple sclerosis treated with MTX standard protocol (using as top limit the cumulative dose of 120mg/m^2), it was observed that until the end of the study (median follow-up duration of 14 months), 18 (14%) patients developed *de novo* cardiotoxicity evidenced by decreased LVEF (46). Of these patients, only three (17%) recovered to normal in the next assessment, six had no further follow-up, and two remained altered until the end of the study (46).

In a single center, open-label, non-randomized study, 42 secondary progressive multiple sclerosis patients were divided in two groups: control (n=11, receiving no treatment) and MTX (n=31, receiving 12mg/m^2 infusion every three months up to a maximum cumulative dose of 120mg/m^2) (20). Ten patients from the MTX group prematurely finished the study due to cardiac complications (heart palpitations, pulmonary edema, and tachycardia). These cardiac complications were classified as severe (decrease of 10% or more from the LVEF baseline) in six patients. However, the post-trial cardiac surveillance, which continued for up two years, revealed that 48% of the total MTX patients presented decreases in the LVEF, that followed by a post-treatment recovered to normal cardiac function (20).

In another open-label study with 23 multiple sclerosis patients receiving 12mg/m^2 at three month intervals (up to a maximum cumulative dose of 140mg/m^2) only one patient, representing 4.3% of the studied population, presented asymptomatic left ventricular hypokinesia and reduced LVEF, which was also reverted after the end of therapy (57). This lower cardiotoxicity incidence might be related to the reduced number of patients.

A retrospective study reviewing 41 multiple sclerosis patients who received MTX previously (12mg/m^2 at three month intervals), evidenced that 9% presented decline greater than 20% from baseline LVEF and 7% patients had decline greater than 10% from baseline LVEF (19). Of patients re-evaluated off-study, all presented improvements in LVEF, also demonstrating that, although the MTX-induced cardiotoxicity is a concern, it may be not permanent if the therapy is conducted with regularly monitoring and interruption is in place adequately (19).

There are few studies trying to elucidate the mechanisms involved in the MTX-induced cardiotoxicity. Frequently, regarding that the clinical manifestations of MTX-cardiotoxicity are similar to those observed to doxorubicin, it was believed that both compounds shared the mechanisms involved in their cardiotoxicity (29,58). However, other studies suggest that the mechanisms are dissimilar (50,59). Considering that the purpose of the present thesis is to contribute to the elucidation of the mechanisms related to MTX-cardiotoxicity, mechanistic studies will be discussed in more details in the Discussion section.

I.6.2. MTX-induced hepatotoxicity

The occurrence of abnormalities in the liver function during the treatment of complex diseases such as cancer and multiple sclerosis can be catastrophic. In fact, it may compromise treatment and even, as a consequence of impaired metabolism, contribute to MTX toxicity (60). In humans, the MTX-induced hepatotoxicity manifests as transient increases in the serum bilirubin concentration and in the activity of hepatic enzymes, occurring in about 15% of treated patients (12mg/m^2) (9,15).

There are few studies focusing on the hepatotoxicity of MTX and it is still unclear whether the hepatic disturbances elicited by MTX are due to a direct hepatotoxic effect or are a consequence of cardiac failure. The hepatotoxicity was observed in mice treated with a single dose of MTX (15mg/kg), which hepatic injury was considered more intense compared to the hepatic lesion promoted by doxorubicin in the same dose and model (49). Existing data demonstrate that oxidative stress is involved in the hepatic injury caused by MTX (33,37,49). A study with HepG2 cell line and rat hepatocytes suggested that the cytotoxic effect of MTX depends on prior oxidation mediated by CYP450 (37). The incubation of MTX (100μM) with HepG2 cells for 6h promoted a slight decrease in the GSH levels (33) that is in accordance with what was found in mice, where decreases in the hepatic antioxidant defenses after MTX treatment were also observed (49). In fact, four days after the intraperitoneal (i.p.) injection of a single dose of MTX (15mg/kg), intense signals of hepatic lipid peroxidation, diminished activity of hepatic superoxide dismutase, catalase, and glutathione peroxidase, and depletion of the hepatic retinol and GSH contents were observed (49). In the same study, hepatic histopathologic results showed intense hydropic vacuolization of the cytoplasm, necrotic areas, picnosis, and nuclear lysis (49).

As mentioned above, *in vitro* studies suggest that the oxidative biotransformation influences MTX toxicity (33,36,37). Hence, the liver is the main destiny of MTX accumulation in humans (26) and, as already described, is also in charge of the MTX detoxifying process through phase II metabolism (1). Thus, it is not surprising that patients presenting hepatic disturbances are prescribed with lower dose of MTX (15).

I.6.3. MTX-induced hematotoxicity

As already addressed, after administration MTX is rapidly attracted to blood cells, causing immediately its hematological effects (1). In fact, concerns were raised since the observation that, 1h after MTX infusion, its concentration in leukemic cells is ten times higher than in plasma and 350 times higher after 2-5h (9). On the other hand, MTX depressor effects among blood cells, namely macrophage, T and B cells proliferation justify its use in the treatment of multiple sclerosis (51).

MTX presents a potential hematotoxicity which can limit and even cause the cessation of therapy (9,61). Firstly, the administration of MTX only can be supported after hematological screening: patients with baseline neutrophil counts ≤ 1,500 cells/mm^3 should not receive MTX (51). The hematotoxicity of MTX involves myelosuppression that manifests mostly as leukopenia, thus being its main dose-limiting effect (9,61). Low hemoglobin (Hb) levels were observed in 21 of 139 (15%) multiple sclerosis patients treated with MTX (12mg/m^2, i.v., monthly for three months until reaching the cumulative dose of 120mg/m^2) (46). The same study observed that anemia was associated with increasing dose and that only women manifested this condition (46). In a study employing high dose regimens (40 to 80mg/m^2) by i.v. 15min administration, the myelosuppression was universal (62), which is in agreement with the high frequency associated with MTX treatment (2,9,24). In a phase II clinical trial, 93% advanced breast cancer patients who received MTX (starting dose of 10mg/m^2) associated with paclitaxel (175mg/m^2) presented leukopenia, which was considered severe in 67% of the patients (63). The administration of MTX (38mg/m^2), via i.p., demonstrated that the observed leukopenia is transient since white blood cell (WBC) counting returned to normal values within 7 days (61). Curiously, patients treated with higher dose regimens tend to present a faster blood count recovery (2). Nonetheless, WBC should be carefully monitored since in severe cases of leukopenia, complications such as sepsis and other infections can occur (64).

During MTX pharmacological use, thrombocytopenia also occurs, but in a lesser extent than neutropenia (9). In most cases, neutropenia and thrombocytopenia are mild (2). Monitoring hematological parameters during MTX-therapy is recommended and drug discontinuation or dose reduction may be warranted with neutrophil counts ≤ 1,000 cells/mm^3 or other signals of strong myelosuppresion (51). However, in spite of the relevance of MTX-induced myelotoxicity, patients treated with MTX require fewer median platelet (PLT) transfusions and are treated with fewer median days of i.v. antibiotics compared to those that received other chemotherapy drugs such as daunorubicin (2).

In MTX-treated patients undergoing autologous bone marrow transplantation, the time of transplant has to be carefully assessed depending on the dose and individual pharmacological profile. It is an important observation since MTX treatment increases the risk of delayed hematopoetic function recovery (14).

Consistent with the long accumulation and sustained efficacy of MTX, the hematotoxicity of MTX also can emerge after the end of treatment (15). In fact, the most serious hematologic manifestation is the development of MTX-associated leukemia, which is also related with other topoisomerase II inhibitors (2). The mechanism involved in the secondary leukemia is still being debated. One hypothesis is that the chromosomal breaks related to perturbations in the topoisomerase II cleavage-religation equilibrium post topoisomerase II inhibition can lead to DNA recombination and the resulting translocations are responsible for the leukemogenesis (65). The most common chromosomal translocations related to the topoisomerase II inhibitors-induced leukemia involve rearrangements in the gene *mll*, chromosome 11q23 (2,17,65).

The occurrence of secondary leukemia is related to familiar history of neoplasia, the concomitant use of other anti-cancer drugs, chemotherapy doses and regimen, and individual immunological condition (17). In most cases, patients develop secondary acute myelogenic leukemia, however, some patients develop acute lymphoblastic leukemia (2). The pattern of acute myelogenic leukemia related to topoisomerase II inhibitors treatment is characterized by a short latent period (usually one year) and it is not associated with a myelodysplastic phase prior to its manifestation (2,17). Trying to avoid the associated leukemia in multiple sclerosis patients, MTX administration is not recommended in patients with previous history of leukemia (15). However, the use of MTX in the treatment of multiple sclerosis has been accompanied by reports of leukemia associated to MTX therapy in patients without previous diagnosis of hematological disorders (2,51). Thus, considering the long-term hematological disturbances, blood cell counts should be continued even after the cessation of MTX therapy (15).

Objectives

II. General objective

In the Introduction section, the therapeutic actions of MTX (as an antineoplastic agent and in the treatment of multiple sclerosis) and the limitations related to its adverse effects and toxicity (cardiotoxicity, hepatotoxicity, and hematotoxicity) were focused in detail. Noteworthy, several case reports were presented evidencing the potential MTX-induced cardiotoxicity (20,46,52,54). However, the mechanisms underlying this toxicity are still not fully elucidated, as will be described in more detail in the Discussion section.

The general objective of the present thesis was to contribute to the clarification of the mechanisms involved in the MTX-induced cardiotoxicity. Additionally, in this work, it was intended to highlight the relevance of MTX metabolic pathways and the mitochondrial role in that process. Finally, it was intended to correlate the effects and mechanisms studied in *in vitro* systems (cellular fractions, organelles, and cell line cultures) to those observed in *in vivo* model (adult male Wistar rats).

II.1. Specific objectives:

- Evaluation of MTX mechanisms of cytotoxicity, through the assessment of viability, oxidative stress, energetic, and mitochondrial parameters after MTX incubation in a cardiomyoblast model (H9c2 cells).
- Evaluation of the *in vitro* mitochondrial toxicity through the assessment of mitochondrial membrane potential, ATP synthase expression and activity after MTX incubation with H9c2 cells.
- Evaluation of the direct mitochondrial toxic effect through the assessment of mitochondrial membrane potential after MTX incubation with cardiac mitochondria isolated from male Wistar rats.
- Evaluation of the *in vivo* cardiotoxicity through the assessment of cardiac optic and transmission electron microscopy, cardiac protein, glutathione, and ATP levels after the administration of three cycles of MTX to male Wistar rats.
- *Ex vivo* evaluation of mitochondrial toxicity through the measurement of mitochondrial membrane potential and complex IV and V activities of the respiratory chain of cardiac mitochondria isolated from male Wistar rats treated with three cycles of MTX.
- Evaluation of the metabolic profile of MTX through the identification of the metabolites generated after the incubation of MTX with hepatic S9 fractions isolated from rats.

- Evaluation of the contribution of MTX metabolism to its cardiotoxicity using *in vitro* promoted metabolism coupled to cytotoxic assays in H9c2 cell line.
- Evaluation of the *in vivo* MTX cumulative sub-chronic toxicity through the assessment of biochemical parameters evaluating cardiac, hepatic, and renal function, hematological parameters, and hepatic measurements (microscopy, hepatic glutathione and ATP levels) after the administration of three cycles of MTX to male Wistar rats.

PART II

Material and Methods

In the present section, all experimental models and protocols employed in this thesis will be addressed.

III.1. Brief considerations on the experimental models and concentrations used in the studies

III.1.1. *In vitro* models

In the present thesis, three *in vitro* models were used, namely hepatic S9 fractions, the H9c2 cell line, and isolated mitochondria from heart of adult rat. In general, the *in vitro* models have some advantages when mechanistic studies are being performed (66). It is well known that the detection of cardiovascular injury at the cellular level can be complicated by interactions between adjacent cells of different types, metabolism of the toxic agent under investigation, and by alterations in the concentration of the xenobiotic at the cell-body fluid interface (67). Thus, an important advantage of *in vitro* models is to allow a better control of the surrounding environment (66), which is imperative in the assessment of cardiotoxicity since humoral, neuronal, and endocrine influences are commonly considered confounding factors in the evaluation of cardiotoxicity *in vivo* (68). Another feature is the fact that *in vitro* studies involve the sacrifice of fewer animals compared to *in vivo* approaches, evidencing an ethical advantage (66).

III.1.1.1. Hepatic S9 fractions isolated from adult male Wistar rat

The hepatic S9 fraction is the supernatant obtained after liver homogenization and centrifugation at 9,000*g* for 20min in a suitable medium (100mM phosphate buffer, pH 7.4). The greatest advantage of this model is the fact that it contains the cytosol (with most of the enzymes responsible for the phase II metabolism, such as glutathione-S-transferases and some enzymes responsible for phase I metabolism, as cytosolic epoxide hydrolase) and microsomes (containing enzymes of phase I metabolism such as CYP450 isoforms and UDP-glucuronosyl transferases responsible for phase II metabolism) (69–71). Hence, liver S9 fractions are reported as the most representative sub-cellular *in vitro* system to study metabolism because it allows the study of the main biotransformation phases at the same time (71), being much more illustrative of a real situation than studies using isolated enzymes or microsomes (69,71). Indeed, S9 fractions can be considered a classic model since it is commonly used in the pharmaceutical industry coupled to Ames test in order to evaluate the possible mutagenic effect after bioactivation of pre-genotoxic compounds (72–74). Moreover, procedures involved in liver S9 fractions isolation and incubation steps are rapid, do not require sophisticated equipment, are easy to perform in laboratory settings, and allow the study of several conditions with a single animal.

In the study using hepatic S9 fractions isolated from male Wistar rats presented in this thesis (Manuscript I), the animals used received phenobarbital 0.2% in drinking water for one week prior to the excision of the livers. This approach aims to induce enzymes involved in the MTX metabolism (32,75) and was adopted due to the difficulties to simulate *in vitro* MTX oxidoreductive metabolism, being commonly used by other authors (28,31–33). In fact, phenobarbital induces CYP450-induced metabolism as well as other enzymatic systems present in the S9 fractions, namely epoxide hydrolase, UDP-glucuronyl transferases, and glutathione-S-transferases (76).

III.1.1.2. H9c2 cell line

Permanent cell lines are frequently used as a model for many cell types (77). However, immortal cardiac cell lines have been difficult to establish because of the heterogeneity of cells present in heart tissue, the inability of isolated cardiomyocytes to multiply in culture, and the low frequency of cardiac tumors necessary to create cell lines (77,78). The studies presented in the Manuscripts I and II on the next section were conducted in the H9c2 cellular model. This clonal muscle cell line derived from embryonic rat heart tissue was established in 1976 by Kimes and Brandt. It was obtained through selective serial passage from BDIX rat cardioblasts (79).

Morphologically, H9c2 cells are spindle-shaped cells. The dividing myoblasts are large, flat, and their nuclei contain from two to four spherical or lobed nucleoli (78,79). The structures and organelles that can be observed in the H9c2 cells are: microtubules (sometimes arranged as a dense network), vacuoles, lysosomes, pinocytotic vesicles, basement membrane, ribosomes, cell surface enlarged by microvilli, and a rich content of mitochondria and rough endoplasmic reticulum (78,79). Golgi *cisternae* are found near the cell nucleus and *caveolae* are absent (78). At low densities, H9c2 cells organize themselves avoiding close contact (Figure 3 A). On the other hand, when they reach confluence, they arranged themselves in linear parallel arrays, maintaining these characteristics at continual passages (Figure 3 B) (79).

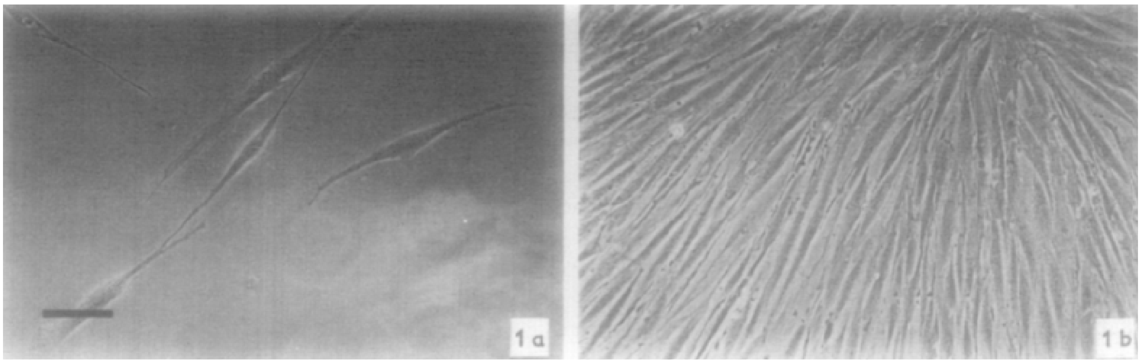

Figure 3: Phase contrast micrographs of H9c2 cells. A) at low densities; B) at confluence (79).

Binding studies for 1,4-dihydropyridine demonstrated H9c2 heart-specific features (78). Additionally, after reaching confluence, H9c2 cells express an L-type calcium current characterized by a slow time course of inactivation, unitary conductance properties, and sensitivity to organic calcium channel blockers, typical characteristics of cardiac cells (78,80). Moreover, at least 2 distinct potassium channels and a nonspecific cation channel were described (80). Densely culture conditions seems to optimize calcium channel expression, since when cells are in the proliferative phase, these channels are sparse (80). However, if H9c2 cells are allowed to reach confluence, the myoblastic population becomes depleted faster (81). In order to prevent this inconvenient, cell cultures used in this thesis were kept at 70-80% confluence. The H9c2 cells also have features of skeletal muscle, namely the tendency of myoblasts to form myotubes, the synthesis of muscle-specific creatine phosphokinase isoenzyme when the mononucleated myoblasts fuse, and the expression of nicotinic receptors (79).

The pattern of membranous signal-transducing G-proteins found in the H9c2 cells shows all characteristics of striated muscle cells (78). They contain two forms of the G_s α-subunit, two forms of the G_iα-subunit, and, as adult rat cardiomyocytes, they lack G_0 subunit (78). H9c2 cells also contain β_1 and β_2 adrenoreceptors and respond to acetylcholine stimulation (81,82). Regarding caveolin, a major structural protein of *caveolae* involved in the AMPc signaling, it was demonstrated that caveolin-1 mRNA expression is similar in H9c2 cells and in canine hearts (83). However, the mRNA of muscle-specific subtype caveolin-3 is abundantly expressed in cardiac tissues while poorly in the H9c2 cells (83). Decreased levels of caveolin-3 expression were associated with the development of cardiac hypertrophy since caveolin-3 regulates the inhibition of cell growth and proliferation in the heart (84). Recently, a study comparing the response patterns after hypertrophic stimulation in primary cardiomyocytes from neonatal rat heart and in the H9c2 cell line demonstrated that both models showed almost identical hypertrophic responses (85). Hence, it was concluded that H9c2 cells are a reliable model for the study of drug-induced hypertrophy with the ethical advantage of being an animal-free protocol, in opposition to neonatal cardiomyocytes (85).

In the present study, we used the H9c2 cells in the undifferentiated state. In this condition, the embryonic-derived H9c2 cells are more reliant on glycolysis accordingly with the fetal phenotype (86). This cellular model expresses thyreoglobulin at the mRNA and protein level. That is an important regulator of cardiac function and cardiovascular hemodynamics (87).

Significant levels of peptidylglycine α-amidating monooxygenase, which catalyzes the formation of bioactive α-amidated peptides from glycine precursors, are found in the H9c2 myoblasts. This observation suggests the ability of H9c2 to make bioactive α-amidated hormones and neuropeptides, however, the activity of this enzyme is lower than in atrium tissues (88). Although the role of peptidylglycine α-amidating monooxygenase in the heart tissue is not fully elucidated, it seems that amidated peptides have a crucial role in the early stages of cardiac development (88).

Furthermore, these myoblasts express multiple CYPs at comparable levels to those expressed in the rat heart. CYP1A1 and CYP1B1 are constitutively expressed in both H9c2 cell line and rat heart, CYP2B1, CYP2B2, CYP2E1, CYP2J3 are expressed in the H9c2 cells at different degrees but in comparable levels to rat heart, and CYP2A1, CYP3A1, CYP3A2 are not expressed either in H9c2 cells or in the rat heart (89). Hence, regarding their metabolic competence, H9c2 cells have been considered a valuable *in vitro* model to study cardiac drug metabolization and the metabolic capacity of the heart (89).

In conclusion, in spite of the H9c2 cellular model characteristics of muscle cells, it preserves several elements of cardiac cells, namely the electrical and hormonal signal pathways (78,79). Thus, this *in vitro* model has been widely accepted as a feasible model to study cardiotoxicity (90–93).

III.1.1.3. Cardiac mitochondria isolated from male Wistar rat

Mitochondria are responsible for supplying between 80-90% of total ATP produced in the cell (94). Due to the high energetic demand in the cardiac muscle, mitochondria occupy 20-30% of cell volume, being the highest distribution of these organelles found in the cardiomyocytes, showing mitochondria relevance for the cardiac performance (94–96). Thus, given their importance, one of the main objectives of this thesis was to investigate mitochondria as a target for the MTX-induced cardiotoxicity. For this purpose, cardiac mitochondria isolated from male Wistar rats were used. Similarly, this model was already employed in the evaluation of the doxorubicin-induced mitochondrionopathy (97–99).

III.1.2. *In vivo* model

For the *in vivo* studies, the laboratory animal model used was *Rattus novergicus.* This animal species is recognized as the most widely *in vivo* model used in medical research and, in toxicology, the rodent species of choice (100,101). The advantages of working with rats comprises the easier monitoring of their physiology, and, in many cases, the physiology is resembled to human conditions (100). Additionally, other advantages include metabolic similarities to humans, their relatively docile nature, short life span, short gestation period, and the large database of rat nutrition, diseases, and general biology (101). Regarding cardiovascular system, the rat is considered an excellent model, especially for stroke and hypertension (100). This animal model has been widely used in the assessment of chemotherapy-induced cardiotoxicity (102,103). Another advantage is that the size of the rat enables both the easy manipulation of the animal in laboratory conditions and serial blood draws (100).

Adult male Wistar rats (Charles River Laboratories, Barcelona, Spain) were housed in cages, with a temperature- and humidity- controlled environment. Food and water were provided *ad libitum* and animals were subjected to a 12h light-dark cycle. Animal experiments were approved by the Ethics Committee of the Faculty of Pharmacy, Porto University, Portugal (protocol number 9/04/2013). Housing and experimental treatment of the animals were in accordance with the Guide for the Care and Use of Laboratory Animals from the Institute for Laboratory Research.

In the experiments presented in the Manuscripts III and IV, one week prior the experiment, animals were acclimatized in the cages and then were distributed into three groups (five animals per group): control, MTX22, and MTX48. Animals were treated by i.p. via with three cycles, (5ml/kg), of saline solution (0.9% NaCl) (control) or MTX 2.5mg/kg (MTX22 and MTX48) on day 0, 10, and 20. The MTX treated groups reached a total cumulative dose of 7.5mg/kg on day 20, as represented in Figure 4. The regimen of administration (one cycle every ten days) was performed aiming to simulate the chemotherapeutic cycles that comprise several administrations. The interval of ten days was defined taking into account the life cycle of the rat and the clinical conditions observed in pilot studies. The MTX22 group suffered euthanasia on day 22, in order to assess the MTX-induced cumulative damage 48h after the last cycle of treatment. MTX48 group suffered euthanasia on day 48, 28 days after the last cycle of treatment, with the objective to evaluate late cumulative responses.

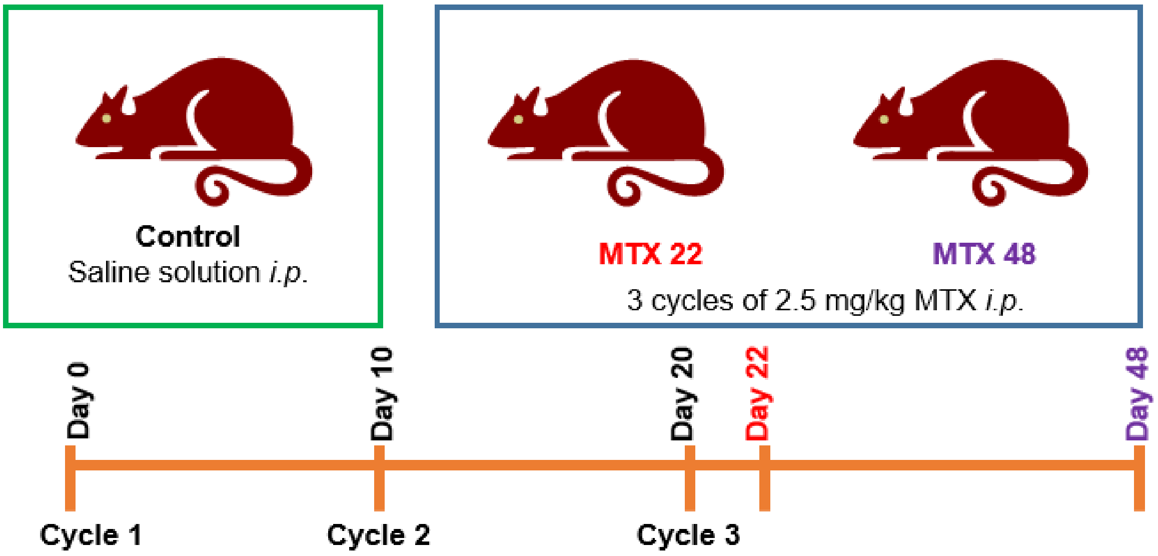

Figure 4: Graphic representation of the *in vivo* experiment design performed in Manuscript III and IV.

During the experiment, daily clinical evaluations of all animals were performed by the veterinary doctor of the team. The parameters evaluated were piloerection, dehydration, hemorrhage and diarrhea, motor function (tone and movement coordination), breathing (rate and depth, gasping), mucosal color (pale, cyanotic), and clinical signals of abdominal pain. The individual weight and consumption of food and water were also recorded every day until the day 30. On the day of euthanasia, animals were anesthetized with xylasine/ketamine (10mg/kg/100mg/kg) and blood was collected through cardiac puncture.

The *in vivo* metabolic study presented in the Manuscript I was also performed aiming to verify the presence of MTX metabolites in liver and heart after MTX i.p. administration to male Wistar rats. Three animals received a single dose of 7.5mg/kg of MTX i.p., and were euthanized 24h after treatment under anesthesia with xylasine/ketamine (10mg/kg/100mg/kg). The livers and hearts were excised and MTX and its metabolites were extracted as described in the Manuscript I to the LC-diode array (DAD)/electrospray ionization interface (ESI)-MS analysis.

III.1.3. MTX concentrations and doses

The human conventional doses of MTX are summarized in the Table 3. The mean maximum plasma concentrations in humans after a 15mg/m^2 or a 90mg/m^2 30min infusion of MTX are about 1.5 and 12µM, respectively (14). Considering tissue levels, it is well known that MTX is extensively distributed and largely accumulates in heart tissue (104). In humans, MTX is detected in the organism for a long period, reaching the amount of 716ng/g wet weight in the heart even 35 days after a single dose (12mg/m^2) (26), evidencing the cardiac accumulation of MTX.

Considering MTX plasma and tissue concentration levels, the MTX working concentrations were selected in order resemble therapeutically relevant concentrations. Thus, for the *in vitro* evaluation of the cytotoxic effects upon H9c2 cells, time and concentration response curves were performed using the low MTX concentrations of 10nM, 100nM, 1µM, 5µM, 10µM, 50µM, and 100µM. Afterward, given the cytotoxic profile in this model, experiments were performed using the MTX selected concentrations of 100nM and 1µM.

Table 3: MTX conventional dose for FDA approved therapeutic indications in humans.

Therapeutic indication	MTX dose	Maximum cumulative dose	References
Acute myeloid leukemia	12mg/m^2/Day	140mg/m^2	(2,12)
Prostate cancer	12mg/m^2 i.v. every three months	140mg/m^2	(2,12)
Multiple sclerosis	12 to 14mg/m^2 i.v. every 21 days	100mg/m^2	(12,19,20)

Regarding the *in vivo* experiment, the dose was also calculated considering previously pilot studies employing three cycles of 2.5mg/kg, 5mg/kg, and 10mg/kg. The body surface area of the rats was also considered in order to correlate the dose in this species with the human top limit of MTX doses. Thus, the majority of experiments were performed using three cycles of MTX 2.5mg/kg (7.5mg/kg as cumulative dose), which corresponds to 16mg/m^2 of a rat weighing 240g, by allometric relationship. The metabolic *in vivo* study was conducted using the single dose of 7.5mg/kg, administered via i.p., in order to correlate with the total cumulative dose used in the *in vivo* study of the MTX-induced cardiotoxicity and to reach the limit of detection of the analytical method used.

III.2. Methods

III.2.2. Evaluation of the metabolic profile of MTX using hepatic S9 fractions by LC-DAD/ESI-MS

The metabolic profile of MTX was evaluated using hepatic S9 fractions isolated from male Wistar rats (32). Three tubes were incubated and further analyzed in order to assess MTX metabolism:

- Blank tube: control supplemented S9 fractions (without MTX), in order to evaluate possible matrix interferences;
- Control tube: 100µM MTX + 1mM NADPH + 4mM GSH (without the S9 fractions), in order to rule out the possibility of artifact formation;
- Sample: supplemented S9 fractions + 100µM MTX, in order to assess the MTX metabolism at times 0 and 4h.

At 0 and 4h, after samples collection, methanol was added (ratio of 1:4 methanol) in order to precipitate the proteins and to extract MTX and the metabolites. Methanol was evaporated under nitrogen flow and the residue was re-suspended in 200µl phosphate buffer saline (for cytotoxicity evaluation) or in 200µl methanol (for LC-DAD/ESI-MS analysis). The experimental protocol of S9 fractions isolation, protein quantification, incubation conditions, and LC-DAD/ESI-MS analysis are described in details in Manuscript I.

III.2.3. Cytotoxicity assays

The cytotoxicity assays employed to evaluate the toxic effects of MTX in the H9c2 cells were the lactate dehydrogenase release (LDH) assay (which correlates with the loss of cell membrane integrity) and the reduction of the 3-(4,5-dimethylthiazol-2-yl)-2,5-diphenyltetrazolium bromide (MTT) assay (which can be used as a mitochondrial viability index since it measures mostly the action of mitochondrial dehydrogenases).

III.2.3.1. LDH leakage Assay

At the end of incubation period (24, 48, 72, and 96h), cellular damage was quantitatively assessed by the evaluation of cell membrane integrity through the measurement of LDH release by means of a kinetic photometric assay. The % of viability was evaluated considering the % of LDH released over the total LDH from the complete lysis of the cells (artificially promoted by the addition of triton X-100). The absorbance was measured at 340 nm in a multi-well plate reader (BioTech Instruments, Vermont, US).

III.2.3.2. MTT reduction assay

The cytotoxic effects of MTX after the incubation period (24, 48, 72, and 96h) were assessed also through the reduction of MTT assay as previously described (105).The reduction of the MTT assay can be used as a mitochondrial viability index since it measures mostly the action of mitochondrial dehydrogenases (106).

Trying to prevent or counteract the observed cytotoxicity of MTX, potential protective studies were performed by co-incubating the agents with MTX (100nM and 1μM) at 37 ºC for 96h. The protective agents employed were: a) the reactive species scavenger and GSH precursor N-acetylcysteine (NAC) (1mM), b) the energetic function enhancer *L*-carnitine (1mM), c) the CYP450 inhibitor MTP (0.5mM), and the CYP2E1 inhibitor diallyl sulfide (DAS) (150μM) (105).

III.2.4. Caspase-3 activity assay

Caspase-3 is a cysteine protease involved in apoptosis, being activated by both intrinsic and extrinsic pathways (107). Caspase-3 activity was assessed after 24h incubation with MTX (100nM and 1μM) in H9c2 cells through the method previously described (108). The CYP450 inhibitor MTP (0.5mM) and the CYP2E1 inhibitor DAS (150μM) were used to possible counteract the activation of caspase-3 caused by MTX (105) (Manuscript II).

III.2.5. Evaluation of oxidative stress

III.2.5.1. Evaluation of reactive species generation

Early and late generation of reactive species was evaluated in the H9c2 cells after incubation with MTX (100nM and 1µM) using two different probes, dihydrorhodamine (DHR) (100µM) (108) or dichlorodihydrofluorescein diacetate (DCFH-DA) (10µM) (109,110). Both are non-fluorescent probes that undergo intracellular oxidation to their respective fluorescent products in the presence of reactive species such as peroxynitrite, and hydroxyl radical (108,111,112). The experimental protocol is described in detail in the Manuscript II.

III.2.5.2. Measurement of intracellular total glutathione (GSHt), GSH, and oxidized glutathione (GSSG) levels

The glutathione status was evaluated after incubation with MTX (100nM and 1µM) in the H9c2 cells. It was also evaluated in liver and heart of male Wistar rats after the administration of MTX (3 cycles of 2.5mg/kg). The glutathione status was assessed by the 5,5-dithio-bis(2-nitrobenzoic) acid (DTNB)-GSSG reductase recycling assay, as previously described (113,114), and the experimental protocols are described in Manuscript II, III, and IV.

III.2.5.3. Evaluation of lipid peroxidation

Malondialdehyde is the most used marker of lipid peroxidation (115). The main method employed to the malondialdehyde quantification is the thiobarbituric acid (TBA) reactive substances (TBARS) assay (116,117). However, this methodology is not specific since TBA also reacts with a variety of compounds such as sugars, aminoacids, aldehydes, and bilirubin, generating colorimetric interferences (116). Thus, trying to counteract this problem, we employed a previously validated HPLC/UV method, with minor adaptations, which presents an extraction step employing butanol that reduces the interferences, being more reliable (116). The protocol is described in the Manuscript II.

III.2.6. Evaluation of the energetic function

III.2.6.1. Measurement of ATP levels

ATP determinations were performed after incubation with MTX (100nM and 1μM) in the H9c2 cells and *in vivo* (liver and heart), after the administration of MTX (three cycles of 2.5mg/kg) to male Wistar rats. The ATP levels were measured through the bioluminescence test (118), as described in Manuscript II, III, and IV.

III.2.6.2. Evaluation of the ATP synthase expression

ATP synthase expression was evaluated in the H9c2 cells after incubation with MTX through western immunoblot (119). The experimental conditions are described in details in the Manuscript II.

III.2.6.3. Evaluation of the ATP synthase activity

The activity of ATP synthase in the H9c2 cells was indirectly determined by analysis of the inorganic phosphate (Pi) released from ATP hydrolysis (119) (experimental protocol described in the Manuscript II).

III.2.6.4. Blue native polyacrylamide gel electrophoresis (BN-PAGE) separation of cardiac mitochondria membrane complexes of MTX-treated rats

The respiratory chain complexes from cardiac mitochondria of MTX treated rats (three cycles of 2.5mg/kg) were evaluated. Mitochondrial isolation and BN-Page separation of the respiratory chain complexes are described in the Manuscript III.

III.2.6.5. In-gel activity of mitochondrial complexes IV and V after MTX treatment

The in-gel activity of cardiac mitochondrial complexes IV and V of control or MTX treated rats (three cycles of 2.5mg/kg) were evaluated. The in-gel activity of complexes IV and V were determined using the methods previously described (95) (Manuscript III).

III.2.6.6. Cardiac mitochondrial DNA quantitation in MTX treated rats

Cardiac mitochondrial DNA of control or MTX treated rats (three cycles of 2.5mg/kg) were quantified using the Qubit® dsDNA BR assay kit. Samples were read in a Qubit® 2.0 Fluoremeter and results are expressed as the ratio between the mitochondrial DNA concentration and heart mass.

III.2.7. Evaluation of the mitochondrial membrane potential after *in vivo* and *in vitro* treatment with MTX

Cardiac mitochondria from control and MTX48 rats were isolated for the assessment of the late and cumulative effects induced by MTX towards the mitochondrial membrane potential. Moreover, an *in vitro* study with mitochondria isolated from control rat heart (not treated with MTX) was also performed in order to assess the direct MTX-induced effects in the mitochondrial function after incubation with MTX (10nM, 100nM, and 1µM).

The evaluation of the mitochondrial function was performed through the measurement of the mitochondrial membrane potential and it was assessed using an ion-selective electrode to measure the distribution of the tetraphenylphosphonium (TPP$^+$), as described before (120) (Manuscript III).

III.2.8. Flow cytometry analysis

Intracellular calcium measurements and the evaluation of the mitochondrial membrane potential in the H9c2 cells were determined through flow cytometry using the Fluo-3 AM (10µM) and TMRM (20nM) fluorescent probes, respectively, following the experimental protocols described in the Manuscript II.

III.2.9. Heart and liver preparation for light and transmission electron microscopy

Heart and liver of MTX treated rats were microscopically evaluated through light and transmission electron histology (121). Samples were processed as described in detail in the Manuscript III and IV.

III.2.10. Plasma biochemical analysis

Plasma parameters of control and both MTX treated rats (three cycles of 2.5mg/kg) were evaluated. On the day of euthanasia, blood was collected into heparinized tubes. Plasma levels of albumin, total proteins, IgG, IgM, IgE, C3 and C4 complement, total and conjugated bilirubin, aspartate transaminase (AST), alanine transaminase (ALT), alkaline phosphatase, transferrin, ferritin, iron, cholesterol, triglycerides, glucose, amylase, creatinine, urea, uric acid, potassium, sodium, calcium, C-reactive protein, α_1 – antitrypsin, δ-glutamyltranspeptidase (GGT), and LDH, creatine kinase (CK), CK-MB, and lactate were evaluated in duplicate on an AutoAnalyzer (PRESTIGE® 24i, PZ Cormay S.A.) using the respective kits and following the manufacturer instructions.

III.2.11. Hematological analysis

Hematologic parameters of control or MTX treated rats (three cycles of 2.5mg/kg) were evaluated. On the day of euthanasia, blood samples (using EDTA as anticoagulant) were collected and processed in order to obtain whole blood. We evaluated the erythrocyte count, Hb concentration, hematocrit (HCT), hematimetric indexes – mean cell volume (MCV), mean cell hemoglobin (MCH), mean cell hemoglobin concentration (MCHC), red cell distribution width (RDW), PLT, plateletcrit (PCT), platelet distribution width (PDW), mean platelet volume (MPV), and WBC count, by using an automated blood cell counter (Sysmex K1000, Hamburg, Germany). Differential leukocyte count was performed on blood smears stained according to Wright (122). Reticulocyte count was performed by microscopic counting on blood smears after vital staining with new methylene blue (Reticulocyte stain, Sigma-Aldrich, St Louis, MO, USA).

III.2.12. Total protein quantification

Except when otherwise specified, the protein levels were determined by Lowry method (123). Samples were suspended in NaOH 0.3M and protein content were evaluated spectrophotometrically using a microplate reader (750nm) (114).

III.2.13. Statistical analysis

Results are presented as means ± standard deviation. The evaluations of the rat relative body weight gain and the consumptions of food and water were followed daily.

Thus, the statistical analysis was performed using repeated measures ANOVA followed by the Student Newman Keuls *post hoc* test. In the other experiments, statistical comparisons between groups were performed with One-Way ANOVA (in case of normal distribution) or Kruskal-Wallis test (one-way ANOVA on ranks – in case distribution is not normal). Significance was accepted at *p* values <0.05.

Results

Manuscript I

The metabolic profile of mitoxantrone and its relation with mitoxantrone-induced cardiotoxicity.

Rossato, L. G., Costa, V. M., De Pinho, P. G., Freitas, V., Viloune, L., Bastos, M.L., Palmeira, C., Remião, F.

Arch Toxicol 2013, 87 (10):1809-20

Arch Toxicol (2013) 87:1809–1820
DOI 10.1007/s00204-013-1040-6

ORGAN TOXICITY AND MECHANISMS

The metabolic profile of mitoxantrone and its relation with mitoxantrone-induced cardiotoxicity

**Luciana Grazziotin Rossato · Vera Marisa Costa · Paula Guedes de Pinho ·
Marcelo Dutra Arbo · Victor de Freitas · Laure Vilain ·
Maria de Lourdes Bastos · Carlos Palmeira · Fernando Remião**

Received: 9 November 2012 / Accepted: 8 March 2013 / Published online: 2 April 2013
© Springer-Verlag Berlin Heidelberg 2013

Abstract Mitoxantrone (MTX) is an antitumor agent that causes cardiotoxicity in 18 % patients. The metabolic profile of MTX was assessed after incubation of 100 μM MTX with hepatic S9 fraction isolated from rats. The presence of MTX and its metabolites was also assessed in vivo through the analysis of liver and heart extracts of MTX-treated rats. The cytotoxic effects of MTX and MTX metabolites were evaluated in the H9c2 cells after 24-h incubation with MTX alone and MTX + metabolites. The influence of CYP450- and CYP2E1-mediated metabolism for the cytotoxicity of MTX was assessed after 96-h incubation with MTX (100 nM and 1 μM) in the presence/absence of CYP450 or CYP2E1 inhibitors. After 4-h incubation in supplemented S9 fraction, the MTX content was 35 % lower and 5 metabolites were identified: an acetoxy ester derivative (never described before), two glutathione conjugates, a monocarboxylic acid derivative, and the naphtoquinoxaline, the later commonly related to MTX pharmacological effects. The presence of MTX and naphtoquinoxaline metabolite was evidenced in vivo in liver and heart of MTX-treated rats. The cytotoxicity caused by MTX + metabolites was higher than that observed in the H9c2 cells incubated with non-metabolized MTX group. The co-incubation of MTX with CYP450 and CYP2E1 inhibitors partially prevented the cytotoxicity observed in the MTX groups incubated with H9c2 cells, highlighting that the metabolism of MTX is relevant for its undesirable effects. The naphtoquinoxaline metabolite is described in heart and liver in vivo, highlighting that this metabolite accumulates in these tissues. It was demonstrated that MTX P450-mediated metabolism contributed to MTX toxicity.

Keywords Mitoxantrone · Metabolism · Bioactivation · LC/MS · S9 fraction · Cardiotoxicity

Abbreviations

DAD	Photodiode array
DAS	Diallyl sulfide
DMEM	Dulbecco's modified eagle's medium
DMSO	Dimethyl sulfoxide
ESI	Electrospray ionization interface
GSH	Reduced glutathione
LC	Liquid chromatography
MS	Mass spectrometry
MTT	3-(4,5-dimethylthiazol-2-yl)-2,5-diphenyltetrazolium bromide
MTP	Metyrapone
MTX	Mitoxantrone
β-NADPH	β-Nicotinamide adenine dinucleotide phosphate

Electronic supplementary material The online version of this article (doi:10.1007/s00204-013-1040-6) contains supplementary material, which is available to authorized users.

L. G. Rossato (✉) · V. M. Costa · P. G. de Pinho ·
M. D. Arbo · L. Vilain · M. de Lourdes Bastos · F. Remião (✉)
REQUIMTE, Laboratório de Toxicologia, Departamento de Ciências Biológicas, Faculdade de Farmácia, Universidade do Porto, Rua Jorge Viterbo Ferreira, 228, Porto 4050-313, Portugal
e-mail: luciana.g.rossato@gmail.com

F. Remião
e-mail: remiao@ff.up.pt

V. de Freitas
Centro de Investigação em Química, Departamento de Química, Faculdade de Ciências, Universidade do Porto, Porto, Portugal

C. Palmeira
Centro de Neurociências e Biologia Celular de Coimbra, Departamento de Ciências da Vida, Universidade de Coimbra, Coimbra, Portugal

Introduction

Mitoxantrone (MTX) is an anticancer drug synthesized in the end of 1970s as an alternative to anthracyclines therapy (Canal et al. 1993). It has been largely used in the treatment of solid tumors, acute leukemia, lymphoma, prostate, and breast cancer (Seiter 2005) and, more recently, in the active forms of relapsing–remitting or secondary progressive multiple sclerosis (Neuhaus et al. 2006). Despite its broad utilization, MTX is potentially cardiotoxic (Seiter 2005; Avasarala et al. 2003).

The pharmacological activity of MTX is based on the ability to intercalate its planar electron-rich chromophore group in the DNA and to allow electrostatic interactions of its side chains with the phosphate moiety of DNA (Ehninger et al. 1990). Furthermore, MTX causes single and double breaks in DNA by stabilization of a complex formed between DNA and topoisomerase II (Ehninger et al. 1990; Seiter 2005). As a consequence, MTX inhibits DNA replication, RNA transcription, and also affects the cell cycle at various stages (Khan et al. 2010; Ehninger et al. 1990).

The oxidoreductive metabolism of MTX has a significant role on its antitumor effects. MTX has particular effectiveness in tumors with high contents of peroxidases (Brück and Brück 2011; Blanz et al. 1991), and it was verified that the inhibitory effect of MTX on cell growth was prevented by inhibiting the activity of cytochrome P450 mixed oxidase function in a human hepatoma-derived cell line (Duthie and Grant 1989). Similar results were obtained with a rat hepatocytes model (Mewes et al. 1993) and with human breast cancer cells (Li et al. 1995). Phorbol ester-stimulated human neutrophils can bioactive MTX through myeloperoxidase metabolism, and the generated metabolites can form adducts with DNA (Panousis et al. 1997). Furthermore, it was already demonstrated that a synthetic cyclic metabolite of MTX, the 8,11-dihydroxy-4-(2-hydroxyethyl)-6-[[2-[(2-hydroxyethyl)amino]ethyl]amino]-1,2,3,4,7,12-hexahydronaphto-[2-3]-quinoxaline-7-12-dione or naphtoquinoxaline metabolite, causes cellular damage in neonatal cardiomyocytes isolated from rats (Shipp et al. 1993). This metabolite was already described as an in vivo MTX biotransformation product in humans, pigs, and rats (Blanz et al. 1991). With the exception of the study mentioned above (Shipp et al. 1993), to the best of our knowledge, there are no studies relating the bioproducts of MTX with its most serious undesirable effect: the late irreversible cardiotoxicity (Avasarala et al. 2003).

Pharmacokinetic studies showed that after intravenous administration, MTX has a rapid distribution followed by a slow elimination phase characterized by an extensive accumulation in highly perfused organs in humans and laboratory animals (Ehninger et al. 1990; Batra et al. 1986). The metabolism of MTX involves the oxidation through the microsomal system and/or peroxidase enzymes such as neutrophil myeloperoxidase (Duthie and Grant 1989; Panousis et al. 1997). Moreover, the phase II metabolism has a relevant role in the MTX detoxification process, namely the conjugation with reduced glutathione (GSH) and glucuronic acid (Ehninger et al. 1990). Considering the interspecies variability, the main metabolic difference between rats and humans is that mono and dicarboxylic acid derivatives of MTX are major bioproducts of human metabolism, while in rats, they are residual (Blanz et al. 1991; Richard et al. 1991).

The difficulty to reproduce the oxidoreductive metabolism of MTX in in vitro conditions is extensively reported (Wolf et al. 1986; Richard et al. 1991; Basra et al. 1985; Kostrzewa-Nowak et al. 2007; Fisher and Patterson 1992; Fisher et al. 1993). Because of that, some authors use exogenously added isolated enzymes such as NADPH cytochrome P450 reductase (Kostrzewa-Nowak et al. 2007; Novak and Kharasch 1985) and peroxidase enzymes system (Blanz et al. 1991; Brück and Brück 2011) in order to circumvent this limitation. Nevertheless, from all in vitro methods, these are the less realistic ones. There are also metabolic studies employing more representative systems, namely using primary cultures of hepatocytes isolated from rats, rabbits, and humans (Richard et al. 1991), microsomes, and cytosol fractions isolated from rat livers (Wolf et al. 1986). The referred studies use HPLC/UV methods to detect and quantify the metabolites (Richard et al. 1991; Wolf et al. 1986), which limit the analysis due to the low sensitivity of UV detector and do not allow the structural elucidation of the metabolites. Alternative methods use liquid scintillation counting equipped with a radioactive flow detector (Richard et al. 1991), which is not commonly available in the majority of analytical laboratories and requires the undesirable use of labeled compounds.

We present herein a study that aims to assess the contribution of MTX metabolism to its cardiotoxicity. The metabolic profile of MTX was studied using the hepatic S9 fraction from phenobarbital-induced animals, which are considered a representative hepatic model for this purpose as it contains both phase I and II enzymes involved in the MTX metabolism (Brandon et al. 2003; Jia and Liu 2007). The MTX metabolites were separated by liquid chromatography (LC) coupled with a UV–VIS photodiode array detector (DAD) and accurately identified by electrospray ionization interface (ESI) mass spectrometry detector (MS) that possess a higher sensitivity and accuracy. The cytotoxic effects of MTX metabolites and the influence of CYP450 and CYP2E1 metabolism in the cytotoxicity of MTX were evaluated in the H9c2 cells, a valuable cardiomyoblast in vitro model (Zordoky and El-Kadi 2007). An in vivo study was also performed in order to investigate whether the MTX metabolites previously found in vitro were also present in the liver and heart of rats after MTX intraperitoneal administration.

Materials and methods

Chemicals

All chemicals and reagents were of analytical grade. MTX hydrochloride, GSH, reduced β-nicotinamide adenine dinucleotide phosphate (β-NADPH), metyrapone (MTP), diallyl sulfide (DAS), and 3-(4,5-dimethylthiazol-2-yl)-2,5-diphenyltetrazolium bromide (MTT) were obtained from Sigma-Aldrich (St. Louis, MO, USA). Methanol, dimethyl sulfoxide (DMSO), and formic acid were obtained from Merck (Darmstadt, Germany).

Dulbecco's modified eagle's medium (DMEM) with 4,500 mg/L glucose and GlutMAX^{TM}, fetal bovine serum FBS, trypsin (0.25 %)—EDTA (1 mM), and antibiotic (10,000 U/mL penicillin, 10,000 g/mL streptomycin) were obtained from Gibco Laboratories (Lenexa, KS, USA).

Animals

Adult male Wistar rats (Charles River Laboratories, Barcelona, Spain) weighing 300–350 g were used. The animals were acclimated, housed in cages, with a temperature- and humidity-controlled environment. Food and water were provided ad libitum, and animals were subjected to a 12-h light–dark cycle. Animal experiments were licensed by Portuguese General Directory of Veterinary Medicine. Housing and experimental treatment of the animals were in accordance with the Guide for the Care and Use of Laboratory Animals from the Institute for Laboratory Research. The experiments complied with current Portuguese laws.

Isolation of the hepatic S9 fraction

The animals used for the hepatic S9 fraction isolation received phenobarbital 0.2 % in drinking water for 1 week prior to the excision of the livers, in order to induce metabolism (Wolf et al. 1986). All the animals were monitored, and no signals of toxicity were observed.

The animals were killed through cervical dislocation. The livers were excised, washed with 100 mM phosphate buffer, pH 7.4 (in order to remove the excess of blood), dried, and weighed. Livers were homogenized in 100 mM phosphate buffer, pH 7.4 (1 g/4 mL of buffer), and centrifuged 9,000×*g*, 20 min, 4 °C. The supernatant contains the S9 fraction. All steps were carefully performed on ice.

An aliquot was used to quantify the protein levels by Lowry method (Rossato et al. 2011, Lowry et al. 1951).

Evaluation of the metabolic profile of MTX

Prior to the incubations, the protein density of the S9 fraction was adjusted to contain 4 mg/mL in 100 mM phosphate buffer, pH 7.4 (Wolf et al. 1986). Samples were supplemented with 1 mM NADPH and 4 mM GSH, as previously reported (Wolf et al. 1986). The incubations were carried out using 100 µM MTX, at 37 °C, for 4-h. Aliquots of this mix were taken at the incubation times 0 and 4-h. One blank tube containing control supplemented S9 fraction (without MTX) was also incubated and further analyzed in order to evaluate possible matrix interferences. One tube containing only 100 µM MTX + 1 mM NADPH + 4 mM GSH (without the S9 fraction) was also evaluated in order to rule out the possibility of artifacts formation.

At 0 and 4-h, methanol was added to the samples (ratio of 1:4 methanol) in order to precipitate the proteins and to extract MTX and the metabolites. Samples were centrifuged at 16,000×*g*, 5 min, 4 °C, and the supernatant was dried under nitrogen flux. The residues were re-suspended in 200 µL of methanol and analyzed by LC/DAD-ESI/MS or in 100 µL phosphate saline buffer for the assessment of cytotoxicity (in detail addressed below).

The incubations with S9 fraction were independently performed in 3 different days with S9 fraction isolated from 3 different animals.

In vivo metabolic study

A study using male Wistar rats was performed in order to verify the presence of MTX metabolites in liver and heart. Three animals received a single dose of 7.5 mg/kg of MTX, via intraperitoneal, and were killed 24-h after treatment. The animals were anesthetized with xilasin/ketamine (10 mg/kg/100 mg/kg) and were killed after diaphragm rupture. The livers and hearts were excised and processed as previously described (An and Morris 2010), with minors adaptations. Briefly, the organs were homogenized with 0.1 M citric buffer containing 100 mg/mL ascorbic acid, pH 3.0. MTX, and its metabolites were extracted after the sequential addition of sulfosalicylic acid (50 µL, final concentration of 5 %) and acetonitrile (150 µL) to the tissue homogenate (200 µL). Samples were centrifuged at 16,000×*g*, 10 min, 4 °C, and the supernatant was dried under nitrogen flux. The residues were re-suspended in 200 µL methanol and analyzed by LC/DAD-ESI/MS, as described below. Control organs (from animals that did not receive MTX) were also evaluated in order to assess matrix interferences.

LC-DAD/ESI–MS analysis

A Finnigan Surveyor series LC, equipped with Lichrocart Purospher® Star reversed-phase column (25 cm × 4.6 mm inner diameter, 5 µM, C18), was used. The samples were analyzed using aqueous 0.5 % (v/v) formic acid as solvent A and acetonitrile as solvent B (Brück and Brück 2011). The pH of the mobile phase was set to 3.0 with formic acid. The gradient profile was 90 % (v/v) A/10 % (v/v) B for 1 min and, subsequently, the percentage of acetonitrile was ramped linearly to 80 % B over a time span of 20 min (Brück and Brück 2011). The analysis was done at a flow rate of 0.5 mL/min. The sample injection volume was 25 µL. The chromatographic column was stabilized with the initial conditions for 10 min. Double-online detection was done by a DAD and MS detectors. The MS detector was a Finnigan LCQ DECA XP MAX (Finnigan Corp., San Jose, CA, USA) quadrupole ion trap equipped with atmospheric pressure ionization source, using ESI. The vaporizer and the capillary voltages were 5 kV and 4 V, respectively. The capillary temperature was set at 325 °C. Nitrogen was used as both sheath and auxiliary gas at flow rates of 90 and 35, respectively (in arbitrary units). Spectra were recorded in positive ion mode between *m/z* 250 and 1,100.

Comparison of the cytotoxic effects of non-metabolized MTX and MTX metabolites in H9c2 cells

The H9c2 cell line was a generous gift from Dr. Vilma Sardão, Center for Neurosciences and Cellular Biology, University of Coimbra, Portugal. Cells were cultured in DMEM supplemented with 10 % fetal bovine serum, 100 U/mL of penicillin, and 100 U/mL of streptomycin in 75 cm^2 tissue culture flasks at 37 °C in a humidified atmosphere of 5 % CO_2, 95 % air atmosphere. Cells were fed every 2–3 days and sub-cultured once they reached 70–80 % confluence (Sardão et al. 2009a, b).

Cells were seeded at a density of 35,000 cells/mL in 48-well plates (final volume of 250 µL; about 8,000 cells/cm^2) and were allowed to grow for 2 days. On the day of experiment, the medium was replaced and cells were divided into four groups (six-well *per* group): (a) control group (without treatment), (b) matrix group (the previously 4-h incubated S9 liver fraction enriched with 1 mM NADPH and 4 mM GSH), (c) MTX + metabolites group (the product of 4-h incubation of S9 liver fraction + 1 mM NADPH + 4 mM GSH + 100 µM MTX), and (d) non-metabolized MTX group (S9 liver fraction + 1 mM NADPH + 4 mM GSH + 100 µM MTX, on time 0 of incubation). The presence/absence of metabolites in the groups (c) and (d), respectively, was confirmed by LC/DAD-ESI/MS prior to the incubations. The cytotoxic effects were assessed after 24-h incubation period at 37 °C through the reduction in MTT assay (described in more detail below). Three independent experiments were performed (with cells seeded on different days and incubated with samples obtained from S9 fraction isolated from 3 different animals).

Assessment of the protective effect of the co-incubation of MTX and P450 cytochrome metabolism inhibitors in H9c2 cells

The CYP450 inhibitor MTP (0.5 mM) (Duthie and Grant 1989; Mewes et al. 1993; Li et al. 1995) and the CYP2E1 subtype inhibitor DAS (150 µM) (Pontes et al. 2010) were co-incubated with MTX (100 nM and 1 µM) at 37 °C for 96-h. MTP was dissolved in DMSO; thus, a group with only the vehicle (DMSO 0.1 %) was also included. The potential protective effect of metabolism inhibitors in the cytotoxicity of MTX was assessed through the MTT assay.

MTT reduction assay

The cytotoxicity upon H9c2 cells was assessed through the reduction of MTT. At the end of incubation period, the medium was removed and the cells were washed with phosphate saline buffer, pH 7.4, followed by the addition of fresh cell culture medium containing 0.5 mg/L MTT and incubated at 37 °C in a humidified, 5 % CO_2, 95 % air atmosphere for 4-h. After this incubation period, the cell culture medium was removed and the formed formazan crystals were dissolved in 100 % DMSO. The absorbance was measured at 550 nm in a multi-well plate reader (BioTek Instruments, Vermont, US). The percent of the MTT reduction relative to control cells was used as the cytotoxicity measure (Silva et al. 2011).

Statistical analysis

Results are presented as mean ± standard deviation ($n = 18$ *per* condition out of 3 independent studies). Since the MTT results passed the normality test, a parametric test was used. One-way ANOVA was performed to compare means of different groups followed by the Student–Newman–Keuls post hoc test. Statistical significance was accepted at p values <0.05.

Results

Metabolic profile of MTX after incubation with supplemented rat hepatic S9 fraction

It was possible to demonstrate the metabolism of MTX using hepatic S9 fraction isolated from adult rats supplemented with 1 mM NADPH and 4 mM GSH. As shown in the Fig. 1, the MTX has a retention time of about 15 min. After 4-h incubation of the MTX with the supplemented S9 fraction, a significant decrease of about 35 % in the MTX peak area was observed, highlighting MTX metabolism in this in vitro system. Moreover, after 4-h, 5 additional chromatographic peaks were present and were numerically identified on the LC-DAD/ESI–MS chromatogram (Fig. 1). The peaks 1 and 3 were present in small amounts in time 0, their areas increasing at time 4-h. The peaks 2, 4 (trace), and 5 were only found after the 4-h incubation period (Fig. 1). In Fig. 2, the UV–VIS DAD spectral properties of MTX and its metabolites are presented, showing that all metabolites identified still possess the tricyclic planar chromophore group.

Data about the retention times, the MS fragmentation pattern, and the proposed structure of MTX and its metabolites are summarized on Table 1. MTX was unequivocally identified on the basis of its already described UV–VIS spectral features (Fig. 2) (Ehninger et al. 1990) and its parent molecular ion mass ($[M + H]^+$) at *m/z* 445 (Brück and Brück 2011). The metabolite 5, the naphtoquinoxaline, was also already reported (Blanz et al. 1991; Brück and Brück 2011), and it has UV–VIS spectrum with maximum absorbance at 583 and 634 nm (Fig. 2). Its parent molecular ion mass ($[M + H]^+$) is *m/z* 443. Both MTX and metabolite 5 have the same MS/MS daughter fragmentation derived from cleavages on the side chain: *m/z* 358 for MTX and *m/z* 356 for metabolite 5 ($[M + H^+] - CH_2 = CHNH_2CH_2CH_2OH$), and *m/z* 384 for MTX and *m/z* 382 for metabolite 5 ($[M + H^+] - NH_2CH_2CH_2OH$].

The metabolites 1 and 2 are probably the MTX conjugates with one and two molecules of GSH, resulting in the parent molecular ion mass ($[M + H]^+$) at *m/z* 750 (metabolite 1) and ($[M + H]^+$) at *m/z* 1,055 (metabolite 2) (Table 1), the same parent molecular ion previously described for these metabolites (Blanz et al. 1991). Regarding metabolite 1, the same pattern of fragmentation of parent ion 750 was obtained ($m/z = 477$ and $m/z = 621$) (Supplementary data). However, considering the metabolite 2, the fragmentation of the ion at *m/z* 1,055 results in fragments (*m/z* 845 and 775) different from those found in the study performed by Blanz and co-workers (*m/z* 926 and 797) (Table 1). Thus, the occurrence of structural rearrangements or the insertion of the GSH molecules in other positions is possible. Metabolite 1 presents maximum absorbance peaks at 619 and 673 nm, and metabolite 2 presents maximum absorbance peaks at 613 and 661 nm (Fig. 2). The LC/DAD-ESI/MS analysis does not allow a conclusion about the site of GSH conjugation. However, we propose the GSH adduct on the dihydroxybenzene part of MTX molecule for metabolite 1 based on the previous work of Mewes and co-workers, which elucidated GSH conjugates chemical structure through two-dimensional ^1H-^{13}C-heteronuclear multiple-bond connectivity NMR technique (Mewes et al. 1993).

The metabolite 3 presents an UV–VIS spectrum similar to MTX (Fig. 2). Its mass spectrum (Table 1) showed a parent molecular ion mass ($[M + H]^+$) at *m/z* 503 and MS/MS fragmentations with *m/z* 442 ($[M + H]^+$–$NH_2CH_2CH_2OH$) and 416 ($[M + H]^+$–$CH_2{=}CHNH_2CH_2CH_2OH$). The parent ion suggests that this compound has a

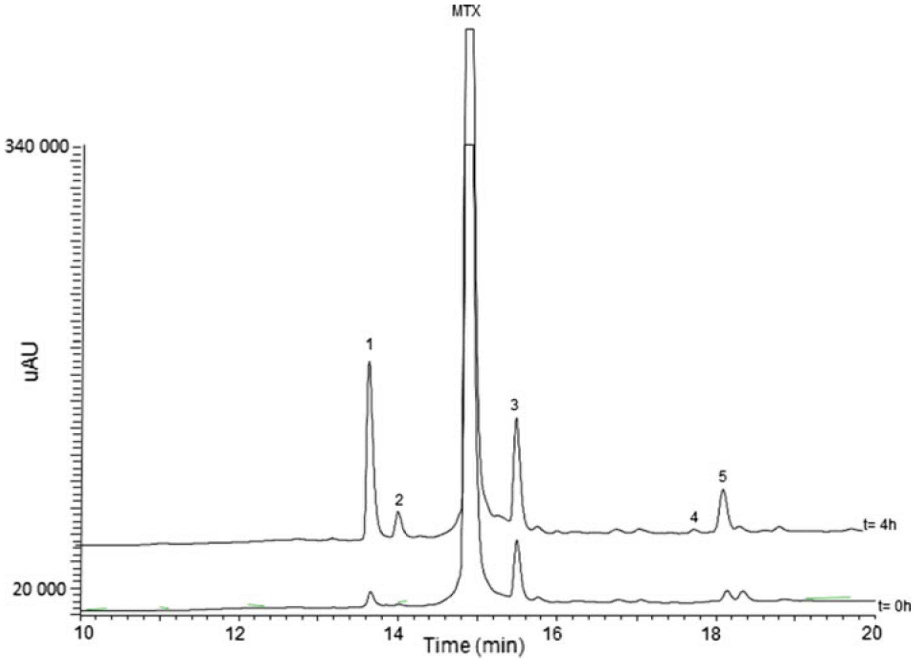

Fig. 1 Overlap of LC/DAD-ESI/MS chromatograms of time 0- and 4-h incubation of rat hepatic S9 fraction (4 mg/mL) with 100 μM MTX + 1 mM NADPH + 4 mM GSH

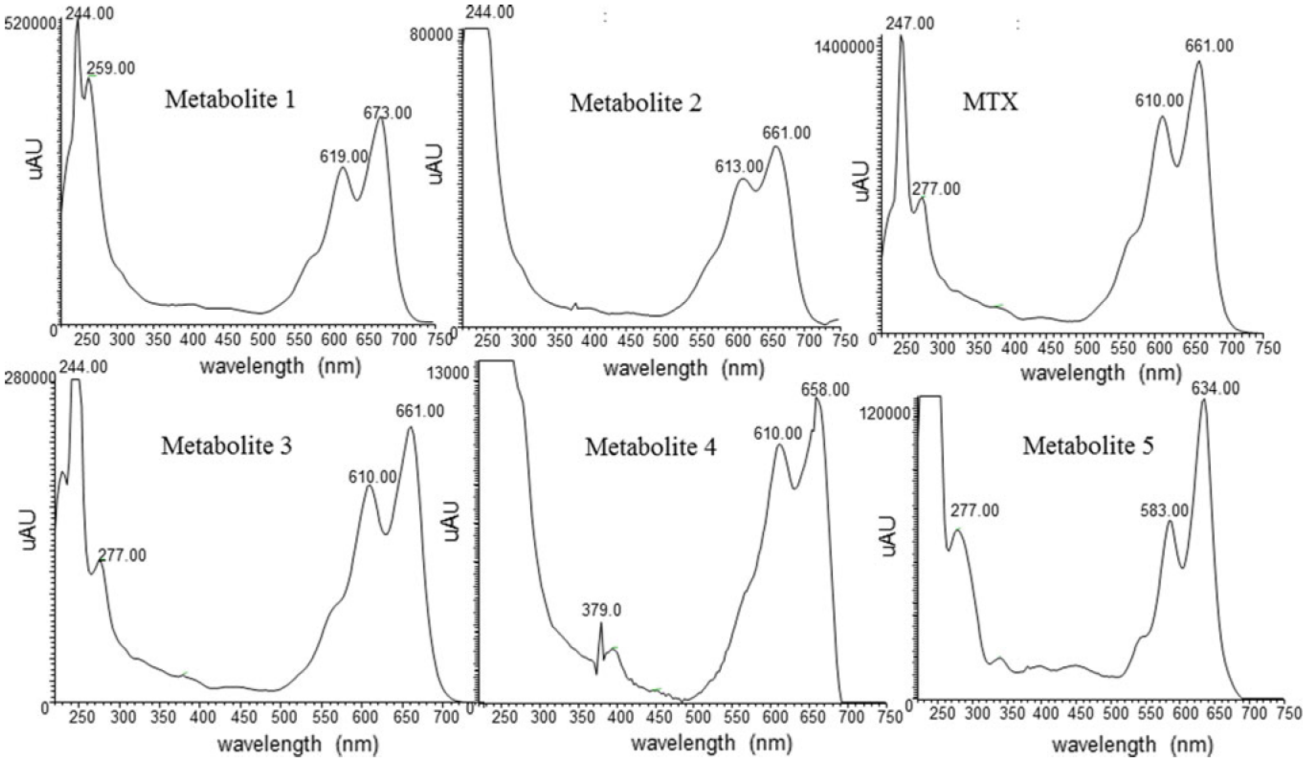

Fig. 2 UV–VIS spectral data (between 240 and 700 nm) of MTX and its metabolites after 4-h incubation with rat hepatic S9 fraction supplemented with 1 mM NADPH + 4 mM GSH. The metabolites number designations are in accordance with the chromatogram showed in Fig. 1

CH_3COO— group introduced in the original molecule of MTX (Table 1).

Metabolite 4 was found as a trace (Fig. 1), and it presents maximum absorbance at 610 and 658 nm (Fig. 2). Due to the small amount of this compound, the only information given by the mass spectrum was the parent ion ($[M + H]^+$) at m/z 455. Based on these data, we proposed for metabolite 4 the chemical structure presented on Table 1. A compound with the same molecular ion mass was previously described and associated with the oxidative metabolism of MTX (Brück and Brück 2011).

The analysis of the blank sample (containing only the supplemented S9 fraction, without the addition of MTX) revealed no relevant interferences from the matrix on the retention times of interest. Similarly, no peaks were observed at the same retention times in the sample containing only 100 µM MTX + 1 mM NADPH + 4 mM GSH (without the S9 fraction) (data not shown).

Metabolic profile of liver and heart extracts of MTX-treated male rats

The metabolic profile was determined in vivo through the evaluation of liver and heart extracts of rats that received 7.5 mg/kg of MTX 24-h before. MTX and its metabolites were extracted and concentrated as described in the "Materials and methods" section and analyzed through LC/DAD-ESI/MS. Control liver and heart extracts were also analyzed in order to determine matrix interferences. More attention was given in the search and identification of the metabolite 5 due to its known pharmacological activity (Brück and Brück 2011; Shipp et al. 1993).

In the liver extracts of the animals treated with MTX (Fig. 3a), it was possible to observe the presence of MTX, with a retention time of about 15 min, and 7 additional peaks when compared to control livers (data not shown). All the compounds identified in the chromatogram as metabolites of MTX are compounds that absorb radiation between 500 and 700 nm. At the retention time of 18.16 min, it was identified the metabolite 5 due to its UV–VIS spectrum characteristics and the MS fragmentation (data not shown). Further structural identification of the other metabolites was not possible due to the huge background presented in the analysis. The metabolites that have the retention times of 13.21 and 13.70 min possess a UV–VIS spectrum profile similar to the metabolite 1, with maximum absorbance in the visible region set at 619 and 673 nm (data not shown). The metabolite with the retention time of 14.04 min has the same absorbance peaks in the visible region of the metabolite 4, namely 610 and 658 nm (data not shown). The metabolites with the retention times of 14.62, 15.39, and 15.79 min have a UV–VIS spectrum

Table 1 Proposed chemical structure, retention times, and mass spectrum of MTX and its metabolites obtained through LC-DAD/ESI–MS after 4-h incubation of 100 μM MTX in supplemented S9 fraction

Compound	Chemical structure	Retention time (LC/MS) (min)	MS parent-ion mass [*m/z*]	MS/MS daughter ions [*m/z*]
MTX	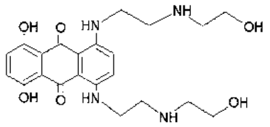	15.01	445	384 + 358
1	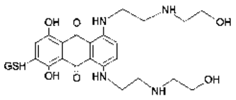	13.74	750	621 + 477
2	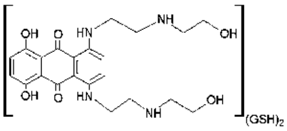	14.10	1,055	845 + 775
3	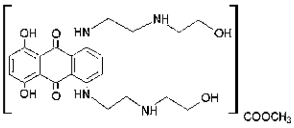	15.61	503	442 + 416
4	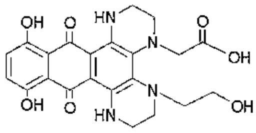	17.86	455	–
5	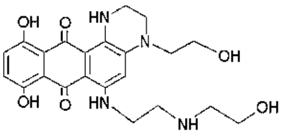	18.28	443	382 + 356

with absorbance set at 610 and 661 nm, which are the absorbance maximum peaks of metabolite 3 and MTX.

In heart extracts (Fig. 3b), it was only observed the presence of MTX (retention time about 15 min) and metabolite 5 (retention time about 18 min), in trace amounts. Both compounds were identified through analysis of their DAD spectrum properties and MS fragmentation. None of the other peaks were identified as other MTX metabolites.

The metabolites of MTX increase the toxicity in a cardiomyoblast in vitro model

The cytotoxicity of MTX and pre-incubated MTX metabolic S9 fraction was assessed in cardiomyoblast model through the reduction of MTT assay after a time period incubation of 24-h. The treatment groups result from the extracts of the previous incubations of the supplemented S9 fraction with 100 μM MTX (with the exception of the matrix group, which did not contain MTX) at time 0 (non-metabolized MTX) or 4-h (MTX and its metabolites). The presence of MTX metabolites after 4-h incubation with S9 fraction was previously confirmed by LC/DAD-ESI/MS analysis, highlighting the presence of peaks of metabolites and a reduction of 35 % of the MTX content at this time point (Fig. 1). Figure 4 presents the cytotoxicity results expressed as percent of the MTT reduction compared to control. As it can be seen, the incubation with the matrix group (S9 fraction + 1 mM NADPH + 4 mM GSH after 4-h incubation at 37 °C) did not reveal any measurable toxic effect compared to control (96 ± 2 % vs. 100 ± 1 %, respectively). The MTX group and the MTX + metabolites group showed a significantly decrease in % of MTT reduction compared to control (79 ± 2 % for the MTX group and 67 ± 2 % for the MTX + metabolites group). In the group MTX + metabolites, the cytotoxic effects were significantly more pronounced, even with 35 % less MTX, compared to MTX group, highlighting that its metabolism increases the cytotoxicity caused by MTX in the cardiomyoblast model.

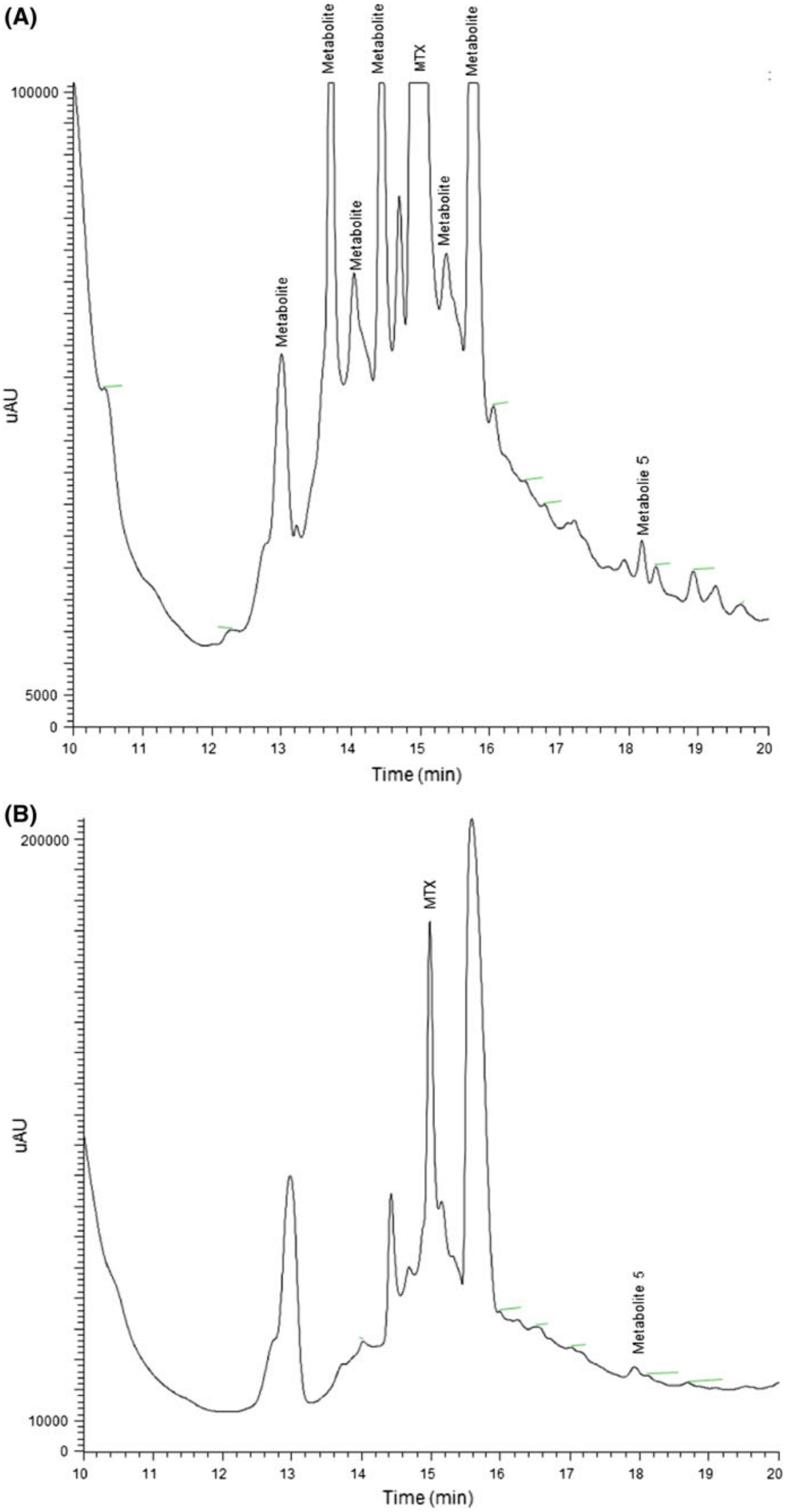

Fig. 3 LC/DAD-ESI/MS chromatograms of (**a**) liver and (**b**) heart extracts of MTX-treated rats. Male Wistar rats received 7.5 mg/kg MTX, via intraperitoneal, and they were euthanized 24-h after treatment. The livers and hearts extracts were obtained as described in the "Materials and methods" section

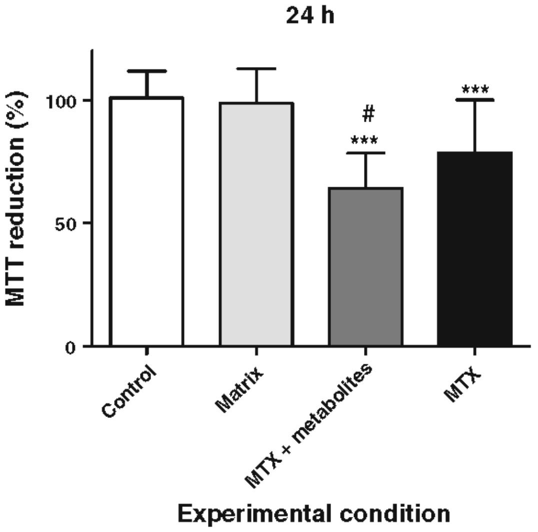

Fig. 4 Cytotoxic effects of MTX and MTX + metabolites in H9c2 cells after 24-h incubation. Results are presented as mean ± standard deviation from 18 *per* condition out of 3 independent experiments. Statistical comparisons were made using One-way ANOVA followed by the Student–Newman–Keuls post hoc test (***$p < 0.001$ vs. control; $^{\#}p < 0.05$ vs. MTX group)

MTX cytotoxicity is prevented by the co-incubation of MTX with CYP450 and CYP2E1 inhibitors

Trying to counteract the cytotoxicity of MTX, the effects of CYP450 inhibitor MTP (0.5 mM) and CYP2E1 inhibitor DAS (150 μM) were evaluated through the MTT reduction assay. MTX (100 nM and 1 μM) was co-incubated with MTP or DAS at 37 °C for 96-h. Data are presented in Fig. 5.

In the presence of MTP, the cytotoxic effects observed after MTX incubation were significantly reduced compared to those observed with MTX alone: the % of MTT reduction was 69 ± 5 % for the MTX (100 nM) group versus 81 ± 5 % for the MTX (100 nM) + MTP (0.5 mM) group and 63 ± 7 % for the MTX (1 μM) group versus 74 ± 1 % for the MTX (1 μM) + MTP (0.5 mM) group (Fig. 5a). The incubation with MTP alone or the DMSO 0.1 % group did not produce any measurable toxic effect (99 ± 5 % and 95 ± 2 %, respectively) compared to control (100 ± 4 %).

A partial reversion of the cytotoxicity of MTX using the CYP2E1 subtype inhibitor DAS (150 μM) was also observed. The co-incubation of MTX (100 nM) + DAS (150 μM) caused less toxic effects (73 ± 5 %) compared to MTX (100 nM) alone (64 ± 4 %). The same was observed in the MTX (1 μM) + DAS (150 μM) (71 ± 4) versus MTX 1 μM group (59 ± 8). The % reduction in MTT in the DAS (150 μM) group (101 ± 4 %) was similar to those observed in the control group (100 ± 6 %) (Fig. 5b).

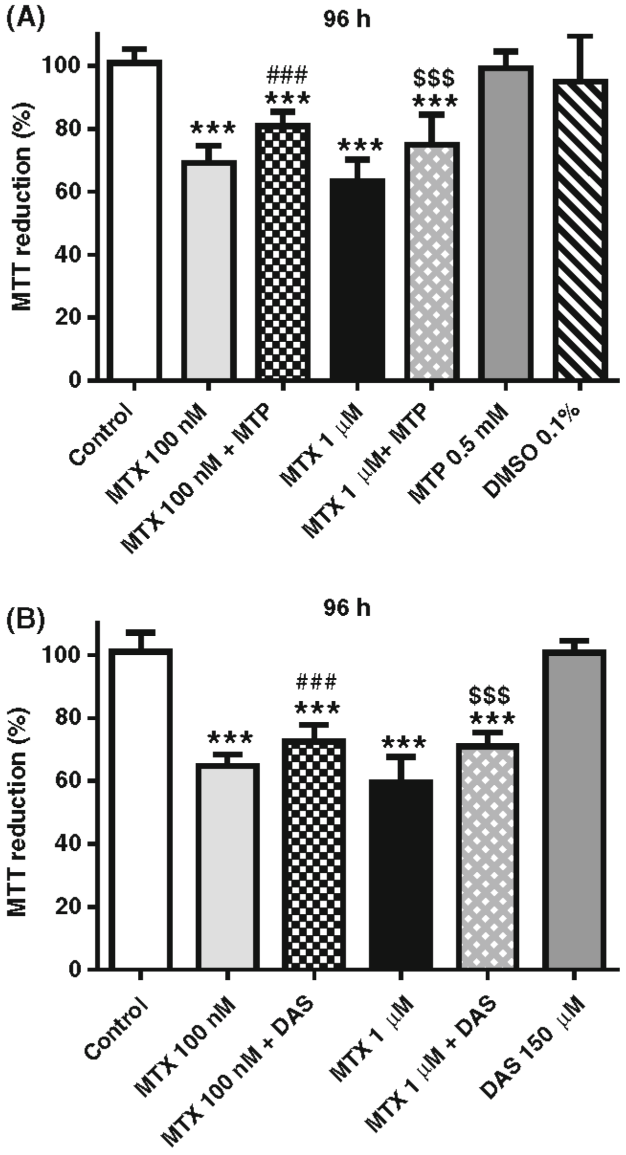

Fig. 5 Protective effects of (**a**) MTP (0.5 mM) and (**b**) DAS (150 μM) in the cytotoxic effects of MTX (100 nM and 1 μM) after 96-h co-incubation. Results are presented as means (%) ± standard deviation ($n = 18$ per condition out of 3 independent experiments). Statistical comparisons were made using One-way ANOVA test followed by the Student–Newman–Keuls post hoc test (***$p < 0.001$ vs. control; $^{\#\#\#}p < 0.001$ vs. 100 nM; $^{\$\$\$}p < 0.001$ vs. 1 μM)

Discussion

The major findings of the present work are as follows: (a) the description of the metabolic profile of MTX after incubation with the rat hepatic S9 fraction; (b) the finding that MTX and the naphtoquinoxaline metabolite are present in the extracts of hearts and livers of male Wistar rats treated with MTX 24-h before; (c) the demonstration of the increase in the MTX cytotoxicity in the presence of its metabolites toward H9c2 cells; and (d) the partial prevention of the MTX cytotoxicity with the inhibition of the CYP450 and CYP2E1 metabolism in the H9c2 cells.

To the best of our knowledge, this is the first time that the metabolism of MTX through the supplemented rat hepatic S9 fraction is presented. Using this approach, 5 MTX metabolites were identified that keep the chromophore group (Fig. 2), including the naphtoquinoxaline metabolite (metabolite 5) and a novel metabolite that was never described before (an acetoxy ester derivative, metabolite 3) (Table 1). The maintenance of the chromophore group suggests that all these metabolites possibly maintain the ability to intercalate into DNA base pairs since the tricyclic planar structure is essential for MTX activity (Hsin et al. 2008).

In order to overpass the described difficulty to stimulate MTX metabolism in vitro (Duthie and Grant 1989; Richard et al. 1991; Kostrzewa-Nowak et al. 2007) animals received, as already reported, 0.2 % phenobarbital in drinking water for 1 week prior to the S9 fraction isolation to induce its metabolic systems (Wolf et al. 1986; Novak and Kharasch 1985). The liver S9 fractions are considered one of the most representative sub-cellular metabolic in vitro systems because these fractions contain phase I and phase II enzymes (Jia and Liu 2007; Yoshihara et al. 2001; Brandon et al. 2003) and are much more illustrative of a real situation than studies using exogenously and purified added enzymes (Jia and Liu 2007; Brandon et al. 2003). Subsequent analysis of S9 obtained extracts through LC/DAD-ESI/MS presented in this work allowed an accurate separation and identification of the metabolic profile of MTX (Fig. 1; Table 1).

Studies discuss whether MTX suffers one-electron reduction or two-electron reduction (Wolf et al. 1986; Butler and Hoey 1987; Duthie and Grant 1989; Fisher and Patterson 1992). In fact, the reduction in MTX by flavin reductases is not facilitated due to its low one-electron reduction potential (Fisher and Patterson 1992). Hence, the preferential pathway of MTX metabolism is the two-electron reduction as evidenced by the prevention of the MTX bioactivation with the inhibition of cytochrome P450-mediated metabolism (Li et al. 1995; Duthie and Grant 1989; Mewes et al. 1993) that was also observed in this work (Fig. 5).

The interest in the study of the metabolism of MTX has emerged due to the discover that the naphtoquinoxaline metabolite, which herein we called metabolite 5 (Table 1), is involved in the anti-tumoral effect of MTX (Feofanov et al. 1997; Mewes et al. 1993; Panousis et al. 1997). The metabolite 5 was already described as the product of MTX metabolism through heme containing enzymes systems, CYP450, and peroxidases (Brück and Brück 2011; Blanz et al. 1991). Other studies suggest that this metabolite certainly has a significant role in the pharmacological activity of MTX (Panousis et al. 1997; Feofanov et al. 1997; Mewes et al. 1993; Shipp et al. 1993) and may be associated with MTX-induced adverse effects since it causes ATP depletion in neonatal cardiomyocytes isolated from rats (Shipp et al. 1993).

The conjugation with GSH, resulting in the metabolites 1 and 2 (Table 1), is the main detoxifying pathway of the MTX (Mewes et al. 1993). These metabolites were previously found in studies with rat hepatic microsomes or cytosol incubated with 1 mM MTX (Wolf et al. 1986) and after incubation of 60 μg/mL MTX with horseradish peroxidase supplemented with 25 mg GSH (Blanz et al. 1991). To the best of our knowledge, the metabolite 3 (Table 1) was never associated with the MTX metabolism, although it is important to refer that it is the first time that a complex enzymatic system coupled to LC/DAD-ESI/MS analysis of MTX metabolites is presented. We suggest that the acetoxy derivative can result from an *N*-oxygenation in the aromatic amine, followed by an acetylation. In fact, in primary and secondary aromatic amines, *N*-oxygenation by cytochrome P450 usually results in the formation of arylhydroxylamines, which can be converted by *N*-acetyltransferases (present in S9 fraction), functioning as *O*-acetyltransferases, to acetoxy esters (Parkinson and Ogilvie 2008).

As already stated, in our work, the metabolite 4 is present only in trace amounts (Fig. 1). Thus, it was not possible to obtain the complete MS fragmentation pattern. However, the MS parent-ion mass of this compound is set at *m/z* 455. Recently, a study with horseradish, lacto, and lignin peroxidases incubated with MTX demonstrated the presence of a metabolite with the same parental ion of metabolite 4 (Brück and Brück 2011). Thus, based on this study, it was suggested that the metabolite 4 could have the proposed structure found on Table 1, the monocarboxylic acid derivative. Mono and dicarboxylic acid MTX derivatives were already associated with rat metabolism in very low and variable levels (Blanz et al. 1991; Richard et al. 1991), which is in accordance with the trace amounts found in our experiment with rat liver S9 fraction. In contrast, they are considered the main metabolites of MTX in rabbits and humans (Blanz et al. 1991; Richard et al. 1991), highlighting the interspecies differences in the metabolic profile of MTX.

An in vivo study was also performed to demonstrate the metabolic profile of MTX and determine the metabolites in the rat liver and heart (Fig. 3). The presence of MTX and the metabolite 5 in both organs was shown. Despite this metabolite has been already described in the urine of humans and many laboratory animals (Blanz et al. 1991), to the best of our knowledge, it is the first time that the presence of the naphtoquinoxaline metabolite is described in these organs in an in vivo situation. Furthermore, in liver extracts, 7 additional metabolites were found that preserve the chromophore group. It is known that MTX is rapidly and extensively distributed in tissues (An and Morris 2010), accumulating in organs such as liver and heart (Ehninger et al. 1990). In humans, MTX was detected 35 days after a single dose of 12 mg/m^2 in liver (1,140 ng/g wet weight) and heart (716 ng/g wet weight) (Batra et al. 1986). The results presented here suggest that, as it happens with MTX, the naphtoquinoxaline metabolite also accumulates in hepatic and cardiac tissue.

In the second part of this work, the effects of the MTX bioactivation in a cardiomyoblast cellular in vitro model were studied. The cellular damage assessed through the MTT reduction assay was evaluated after 24-h incubation with the extracts of previous incubation of supplemented hepatic S9 fraction with 100 µM MTX at time 0 or 4-h (containing about 35 % less MTX than at time 0 and the metabolites presented in the Fig. 1; Table 1). As it can be seen in the Fig. 4, even with less amounts of MTX, the presence of the metabolites significantly increased the cytotoxicity when compared to the non-metabolized MTX group. A complex metabolic extract containing 5 in vitro obtained metabolites (including the metabolite 5) was used, and the results presented herein suggest the relevance of MTX metabolism for cardiac damage. The unique study correlating the bioactivation of MTX with its cardiotoxicity is in agreement with our results since it shows that the incubation of the previously synthesized and purified cyclic metabolite (39 µM) (here named as metabolite 5, Table 1) in neonatal cardiomyocytes isolated from rats caused a partial depletion of the ATP content (Shipp et al. 1993). Thus, it seems that the bioactivation of MTX can be involved in both antitumoral and cardiotoxic effects. However, the mechanisms of pharmacological and adverse effects of MTX may differ since it was already demonstrated that the iron chelator ICRF-7 elicits cardioprotective effects in isolated neonatal rat cardiomyocytes and prevents the high-dose MTX lethality on CD-1 mice without counteracting the antitumor effect in two different tumor cell lines and in an in vivo model of leukemia (Shipp et al. 1993).

This is the first time that the prevention of MTX-induced cytotoxic effects by co-incubation with CYP450 metabolism inhibitors is evidenced in a cardiomyoblast model. As shown in the Fig. 5, the inhibition of CYP450-mediated metabolism significantly decreased the cytotoxicity observed with the same concentration of MTX in the absence of the broad CYP inhibitor MTP, highlighting that the in situ metabolism of MTX may also contribute to its toxicity. Another major finding of this work is that, for the first time, it is shown that similar protective results are obtained with the co-incubation with DAS, a CYP2E1 subtype inhibitor (Fig. 5b). The heart is an organ expressing both cytochrome P450 enzymes and NADPH cytochrome reductase (Duthie and Grant 1989; Yoshihara et al. 2001). CYP2E1 is markedly abundant in heart, and we showed here that it contributes to MTX cytotoxicity. The partial protection evidenced by the CYP inhibitors may be related to the direct toxic effect of MTX or the involvement of other enzymes present in the H9c2 cells that can promote the bioactivation of MTX. There are studies showing that the use of MTP prevents the cytotoxicity of MTX, namely in MCF7 human breast cancer cells (Li et al. 1995), in human hepatoma-derived cells (Duthie and Grant 1989; Mewes et al. 1993), and rat hepatocytes (Mewes et al. 1993). Moreover, it was observed a proportional relationship between the cellular metabolic competences and the sensibility to MTX cellular damage, since rat hepatocytes are more susceptible to the cytotoxicity than hepatoma-derived cells (Mewes et al. 1993).

In summary, we presented the metabolic profile of MTX after incubation with rat hepatic S9 fraction. Five potentially MTX metabolites were presented, including the metabolite 3 that was never described before and the naphtoquinoxaline metabolite (metabolite 5). The metabolite 5 is considered the main bioactive product of MTX metabolism (Mewes et al. 1993; Panousis et al. 1997). We showed for the first time that this metabolite can be found in rat liver and heart, prolonging the exposure period of cardiac and hepatic cells to this bioactive compound. As demonstrated in vitro, the presence of MTX metabolites enhances the toxicity in a cardiomyoblast model. Furthermore, it was proved that the bioactivation of MTX mediated through CYP450 and namely CYP2E1 metabolism that occurs in loco in the cardiomyoblasts exerts a significant role in the cellular damage promoted by MTX. Thus, these results suggest that besides the relevance of MTX metabolism to its pharmacological action, the biotransformation fate of MTX might also be involved in its cardiotoxicity.

Acknowledgments Authors are grateful to Dr. Zelia dos Santos Azevedo, from Faculty of Sciences, University of Porto, for gently lend us the LC/DAD-ESI/MS and for all precious technical assistance. This work was supported by the Fundação para a Ciência e Tecnologia (FCT)—project [EXPL/DTP-FTO/0290/2012]—QREN initiative with EU/FEDER financing through COMPETE—Operational Programme for Competitiveness Factors. LGR and VMC thank FCT for their Ph.D. grant (SFRH/BD/63473/2009) and Post-doc grant (SFRH/BPD/63746/2009), respectively. The authors are also grateful to Fundação para a Ciência e a Tecnologia (FCT) for Grant No. PEst-C/EQB/LA0006/2011

References

An G, Morris ME (2010) HPLC analysis of mitoxantrone in mouse plasma and tissues: application in a pharmacokinetic study. J Pharm Biomed Anal 51(3):750–753

Avasarala JR et al (2003) Rapid onset mitoxantrone-induced cardiotoxicity in secondary progressive multiple sclerosis. Mult Scler 9:59–62

Basra J et al (1985) Evidence for human liver mediated-free radical formation by doxorubicin and mitozantrone. Anticancer Drug Des 1:45–52

Batra VK et al (1986) Pharmacokinetics of mitoxantrone in man and laboratory animals. Drug Metab Rev 17:311–329

Blanz J et al (1991) Evidence for oxidative activation of mitoxantrone in human, pig, and rat. Drug Metab Dispos 19(5):871–880

Brandon EF et al (2003) An update on in vitro test methods in human hepatic drug biotransformation research: pros and cons. Toxicol Appl Pharmacol 189(3):233–246

Brück TB, Brück DW (2011) Oxidative metabolism of the anti-cancer agent mitoxantrone by horseradish, lacto-and lignin peroxidase. Biochimie 93(2):217–226

Butler J, Hoey BM (1987) Are reduced quinones necessarily involved in the antitumour activity of quinone drugs? Br J Cancer 8:53–59

Canal P et al (1993) Plasma and cellular pharmacokinetics of mitoxantrone in high-dose chemotherapeutic regimen for refractory lymphomas. Cancer Res 53(20):4850–4854

Duthie SJ, Grant MH (1989) The role of reductive and oxidative metabolism in the toxicity of mitoxantrone, adriamycin and menadione in human liver derived Hep G2 hepatoma cells. Br J Cancer 60(4):566–571

Ehninger G et al (1990) Pharmacokinetics and metabolism of mitoxantrone. A review. Clin Pharmacokinet 18(5):365–380

Feofanov A et al (1997) Quantitative confocal spectral imaging analysis of mitoxantrone within living K562 cells: intracellular accumulation and distribution of monomers, aggregates, naphtoquinoxaline metabolite, and drug-target complexes. Biophys J 73(6):3328–3336

Fisher GR, Patterson LH (1992) Lack of involvement of reactive oxygen in the cytotoxicity of mitoxantrone, CI941 and ametantrone in MCF-7 cells: comparison with doxorubicin. Cancer Chemother Pharmacol 30(6):451–458

Fisher G, Patterson LH, Gutierrez PL (1993) A comparison of free radical formation by quinone anti-tumour agents in MCF-7 cells and the role of NAD(P)H (quinone-acceptor) oxidoreductase (DT-diaphorase). Chem Biol Interact 88:137–153

Hsin L-W et al (2008) Synthesis, DNA binding, and cytotoxicity of 1,4-bis(2-amino-ethylamino)anthraquinone-amino acid conjugates. Bioorg Med Chem 16(2):1006–1014

Jia L, Liu X (2007) The conduct of drug metabolism studies considered good practice (II): in vitro experiments. Curr Drug Metab 8(8):822–829

Khan SN et al (2010) Effect of mitoxantrone on proliferation dynamics and cell cycle progression. Biosci Rep 30(6):375–381

Kostrzewa-Nowak D et al (2007) Bioreductive activation of mitoxantrone by NADPH cytochrome P-450 reductase. Implications for increasing its ability to inhibit the growth of sensitive and multidrug resistant leukaemia HL60 cells. Cancer Lett 245(1–2): 252–262

Li SJ, Rodgers EH, Grant MH (1995) The activity of xenobiotic enzymes and the cytotoxicity of mitoxantrone in MCF 7 human breast cancer cells treated with inducing agents. Chem Biol Interact 97(2):101–118

Lowry OH, Rosebrough NJ, Farr AL, Randall RJ (1951) Protein measurement with the folin phenol reagent, J Biol Chem (193): 265–272

Mewes K et al (1993) Cytochrome P-450-induced cytotoxicity of mitoxantrone by formation of electrophilic intermediates. Cancer Res 53(21):5135–5142

Neuhaus O, Kieseier BC, Hartung H-P (2006) Therapeutic role of mitoxantrone in multiple sclerosis. Pharmacol Ther 109(1–2): 198–209

Novak RF, Kharasch ED (1985) Mitoxantrone: propensity for free radical formation and lipid peroxidation-implications for cardiotoxicity. Invest New Drugs 3(2):95–99

Panousis C, Kettle AJ, Phillips DR (1997) Neutrophil-mediated activation of mitoxantrone to metabolites which form adducts with DNA. Cancer Lett 113(1–2):173–178

Parkinson A, Ogilvie B (2008) Biotransformation of xenobiotics. In: Klaassen C (ed) Casarett & Doull's toxicology: the basic science of poisons. McGraw-Hill, New York, p 1331

Pontes H et al (2010) Metabolic interactions between ethanol and MDMA in primary cultured rat hepatocytes. Toxicology 270(2–3):150–157

Richard B et al (1991) Interspecies variability in mitoxantrone metabolism using primary cultures of hepatocytes isolated from rat, rabbit and humans. Biochem Pharmacol 41(2):255–262

Rossato LG et al (2011) Structural isomerization of synephrine influences its uptake and ensuing glutathione depletion in rat-isolated cardiomyocytes. Arch Toxicol 85(8):929–939

Sardão V et al (2009a) Doxorubicin-induced mitochondrial dysfunction is secondary to nuclear p53 activation in H9c2 cardiomyoblasts. Cancer Chemother Pharmacol 64(4):811–827

Sardão V et al (2009b) Morphological alterations induced by doxorubicin on H9c2 myoblasts: nuclear, mitochondrial, and cytoskeletal targets. Cell Biol Toxicol 25(3):227–243

Seiter K (2005) Toxicity of the topoisomerase II inhibitors. Expert Opin Drug Saf 4(2):219–234

Shipp NG et al (1993) Characterization of experimental mitoxantrone cardiotoxicity and its partial inhibition by ICRF-187 in cultured neonatal rat heart cells. Cancer Res 53(3):550–556

Silva R et al (2011) In vitro study of P-glycoprotein induction as an antidotal pathway to prevent cytotoxicity in Caco-2 cells. Arch Toxicol 85(4):315–326

Wolf CR, Macpherson JS, Smyth JF (1986) Evidence for the metabolism of mitozantrone by microsomal glutathione transferases and 3-methylcholanthrene-inducible glucuronosyl transferases. Biochem Pharmacol 35(9):1577–1581

Yoshihara S et al (2001) Metabolic activation of bisphenol A by rat liver S9 fraction. Toxicol Sci 62(2):221–227

Zordoky BNM, El-Kadi AOS (2007) H9c2 cell line is a valuable in vitro model to study the drug metabolizing enzymes in the heart. J Pharmacol Toxicol Methods 56(3):317–322

Manuscript II

Therapeutic concentrations of mitoxantrone elicit energetic imbalance in H9c2 cells as an earlier event.

Rossato, L. G., Costa, V. M., Villas-Boas, V., Bastos, M.L., Rolo, A., Palmeira, C., Remião, F.

Cardiovasc Toxicol 2013 *In Press.* DOI: 10.1007/s12012-013-9224-0

Cardiovasc Toxicol
DOI 10.1007/s12012-013-9224-0

Therapeutic Concentrations of Mitoxantrone Elicit Energetic Imbalance in H9c2 Cells as an Earlier Event

Luciana Grazziotin Rossato · Vera Marisa Costa · Vânia Vilas-Boas · Maria de Lourdes Bastos · Anabela Rolo · Carlos Palmeira · Fernando Remião

© Springer Science+Business Media New York 2013

Abstract Mitoxantrone (MTX) is a chemotherapeutic agent that emerged as an alternative to anthracycline therapy. However, MTX also causes late cardiotoxicity, being oxidative stress and mitochondrial-impaired function proposed as possible mechanisms. This work aimed to investigate the relevance of these mechanisms to the MTX toxicity in H9c2 cells, using therapeutic concentrations. The observed cytotoxicity of MTX was time and concentration dependent in both lactate dehydrogenase leakage assay and MTT reduction assay. Two therapeutic concentrations (100 nM and 1 μM) and three time points were selected (24, 48, and 96 h) for further studies. Both MTX concentrations caused a significant increase in caspase-3 activity, which was not prevented by inhibiting MTX CYP450-metabolism. Significant decreases were observed in the total and reduced glutathione levels only in MTX 100 nM at 96 h; however, neither alterations in oxidized glutathione nor increases in the malondialdehyde levels were observed at any time or concentrations tested. On the other hand, changes in the intracellular ATP levels, mitochondrial membrane potential, and intracellular calcium levels were observed in both concentrations and all time tested. Noteworthy, decreased levels of ATP-synthase expression and activity and increases in the reactive species generation were observed at 96 h in both working concentrations. However, the radical scavenger *N*-acetylcysteine or the mitochondrial function enhancer *L*-carnitine did not prevent MTX cytotoxicity. Thus, this work evidenced the early MTX-induced energetic crisis as a possible key factor in the cell injury.

Keywords Mitoxantrone · Cardiotoxicity · Energetic failure · Oxidative stress · Energetic imbalance

Abbreviations

DCFH-DA	Dichlorodihydrofluorescein diacetate
DHR	Dihydrorhodamine 123
DMEM	Dulbecco's modified eagle's medium
DMSO	Dimethyl sulfoxide
DTNB	5,5-Dithio-bis(2-nitrobenzoic) acid
FBS	Fetal bovine serum
FI	Fluorescence intensity
GSH	Reduced glutathione
GSHt	Total glutathione
i.p	Intraperitoneal
GSSG	Oxidized glutathione
LDH	Lactate dehydrogenase
MTT	3-(4,5-Dimethylthiazol-2-yl)-2,5-diphenyltetrazolium bromide
MTX	Mitoxantrone
NAC	*N*-acetylcysteine
β-NADH	Reduced β-nicotinamide adenine dinucleotide
Pi	Inorganic phosphate
SD	Standard deviation
TBA	Thiobarbituric acid
TMRM	Tetramethylrhodamine

L. G. Rossato (✉) · V. M. Costa · V. Vilas-Boas ·
M. de Lourdes Bastos · F. Remião (✉)
REQUIMTE, Laboratório de Toxicologia, Departamento de Ciências Biológicas, Faculdade de Farmácia, Universidade do Porto, Rua Jorge Viterbo Ferreira, 228, 4050-313 Porto, Portugal
e-mail: luciana.g.rossato@gmail.com

F. Remião
e-mail: remiao@ff.up.pt

A. Rolo · C. Palmeira
Departamento de Ciências da Vida, Centro de Neurociências e Biologia Celular de Coimbra, Universidade de Coimbra, Coimbra, Portugal

Published online: 18 September 2013

Introduction

Mitoxantrone (MTX) is an anthracenedione chemotherapeutic agent used in the treatment of solid tumors, such as breast and prostate cancer, and hematological malignances, namely acute leukemia and lymphoma [1]. Due to its immunosuppressive properties, MTX has been also employed in the treatment of multiple sclerosis [2]. MTX acts as an intercalating agent being a powerful inhibitor of DNA and RNA synthesis, and affects the cell cycle at various stages [3]. Moreover, MTX is an inhibitor of topoisomerase II [1], and, recently, the MTX potential epigenetic effects were demonstrated given its high affinity to bind to histone H1 and core histones in vitro [4].

Due to their similar chemical structure and anticancer mechanisms, MTX was considered an alternative to anthracycline chemotherapy with the advantage of allowing the administration of lower relative doses than doxorubicin [5]. However, it became evident after its clinical use that MTX also promoted late irreversible cardiotoxicity in up to 18 % of treated patients, which sometimes is clinically diagnosed several years after treatment [1]. Furthermore, this risk is increased with higher cumulative doses [1]. MTX is extensively distributed and accumulates in heart tissue. In fact, MTX is still detected in the human heart (716 ng/g wet weight) 35 days after a single dose (12 mg/m^2) [6], showing that cardiac cells maintain a prolonged contact after MTX administration.

The observed heart failure promoted by MTX is clinically similar to that caused by doxorubicin [1]; however, mechanistic studies of MTX-induced cardiotoxicity are scarce on the available literature. The cardiac side effects promoted by doxorubicin have been extensively related to oxidative stress [7] and to mitochondrial-impaired function [8]. Studies demonstrated that the oxidoreductive metabolism of MTX produces reactive intermediates [9, 10] and that MTX shows particular effectiveness against tumors expressing high content of heme-peroxidases [11], suggesting the involvement of reactive species in its successful antitumor action. Additionally, its cytotoxicity has already been prevented by the inhibition of CYP450-mediated metabolism in human hepatoma-derived cell line [10, 12], in isolated adult rat hepatocytes [12], and in MCF-7 human breast cancer cells [13]. In fact, recently, our research group highlighted that the bioactivation of MTX may also be involved in its undesirable cardiac side effects since the cytotoxicity of MTX was partially prevented in a cardiomyoblast H9c2 cell model by inhibiting CYP450- and CYP2E1-mediated metabolism [14].

Energetic imbalance was suggested to be a consequence of MTX treatment. In cultured neonatal rat heart cells, the 3 h incubation with MTX (about 0.1–10 μM) caused a concentration-dependent decline in the ATP levels after 72 h [15]. Mitochondrial swelling was observed after electron and light microscopy in hearts excised from female BALB/c mice killed 1 week after treatment with MTX (0.2 mg/kg), intraperitoneal (i.p.), weekly, for 12-week [5]. Furthermore, cardiac mitochondria isolated from rats treated with MTX (1 mg/kg i.p.), twice a week, for 4 weeks, showed a reduction in the electron transfer and the respiratory chain activity and uncoupling of oxidative phosphorylation [16]. In spite of these 3 studies, the mitochondrial role on MTX-induced cardiotoxicity and the mechanisms involved are still poorly understood due to the lack of focused studies on their functionality while facing MTX.

This work aimed to evaluate the mechanisms involved in the MTX cardiotoxicity using the H9c2 cells as cellular model exposed to therapeutic concentrations of this drug. H9c2 is a cell line derived from rat heart, that is considered a valuable model to assess in vitro cardiotoxicity [17], specially due to its metabolic features, which are comparable to those found in rat heart [18]. The work used this in vitro model to evaluate several mitochondrial and mitochondrial-related pathways, namely ATP levels, mitochondrial membrane potential, or ATP-synthase activity or expression. Other cellular components, which could be related to mitochondrial functionality, namely calcium levels, formazan metabolization, reactive species generation, or glutathione levels were also evaluated. The use of a CYP450 inhibitor (metyrapone), a CYP2E1 inhibitor (diallyl sulfide), a reactive species scavenger (*N*-acetylcysteine [NAC]), and a mitochondrial function enhancer (*L*-carnitine) was also performed to evaluate the role of the respective pathways in MTX cytotoxicity.

Methods

Chemicals

All chemicals and reagents were of analytical grade or of the highest grade available. MTX hydrochloride, NAC, *L*-carnitine, reduced glutathione (GSH), oxidized glutathione (GSSG), glutathione reductase (GR, EC 1.6.4.2), 2-vinylpyridine, reduced β-nicotinamide adenine dinucleotide (β-NADH), 3-(4,5-dimethylthiazol-2-yl)-2,5-diphenyltetrazolium bromide (MTT), 5,5-dithio-bis(2-nitrobenzoic) acid (DTNB), the caspase-3 substrate (*N*-Acetyl-Asp-Glu-Val-Asp *p*-nitroanilide), dihydrorhodamine 123 (DHR), luciferin, luciferase, thiobarbituric acid (TBA), protease inhibitors cocktail, anti-goat actin monoclonal antibody, and anti-rabbit ATP-synthase polyclonal antibody were obtained from Sigma-Aldrich (St. Louis, MO). Dichlorodihydrofluorescein diacetate (DCFH-DA), tetramethylrhodamine (TMRM), and Fluo-3 AM were obtained from Molecular Probes (Eugene, OR). Dimethyl sulfoxide (DMSO) and perchloric acid ($HClO_4$) were obtained from Merck (Darmstadt, Germany). The nitrocellulose membranes (Hybond ECL), ECL chemiluminescence detection reagents, the anti-rabbit and anti-goat IgG peroxidase secondary antibody were obtained from GE Healthcare (Buckinghamshine, UK). Flow cytometry reagents (BD Facs-Flow^{TM} and Facs-Clean^{TM}) were purchased from Becton, Dickinson, and Company (São Jose, CA). Bio-Rad DC protein assay kit was purchased from Bio-Rad laboratories (Hercules, CA).

Dulbecco's modified eagle's medium (DMEM) with 4,500 mg/L glucose and GlutaMAX^{TM}, fetal bovine serum (FBS), trypsin (0.25 %)–EDTA (1 mM), and antibiotic (10,000 U/ml penicillin, 10,000 g/ml streptomycin) were obtained from Gibco Laboratories (Lenexa, KS).

H9c2 Cell Culture

The H9c2 cell line was a generous gift from Dr. Vilma Sardão, Center for Neurosciences and Cellular Biology, University of Coimbra, Portugal. Cells were cultured in DMEM supplemented with 10 % FBS, 100 U/ml of penicillin, and 100 U/ml of streptomycin in 75 cm^2 tissue culture flasks at 37 °C in a humidified 5 % CO_2-95 % air atmosphere. Cells were fed every 2–3 days, and sub-cultured once they reached 70–80 % confluence. After seeding, cells were allowed to grow for 2 days, and then, the medium was replaced to start the treatments.

Cytotoxicity Assays

Cells were seeded at a density of 35,000 cells/ml in 48-well plates (final volume of 250 μl; about 8,000 cells/cm^2), as previously described [14]. Concentration–response and time–response curves of MTX were performed using incubation times of 24, 48, 72, and 96 h with MTX concentration range of 10 nM to 100 μM (10, 100 nM, 1, 5, 10, 50, and 100 μM). Cellular damage was quantitatively assessed through the measurement of LDH release [19] and also through the MTT reduction assay [14], as previously described. For the following experiments, MTX working concentrations selected were 100 nM and 1 μM based on cytotoxicity test results.

Studies were also performed by co-incubating for 96 h MTX with potential protective agents, the reactive species scavenger and GSH precursor NAC (1 mM) [20], and the energetic function enhancer *L*-carnitine (1 mM) [21].

Caspase-3 Activity Assay

Caspase-3 activity was determined in H9c2 cells after 100 nM or 1 μM MTX incubation. The incubation period was defined after pilot studies at 6, 24, and 96 h incubation period and chosen to be 24 h. The CYP450 inhibitor metyrapone (0.5 mM) and the CYP2E1 inhibitor diallyl sulfide (150 μM) were used as possible counteracting agents to the activation of caspase-3 caused by MTX [14]. Cells were seeded at a density of 35,000 cells/ml in 6-well plates (final volume of 2.5 ml, about 9,000 cells/cm^2) and allowed to grow for 2 days. The medium was replaced and cells were incubated with MTX (100 nM or 1 μM), in the presence or absence of each metabolism inhibitor, 2 wells per condition. After 24 h incubation, cells were detached and collected to tubes (2 wells for one tube). Cells were centrifuged at 210×*g* for 5 min, at 4 °C, and the supernatant was discarded. One hundred and fifty microliters of lysis buffer (50 mM HEPES, 0.1 mM EDTA, 0.1 % CHAPS, 1 mM DTT) was added to the pellets. After complete lysis, samples were centrifuged at 16,000×*g*, for 10 min, at 4 °C. The supernatant, which contains the cytoplasmatic fraction, was collected to another tube. All steps were performed on ice. Caspase-3 activity was determined at 405 nm in a multi-well plate reader (BioTech Instruments, Vermont, US) as previously described [19].

The protein content in the cell lysate was quantified using the Bio-Rad DC protein assay kit as described by the manufacturer, and albumin solutions were used as standards.

Evaluation of Oxidative Stress

Evaluation of Reactive Species Generation

Cells were seeded at a density of 35,000 cells/ml in 48-well plates (final volume of 250 μl, about 8,000 cells/cm^2) and allowed to grow for 2 days.

In order to assess the early reactive species generation, the medium was replaced and cells were incubated with two different probes, DHR (final concentration 100 μM) [19] or DCFH-DA (final concentration 10 μM) as previously described [22], for 30 min at 37 °C and in the dark. After washing cells twice with phosphate-buffered saline in order to remove non-internalized probes, the new medium was placed and cells were incubated with MTX (100 nM and 1 μM). H_2O_2 (150 μM) was used as a positive control for the probes [22]. Cells were kept in the dark at 37 °C. The detection and quantification of intracellular reactive species was performed using a fluorescence plate reader (baseline 485 nm excitation, 528 nm emission), every hour, until 10 h incubation.

In order to evaluate the late generation of reactive species, cells were first incubated with MTX (100 nM and 1 μM). After 96 h incubation at 37 °C, the medium was replaced and cells were incubated with DCFH-DA (10 μM), for 30 min, at 37 °C, in the dark. At the end of incubation period, the medium was replaced and the detection was performed as described above.

Measurement of Intracellular Total Glutathione (GSHt), GSH, and GSSG Levels

Cells were seeded at a density of 35,000 cells/ml in 55 cm^2 Petri dishes (final volume of 12.5 ml, about 8,000 cell/cm^2). After growing for 2 days, the medium was replaced and MTX (100 nM and 1 μM) was added. After a 24, 48, and 96 h incubation period, the intracellular levels of GSHt and GSSG in the H9c2 cells were evaluated by the DTNB-GSSG reductase recycling assay, as previously described [20].

The protein content was assayed by the Lowry method, using albumin solutions as standards, as previously described [20]. GSHt, GSH, and GSSG contents were normalized to total protein content, and the final results were expressed as nmol of GSH or GSSG per mg of protein.

Evaluation of Lipid Peroxidation

Cells were seeded at a density of 35,000 cells/ml in 6-well plates (final volume of 2.5 ml, about 9,000 cells/cm^2). After growing for 2 days, the medium was replaced for fresh medium and MTX (100 nM and 1 μM) was added. Each condition (control, MTX 100 nM, or MTX 1 μM) was performed in duplicate. After 24, 48, or 96 h incubation at 37 °C, the medium was removed and cells of two wells were collected with phosphate-buffered saline, pH = 7.4, on ice to the same centrifuge tube. Cells were centrifuged (210×*g*, 5 min, 4 °C) and the supernatant was removed. The obtained pellet of cells was lysed with 100 μl of 5 % $HClO_4$, homogenized, and centrifuged (16,000×*g*, 10 min, 4 °C). Lipid peroxidation was assessed by measuring malondialdehyde in the supernatant fraction through a HPLC/UV method previously described [23], with some adaptations. The pellet was dissolved in 100 μl NaOH 0.3 M, and the protein levels were determined by Lowry method, using albumin solutions as standards.

The HPLC analysis was carried out on a system consisting of a Gilson equipped with UV–VIS detection ($\lambda = 532$ nm). Chromatographic separation was achieved using a Waters C18 Spherisorb 5 μM ODS2 4.6 × 250 mm column. The mobile phase consisted in 50 mM ammonium acetate (pH = 5.5): methanol (1:1) + 0.1 % triethylamine. The flow rate was maintained isocratically at 0.6 ml/min, and the total run time was 8 min.

Evaluation of the Energetic Function

Measurement of Intracellular ATP Levels

Cells were seeded and allowed to grow following the same protocol used for the measurement of glutathione levels. Conversely, the cells were scrapped and treated with the same protocol described for the evaluation of glutathione levels (detailed above). ATP intracellular levels were measured as previously described [24].

Evaluation of the ATP-synthase Expression

For the in vitro assessment of the ATP-synthase expression, cells were seeded at a density of 35,000 cells/ml in Petri dishes (final volume of 12.5 ml, about 8,000 cell/cm^2). After growing for 2 days, the medium was replaced and MTX (100 nM and 1 μM) was added. After the incubation periods of 24, 48, and 96 h at 37 °C, cells were collected with phosphate-buffered saline, pH = 7.4, and centrifuged (210×*g*, 5 min, 4 °C). The supernatant was discarded and the pellet was lysed with RIPA buffer [50 mMTris-HCl, 150 Mm NaCl, 1 % Igepal CA 630 (v/v), 0.5 % sodium deoxycholate (w/v), and 0.1 % SDS (w/v), pH = 7.4] supplemented with protease inhibitors cocktail. The ATP-synthase expression was evaluated through western immunoblot. Equal amounts of protein (quantified using the Bio-Rad DC protein assay kit) were loaded and electrophoresed on 10 % SDS–polyacrylamide gel and transferred to polyvinylidenedifluoride membrane. Membranes were blocked with 5 % non-fat milk and incubated with the ATP-synthase antibody (1:500), overnight at 4 °C. Actin (1:500) was used as loading control. The bands obtained through western blot were quantified with QuantityOne® software (Bio-Rad).

Evaluation of the ATP-synthase Activity

The activity of ATP-synthase was indirectly determined by analysis of the inorganic phosphate (Pi) released from ATP hydrolysis. Cells were seeded at a density of 35,000 cells/ml in Petri dishes (final volume of 12.5 ml, about 8,000 cell/cm^2). Cells were allowed to grow for 2 days, the medium was replaced, and MTX (100 nM and 1 μM) was added. Cells were incubated for 96 h at 37 °C.

After the incubation period, cells were scrapped and treated with the same protocol described for the evaluation of ATP-synthase expression (detailed above). The ATP-synthase activity was determined in the cell lysate using 0.75 mg protein (quantified using the Bio-Rad DC protein assay kit). The cell lysates were incubated with 2 ml reaction medium (125 mM sucrose, 65 mM KCl, 2.5 mM $MgCl_2$, 50 mM HEPES, pH 7.4), at 37 °C. Each condition (control, MTX 100 nM or MTX 1 μM) was performed in two independent tubes, one of them in the presence of 2 μl of 1 mg/ml oligomycin (inhibitor of mitochondrial ATP-synthase). The reaction was started with the addition of 50 μl of 100 mM ATP and was stopped with the addition of 1 ml 40 % trichloroacetic acid. Then, 1 ml of the product of this reaction was incubated with 2 ml of freshly prepared ammonium molybdate reagent containing ferrous sulfate and 2 ml distilled water, for 5 min. ATP-synthase activity is quantified subtracting the difference between the Pi released by ATP hydrolysis in the presence and absence of oligomycin. A standard curve of Pi was performed using KH_2PO_4. The absorbance of the reaction was measured at 665 nm, and the results were expressed as nmol Pi/mg/min.

Flow Cytometry Analysis

Intracellular calcium and the evaluation of the mitochondrial membrane potential were determined through flow cytometry using the Fluo-3 AM and TMRM fluorescent probes, respectively. Cells were seeded at a density of 35,000 cells/ml in 6-well plates (final volume of 2.5 ml, about 9,000 cells/cm^2). After growing for 2 days, the medium was replaced and MTX (100 nM and 1 µM) was added (3 wells per condition).

Fluorescence measurements of the cell suspensions were taken with a flow cytometer (FACSCalibur, Becton Dickinson Biosciences) equipped with a 488-nm argon ions laser. The green fluorescence of Fluo-3 AM was measured through a 530-nm band-pass filter (FL1), and the red fluorescence of TMRM was measured through a 575-nm band-pass filter (FL2). Acquisition data for 15,000 cells were gated to include only viable cells based on their forward and side light scatters and the propidium iodide (5 µg/ml) incorporation. Logarithmic fluorescence was recorded and analyzed by the BDIS CellQuest Pro software (Becton Dickinson Biosciences). Non-labeled cells (with or without MTX) were analyzed in FL1 and FL2 in order to detect a possible contribution from cells autofluorescence to the analyzed fluorescence signals. Results were presented as mean fluorescence intensity (FI).

Assessment of the Mitochondrial Membrane Potential

After 24, 48, and 96 h incubation, the medium was removed and cells were washed with phosphate-buffered saline, pH 7.4, and tripsinized with 0.25 % trypsin/1 mM EDTA in order to obtain a cell suspension. Cells were centrifuged (250×*g,* 5 min), the supernatant was discarded, and cells were suspended in 50 µl culture medium containing 20 nM TMRM [25]. Cells were incubated for 30 min, at 37 °C, in the dark. After that, cells were washed twice with phosphate-buffered saline, pH 7.4, centrifuged (210×*g*, 5 min), and kept on ice until flow cytometry analysis.

Assessment of the Intracellular Calcium Levels

The collection and preparation of the cells was done as in the assessment of the mitochondrial membrane potential (see above). The assessment of the intracellular calcium levels was performed as previously described [26].

Statistical Analysis

Results are presented as means ± the standard deviation (SD) from independent experiments. Statistical comparisons between groups were performed with one-way ANOVA (in case of normal distribution) or Kruskal–Wallis test (one-way ANOVA on ranks—in case distribution is not normal). Significance was accepted at p values <0.05. Details of statistical analysis are found in the legend of the figures.

Results

Low Concentrations of MTX Elicit Cytotoxic Effects in a Time- and Concentration-Dependent Manner

The cytotoxicity of MTX was demonstrated at different concentrations and time points, through the decline in the cell viability observed in the LDH leakage assay (Fig. 1) and through the decrease in the MTT reduction activity (Fig. 2). The cytotoxic effects observed in these two assays were dependent on MTX concentration and time of incubation, as shown in the Figs. 1 and 2 (time–response and concentration–response curves).

The decrease in the cell viability in observed the LDH leakage assay is related to cell rupture, and results are shown in the Fig. 1. After 24 h incubation, the lower concentrations tested (10 nM, 100 nM, and 1 µM) did not cause significant decreases in the cell viability compared to control. However, the 24 h incubation with 5 and 10 µM MTX caused a significant decrease in cellular integrity, which was more notorious for the highest concentrations tested, namely 50 and 100 µM MTX. After 48 h, only the incubation with 10 nM MTX did not decrease cell viability compared to control cells. The 48 h incubation with 100 nM, 1, 5, 10, 50, and 100 µM caused significant decreases in cell viability. After 72 h incubation, the cytotoxicity observed with the 10, 100 nM, and 1 µM MTX remained similar to the control values. The 72 h incubation with the other concentrations (5, 10, 50, and 100 µM) caused significant decreases in the cell viability. The cytotoxicity of MTX was even more evident in the longest incubation period (96 h). Ten nM MTX did not change cell viability compared to control; however, slight decreases were observed with the incubation with 100 nM and 1 µM MTX, and dramatic effects were observed with the higher concentrations of 5, 10, and 50 µM.

The reduction of MTT leads to the formation of formazan crystals, mostly by the action of mitochondrial

Fig. 1 Effect of different concentrations of MTX on the H9c2 viability after 24 h (**a**), 48 h (**b**), 72 h (**c**), and 96 h (**d**) of incubation at 37 °C evaluated by the LDH leakage assay. Results are presented as means (%) ± SD ($n = 24$ per condition out of 4 independent experiments) (***$p < 0.001$ vs. Control). Statistical comparisons were made using one-way ANOVA test followed by the Bonferroni post hoc test

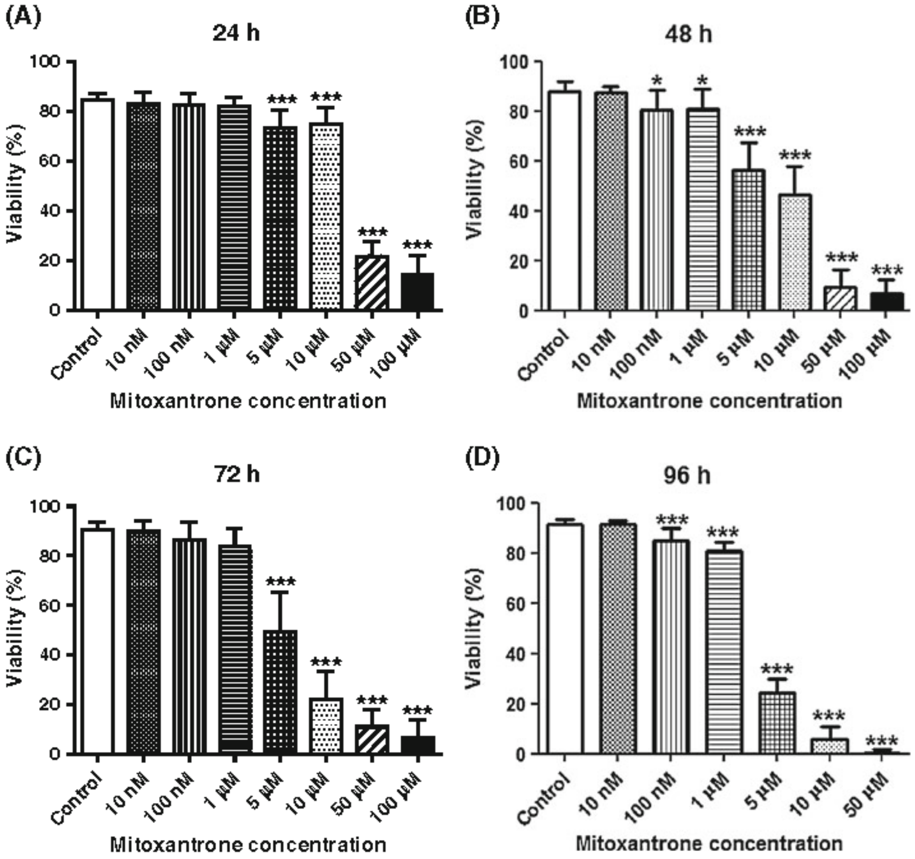

Fig. 2 Effect of different concentrations of MTX after 24 h (**a**), 48 h (**b**), 72 h (**c**), and 96 h (**d**) incubation at 37 °C with H9c2 cells evaluated by the MTT reduction activity assay. Results are presented as means (%) ± SD ($n = 18$ per condition out of 3 independent experiments). Statistical comparisons were made using one-way ANOVA test (***$p < 0.001$ vs. Control) followed by the Bonferroni post hoc test

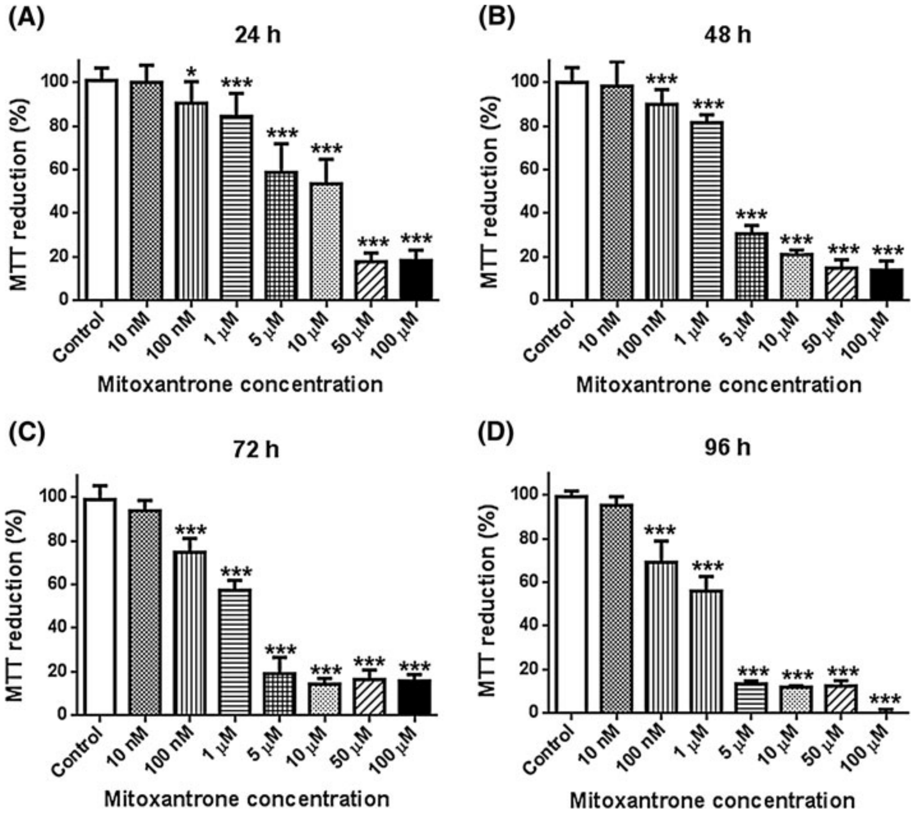

dehydrogenases, thereby can be used as a mitochondrial viability index. After 24 h, the %MTT reduction observed in the 10 nM MTX incubation was similar to control values. The incubation with 100 nM or 1 µM MTX caused slight, but significant, decreases in the %MTT reduction. More pronounced cytotoxic effects were observed with the 24 h MTX incubation at 5, 10, 50, and 100 µM concentrations. After 48 h incubation, the %MTT reduction values in the 10 nM MTX concentration remained similar to that in the control cells. MTX 100 nM and 1 µM caused slight significant decreases. Again, more notorious cytotoxic effects were observed with the higher concentrations of 5, 10, 50, and 100 µM. After 72 h incubation, the %MTT reduction values observed with 10 nM were similar to the control values. The 72 h incubations with higher concentrations (100 nM, 1, 5, 10, 50, and 100 µM) caused significant decreases in %MTT reduction. Similar to what was observed in the LDH leakage assay, the cytotoxicity observed by MTT assay was time dependent being the cytotoxicity higher with the longest incubation period (96 h). The incubation with 10 nM MTX did not cause any significant changes in the %MTT reduction compared to control. The co-incubation with the radical scavenger NAC (1 mM) or the mitochondrial function enhancer *L*-carnitine (1 mM) did not prevent the cytotoxic effects observed with the incubation of MTX (100 nM and 1 µM) for 96 h in the reduction of MTT test (*data not shown*).

MTX Incubation Elicits an Increase in the Caspase-3 Activity After 24 h

As can be observed in the Fig. 3, the incubation of 100 nM and 1 µM MTX, for 24 h, at 37 °C, caused an increase in caspase-3 activity (0.033 ± 0.007 OD/mg protein and 0.039 ± 0.010 OD/mg protein, respectively), compared to control cells (0.025 ± 0.003 OD/mg protein). The co-incubation of MTX (in the same concentrations) with the CYP450 inhibitor metyrapone (0.5 mM) or with the CYP2E1 inhibitor diallyl sulfide (150 µM) did not prevent the observed effects in the caspase-3 assay (*data not shown*).

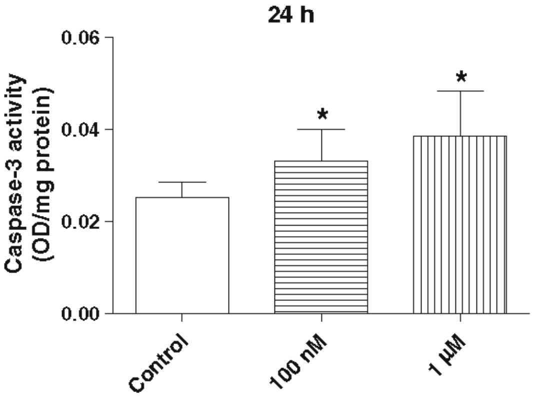

Fig. 3 Levels of caspase-3 activity in the H9c2 cells after 24 h incubation with MTX (100 nM and 1 µM). Results are presented as mean ± SD ($n = 6$ independent experiments). Statistical comparisons were made using Kruskal–Wallis test followed by the Student–Newman–Keuls post hoc test (*$p < 0.05$ vs. Control)

Reactive Species Generation and GSH Depletion after 96 h: No GSSG Formation or Lipid Peroxidation

The effect of MTX in the generation of reactive species was assessed using two different fluorescent probes, DCFH-DA (10 µM) and DHR (100 µM). In all the early time points tested (1, 2, 3, 4, 5, 6, 7, 8, 9, or 10 h), no changes in intracellular reactive species generation with any of MTX-tested concentrations (100 nM and 1 µM) were observed (*data not shown*). However, as evidenced in the Fig. 4a), incubations with DCFH-DA after 96 h pre-incubation with MTX in both working concentrations caused a significant increase in the generation of reactive species (137 ± 46.7 % in the MTX 100 nM group and 141 ± 56.9 % in the MTX 1 µM group compared to 100 ± 10.3 % in the control group).

No changes in the GSHt, GSH, and GSSG intracellular levels after the 24 and 48 h incubations with MTX (100 nM and 1 µM) were observed (*data not shown*). Only when cells were incubated with MTX (100 nM) for 96 h, a significant decrease was observed in GSHt and GSH intracellular levels when compared with control group, as shown in Fig. 4b and c, respectively. No differences were found in GSSG levels in the previous conditions (*data not shown*). No significant changes were observed with the concentration of MTX 1 µM for GSH, GSHt, or GSSG intracellular levels (*data not shown*).

No significant changes were observed in the malondialdehyde levels after incubation with MTX (100 nM and 1 µM) at any time point tested (24, 48, or 96 h) in comparison with control levels (*data not shown*).

MTX-Induced Energetic Impairment and Increased Levels of Intracellular Calcium at All Time Points

ATP intracellular levels after MTX incubation were assessed through the bioluminescence test. Significant decreases in the ATP levels were observed in all time point tested, as shown in the Fig. 5: after 24 h incubation with MTX (100 nM and 1 µM), the ATP intracellular levels were about 0.63 ± 0.48 nmol/mg protein and 0.87 ± 0.50 nmol/mg protein, respectively, compared to 1.77 ± 0.49 nmol/mg protein for the control group. At the end of 48 h incubation, ATP levels were 1.23 ± 0.37 nmol/mg protein in the MTX

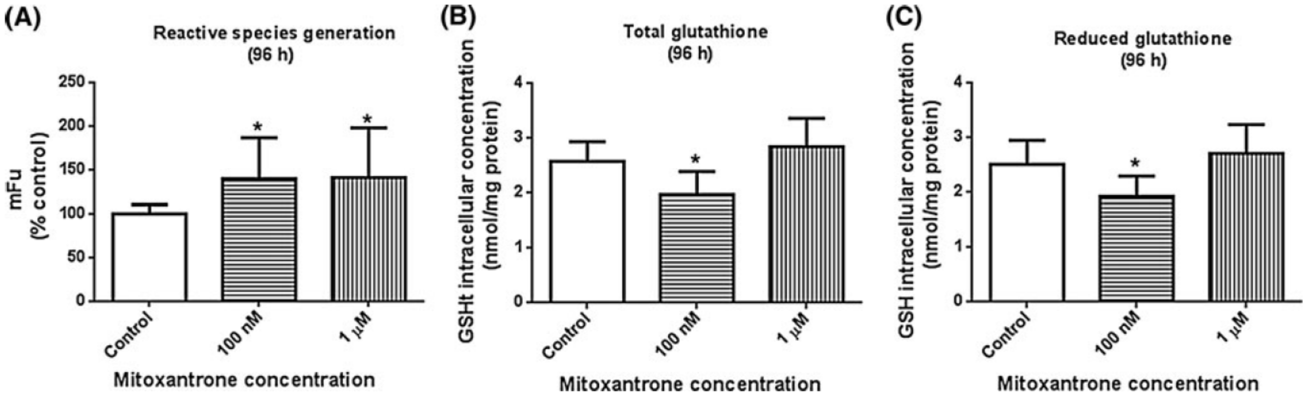

Fig. 4 Markers of oxidative stress after MTX incubation with H9c2 cells. **a** Intracellular levels of reactive species detected after incubation with DCFH-DA (10 μM) fluorescent probe after 96 h pre-incubation with MTX (100 nM and 1 μM). Results are presented as means (%) ± SD ($n = 6$ independent experiments). Intracellular levels of **b** GSHt and **c** GSH after 96 h incubation with MTX (100 nM and 1 μM). Results are presented as mean ± SD ($n = 7$ independent experiments). Statistical comparisons were made using Kruskal–Wallis test followed by the Student–Newman–Keuls post hoc test ($^*p < 0.05$ vs. Control)

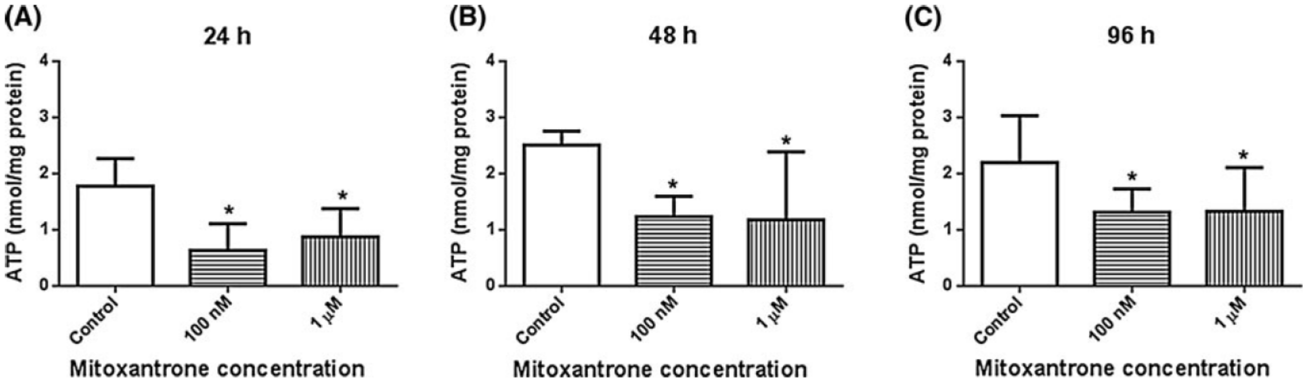

Fig. 5 ATP intracellular levels after MTX (100 nM and 1 μM) incubation for **a** 24 h, **b** 48 h, and **c** 96 h. Results are presented as mean ± SD ($n = 5$ independent experiments). Statistical comparisons were made using Kruskal–Wallis test followed by the Student–Newman–Keuls post hoc test ($^*p < 0.05$ vs. Control)

100 nM group and 1.18 ± 1.21 nmol/mg protein in the MTX 1 μM group versus 2.50 ± 0.25 nmol/mg protein for the control group. After 96 h incubation with MTX (100 nM and 1 μM), the ATP intracellular levels were about 1.31 ± 0.42 nmol/mg protein and 1.33 ± 0.78 nmol/mg protein, respectively, compared to 2.20 ± 0.83 nmol/mg protein for the control group.

The expression of ATP-synthase was evaluated through western immunoblotting in all time points (24, 48, and 96 h), after incubation with MTX in both working concentrations. Results were normalized to the actin content and were expressed as the optic density ratio between ATP-synthase/actin (% relative to the control). No significant changes were observed after 24 or 48 h incubation (*data not shown*). In contrast, after the 96 h incubation, significant decrease in the ATP-synthase expression was observed in both treated groups, as evidenced in Fig. 6a, b. The expression of ATP-synthase was about 86 ± 3.1 % in the MTX 100 nM group, 84 ± 3.6 % in the MTX 1 μM versus 100 ± 0.6 % in the control cells. Considering these differences, the ATP-synthase activity was also evaluated in MTX-treated cells after 96 h incubation. As shown in Fig. 6c, after 96 h incubation with MTX (100 nM and 1 μM), the ATP-synthase activity was dramatically decreased (6.8 ± 3.8 nmol Pi/mg/min and 5.1 ± 1.5 nmol Pi/mg/min, respectively) compared to control cells (18.2 ± 4.4 nmol Pi/mg/min).

After incubation with MTX for 24, 48, and 96 h, the mitochondrial membrane potential and the calcium intracellular levels were evaluated using the TMRM and the Fluo-3 AM fluorescent probes, respectively. As shown in the Fig. 7a, after 24 h incubation period, there was an accumulation of the TMRM probe only with the lower concentration tested (100 nM) (60 ± 11.9 mean FI), compared to control (48 ± 10.6 mean FI). The incubation with MTX 1 μM did not cause significant changes (43 ± 13.3 mean FI) compared to control values. At the same time point, the change in the mitochondrial

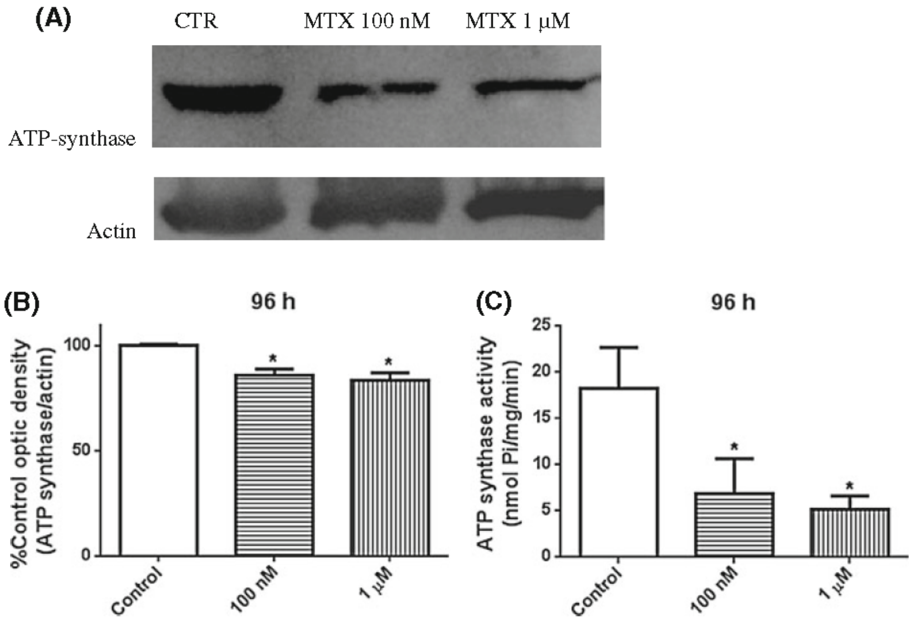

Fig. 6 **a** Representative western blot gel of ATP-synthase expression in the H9c2 cells after 96 h incubation with MTX (100 nM and 1 μM). Actin was used as a loading control. On **b**, a graphic representation of the ATP-synthase expression is presented. Results are normalized to the actin content and are presented as mean ± SD ($n = 3$ independent experiments). **c** ATP-synthase activity in the H9c2 cells after 96 h incubation with MTX (100 nM and 1 μM). Statistical comparisons were made using Kruskal–Wallis test followed by the Student–Newman–Keuls post hoc test ($^*p < 0.05$ vs. Control)

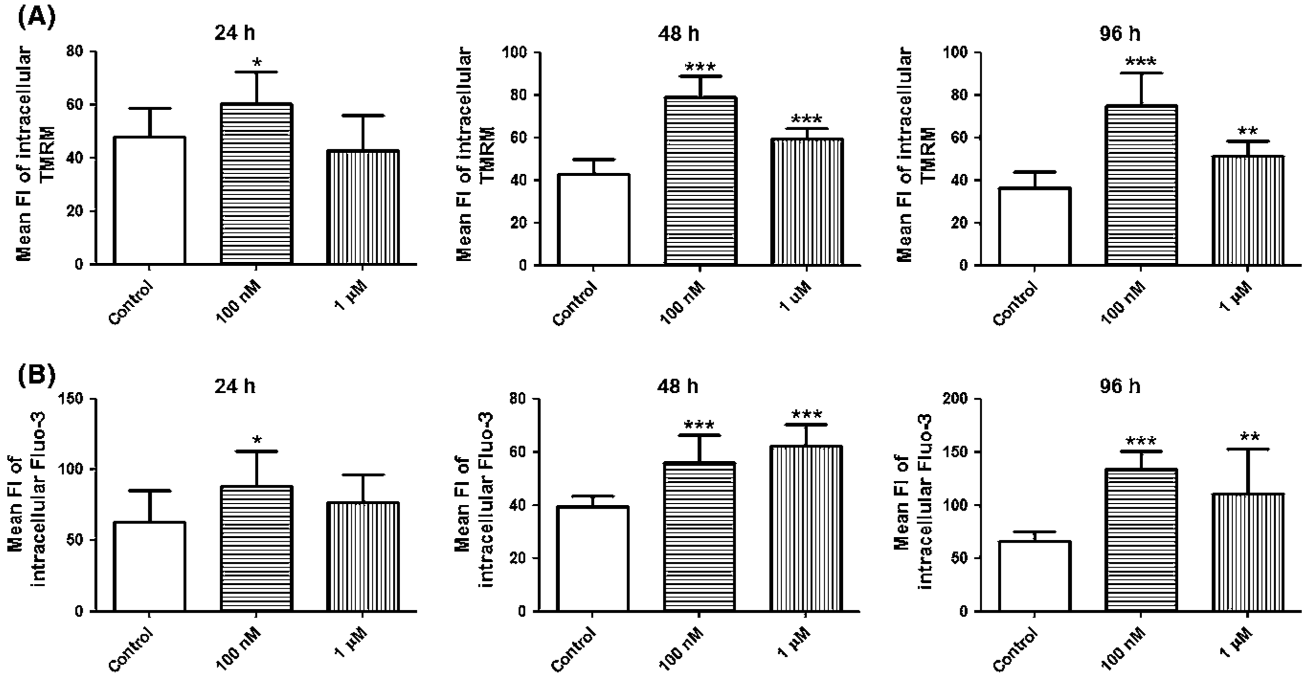

Fig. 7 **a** Mitochondrial membrane potential values and **b** intracellular calcium levels in the H9c2 cells after incubation with MTX (100 nM and 1 μM) for 24, 48, and 96 h. Results are presented as mean ± SD ($n = 3$ independent experiments). Statistical comparison were made using Kruskal–Wallis test followed by the Student–Newman–Keuls post hoc test ($^*p < 0.05$ vs. Control, $^{**}p < 0.01$ vs. Control, $^{***}p < 0.001$ vs. Control)

membrane potential was accompanied by a significant increase in the intracellular calcium levels only in the MTX 100 nM group (88 ± 25.3 mean FI), compared to MTX 1 μM (77 ± 19.3 mean FI) and control group (63 ± 22.6 mean FI) (Fig. 7b). However, after 48 h, both concentrations tested caused a dramatic hyperpolarization of the mitochondrial membrane potential (79 ± 10.0 mean FI for MTX 100 nM group and 59 ± 5.2 mean FI for MTX 1 μM group, compared to 43 ± 7.1 mean FI for control cells) (Fig. 7a) and increases in the intracellular calcium levels (56 ± 9.7 mean FI for MTX 100 nM group, 62 ± 7.7 mean FI for MTX 1 μM vs. 40 ± 3.6 mean FI for control cells) (Fig. 7b). At the last time tested (96 h), the mitochondrial membrane potential did not recover to control values, keeping the same trend observed earlier (75 ± 15.8 mean FI for MTX 100 nM group, 51 ± 7.0 mean FI for MTX 1 μM group vs. 36 ± 7.6 mean FI for control cells). Conversely, the calcium intracellular levels of treated cells remained higher than control cells (134 ± 16.4 mean FI for MTX 100 nM group, 111 ± 41.8 mean FI for MTX 1 μM group vs. 66 ± 8.8 mean FI for control cells) (Fig. 7b).

Discussion

In the present work, we showed a time- and concentration-dependent response to MTX incubation in H9c2 cells, through two different cytotoxicity tests (LDH leakage assay and MTT reduction test, Figs. 1 and 2, respectively). We also contributed to the elucidation of the mechanisms involved in MTX cellular injury. Our results suggest an important energetic crisis caused by MTX evidenced by substantial and early decreases in the ATP intracellular levels, late inhibition of the ATP-synthase expression and activity, hyperpolarization of the mitochondrial membrane potential, and increase in the intracellular calcium levels. Another 24 h event elicited by MTX was the increase in the caspase-3 activity, while in our model, oxidative stress markers were only changed at the longest incubation time tested.

As already stated, by using several MTX concentrations, we observed a time- and concentration-dependent cytotoxicity pattern in both cytotoxicity tests used, being the toxic effects observed earlier in the MTT reduction assay than in the LDH leakage assay in all times tested (Figs. 1, 2). These results suggest that mitochondrial effects anticipate cellular membrane rupture in the MTX toxicity.

For studying the mechanisms of MTX cardiotoxicity, we have selected 2 working concentrations: 100 nM and 1 μM. Indeed, both MTX concentrations are clinically relevant given the plasma and tissue levels of MTX found in the literature [6, 27]. In fact, the mean maximum plasma concentrations in humans after a 15 mg/m^2 or a 90 mg/m^2 30-min infusion of MTX are about 1.5 and 12 μM, respectively [27]. For the caspase-3 activity assay, the incubation period of 24 h was selected due to the measurable decreases in the cytotoxicity observed in the reduction of MTT test at this time point in both working concentrations (indicating mitochondrial damage) (Fig. 2) and the absence of significant decreases in the LDH leakage in the same conditions (indicative of necrosis). In fact, after 24 h incubation, despite the absence of significant loss of viability seen on the LDH leakage assay, both chosen MTX concentrations caused activation of caspase-3 (Fig. 3), which was in accordance with the described bimodal mechanism of cell death induced by MTX: apoptosis at lower concentrations and necrosis at higher concentrations [28]. Similar signals of apoptosis were already described after 24 and 48 h of MTX (1.60 μM) incubation in the H9c2 cells [29]. Noteworthy, the late effects of MTX in the human heart are more related with loss of functionality of the cells rather than necrosis and lysis.

We recently demonstrated a partial protection toward MTX cytotoxicity (100 nM and 1 μM) in the same cellular model after 96 h, with the co-incubation with the CYP450 inhibitor metyrapone (0.5 mM) or with the CYP2E1 inhibitor diallyl sulfide (150 μM) [14]. However, in the present study, the co-incubation with these metabolism inhibitors did not prevent the increase in the caspase-3 activity. Altogether, these results suggest that the previous partial protection obtained with the metabolism inhibitors is not related to this caspase-dependent activation. In fact, that protective effect occurred at a late incubation time, and as we can observe in the present work, the features of MTX cytotoxicity are rather dissimilar in the time course.

Oxidative stress is described as a possible cellular mechanism involved in MTX cardiotoxicity, as an attempt to reveal similarities to the cardiotoxicity caused by doxorubicin [13]. In fact, MTX contains a quinone group within its chemical structure that can potentially suffer oxidative activation leading to reactive species generation [12, 13]. Both probes employed in the present study are non-fluorescent that undergo intracellular oxidation to their respective fluorescent products in the presence of reactive species such as peroxynitrite, hydroxyl radical, and superoxide. However, herein, we did not find any strong evidence of reactive species involvement in earlier MTX cytotoxicity for 100 nM and 1 μM concentrations. In fact, until 10 h of incubation, no free radical (peroxynitrite, hydroxyl radical, or superoxide) generation was observed by using two different probes, DHR and DCFH-DA. In accordance, only a very low superoxide anion generation was described in MCF-7 S9 fractions after incubation with MTX 100 μM for 30 min, with no hydroxyl radical or semiquinone formation even for 400 μM MTX [30]. These results can eventually explain the absence of any lipid peroxidation or changes in GSHt, GSH, and GSSG intracellular levels observed by us, at 24 and 48 h MTX incubation. After 96 h MTX incubation, a slight decrease in intracellular GSH for 100 nM MTX (Fig. 4c), a reduction in GSHt levels (Fig. 4b), and no significant changes in GSSG and lipid peroxidation were observed. Noteworthy, we also found a reactive species generation for 100 nM and 1 μM MTX at this late time point (Fig. 4a), which is in accordance with the previous observation that peroxides production occurs only after a prolonged incubation with MTX (1.60 μM) in the H9c2 cells [29]. However, no changes in intracellular GSH content were observed for 1 μM of MTX: this probably results in some adaptive and early phenomenon. In fact, oxidative alterations seem to occur quite late. One possible explanation is that MTX has a reduced ability to enter in redox cycle and, consequently, to produce reactive species in a enzymatic catalyzed fashion as its congener doxorubicin, while the preferential metabolic pathway of MTX is two-electron reduction rather than one-electron reduction [13, 30]. Nevertheless, we tested NAC in our experimental conditions. Consistently, the co-incubation with the radical scavenger NAC (1 mM) did not prevent any of the cytotoxic effects observed with the MTX (100 nM and 1 μM) incubation for 96 h in the MTT reduction test. However, in vivo and in vitro protective studies using NAC have demonstrated the efficacy of NAC in reversing the drug-induced cardiomyopathy related to oxidative stress [20, 31, 32]. The use of NAC is based on its antioxidant properties and actions upon the GSH pathways; thus, the lack of protective effects of NAC in the present study may result in the fact that other mechanisms involved in MTX toxicity exert a major role when compared to oxidative stress. Conversely, the observed absence of lipid peroxidation is in accordance with the results obtained in heart homogenates from MTX-treated mice (15 mg/kg, i.p.) [33]. Noteworthy, the inhibition of lipid peroxidation was already associated with MTX in in vitro incubations. In liver microsomes, heart sarcosomes, and mitochondria isolated from rabbit incubated with MTX (50, 100, and 200 μM), the levels of lipid peroxidation were significantly lower than those observed in controls [34]. These inhibitory effects in lipid peroxidation still remain unclear, but MTX was described as having some antioxidant properties [34].

The major finding presented herein is the energetic imbalance observed in the cells after incubation with MTX (100 nM and 1 μM). Despite the low MTX concentrations used, the cellular ATP content decreased around 50 % in all time tested (24, 48, and 96 h) (Fig. 5). It is known that H9c2 is a cellular model that privileges the glycolytic pathway, and MTX seems to interfere with this pathway. This early ATP crisis could precipitate fatal changes in the cell. This event can lead to a less efficient calcium control and mitochondrial electron chain regulation, as we can see with the increase in intracellular calcium content and the hyperpolarization of the mitochondrial membrane potential (Fig. 7). The mitochondrial hyperpolarization should drive more calcium into the mitochondria matrix and impair electron chain mitochondrial activity, as we can indirectly observe in the MTT reduction test and ATP-synthase activity. The mitochondrial membrane potential may also be elevated as an attempt to provide motive force to restore the energetic homeostasis. The increase in the mitochondrial membrane potential was also observed in pathological conditions in ischemic cardiomyocytes during reperfusion [35], in vascular endothelial cells after pulsatile shear stress [36], and physiologically during preimplantation stages of human and mouse embryo development, in response to metabolic demand [37]. On the other hand and in contrast to our present work, the incubation of 1.60 μM MTX for 24 h with the H9c2 cells was enough to cause a drop in the mitochondrial membrane potential [29], while in our lower concentrations, a hyperpolarization was observed. Considering the energetic failure, *L*-carnitine was used by us to study a possible protection to MTX effects. *L*-carnitine (1 mM) is considered a mitochondrial enhancer by improving the mitochondrial β-oxidation of fatty acids, the *trans*-esterification/excretion of acyl-CoA esters, the oxidation of α-ketoacids, and the removal of toxic acylcarnitine ester from the mitochondria, providing this metabolic pathway as a source of ATP synthesis [38, 39, 40]. *L*-carnitine was already employed in the H9c2 cell model to study the possible protection against doxorubicin [40]. However, it did not protect the H9c2 cells from the cytotoxicity induced by MTX incubation (96 h), evaluated through the MTT reduction test. Therefore, other mechanisms must be involved in the MTX toxicity towards ATP pathways.

In our study, a decrease in ATP-synthase expression, but mostly a drastic reduction in ATP-synthase activity, was found after 96 h of MTX incubation (Fig. 6). These effects were not described before for MTX. The decrease in the ATP-synthase content and activity (Fig. 6) can contribute to the observed increases in the reactive species generation at late periods (Fig. 4). This late generation of reactive species possibly contributes to decrease in GSH. We evaluated early and late time points of reactive species formation (until 10 h and after 96 h), but it is easy to assume that 1 μM MTX caused the formation of reactive species after those 10 h and before 96 h, allowing an adaptation feature of GSH synthesis. Noteworthy, GSH is mainly concentrated in mitochondria and functions as an internal intracellular antioxidant buffer for the most important target of oxidative stress in the heart, the mitochondria [41].

The energetic dysfunction can result in calcium regulation impairment, since the cellular mechanisms involved in calcium handling are ATP driven. Thus, at low energetic levels, calcium pumping activity decreases, resulting in cytosolic calcium increases [35]. A sustained elevation in calcium levels can, ultimately, determine the loss of mitochondrial membrane potential and trigger the cell to the “no return point,” leading to cell death [42]. Moreover, the calcium increase may be responsible for the early activation of caspase-3 observed (Fig. 3). Although the effects are clear and consistent, it is still difficult to point out the cause of the initial decrease in ATP level. Noteworthy, significant decreased levels of ATP were already demonstrated 72 h after the 3 h pre-incubation of MTX (about 0.1–10 μM) in cultured neonatal rat cardiac cells

[15], evidencing that even after cessation of that short-period MTX incubation, the cardiac cells were unable to recover energetic levels.

Our results suggest that the mild oxidative stress observed in our study with MTX does not seem to be related to its redox cycle being secondary to a more dramatic and earlier event: the energetic imbalance. The main results of this study are related to the energetic toxic effects, evidenced by decreases in the ATP levels, hyperpolarization of the mitochondrial membrane potential, increases in the intracellular calcium levels, and late inhibition of the ATP-synthase expression and activity, observed after MTX incubation with expected therapeutic concentrations. It is well known that changes in cardiac energetics can lead to a heart failure condition. Thus, the results presented here contribute to the elucidation of mechanisms involved in the cardiotoxicity of MTX.

Acknowledgments This work received financial support from "Fundação para a Ciência e Tecnologia (FCT)," Portugal (EXPL/DTP-FTO/0290/2012) and by "Fundo Comunitário Europeu" (FEDER) under the frame of "Eixo I do Programa Operacional Fatores de Competitividade (POFC) do QREN" (COMPETE: FCOMP-01-0124-FEDER-027749). The work was also supported by FCT within the framework of Strategic Projects for Scientific Research Units of R&D (project PEst-C/EQB/LA0006/2011). LGR and VVB thank FCT for their PhD Grant (SFRH/BD/63473/2009 and SFRH/BD/82556/2011, respectively) and VMC thank FCT for her Post-doc Grant (SFRH/BPD/63746/2009). Authors are grateful to Dr. Vilma Sardão, from University of Coimbra, for gently providing us with the cellular model used in this work.

References

1. Seiter, K. (2005). Toxicity of the topoisomerase II inhibitors. *Expert Opinion on Drug Safety, 4*, 219–234.
2. Kingwell, E., Koch, M., Leung, B., Isserow, S., Geddes, J., Rieckmann, P., et al. (2010). Cardiotoxicity and other adverse events associated with mitoxantrone treatment for MS. *Neurology, 74*, 1822–1826.
3. Khan, S. N., Lai, S. K., Kumar, P., & Khan, A. U. (2010). Effect of mitoxantrone on proliferation dynamics and cell cycle progression. *Bioscience Reports, 30*, 375–381.
4. Hajihassan, Z., & Rabbani-Chadegani, A. (2011). Interaction of mitoxantrone, as an anticancer drug, with chromatin proteins, core histones and H1, in solution. *International Journal of Biological Macromolecules, 48*, 87–92.
5. Alderton, P. M., Gross, J., & Green, M. D. (1992). Comparative study of doxorubicin, mitoxantrone, and epirubicin in combination with ICRF-187 (ADR-529) in a chronic cardiotoxicity animal model. *Cancer Research, 52*, 194–201.
6. Batra, V. K., Morrison, J. A., Woodward, D. L., Siverd, N. S., & Yacobi, A. (1986). Pharmacokinetics of mitoxantrone in man and laboratory animals. *Drug Metabolism Reviews, 17*, 311–329.
7. Sereno, M., Brunello, A., Chiappori, A., Barriuso, J., Casado, E., Belda, C., et al. (2008). Cardiac toxicity: Old and new issues in anti-cancer drugs. *Clinical and Translational Oncology, 10*, 35–46.
8. Wallace, K. B. (2003). Doxorubicin-induced cardiac mitochondrionopathy. *Pharmacology and Toxicology, 93*, 105–115.
9. Brück, T. B., & Brück, D. W. (2011). Oxidative metabolism of the anti-cancer agent mitoxantrone by horseradish, lacto-and lignin peroxidase. *Biochimie, 93*, 217–226.
10. Duthie, S. J., & Grant, M. H. (1989). The role of reductive and oxidative metabolism in the toxicity of mitoxantrone, adriamycin and menadione in human liver derived Hep G2 hepatoma cells. *British Journal of Cancer, 60*, 566–571.
11. Panousis, C., Kettle, A., & Phillips, D. R. (1995). Myeloperoxidase oxidises mitoxantrone to metabolites which bind covalently DNA and RNA. *Anticancer drug designer, 10*, 593–605.
12. Mewes, K., Blanz, J., Ehninger, G., Gebhardt, R., & Zeller, K. P. (1993). Cytochrome P-450-induced cytotoxicity of mitoxantrone by formation of electrophilic intermediates. *Cancer Research, 53*, 5135–5142.
13. Li, S. J., Rodgers, E. H., & Grant, M. H. (1995). The activity of xenobiotic enzymes and the cytotoxicity of mitoxantrone in MCF 7 human breast cancer cells treated with inducing agents. *Chemico Biological Interactions, 97*, 101–118.
14. Rossato, L., Costa, V., De Pinho, P., Freitas, V., Viloune, L., Bastos, M., et al. (2013). The metabolic profile of mitoxantrone and its relation with mitoxantrone-induced cardiotoxicity. *Archives of Toxicology*. doi:10.1007/s00204-013-1040-6.
15. Shipp, N. G., Dorr, R. T., Alberts, D. S., Dawson, B. V., & Hendrix, M. (1993). Characterization of experimental mitoxantrone cardiotoxicity and its partial inhibition by ICRF-187 in cultured neonatal rat heart cells. *Cancer Research, 53*, 550–556.
16. Bachmann, E., Weber, E., & Zbinden, G. (1987). Effect of mitoxantrone and doxorubicin on energy metabolism of the rat heart. *Cancer Treatment Reports, 71*, 361–366.
17. Kimes, B. W., & Brandt, B. L. (1976). Properties of a clonal muscle from rat heart. *Experimental Cell Research, 98*, 367–381.
18. Zordoky, B. N. M., & El-Kadi, A. O. S. (2007). H9c2 cell line is a valuable in vitro model to study the drug metabolizing enzymes in the heart. *Journal of Pharmacological and Toxicological Methods, 56*, 317–322.
19. Costa, V. M., Silva, R., Ferreira, R., Amado, F., Carvalho, F., Bastos, M. L., et al. (2009). Adrenaline in pro-oxidant conditions elicits intracellular survival pathways in isolated rat cardiomyocytes. *Toxicology, 257*, 70–79.
20. Rossato, L. G., Costa, V. M., De Pinho, P. G., Carvalho, F., Bastos, M. L., & Remião, F. (2011). Structural isomerization of synephrine influences its uptake and ensuing glutathione depletion in rat-isolated cardiomyocytes. *Archives of Toxicology, 85*, 929–939.
21. Sayed-Ahmed, M. M., Shaarawy, S., Shouman, S. A., & Osman, A. M. (1999). Reversal of doxorubicin-induced cardiac metabolic damage by L-carnitine. *Pharmacological Research, 39*, 289–295.
22. Angeloni, C., Spencer, J. P. E., Leoncini, E., Biagi, P. L., & Hrelia, S. (2007). Role of quercetin and its in vivo metabolites in protecting H9c2 cells against oxidative stress. *Biochimie, 89*, 73–82.
23. Grotto, D., Santa Maria, L. D., Boeira, S., Valentini, J., Charão, M. F., Moro, A. M., et al. (2007). Rapid quantification of malondialdehyde in plasma by high performance liquid chromatography-visible detection. *Journal of Pharmaceutical and Biomedical Analysis, 43*, 619–624.
24. Costa, V. M., Silva, R., Ferreira, L. M., Branco, P. S., Carvalho, F., Bastos, M. L., et al. (2007). Oxidation process of adrenaline in freshly isolated rat cardiomyocytes: Formation of adrenochrome, quinoproteins, and GSH adduct. *Chemical Research in Toxicology, 20*, 1183–1191.
25. Floryk, D., & Houstěk, J. (1999). Tetramethyl rhodamine methyl ester (TMRM) is suitable for cytofluorometric measurements of mitochondrial membrane potential in cells treated with digitonin. *Bioscience Reports, 19*, 27–34.
26. Carvalho, M., Remião, F., Milhazes, N., Borges, F., Fernandes, E., Monteiro, M. D. C., et al. (2004). Metabolism is required for

the expression of ecstasy-induced cardiotoxicity in vitro. *Chemical Research in Toxicology, 17*, 623–632.

27. Canal, P., Attal, M., Chatelut, E., Guichard, S., Huguet, F., Muller, C., et al. (1993). Plasma and cellular pharmacokinetics of mitoxantrone in high-dose chemotherapeutic regimen for refractory lymphomas. *Cancer Research, 53*, 4850–4854.
28. Neuhaus, O., Kieseier, B. C., & Hartung, H.-P. (2006). Therapeutic role of mitoxantrone in multiple sclerosis. *Pharmacology & Therapeutics, 109*, 198–209.
29. Kluza, J., Marchetti, P., Gallego, M.-A., Lancel, S., Fournier, C., Loyens, A., et al. (2004). Mitochondrial proliferation during apoptosis induced by anticancer agents: Effects of doxorubicin and mitoxantrone on cancer and cardiac cells. *Oncogene, 23*, 7018–7030.
30. Fisher, G. R., & Patterson, L. H. (1992). Lack of involvement of reactive oxygen in the cytotoxicity of mitoxantrone, CI941 and ametantrone in MCF-7 cells: comparison with doxorubicin. *Cancer Chemotherapy and Pharmacology, 30*, 451–458.
31. Chen, F., Lewis, W., Hollander, J. M., Baseler, W., & Finkel, M. S. (2012). *N*-acetylcysteine reverses cardiac myocyte dysfunction in HIV-Tat proteinopathy. *Journal of Applied Physiology, 113*, 105–113.
32. Chen, F., Hadfield, J., Berzingi, C., Hollander, J., Miller, D., Nichols, C., et al. (2013). *N*-acetylcysteine reverses cardiac myocyte dysfunction in a rodent model of behavioral stress. *Journal of Applied Physiology, 115*, 514–524.
33. Arnaiz, S. L., & Llesuy, S. (1993). Oxidative stress in mouse heart by antitumoral drugs: A comparative study of doxorubicin and mitoxantrone. *Toxicology, 77*, 31–38.
34. Novak, R. F., & Kharasch, E. D. (1985). Mitoxantrone: Propensity for free radical formation and lipid peroxidation-implications for cardiotoxicity. *Investigational New Drugs, 3*, 95–99.
35. Dong, Z., Saikumar, P., Weinberg, J. M., & Venkatachalam, M. A. (2006). Calcium in cell injury and death. *Annual Review of Pathology: Mechanisms of Disease, 1*, 405–434.
36. Li, R., Beebe, T., Cui, J., Rouhanizadeh, M., Ai, L., Wang, P., et al. (2009). Pulsatile shear stress increased mitochondrial membrane potential: Implication of Mn-SOD. *Biochemical and Biophysical Research Communications, 388*, 406–412.
37. Acton, B. M. (2004). Alterations in mitochondrial membrane potential during preimplantation stages of mouse and human embryo development. *Molecular Human Reproduction, 10*, 23–32.
38. Zammit, V. A., Ramsay, R. R., Bonomini, M., & Arduini, A. (2009). Carnitine, mitochondrial function and therapy. *Advanced Drug Delivery Reviews, 61*, 1353–1362.
39. Mijares, A., & López, J. R. (2001). L-carnitine prevents increase in diastolic [Ca^{2+}] induced by doxorubicin in cardiac cells. *European Journal of Pharmacology, 425*, 117–120.
40. Newman, R., Hacker, M., & Krakoff, I. (1981). Amelioration of adriamycin and daunorubicin myocardial toxicity by adenosine. *Cancer Research, 41*, 3483–3488.
41. Costa, V. M., Carvalho, F., Bastos, M. L., Carvalho, R. A., Carvalho, M., & Remião, F. (2011). Contribution of catecholamine reactive intermediates and oxidative stress to the pathologic features of heart diseases. *Current Medical Chemistry, 18*, 2272–2314.
42. Trump, B. F., & Berezesky, I. K. (1995). Calcium-mediated cell injury and cell death. *FASEB, 9*, 219–228.

Manuscript III

Mitochondrial cumulative damage induced by mitoxantrone: late onset cardiac energetic impairment.

Rossato, L. G., Costa, V. M., Dallegrave, E., Arbo, M., Silva, R., Ferreira, R., Amado, F., Dinis-Oliveira, R.J., Duarte, J.A., Bastos, M.L., Palmeira, C., Remião F.

Cardiovasc Toxicol 2013 *In Press.* DOI: 10.1007/s12012-013-9230-2.

Cardiovasc Toxicol
DOI 10.1007/s12012-013-9230-2

Mitochondrial Cumulative Damage Induced by Mitoxantrone: Late Onset Cardiac Energetic Impairment

**Luciana Grazziotin Rossato · Vera Marisa Costa · Eliane Dallegrave ·
Marcelo Arbo · Renata Silva · Rita Ferreira · Francisco Amado ·
Ricardo Jorge Dinis-Oliveira · José Alberto Duarte · Maria de Lourdes Bastos ·
Carlos Palmeira · Fernando Remião**

© Springer Science+Business Media New York 2013

Abstract Mitoxantrone (MTX) is a chemotherapeutic agent, which presents late irreversible cardiotoxicity. This work aims to highlight the mechanisms involved in the MTX-induced cardiotoxicity, namely the effects toward mitochondria using in vivo and in vitro studies. Male Wistar rats were treated with 3 cycles of 2.5 mg/kg MTX at day 0, 10, and 20. One treated group was euthanized on day 22 (MTX22) to evaluate the early MTX cardiac toxic effects, while the other was euthanized on day 48 (MTX48), to allow the evaluation of MTX late cardiac effects. Cardiac mitochondria isolated from 4 adult untreated rats were also used to evaluate in vitro the MTX (10 nM, 100 nM, and 1 μM) direct effects upon mitochondria functionality. Two rats of MTX48 died on day 35, and MTX treatment caused a reduction in relative body weight gain in both treated groups with no significant changes in water and food intake. Decreased levels of plasma total creatine kinase and CK-MB were detected in the MTX22 group, and increased plasma levels of lactate were seen in MTX48. Increased cardiac relative mass and microscopic changes were evident in both treated groups. Considering mitochondrial effects, for the first time, it was evidenced that MTX induced an increase in the complex IV and complex V activities in MTX22 group, while a decrease in the complex V activity was accompanied by the reduction in ATP content in the MTX48 rats. No alterations in mitochondria transmembrane potential were found in isolated mitochondria from MTX48 rats or in isolated mitochondria directly incubated with MTX. This study highlights the relevance of the cumulative MTX-induced in vivo mitochondriopathy to the MTX cardiotoxicity.

L. G. Rossato (✉) · V. M. Costa · E. Dallegrave · M. Arbo ·
R. Silva · R. J. Dinis-Oliveira · M. de Lourdes Bastos ·
F. Remião (✉)
REQUIMTE, Laboratório de Toxicologia, Departamento de Ciências Biológicas, Faculdade de Farmácia, Universidade do Porto, Porto, Portugal
e-mail: luciana.g.rossato@gmail.com

F. Remião
e-mail: remiao@ff.up.pt

E. Dallegrave
Universidade Federal de Ciências da Saúde de Porto Alegre, Porto Alegre, Brazil

R. Ferreira
QOPNA, Departamento de Química, Universidade de Aveiro, Aveiro, Portugal

F. Amado
Escola Superior de Saúde, Universidade de Aveiro (ESSUA), Aveiro, Portugal

R. J. Dinis-Oliveira
Departamento de Medicina Legal e Ciências Forenses, Faculdade de Medicina, Universidade do Porto, Porto, Portugal

R. J. Dinis-Oliveira
Department of Sciences, Advanced Institute of Health Sciences - North, CESPU, CRL, Gandra, Portugal

J. A. Duarte
CIAFEL, Faculdade de Desporto, Universidade do Porto, Porto, Portugal

C. Palmeira
Centro de Neurociências e Biologia Celular de Coimbra, Departamento de Ciências da Vida, Universidade de Coimbra, Coimbra, Portugal

Published online: 05 October 2013

Keywords Mitoxantrone · Cardiotoxicity · Mitochondria

Abbreviations

ATP	Adenosine 5′-triphosphate
AST	Aspartate aminotransferase
BN-PAGE	Blue native polyacrylamide gel electrophoresis
CK	Creatine kinase
DAB	Diaminobenzidine
DTNB	5,5-Dithio-bis(2-nitrobenzoic acid)
GSH	Reduced glutathione
GSHt	Total glutathione
GSSG	Oxidized glutathione
$HClO_4$	Perchloric acid
LDH	Lactate dehydrogenase
MTX	Mitoxantrone
β-NADPH	Reduced β-nicotinamidephosphate adenine dinucleotide
TPP^+	Tetraphenylphosphonium

Introduction

Mitoxantrone (MTX) is an antitumor agent used in the treatment of breast and prostate cancer, acute leukemia, lymphoma, and in the treatment of multiple sclerosis due to its immunosuppressive properties [1, 2]. However, the cumulative cardiotoxic profile of MTX is well known, and it can affect up to 18 % of treated patients [1]. The MTX-induced cardiotoxicity is irreversible, dose-dependent, and it may occur years after treatment [3]. Clinically, MTX cardiotoxicity is mainly characterized by a reduction in left ventricular stroke volume and congestive heart failure [1, 3].

The risk of MTX-induced cardiac side effects increases greatly with cumulative dose up to 140 mg/m^2 [2, 3]. Human mean maximum MTX plasma concentrations are about 1.5 and 12 μM 30 min after 15 or 90 mg/m^2 intravenous infusion, respectively [4]. The accumulation of MTX in the heart tissue is well documented [5, 6], with described concentrations around 716 ng/g wet tissue 35 days after MTX single dose of 12 mg/m^2 [6]. Furthermore, we highlighted that at least one biotransformation product of MTX, the naphthoquinoxaline metabolite (described as toxic), also accumulates in the rat heart, evidencing a prolonged exposure of the cardiac cells to MTX and this bioactive product [7].

Recently, we showed that therapeutic concentrations of MTX (100 nM and 1 μM) caused an important energetic imbalance evidenced by decreased ATP levels, hyperpolarization of the mitochondrial membrane potential, and a rise in the intracellular calcium levels after 24, 48, and 96 h of MTX incubation in a cardiomyoblast cell model (H9c2 cells) [8]. Additionally, MTX caused late inhibition of ATP-synthase expression and activity with concomitant increase in the reactive species generation after 96 h incubation with both previously referred concentrations [8]. In other studies, energetic imbalance was also observed in cultured neonatal rat heart cells after MTX incubation [9], and mitochondrial swelling was described in female BALB/c mice heart after MTX treatment [10]. Furthermore, uncoupling of oxidative phosphorylation was described in cardiac mitochondria isolated from rats treated with MTX [11]. Even so, studies to elucidate the mechanisms involved in the cardiotoxicity of MTX in vivo are scarce, especially with focus on mitochondrial functionality. Thus, the present work aims to contribute to the better understanding the in vivo MTX-induced cumulative cardiotoxicity using male adult Wistar rats subjected to 3 cycles of MTX treatment. MTX total cumulative dose was 7.5 mg/kg, which corresponds to 48 mg/m^2 by the allometric relationship, and therefore a clinical therapeutic dose. Early and late toxic effects (2 vs. 28 days after reaching the MTX total cumulative dose) were evaluated in order to assess the maladaptive responses involved in the MTX-induced cardiotoxicity. Furthermore, a complementary in vitro study, using rat-isolated cardiac mitochondria, was performed to understand the direct effects of MTX in the cardiac mitochondrial function.

Materials and Methods

Chemicals

All chemicals were of analytical grade. MTX hydrochloride, reduced glutathione (GSH), oxidized glutathione (GSSG), glutathione reductase (GR, EC 1.6.4.2), 2-vinylpyridine, reduced β-nicotinamide phosphate adenine dinucleotide (β-NADPH), adenosine 5′-triphosphate (ATP), cytochrome c, defatted bovine serum albumin, subtilopeptidase A type VIII, 5,5-dithio-bis(2-nitrobenzoic acid) (DTNB), luciferin, luciferase, subtilisin A protease, diaminobenzidine (DAB), glutaraldehyde, formaldehyde, and osmium tetroxide were purchased from Sigma-Aldrich (St. Louis, MO). HMW-native marker was purchased from GE Healthcare, Buckinghamshire, UK. Perchloric acid ($HClO_4$) and propylene oxide were obtained from Merck (Darmstadt, Germany). The reagents for the creatine kinase (CK), CK-MB, and lactate analysis were purchased from PZ Cormay S.A.

Animals

For the in vivo study, 15 adult male Wistar rats (Charles River Laboratories, Barcelona, Spain) weighing 240–300 g were used. Four additional male Wistar rats, weighting

200–250 g, were utilized for the in vitro study. The animals were housed in cages, with a temperature and humidity controlled environment. Food and water were provided ad libitum, and animals were subjected to a 12 h light–dark cycle. Animal experiments were approved by the Ethical Committee of Faculty of Pharmacy of the University of Porto (protocol number 09/04/2013). Housing and experimental treatment of the animals were in accordance with the Guide for the Care and Use of Laboratory Animals from the Institute for Laboratory Research. The experiments complied with current Portuguese laws.

Dose Regimen

For 1 week prior to the in vivo experiment, animals were acclimatized in cages. Animals were distributed into 3 groups (5 animals per group): control, MTX22, and MTX48; however, in order to allow individual measurements of food/water consumption, rats were distributed as 1 animal per cage. Animals were treated with 3 cycles by intraperitoneal route (5 ml/kg), of saline solution (0.9 % NaCl) (control) or MTX 2.5 mg/kg (MTX22 and MTX48) on day 0, 10, and 20, the MTX-treated groups reaching a total cumulative dose of 7.5 mg/kg on day 20. The dose was calculated taking into account previously pilot studies and the body surface area of the rats in order to correlate the dose in this species considering human top limit of the commonly used doses [5]. Thus, 2.5 mg/kg corresponds to 16 mg/m^2 of a rat weighing 240 g, being similar to the dose administered in humans and about one-tenth of the maximum dose allowed in humans (140 mg/m^2) [1]. The regimen of administration (1 cycle every 10 days) was performed aiming to simulate the human chemotherapeutic cycles. The interval of 10 days was defined taking into account the life cycle of the rat and the clinical conditions observed in pilot studies.

During the experiment, daily clinical evaluations of all animals were performed by the veterinary doctor of the team. The parameters evaluated were as follows: piloerection, dehydration, hemorrhage and diarrhea, motor function (tone and movement coordination), breathing (rate and depth, gasping), mucosal color (pale, cyanotic), and clinical signals of abdominal pain. The individual weight and consumption of food and water were also evaluated daily until day 30.

The MTX22 group was euthanized on day 22, in order to assess the MTX-induced cumulative damage 2 days after the last cycle of treatment. MTX48 group was euthanized on day 48, i.e., 28 days after the last cycle of treatment, in order to evaluate the late cumulative responses. Animals were anesthetized with xylazine/ketamine (10–100 mg/kg), and blood was collected through cardiac puncture. All the procedures were equally performed for control and treated rats.

Plasma Biochemical Analysis

Blood was collected into heparinized tubes. Plasma levels of aspartate aminotransferase (AST), CK, CK-MB, and lactate were evaluated in duplicate on an AutoAnalyzer (PRESTIGE® 24i, PZ Cormay S.A.) using the respective kits and following the manufacturer instructions.

Tissue Preparation for Light and Transmission Electron Microscopy

For light microscopy, heart (right and left ventricle) was sliced in 2–4 mm^3 pieces, approximately, and fixed in 4 % formaldehyde (10–20 h, 4 °C), which were further dehydrated with graded ethanol (Panreac, Barcelona, Spain) concentrations and mounted in paraffin (MERK, Darmstadt, Germany) following routine standard procedures. Semi-thin sections (5 µm) were cut in a microtome (Leica Microsystems, Model RM2125) and mounted on silane-coated slides (Sigma, S4651-72EA). After dewaxed in xylene and hydrated through graded alcohol concentrations, tissue sections were stained with haematoxylin–eosin (Atom Scientific Ltd, England) and analyzed under a light microscope coupled to a digital camera (Axio Imager A1, Carl Zeiss, Oberkochen, Germany).

For transmission electron microscopy, 1 mm^3 right and left ventricle pieces were fixed in 2 % glutaraldehyde (2 h, 4 °C), post-fixed with 2 % osmium tetroxide, dehydrated in graded ethanol and later embedded in Epon (TAAB 812 Resin, Kit Cat. No. T024), using routine standard procedures. Ultrathin (100 nm) sections obtained in an ultramicrotome (Reichert Ultracut) were mounted in copper grids (300 Mesh, from TAAB Laboratories Equipment Ltd, England) and further contrasted with uranyl acetate and lead citrate for transmission electron microscopy analysis (Zeiss EM 10A) at an accelerating voltage of 60 kV.

Isolation of Cardiac Mitochondria for the Evaluation of Complexes IV and V Activities and Cardiac Mitochondrial Content

Cardiac mitochondria from control and MTX-treated rats were isolated for the evaluation of in-gel activity of complexes IV and V and cardiac mitochondrial content. Hearts were minced with scissors in homogenization buffer [250 mM sucrose, 10 mM HEPES, 0.5 mM EGTA (pH 7.4)], supplemented with subtilpeptidase A type VIII (1 mg/g tissue). Following 10 min of incubation on ice, albumin fat-free was added to a final concentration of 10 mg/mL. The tissue was subsequently rinsed three times with buffer, homogenized with a tightly fitted Potter–Elvehjen homogenizer and Teflon pestle, and centrifuged (14,500*g*, 10 min, 4 °C). The resulting pellet was resuspended in homogenization buffer free of enzyme, homogenized, and centrifuged (750*g*, 10 min, 4 °C). Mitochondria-enriched pellet was obtained by centrifuging the resulting supernatant (12,500*g*, 20 min, 4 °C), washed twice, and then aliquoted for subsequent analysis [12]. Protein content was determined with RC DC Protein Assay kit (Bio-Rad, Hercules, CA, USA) using bovine serum albumin as standard.

Blue Native (BN)-PAGE Separation of Mitochondria Membrane Complexes

The BN-PAGE separation of mitochondrial membrane complexes was performed as already described [12] using 4 animals per group. Mitochondria (200 µg of protein) were pelleted by centrifugation (20,000*g*, 10 min, 4 °C) and then resuspended in solubilization buffer (50 mM NaCl, 50 mM imidazole, 2 mM 6-aminohexanoic acid, 1 mM EDTA pH 7.0) with 1 % (w/v) digitonin. After 10 min on ice, insoluble material was removed by centrifugation (20,000*g*, 20 min, 4 °C). Soluble components were combined with 0.5 % (w/v) Coomassie Blue G250, 50 mM ε-amino *n*-caproic acid, and 4 % (w/v) glycerol and separated on a 4–13 % gradient acrylamide gradient gel with 3.5 % sample gel on top. Anode buffer contained 25 mM imidazole pH 7.0. Cathode buffer (50 mM tricine and 7.5 mM imidazole pH 7.0) containing 0.02 % (w/v) Coomassie Blue G250 was used during 1 h at 70 V, the time needed for the dye front to reach approximately one-third of the gel. Cathode buffer was then replaced for one containing only 0.002 % (w/v) Coomassie Blue G250, and the native complexes were separated at 200 V for 4 h at 4 °C. A native protein standard HMW-native marker (GE Healthcare) was used. The gels were stained with Coomassie Colloidal for protein visualization and scanned with Gel Doc XR System (Bio-Rad, Hercules, CA, USA). Band detection, quantification, and matching were performed using QuantityOne Imaging software (v4.6.3, Bio-Rad). Mitochondrial DNA was quantified using the Qubit® dsDNA BR assay kit (Invitrogen, Carlsbad, CA, USA). Samples were read in a Qubit® 2.0 Fluorometer, and results were expressed as the ratio between the mitochondrial DNA concentration and the heart mass.

In-Gel Activity of Mitochondrial Complexes IV and V

The in-gel activity of complexes IV and V was determined using the methods described elsewhere [12]. Briefly, complex IV-specific heme stain in BN-PAGE gels was determined using 10-µL horse-heart cytochrome c (5 mM) and 0.5 mg DAB dissolved in 1 ml of 50 mM sodium-phosphate, pH 7.2. The reaction was stopped by 50 % (v/v) methanol and 10 % (v/v) acetic acid, and the gels were then transferred to water.

ATP hydrolysis activity of complex V was analyzed by incubating the native gels with 35 mM Tris, 270 mM glycine buffer, pH 8.3 at 37 °C, supplemented with 14 mM $MgSO_4$, 0.2 % (w/v), $Pb(NO_3)_2$, and 8 mM ATP. Lead phosphate precipitation is proportional to the enzymatic ATP hydrolysis activity. The reaction was stopped by incubation with 50 % (v/v) methanol for 30 min, and the gels were then transferred to water.

Gels were scanned with Gel Doc XR System (Bio-Rad, Hercules, CA, USA). Band quantification was performed using QuantityOne Imaging software (v4.6.3, Bio-Rad).

Determinations in the Cardiac Tissue

After the excision of hearts, they were washed in a phosphate-saline buffer solution (pH 7.4), dried, and weighted to assess the relative mass of the heart (calculated as a percentage of the total body weight on the day of euthanasia). Afterward, heart tissue samples were homogenized [1:4 (m/v)] in ice-cold phosphate buffer solution (pH 7.4), with an Ultra-Turrax® homogenizer and centrifuged (3,000*g*, 10 min, 4 °C). Aliquots were taken to determine the glutathione status, ATP levels, and total protein levels.

Total Glutathione (GSHt), GSH, and GSSG Levels in the Cardiac Tissue

An aliquot of the supernatant referred previously was added to an equal volume of $HClO_4$ 10 % (5 % as final concentration). Samples were again homogenized and centrifuged (16,000*g*, 10 min, 4 °C), and the supernatant was used to determinate the glutathione status [13]. The GSHt and GSSG levels were evaluated by the DTNB–GSSG reductase recycling assay, as previously described [14, 15]. Briefly, for GSHt quantification, 200 µL of supernatant was neutralized with 200 µL of 0.76 M $KHCO_3$ and centrifuged (16,000*g*, 5 min, 4 °C). For GSSG quantification, 10 µL of 2-vinylpyridine was added to 200 µL of acid supernatant and shaken during 1 h on ice prior to the neutralization step. In 96-well plates, 100 µL of sample, standard, or blank were added in triplicate and mixed with 65 µL of fresh reagent solution containing DTNB and β-NADPH. Plates were incubated at 30 °C for 15 min in a plate reader (PowerWaveX, Bio-Tek Instruments) prior to the addition of 40-µL glutathione reductase solution (10 U/mL). The final product of this reaction is a colored substance, and its formation was monitored for 3 min, at 415 nm, and compared with a standard curve. GSH and GSSG standard solutions were prepared in $HClO_4$ 5 % [15]. Results were expressed as nmol/mg protein.

Cardiac ATP Levels

An aliquot of supernatant obtained in "Determinations in the Cardiac Tissue" section was added to an equal volume of $HClO_4$ 10 % (5 % as final concentration). Samples were again homogenized and centrifuged (16,000*g*, 10 min, 4 °C), and the supernatant was used to determine the ATP levels as described before [8]. One hundred µL of tissue homogenate was neutralized with 100 µL of 0.76 M $KHCO_3$ and centrifuged (16,000*g*, 10 s, 4 °C). The ATP levels were quantified by the bioluminescence test after the reaction of 100-µL neutralized supernatant with luciferin/luciferase solution. ATP standards were prepared in 5 % $HClO_4$. ATP intracellular contents were normalized to the total protein content (nmol/mg of protein).

Cardiac Total Protein Quantification

An aliquot of the supernatant obtained in the "Determinations in the Cardiac Tissue" section was diluted in 0.3 M NaOH and was used to assess the total protein levels in the cardiac tissue. The protein levels were determined, by a procedure based in the Lowry method, spectrophotometrically (750 nm), and using a microplate reader as previously described [14, 16].

Evaluation of the Mitochondrial Membrane Potential After In Vivo and In Vitro Treatment with MTX

Cardiac mitochondria from control and MTX48 rats were isolated for the assessment of the late cumulative effects induced by MTX toward the mitochondrial membrane potential. Moreover, an in vitro study with mitochondria isolated from 4 untreated rat hearts (not treated with MTX), which were euthanized through cervical dislocation, was also performed in order to assess the direct MTX effects in the mitochondrial function after incubation with MTX (10 nM, 100 nM, and 1 µM).

Isolation of Cardiac Mitochondria

Hearts were minced with scissors in homogenization buffer (250 mM sucrose, 1 mM EGTA, HEPES–KOH 5 mM, pH 7.4, and 0.1 % fat-free bovine serum albumin) supplemented with 0.5 mg/g tissue of protease. Samples were homogenized using a Potter–Elvehjen homogenizer for 30 s. The suspension was then incubated on ice for 1 min, and the homogenization step was repeated for more 30 s. After centrifugation (11,000*g*, 10 min, 4 °C), the pellet was gently homogenized in the homogenization buffer and centrifuged (800*g*, 10 min, 4 °C). The obtained supernatant was centrifuged (12,000*g*, 10 min, 4 °C), and the mitochondria pellet was washed twice with homogenization buffer without EGTA and bovine serum albumin. Protein content was determined through the Biuret method.

Mitochondrial Transmembrane Potential Measurement

The mitochondrial membrane potential was measured using an ion-selective electrode to measure the distribution of the tetraphenylphosphonium (TPP^+), as described before [17]. The reference electrode used was a $Ag/AgCl_2$, and mitochondria (1 mg) were incubated with 1 ml respiratory medium (130 mM sucrose, 50 mM KCl, 2.5 mM KH_2PO_4, 5 mM HEPES, pH 7.4), supplemented with 2 µM TPP^+ and 1.5 mM rotenone, with constant stirring, at 25 °C. MTX (10 nM, 100 nM, or 1 µM) was added to the incubation chamber. Mitochondria were energized by adding 5 mM succinate [18]. The electrode was calibrated with TPP^+ assuming Nerstian distribution of the ion across the synthetic membrane. The mitochondrial membrane potential was expressed in mV.

Statistical Analysis

Results are presented as mean ± standard deviation. The evaluations of the rat relative body weight gain and the consumptions of food and water were followed daily; thus, the statistical analysis was performed using repeated measures ANOVA followed by the Student–Newman–Keuls post hoc test. In the other experiments, statistical comparisons between groups were performed with one-way ANOVA (in case of normal distribution) or Kruskal–Wallis test (one-way ANOVA on ranks—in case of not normal distribution). Significance was accepted at p values <0.05.

Results

Cumulative signs of Toxicity After MTX Treatment

On the day 22 (2 days after the last MTX cycle), 2 rats from the MTX22 group presented moderate piloerection. On the day 25 (5 days after the last MTX cycle), 3 animals from the group MTX48 showed moderate signals suggestive of toxicity, namely slight dehydration, cyanosis, and slight bleeding. In the following days, 1 of these animals fully recovered, but the other 2 died on the day 35. The 2 remaining rats from MTX48 group did not show any significant clinical alteration during all time course of the study. As it can be seen in the Fig. 1, animals treated with MTX started to decrease the relative body weight gain compared to control group since the second cycle of drug administration. These decreases were statistically significant after the third cycle, when the animals treated with

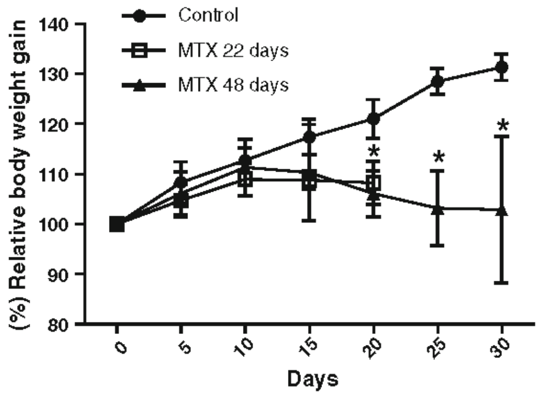

Fig. 1 Relative body weight (%) gain of the animals treated with MTX (3 cycles of 2.5 mg/kg) and control group. Results are presented as mean ± standard deviation. Statistical analysis was performed using repeated measures ANOVA followed by the Student–Newman–Keuls post hoc test (*$p < 0.05$ vs. control)

MTX reached a cumulative dose of 7.5 mg/kg, until the day 30. This change is indicative of toxicity, and it was not accompanied by significant alterations in food or water consumptions (data not shown).

Plasma Changes Induced by MTX Treatment

As demonstrated in Table 1, plasma biochemical analysis revealed a significant transient decrease in the CK levels in the MTX22 group when compared to MTX48 group and control group. Conversely, the CK-MB isoenzyme presented the same trend: a significant decrease in the MTX22 group versus control. Values similar to control levels were found in the MTX48 group. The plasma lactate levels significantly increased in the MTX48 group compared to MTX22 and control groups (Table 1). No significant changes were observed in the plasma AST levels in MTX-treated groups compared to control animals (data not shown).

Table 1 Plasma biochemical parameters of the animals treated with MTX (3 cycles of 2.5 mg/kg) and control group

Plasma biomarker	Group		
	Control	MTX22	MTX48
CK (U/L)	537.8 ± 195.6	326.5 ± 71.0*	441.3 ± 26.9 ns
CK/MB (U/L)	572.8 ± 125.9	390.3 ± 58.7*	595.6 ± 151.2 ns
Lactate (mmol/L)	1.3 ± 0.4	1.6 ± 0.3 ns	2.6 ± 1.7*

Results are presented as mean ± standard deviation. Statistical analysis was performed using one-way ANOVA followed by the Student–Newman–Keuls post hoc test (*$p < 0.05$ vs. control)

ns not significant

*$p < 0.05$ vs. control

Microscopic Changes in the Cardiac Structure After MTX Treatment

Structural and ultrastructural analysis from control group revealed a preserved cellular and tissue morphology (data not shown). However, as shown in the Fig. 2, in both MTX-treated hearts, light microscopy revealed dispersed cellular and interstitial edema, diffusion of inflammatory cells, and proliferation of connective tissue (A and B). In the MTX48 group, dispersed areas of a more intense proliferation of the connective tissue with abundant cellular infiltration, probably by fibroblasts, and signs of obstruction in some small caliber arteries (A and B) were seen. The transmission electron microscopy revealed edema of cardiomyocytes (C, D, and E), lysosome activation in the cardiomyocytes, proliferation of connective tissue (F and E) and fibroblasts, and occupation of the endothelial space by digiforme endothelial projections (C and E). In general, mitochondria showed clearly defined cristae, however, with abnormal orientations, but no signs of mitochondrial swelling were observed. Giant mitochondria with aberrant morphology (C, D, and E) were frequently interspaced with normal morphology and dimensions ones. Abundant collagen deposition in the interstitial space was frequently observed in MTX48 (D and E). It is important to refer that the cardiac damage shown in the histology was observed in both right and left ventricles, suggesting that both sides were equally affected by MTX. The sub-endocardial region was more affected compared to the sub-pericardial since the cellular edema and fibrosis were more pronounced in this region.

Cardiac Alterations Induced by MTX

The cardiac relative mass (%) was evaluated as an indicator of cardiotoxicity (Fig. 3). The animals, which were euthanized on the day 22 (MTX22), did not show any changes in the cardiac relative mass (0.27 ± 0.02 %) compared to control group (0.27 ± 0.03 %). However, the cardiac relative mass in the MTX48 group was significantly higher (0.33 ± 0.03 %) when compared to control or MTX22 group, evidencing a late cardiac response (Fig. 3). These changes in the cardiac relative mass were not accompanied by alterations in the cardiac total protein levels (data not shown). No significant changes in the GSHt, GSH, or GSSG cardiac levels were observed in any of the end time points (data not shown).

Isolated cardiac mitochondria were used to evaluate the activity of complexes IV and V of the mitochondrial respiratory chain of the treated rats. As shown in the Fig. 4a), the organization pattern of the five respiratory chain complexes is in accordance with the described in the literature for heart tissue [12]. No significant qualitative or

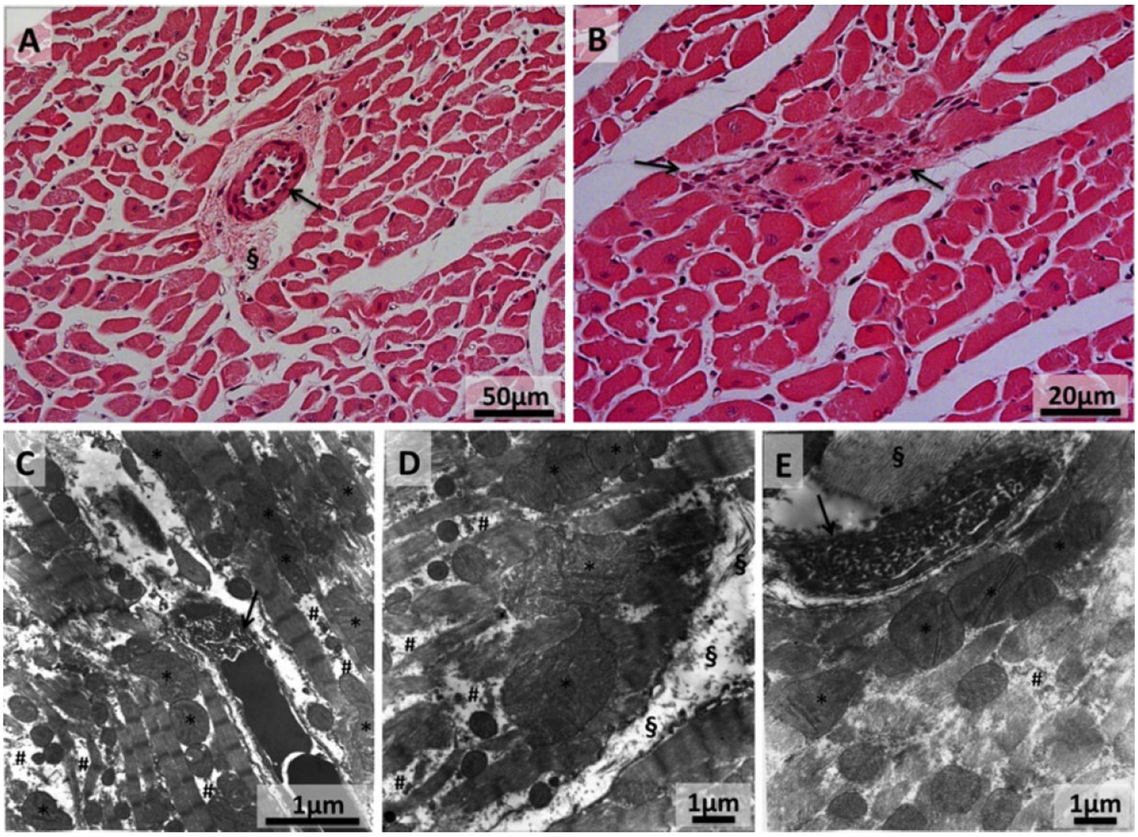

Fig. 2 Light (**a**, **b**) and electron micrographs (**c**, **d**, **e**) of heart tissue sections representative of the common structural and ultrastructural modifications observed in MTX-treated animals. In **a** (MTX48), it can be observed an arteriole, with its lumen partially obstructed (*arrow*), surrounded by an area of connective tissue (§); a general enlargement of the interstitial space with dispersed swollen cardiomyocytes (with increased inter-myofibril space) is also depicted. A focal area of fibrosis (*arrows*) with abundant cellular infiltration is shown in **b** (MTX48). At the ultrastructural level, an enlargement of inter-myofibril space (#) and several giant and/or aberrant mitochondria with abnormal cristae (*asterisk*) can be observed in **c** (MTX48), **d** (MTX48), and **e** (MTX48); capillaries with their lumen occupied by digiform structures are shown in **c** and **e** (*arrow*); interstitial collagen fibers are also illustrated in **d** and, with a special amount, in **e** (§). The figures refer to the *left ventricle*; however, similar cardiac changes were found in the *right ventricle*

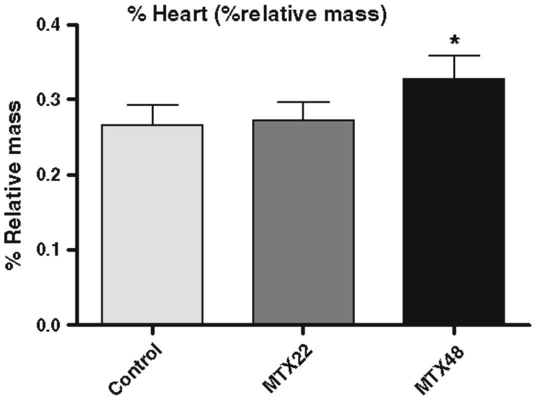

Fig. 3 Heart relative mass (%) of the animals treated with MTX (3 cycles of 2.5 mg/kg) and control group. Results are presented as mean ± standard deviation. Statistical analysis was performed using one-way ANOVA followed by the Student–Newman–Keuls post hoc test (*$p < 0.05$ vs. control)

quantitative differences in the band pattern were observed between groups in the BN-PAGE. The in-gel activity of complex IV revealed significantly higher activity level in the cardiac mitochondria from rats treated with MTX (155.8 ± 33.6 % for the MTX22 group, 148.3 ± 14.4 % for the MTX48 group *vs.* 100.0 ± 2.8 % for the control group) (Fig. 4b). Considering the complex V activity, a significant increase in MTX22 (172.6 ± 20.0 %) and a significant decrease in MTX48 (58.1 ± 21.0 %) were observed in comparison with the control (100.0 ± 8.3 %; Fig. 4c). Regarding cardiac ATP levels, a significant decrease in the MTX48 group (7.8 ± 1.5 nmol/mg) compared to control (16.0 ± 2.8 nmol/mg) or MTX22 (17.6 ± 6.7 nmol/mg) groups was observed, as demonstrated in the Fig. 5. However, no significant changes in the ratio between mitochondrial DNA concentration and heart mass were found (data not shown).

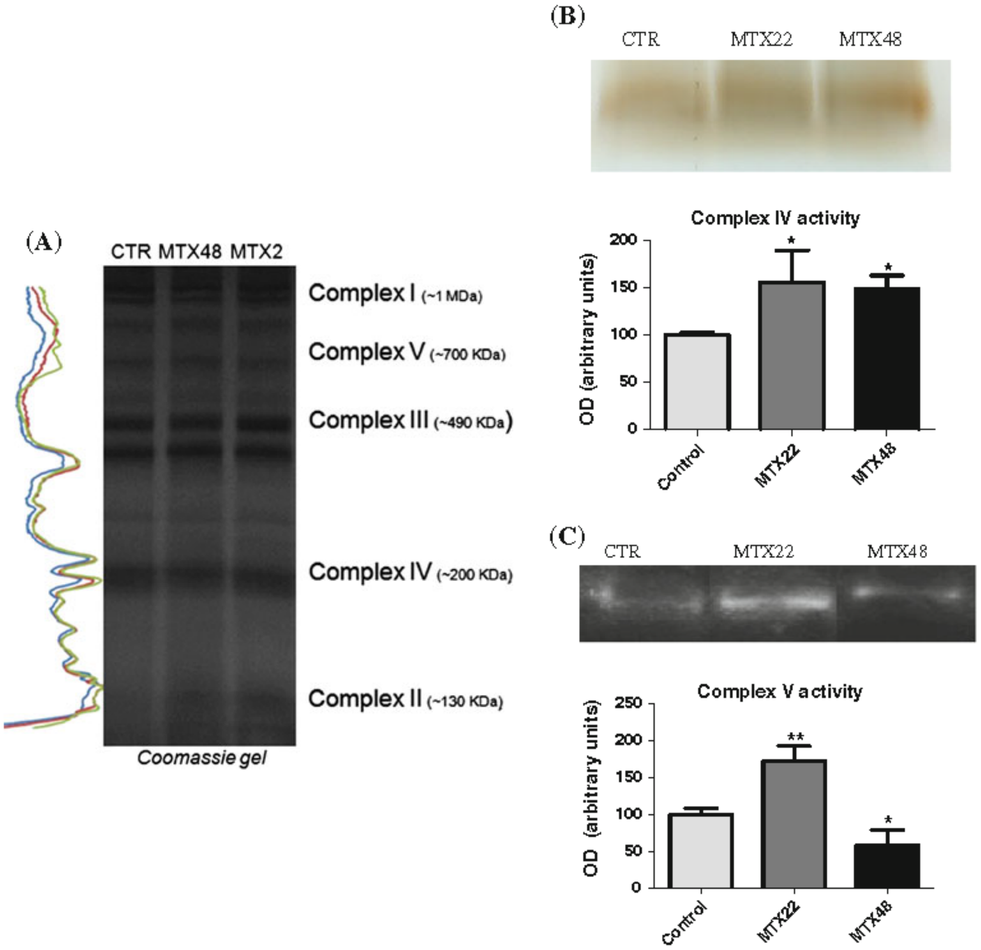

Fig. 4 **a** BN-PAGE profile of mitochondria isolated from control, MTX22, and MTX48 groups. An overlap of the density variation in the *lanes* of the 3 groups is presented on the left. **b** Representative image and graphic representation of histochemical staining of the in-gel activity of complex IV. **c** Representative image and graphic representation of histochemical staining of the in-gel activity of complex V. Results are presented as mean ± standard deviation. Statistical analysis was performed using Kruskal Wallis test (ANOVA on ranks) followed by the Student Newman Keuls post hoc test ($*p < 0.05$ vs. control)

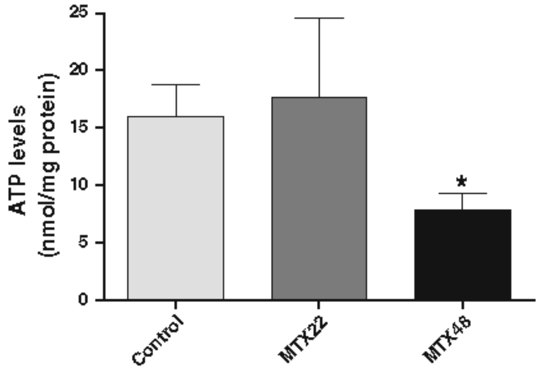

Fig. 5 Cardiac ATP levels of the animals treated with MTX (3 cycles of 2.5 mg/kg) and control group. Results are presented as mean ± standard deviation. Statistical analysis was performed using Kruskal Wallis test (ANOVA on ranks) followed by the Student Newman Keuls post hoc test ($*p < 0.05$ vs. control)

Evaluation of the Transmembrane Potential in Cardiac-Isolated Mitochondria

Transmembrane potential sustained by mitochondria upon energization is essential for mitochondrial function. Given the previously presented results found in vivo, we investigated the possible mitochondrial deleterious effect of MTX using cardiac mitochondria isolated from MTX48 group. Altogether, no significant changes in the TPP^+ assay were observed for the MTX48 mitochondria compared to control group. However, mitochondria from 2 animals presented an increased lag phase, demonstrating a difficulty to repolarize and sustain the mitochondrial potential (data not shown).

When mitochondria from untreated rats were incubated with 3 different MTX concentrations (10 nM, 100 nM, and 1 μM), energization phase (initial transmembrane potential, depolarization induced by the addition of ADP, repolarization, or lag phase) was not affected when compared to control (data not shown).

Discussion

In the present work, for the first time, the MTX-induced cumulative cardiotoxicity was ensued after the administration of reliable doses of MTX to rats evaluated at 2 different endpoints: 2 days after the last cycle of treatment (MTX22) and 28 days after the last MTX administration (MTX48). The cardiotoxicity of MTX was verified through the changes in the cardiac structure as showed by the transmission electron and optic microscopy (Fig. 2) and by the increases in the % of relative heart mass per body weight observed in the MTX48 group (Fig. 3). The major contribution of this study was to show, for the first time, the different effects on mitochondrial respiratory chain with similar MTX dose and schedule regime of administration in vivo when animals were euthanized at two distinct endpoints. It became evident that mitochondrial function alterations were more pronounced in the later time point, as seen by the presence of aberrant mitochondria, changes of mitochondrial complexes IV and V activities, and depletion of cardiac ATP levels all in MTX48 animals. On the other hand, in MTX22 rats, increases in mitochondrial complexes IV and V was observed with no significant alteration in cardiac ATP levels when compared to control rat hearts.

The in vivo model employed in the present work seems to be appropriate to study cumulative toxicity induced by MTX treatment, since it reproduced human clinical observations, such as the late development of cardiotoxicity. This is an important point regarding the difficulties to pharmacologically induce a heart failure condition in laboratory animal models [19].

Although clinical aspects of doxorubicin and MTX are partially the same, the underlying mechanisms seem to differ. In fact, the MTX-induced cardiotoxicity may have its origin in its interference with cardiac energetic metabolism instead of oxidative stress [8, 10, 11, 20, 21]. In the present study, no observed significant alterations in the cardiac glutathione levels (GSHt, GSH, and GSSG) were found, which is in accordance with our previous in vitro results [8]. Even so, significant changes in ATP levels were found in MTX48 group. The sequence of events in the establishment of a failing and energy-starved heart usually follows a time course, first with decreases in the phosphocreatine levels, followed by the creatine loss, and, ultimately, by ATP depletion [22]. Decreases in the total CK activity and CK-MB, as observed in the MTX22 group (Table 1), may be interpreted as a hallmark of the heart failure development [23]. However, all signaling pathways involved in CK alterations remain to be elucidated [23]. The development of late MTX-induced cardiotoxicity was characterized by the energetic depletion observed in the MTX48 group. It is well known that the loss of ATP in the failing myocardium is a slow and progressive phenomenon, only being detectable in the presence of a severe heart failure [22]. Plasma lactate levels increased in the MTX48 group in comparison with MTX22 and control levels (Table 1), and it was accompanied by depletion in the ATP cardiac levels and increase in the cardiac relative mass, suggesting a cardiac failure condition. Increased levels of plasma lactate, as observed in the MTX48 group (Table 1), are suggestive of lactic acidosis and occur in response to tissue hypoxia, uncoupling of oxidative phosphorylation, congestive heart failure, generalized cachexia (due to increased anaerobic glycolysis in the skeletal muscle), or in situations where the hepatic clearance is compromised [23, 24]. At MTX48, apparently, an energetic shift occurred, and the glycolytic pathway seems to be the major supplier of cardiac ATP, not being enough to warrant a healthy heart. In fact, when failing, the heart assumes the fetal pattern, switching the main energetic substrate source from fatty acids to glucose [23]. However, as efficiency of glucose oxidation is reduced, more lactate is generated [23], and the energetic impairment was evidenced by the depletion of the ATP cardiac levels in MTX48 rats (Fig. 5). In fact, it was described that failing human hearts have about 25–40 % less ATP than healthy hearts, and hearts in energetic starvation fail to support an increase in the workload [22, 25]. Indeed, the length of time that the heart can survive with such ATP depletion still remains unclear [22]. The energetic imbalance caused by MTX was already demonstrated in vitro, after incubation of MTX with cultured neonatal cardiomyocytes isolated from rats [9] and with H9c2 cells [8].

The late MTX-induced mitochondrial degeneration was also evidenced by aberrant mitochondrial morphology and subsequent functional studies. Microscopic changes in the cardiac mitochondrial architecture (namely cristolysis and swelling) were observed in vitro [26] and in vivo [10, 11] with MTX. In the present study, the mitochondrial cristae are well defined, but in many organelles, they are abnormally oriented, without signs of swelling. The mitochondrial morphologic changes are restricted to giant and aberrant aspect (Fig. 2). One hypothesis that could explain this finding is the MTX ability to intercalate into the DNA molecule causing double and single breaks and inhibiting DNA and RNA synthesis [27], which may compromise the mitochondrial turnover.

The activity of mitochondrial IV and V complexes was also evaluated in both time points. Increased levels of the complex IV activity were found (Fig. 4), while interestingly, when considering complex V, its activity increased in MTX22 group and decreased in the MTX48 (Fig. 4). At MTX22, increases in the activity of the complexes IV and V may be the result of a mitochondrial adaptation to produce more ATP in response to MTX toxic effects. Indeed, in the MTX22 group, no significant differences in the ATP cardiac content compared to control rats were observed (Fig. 5), showing at this time point that the increased activity of the mitochondrial complexes is sufficient to maintain ATP overall levels. However, about one month after the last MTX administration, despite the increase in the complex IV activity, a decrease in complex V activity was observed. In fact, MTX48 rats failed to support the cardiac ATP demand, as observed by decreased cardiac overall ATP levels (Fig. 5). To the best of our knowledge, these results were evidenced for the first time in vivo and were corroborated in vitro (using H9c2 cells) by our research group on ATP-synthase activity using low MTX levels [8]. Conversely, a reduction in the electron transfer activity of state III and a concomitant uncoupling of oxidative phosphorylation were already observed in cardiac mitochondria isolated from MTX-treated female rats (2 mg/kg, twice a week, for 4 weeks) [11]. ATP decreased levels can be associated with an inhibited ATP synthesis inhibition (as suggested in this work by the late decreases in the complex V activity), but changes in the ATP levels in the failing myocardium can also be related to the loss of total tissue purines [25], whose levels were not evaluated in the present work.

The mitochondrial effects herein demonstrated in vivo were not observed by the direct incubation of MTX with cardiac mitochondria isolated from untreated rats. The cardiac mitochondria incubated with MTX did not show any change in the mitochondrial functionality evaluated by the distribution of TPP^+ assay. As already stated, MTX metabolism exerts a pivotal role to the MTX-induced toxicity [7]. Thus, the direct toxic effect mediated by MTX may be residual and insufficient to elicit significant alterations in this in vitro model without previous biotransformation. Moreover, when cardiac mitochondria were isolated from MTX-treated rats and subjected to the TPP^+ assay, remarkable heterogeneous results were seen: some animals had fully functional mitochondria, and others presented mitochondria with prolonged lag phase (data not shown). Hence, these data are suggestive that the MTX metabolism seems to be decisive to the toxicity induced by MTX, and differences in the metabolic rate might be behind the intersubject variability observed in the clinical evaluations presented in this work and in human MTX therapy.

In summary, it was demonstrated that MTX induces a relevant cumulative mitochondriopathy evidenced by several indicators of mitochondrial damage: MTX causes aberrant mitochondria and interferes in vivo with the mitochondrial functionality causing an imbalance in the mitochondrial function that results in late ATP depletion and, consequently, a dysfunctional heart. After depletion of its energetic content, the cardiac performance is impaired. Hence, this study highlights the relevance of the MTX-induced mitochondrial toxicity to the MTX-related cardiomyopathy.

Acknowledgments This work was supported by the Fundação para a Ciência e Tecnologia (FCT)—project (EXPL/DTP-FTO/0290/2012)—QREN initiative with EU/FEDER financing through COMPETE—Operational Programme for Competitiveness Factors. LGR, VMC, and RJD-O thank FCT for their PhD Grant (SFRH/BD/63473/2009) and Post-doc Grants (SFRH/BPD/63746/2009) and (SFRH/BPD/36865/2007), respectively. The authors are grateful to Fundação para a Ciência e Tecnologia for grant no. Pest C/EQB/LA0006/2011.

References

1. Seiter, K. (2005). Toxicity of the topoisomerase II inhibitors. *Expert Opinion on Drug Safety, 4*, 219–234.
2. Kingwell, E., Koch, M., Leung, B., Isserow, S., Geddes, J., Rieckmann, P., et al. (2010). Cardiotoxicity and other adverse events associated with mitoxantrone treatment for MS. *Neurology, 74*, 1822–1826.
3. Avasarala, J. R., Cross, A. H., Clifford, D. B., Singer, B. A., Siegel, B. A., & Abbey, E. E. (2003). Rapid onset mitoxantrone-induced cardiotoxicity in secondary progressive multiple sclerosis. *Multiple Sclerosis, 9*, 59–62.
4. Canal, P., Attal, M., Chatelut, E., Guichard, S., Huguet, F., Muller, C., et al. (1993). Plasma and cellular pharmacokinetics of mitoxantrone in high-dose chemotherapeutic regimen for refractory lymphomas. *Cancer Research, 53*, 4850–4854.
5. Ehninger, G., Schuler, U., Proksch, B., Zeller, K. P., & Blanz, J. (1990). Pharmacokinetics and metabolism of mitoxantrone. A review. *Clinical Pharmacokinetics, 18*, 365–380.
6. Batra, V. K., Morrison, J. A., Woodward, D. L., Siverd, N. S., & Yacobi, A. (1986). Pharmacokinetics of mitoxantrone in man and laboratory animals. *Drug Metabolism Reviews, 17*, 311–329.
7. Rossato, L., Costa, V. M., De Pinho, P., Freitas, V., Viloune, L., Bastos, M., et al. (2013). The metabolic profile of mitoxantrone and its relation with mitoxantrone-induced cardiotoxicity. *Archives of Toxicology, 10*, 1809–1820. doi:10.1007/s00204-013-1040-6.
8. Rossato, L. G., Costa, V. M., Villas-Boas, V., de Lourdes Bastos, M., Rolo, A., Palmeira, C., et al. (2013). Therapeutic concentrations of mitoxantrone elicit energetic imbalance in H9c2 cells as an earlier effect. *Cardiovascular Toxicology*. doi:10.1007/s12012-013-9224-0.
9. Shipp, N. G., Dorr, R. T., Alberts, D. S., Dawson, B. V., & Hendrix, M. (1993). Characterization of experimental mitoxantrone cardiotoxicity and its partial inhibition by ICRF-187 in cultured neonatal rat heart cells. *Cancer Research, 53*, 550–556.
10. Alderton, P. M., Gross, J., & Green, M. D. (1992). Comparative study of doxorubicin, mitoxantrone, and epirubicin in combination with ICRF-187 (ADR-529) in a chronic cardiotoxicity animal model. *Cancer Research, 52*, 194–201.
11. Bachmann, E., Weber, E., & Zbinden, G. (1987). Effect of mitoxantrone and doxorubicin on energy metabolism of the rat heart. *Cancer Treatment Reports, 71*, 361–366.

12. Padrão, A. I., Ferreira, R. M. P., Vitorino, R., Alves, R. M. P., Neuparth, M. J., Duarte, J. A., et al. (2011). OXPHOS susceptibility to oxidative modifications: The role of heart mitochondrial subcellular location. *Biochimica et Biophysica Acta, 1807*, 1106–1113.
13. Pontes, H., Duarte, J. A., De Pinho, P. G., Soares, M. E., Fernandes, E., Dinis-Oliveira, R. J., et al. (2008). Chronic exposure to ethanol exacerbates MDMA-induced hyperthermia and exposes liver to severe MDMA-induced toxicity in CD1 mice. *Toxicology, 252*, 64–71.
14. Rossato, L. G., Costa, V. M., De Pinho, P. G., Carvalho, F., Bastos, M. L., & Remião, F. (2011). Structural isomerization of synephrine influences its uptake and ensuing glutathione depletion in rat-isolated cardiomyocytes. *Archives of Toxicology, 85*, 929–939.
15. Barbosa, D. J., Capela, J. P., Oliveira, J. M., Silva, R., Ferreira, L. M., Siopa, F., et al. (2012). Pro-oxidant effects of ecstasy and its metabolites in mouse brain synaptosomes. *British Journal of Pharmacology, 165*, 1017–1033.
16. Lowry, O., & Rosebrough, N. (1951). Protein measurement with the Folin phenol reagent. *Journal of Biological Chemistry, 193*, 265–272.
17. Rolo, A. P., Oliveira, P. J., Moreno, A. J., & Palmeira, C. M. (2000). Bile acids affect liver mitochondrial bioenergetics: Possible relevance for cholestasis therapy. *Toxicological Sciences, 57*, 177–185.
18. Duarte, F. V., Simões, A. M., Teodoro, J. S., Rolo, A. P., & Palmeira, C. M. (2011). Exposure to dibenzofuran affects lung mitochondrial function in vitro. *Toxicology Mechanisms and Methods, 21*, 571–576.
19. Patten, R. D., & Hall-Porter, M. R. (2009). Small animal models of heart failure: Development of novel therapies, past and present. *Circulation, 2*, 138–144.
20. Novak, R. F., & Kharasch, E. D. (1985). Mitoxantrone: Propensity for free radical formation and lipid peroxidation-implications for cardiotoxicity. *Investigational New Drugs, 3*, 95–99.
21. Kharasch, E. D., & Novak, R. F. (1983). Inhibitory effects of anthracenedione antineoplastic agents on hepatic and cardiac lipid peroxidation. *Journal of Pharmacology and Experimental Therapeutics, 226*, 500–506.
22. Ingwall, J. S., & Weiss, R. G. (2004). Is the failing heart energy starved? On using chemical energy to support cardiac function. *Circulation Research, 95*, 135–145.
23. Ventura-Clapier, R., Garnier, A., & Veksler, V. (2004). Energy metabolism in heart failure. *Journal of Physiology, 555*, 1–13.
24. Luft, F. C. (2001). Lactic acidosis update for critical care clinicians. *Journal of the American Society of Nephrology, 12*, S15–S19.
25. Dzeja, P. P., Redfield, M. M., Burnett, J. C., & Terzic, A. (2000). Failing energetics in failing hearts. *Current Cardiology Reports, 2*, 212–217.
26. Kluza, J., Marchetti, P., Gallego, M.-A., Lancel, S., Fournier, C., Loyens, A., et al. (2004). Mitochondrial proliferation during apoptosis induced by anticancer agents: Effects of doxorubicin and mitoxantrone on cancer and cardiac cells. *Oncogene, 23*, 7018–7030.
27. Khan, S. N., Lai, S. K., Kumar, P., & Khan, A. U. (2010). Effect of mitoxantrone on proliferation dynamics and cell cycle progression. *Bioscience Reports, 30*, 375–381.

Manuscript IV

Cumulative mitoxantrone-induced haematologic and hepatic adverse effects in a sub-chronic *in vivo* model

Rossato, L., Costa, V., Dallegrave, E., Arbo, M., Dinis-Oliveira, R.J., Silva, A., Duarte, J.A., Bastos, M.L., Palmeira, C., Remião, F

Basic Clin Pharmacol Toxicol 2013 *In Press.* DOI: 10.1111/bcpt.12143

Basic & Clinical Pharmacology & Toxicology

Basic & Clinical Pharmacology & Toxicology Doi: 10.1111/bcpt.12143

Cumulative Mitoxantrone-Induced Haematological and Hepatic Adverse Effects in a Subchronic *In vivo* Study

Luciana G. Rossato[1], Vera M. Costa[1], Eliane Dallegrave[1,2], Marcelo Arbo[1], Ricardo J. Dinis-Oliveira[1,3,4], Alice Santos-Silva[5], José A. Duarte[6], Maria de Lourdes Bastos[1], Carlos Palmeira[7] and Fernando Remião[1]

[1]REQUIMTE, Toxicology Laboratory, Biological Sciences Department, Faculty of Pharmacy, University of Porto, Porto, Portugal, [2]Federal University of Health Sciences from Porto Alegre, Porto Alegre, Brazil, [3]Department of Legal Medicine, Faculty of Medicine, University of Porto, Porto, Portugal, [4]Department of Sciences, Advanced Institute of Health Sciences - North, CESPU, CRL, Gandra, Portugal, [5]Institute of Molecular and Celular Biology & Laboratory of Biochemistry, Biological Sciences Department, Faculty of Pharmacy, University of Porto, Porto, Portugal, [6]CIAFEL, Faculty of Sport Sciences and Physical Education, University of Porto, Porto, Portugal and [7]Center for Neurosciences and Cell Biology, University of Coimbra, Coimbra, Portugal

(Received 5 July 2013; Accepted 10 September 2013)

Abstract: Mitoxantrone (MTX) is an antineoplastic agent that can induce hepato- and haematotoxicity. This work aimed to investigate the occurrence of cumulative early and late MTX-induced hepatic and haematological disturbances in an *vivo* model. A control group and two groups treated with three cycles of 2.5 mg/kg MTX at days 0, 10 and 20 were formed. One of the treated groups suffered euthanasia on day 22 (MTX22) to evaluate early MTX toxic effects, while the other suffered euthanasia on day 48 (MTX48), to allow the evaluation of MTX late effects. An early immunosuppression with a drop in the IgG levels was observed, causing a slight decrease in the plasma total protein content. The early bone marrow depression was followed by signs of recovery in MTX48. The genotoxic potential of MTX was demonstrated by the presence of several micronuclei in MTX22 leucocytes. Increases in plasma iron and cholesterol levels in the MTX22 rats were observed, while in both groups increases in the unconjugated bilirubin, C4 complement, and decreases in the triglycerides, alanine aminotransferase, alkaline phosphatase and transferrin were found in plasma samples. On MTX 48, the liver histology showed more hepatotoxic signs, the hepatic levels of reduced and oxidized glutathione were increased, and ATP hepatic levels were decreased. However, the hepatic total protein levels were decreased only in the livers of MTX22 group. Results demonstrated the MTX genotoxic effects, haemato- and direct hepatotoxicity. While the haematological toxicity is ameliorated with time, the same was not observed in the hepatic injury.

Mitoxantrone (MTX) is an anticancer and immunosuppressive drug that has been used in the treatment of tumours such as acute leukaemia, lymphoma, prostatic and breast cancer [1] and in the active forms of relapsing-remitting or secondary progressive multiple sclerosis [2]. MTX acts as an intercalating agent that causes double breaks in DNA by stabilization of a complex formed between DNA and topoisomerase II [1,3]. The regimen of MTX administration varies depending on disease progression and the clinical condition of the patient. Additionally, MTX is a substrate of membrane efflux pumps, namely the transporter breast cancer resistance protein (BCRP), which could interfere in MTX biodisposition [4]. However, the doses commonly employed range between 12 14 mg/m^2 and the maximum recommended cumulative dose is 140 mg/m^2 [1].

One of the most serious adverse events related to MTX therapy is the late and irreversible cardiotoxicity [1], whose underlying mechanisms have been studied by us [5 7]. It is known that cardiotoxic drugs such as MTX can cause acute liver failure as a result of a primary congestive heart failure with low cardiac output and consequent reduced hepatic blood flow [8]. However, the precise origin of liver failure, due to a direct effect or secondary to the cardiomyopathy, is not easy to define, because clinical signs of cardiac decompensating can be undetected in a first moment delaying the diagnosis [8]. Additionally, MTX has been considered more hepatotoxic than other antineoplastic agents such as doxorubicin [9].

In human beings, the MTX-induced hepatotoxicity manifests as transient increases in the serum bilirubin concentration and in the activity of hepatic enzymes, occurring in about 15% of treated patients (12 mg/m^2) [2,10]. Indeed, the inhibition of CYP450 metabolism in HepG2 cells and rat isolated hepatocytes prevented the MTX cytotoxicity [11], demonstrating the relevance of MTX oxidative metabolism to its noxious effects. MTX has at least one pharmacologically and toxicologically relevant metabolite, naphthoquinoxaline (the 8, 11-dihydroxy-4-[2-hydroxyethyl]-6-[[2-[[2-hydroxyethyl]amino] ethyl]amino]-1,2,3,4,7,12-hexahydronaphto-[2,3]-quinoxaline-7-12-dione), which has proven antitumour effects and has been related to MTX toxicity [5,10]. Recently, we demonstrated that, as it happens with MTX, the naphthoquinoxaline metabolite also distributes to highly perfused tissues and accumulates in organs such as liver and heart in rats [5]. The liver is subjected to a prolonged exposure to MTX and, possibly, to

---

Author for correspondence: Luciana G. Rossato and Fernando Remião, REQUIMTE, Departamento de Toxicologia, Faculdade de Farmácia, Universidade do Porto, Rua Jorge Viterbo Ferreira, 228, 4050-313 Porto, Portugal (fax +351 226 093 390, e-mails: luciana.g.rossato@gmail.com and remiao@ff.up.pt).

© 2013 Nordic Pharmacological Society. Published by John Wiley & Sons Ltd

this toxic metabolite that may contribute to its direct hepatotoxicity.

Haematological parameters should be monitored during therapy and the occurrence of neutropenia and thrombocytopenia can limit the dose administered or obligate the cessation of MTX therapy [1,12], demonstrating the haematological effects induced by MTX. The late haematological effects of MTX involves the development of MTX-associated leukaemia, which is also related to other topoisomerase II inhibitors [1].

Considering that the occurrence of liver dysfunction, as well as MTX-induced haematological toxicity in the treatment of complex diseases such as cancer and multiple sclerosis, can compromise the therapy [13], this work aimed to characterize the potential hepatotoxicity and haematological toxicity after therapeutic doses of MTX administration in male Wistar rats in 2 experimental settings. Animals were subjected to 3 cycles of 2.5 mg/kg MTX (cumulative dose of 7.5 mg/kg, which corresponds to 48 mg/m^2 by the allometric relationship). The toxic effects were evaluated 48 hr (day 22) after the last administration to assess immediate toxicity and also 28 days after the last administration (day 48) to determine whether the effects were cumulative or whether adaptation responses occurred in the hepatic tissue and blood.

Materials and Methods

Chemicals. All chemicals and reagents were of analytical grade. MTX hydrochloride, reduced glutathione (GSH), oxidized glutathione (GSSG), glutathione reductase (GR, EC 1.6.4.2), 2-vinylpyridine, reduced β-nicotinamide phosphate adenine dinucleotide (β-NADPH), 5,5-dithio-bis(2-nitrobenzoic acid) (DTNB), luciferin and luciferase were purchased from Sigma-Aldrich (St. Louis, MO, USA). Perchloric acid ($HClO_4$) was obtained from Merck (Darmstadt, Germany). The reagents for biochemical analyses were purchased from PZ Cormay S.A.

Animals. Adult male Wistar rats (Charles River Laboratories, Barcelona, Spain) weighing 240–300 g were used. The animals were housed in individual cages, in a temperature- and humidity-controlled environment and acclimated for 1 week prior to the study. Food and water were provided *ad libitum*, and animals were subjected to a 12-hr light/dark cycle. Animal experiments were approved by the Ethical Committee of Faculty of Pharmacy of the University of Porto (protocol number 09/04/2013). Housing and experimental treatment of the animals were in accordance with the Guide for the Care and Use of Laboratory Animals from the Institute for Laboratory Research. The experiments complied with current Portuguese laws.

Dose regimen. Animals were divided into three groups (five animals per group): control, MTX22 and MTX48. Animals were treated with three administrations, 5 mL/kg, intraperitoneal, of saline solution (0.9% NaCl) (control) or MTX 2.5 mg/kg (MTX22 and MTX48) on days 0, 10 and 20. The MTX-treated groups reached a total cumulative dose of 7.5 mg/kg on day 20. Animals belonging to the MTX22 group suffered euthanasia on day 22, to evaluate the early MTX-induced cumulative damage (i.e. 2 days after the last cycle of treatment). Animals from the MTX48 group suffered euthanasia on day 48, corresponding to 28 days after the last administration, to evaluate late cumulative responses [6]. Two animals of control group suffered euthanasia on day 22 and the others on day 48.

The used dose of MTX is clinically realistic (2.5 mg/kg corresponds to 16 mg/m^2 of a rat weighing 240 g, being similar to the dose administered in human beings and about one-tenth of the maximum dose recommended in human beings). The regimen of administration (one administration every 10 days) was scheduled aiming to simulate the human chemotherapeutic cycles. The interval of 10 days was defined considering the life cycle of the rat and the clinical conditions noted in pilot studies.

Euthanasia was performed under anaesthesia with xylazine/ketamine (10 mg/kg and 100 mg/kg), and blood was collected through cardiac puncture. A necropsy was performed to all animals.

Plasma biochemical analysis. On the day of euthanasia, blood was collected into heparinized tubes to perform biochemical analysis and into EDTA tubes to the haematological evaluations. Plasma levels of albumin, total proteins, IgG, IgM, IgE, C3 and C4 complement, total and conjugated bilirubin, alanine aminotransferase (ALT), alkaline phosphatase, transferrin, ferritin, iron, cholesterol, triglycerides, glucose, amylase, creatinine, urea, uric acid, potassium sodium, calcium, C-reactive protein, α_1-antitrypsin, δ-glutamyltranspeptidase (GGT) and lactate dehydrogenase (LDH) were evaluated in duplicate on an AutoAnalyzer (PRESTIGE® 24i, PZ Cormay S.A.) using the respective kits and following the manufacturer instructions.

Haematological analysis. Whole blood samples (collected using EDTA as anticoagulant) were used to evaluate erythrocyte count, haemoglobin (Hb) concentration, haematocrit, haematological indexes – mean cell volume (MCV), mean cell haemoglobin (MCH), mean cell haemoglobin concentration (MCHC), red cell distribution width (RDW), platelet count (PLT), plateletcrit (PCT), platelet distribution width (PDW), mean platelet volume (MPV) and total white blood cell (WBC) count, using an automated blood cell counter (Sysmex K1000, Hamburg, Germany). Differential leucocyte count was performed on blood smears stained according to Wright [14]. Reticulocyte count was performed by microscopic counting on blood smears after vital staining with new methylene blue (Reticulocyte stain; Sigma-Aldrich).

Tissue preparation for light and transmission electron microscopy. For light microscopy analysis, pieces of 2–4 mm^3 from all liver lobes were fixed in 4% formaldehyde during 24 hr. The pieces were further dehydrated with graded ethanol (Panreac, Barcelona, Spain) and included in paraffin blocks (MERCK) after standard procedures. Semithin sections (5 μm) were cut (Leica Microsystems, Model RM2125) and mounted on silane-coated slides (Sigma-Aldrich). After dewaxed in xylene and hydrated through graded alcohol concentrations, tissue sections were stained with haematoxylin-eosin (Atom Scientific Ltd, Manchester, UK) and analysed under a light microscope coupled to a digital camera (Axio Imager A1; Carl Zeiss, Oberkochen, Germany).

For transmission electron microscopy, 1 mm^3 tissue pieces from all liver lobes were fixed in 2% glutaraldehyde, post-fixed with 2% osmium tetroxide, dehydrated in graded ethanol, and later embedded in Epon (TAAB 812 Resin, Kit Cat. No. T024) according to standard procedures. Ultrathin (100 nm) sections obtained in an ultra microtome (Reichert Ultracut) were mounted in copper grids (300 Mesh; from TAAB Laboratories Equipment Ltd, West Berkshire, UK) and further contrasted with uranyl acetate and lead citrate for analysis at an accelerating voltage of 60 Kv (Zeiss EM 10A; Carl Zeiss).

Biochemical determinations in the hepatic tissue. After the excision from each animal, the liver was washed in a phosphate-buffered saline solution, pH 7.4, dried and weighed to assess the relative mass of the organ (calculated as a percentage of the total body-weight on the day of euthanasia). Liver samples were homogenized [1:4 (m/v)] in ice-cold phosphate-buffered solution, pH 7.4, with an Ultra-Turrax®

© 2013 Nordic Pharmacological Society. Published by John Wiley & Sons Ltd

homogenizer and centrifuged (3000 × *g*, 10 min., 4°C). Aliquots of the supernatant were taken to determine the glutathione status, ATP levels and total protein levels.

Total glutathione (GSHt), GSH and GSSG levels in the hepatic tissue. An aliquot of previous supernatant was added to an equal volume of $HClO_4$ 10% (5% final concentration). Samples were again homogenized, centrifuged (16 000 × *g*, 10 min., 4°C), and the supernatant was used to determine the glutathione status [15]. The GSHt and GSSG levels were evaluated by the DTNB-GSSG reductase recycling assay, as previously described [16,17]. Briefly, for GSHt quantification, 200 μL of the acidic supernatant was neutralized with 200 μL of 0.76 M $KHCO_3$ and centrifuged (16 000 × *g*, 5 min., 4°C). For GSSG quantification, 10 μL of 2-vinylpyridine was added to 200 μL of acidic supernatant, and the samples were shaken during 1 hr on ice prior to the neutralization step. In 96-well plates, 100 μL of sample, standard or blank was added in triplicate and mixed with 65 μL of fresh reagent solution containing DTNB and β-NADPH. Plates were incubated at 30°C for 15 min. in a plate reader (PowerWaveX; Bio-Tek Instruments, Winooski, VT, USA) prior to the addition of 40 μL glutathione reductase solution (10 U/mL). The final product of this reaction is a coloured substance, and its formation was monitored for 3 min., at 415 nm, and compared with a standard curve. GSH and GSSG standard solutions were prepared in $HClO_4$ 5% [15]. Results were expressed as nmol/mg protein.

Hepatic ATP levels. An aliquot of the supernatant obtained as described above was added to an equal volume of $HClO_4$ 10% (5% final concentration). Samples were again homogenized, centrifuged (16 000 × *g*, 10 min., 4°C), and the supernatant was used to determine the ATP levels as described before [6]. One hundred microliter of tissue homogenate was neutralized with 100 μL of 0.76 M $KHCO_3$ and centrifuged (16 000 × *g*, 10 sec., 4°C). The ATP levels were quantified by the bioluminescence test after the reaction of 100 μL neutralized supernatant with luciferin/luciferase solution. ATP standards were prepared in 5% $HClO_4$. ATP intracellular levels were normalized to total protein content (nmol/mg of protein).

Hepatic total protein quantification. An aliquot of the supernatant obtained after centrifugation described in the section '*Biochemical determinations in the hepatic tissue*' was diluted in 0.3 M NaOH and used to assess the total hepatic protein levels. The protein levels were determined by the Lowry method using a microplate reader (750 nm), as previously described [16].

Statistical analysis. Results are presented as means ± standard deviation. Statistical comparisons between groups were performed with one-way ANOVA (in case of normal distribution: haematological and plasma biomarkers) or the Kruskal–Wallis test (one-way ANOVA on ranks – in case of not normal distribution: hepatic protein levels, hepatic glutathione levels and ATP levels). Significance was accepted at p values < 0.05. Details of statistical analysis are found in the legend of the figures in the results section.

Results

Plasma and haematological changes induced by MTX cumulative doses.

The results from plasma and haematological biomarkers at the end of the experiment which presented significant changes (in at least one of the treated groups) compared with control rats, are shown in Table 1. A transient decrease in total protein and IgG plasma levels was observed in the MTX22 group. Transient decreases in RBC count, HCT, Hb, WBC and reticulocytes were evident in the MTX22 group. The leucocyte group

Table 1.
Plasma and haematological parameters of the animals treated with MTX (three cycles of 2.5 mg/kg) and control group.

	Groups		
Parameter	Control	MTX22	MTX48
Total proteins (g/dL)	56.8 ± 3.3	48.3 ± 4.9*	52.4 ± 2.1
IgG	48.6 ± 19.9	10.2 ± 6.5**	32.0 ± 13.9
Complement C4 (mg/dL)	2.4 ± 0.9	4.8 ± 0.5**	3.7 ± 0.6*
Conjugated bilirubin (mg/dL)	0.10 ± 0.02	0.07 ± 0.02*	0.06 ± 0.02*
ALT (U/L)	34.8 ± 7.4	13.0 ± 5.3**	19.5 ± 5.0**
Alkaline phosphatase (U/L)	278.6 ± 61.0	133.2 ± 54.9**	149.0 ± 35.8**
Cholesterol (mg/dL)	44.6 ± 2.8	65.28 ± 11.3**	52.47 ± 7.6
Triglycerides (mg/dL)	93.8 ± 9.9	40.6 ± 7.28***	64.3 ± 19.5*
Iron (μg/dL)	176.9 ± 27.8	250 ± 27.0**	169.7 ± 14.3
Transferrin (mg/dL)	105.2 ± 5.2	73.6 ± 17.0**	82.7 ± 15.5*
RBC ($\times 10^6$/mm^3)	7.8 ± 0.9	6.0 ± 1.0*	6.6 ± 0.6
Haematocrit (%)	43.78 ± 4.9	32.7 ± 5.5*	43.7 ± 3.2
Hb(g/dL)	14.6 ± 1.1	11.4 ± 1.8**	14.4 ± 0.7
MCH (pg)	18.8 ± 0.9	19.1 ± 0.3	22.1 ± 1.2***
RDW (%)	12.5 ± 0.4	12.9 ± 0.9	17.9 ± 1.1***
MCV (fL)	56.2 ± 1.1	54.5 ± 1.3	66.3 ± 2.1***
Platelet ($\times 10^3$/mm^3)	599.4 ± 79.24	592.0 ± 246.2	785.0 ± 74.0
MPV (fL)	7.4 ± 0.4	8.4 ± 1.0*	6.9 ± 0.4
Reticulocytes (%)	1.6 ± 0.5	0.0 ± 0.0**	2.9 ± 0.6**
WBC ($\times 10^3$/mm^3)	2.8 ± 1.3	1.6 ± 0.8*	2.3 ± 0.7

Results are presented as means ± standard deviation.
Statistical analysis was performed using one-way ANOVA followed by the Student Newman Keuls *post hoc* test (*$p < 0.05$ *versus* control, **$p < 0.01$ *versus* control, ***$p < 0.001$ *versus* control).

© 2013 Nordic Pharmacological Society. Published by John Wiley & Sons Ltd

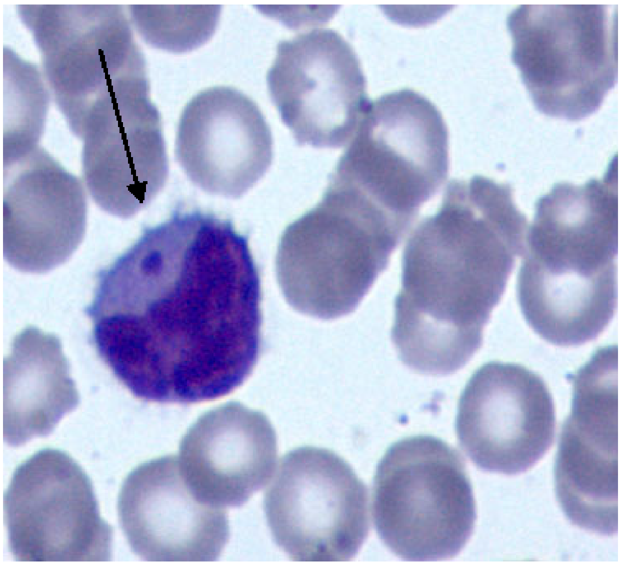

Fig. 1. Representative blood smears from the MTX22 group, demonstrating a monocyte with the presence of a micronucleus (arrow).

that mostly contributed to this decrease were lymphocytes (diminished in both groups). Additionally, increased levels of MPV were observed in the MTX22 group and microscopic analysis of the blood smears from the MTX22 group revealed the presence of several nucleated cells with micronucleus for all the animals (Fig. 1). Transient bone marrow suppression was observed in the MTX22 group, as shown by the absence of circulating reticulocytes. However, in MTX48, a recovery was observed and circulating reticulocytes were significantly higher than controls, representing an adaptation process to MTX exposure (Table 1).

A significant increase in the C4 complement and reduced levels of transferrin, conjugated bilirubin, ALT and alkaline phosphatase were evident in both treated groups. The MTX48 group had significant increases in the MCH, RDW and MCV levels, while WBC returned to control levels at MTX48.

Glucose, amylase, albumin, creatinine, urea, uric acid, calcium, potassium, sodium, C-reactive protein, α_1-antitrypsin, GGT, C3 complement, LDH, total bilirubin and IgM, and IgE plasma levels in the treated animals did not show any changes in comparison with control levels (data not shown). PLT, PCT, MCHC, platelet distribution width, neutrophil, eosinophil, basophil and monocytes levels remained constant in all groups at the time-points evaluated.

MTX administration induced macro- and microscopic changes in hepatic tissue.

Hepatic macroscopic alterations were evident in the necropsy of MTX-treated rats (Fig. 2). The livers, presenting a dark red colour with brilliant surface, were swollen with all lobes showing rounded edges. Their consistency was firm but friable during the cut. These alterations were more notorious in the MTX48 group. No macroscopic changes were observed in control livers.

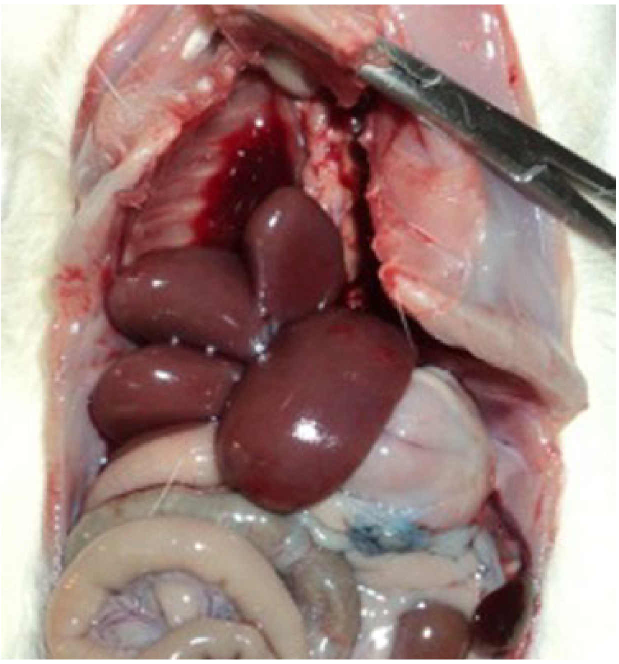

Fig. 2. Necropsy of an animal from the MTX48 group, demonstrating the liver macroscopic alterations observed in all MTX treated rats, being more evident in the MTX48 group. The liver presents a swollen aspect with rounded edges in all lobes, having a dark red colour and brilliant surface. Male Wistar rats were subjected to MTX treatment (three cycles of 2.5 mg/kg) and suffered euthanasia 28 days after the last MTX administration.

The microscopic analysis did not reveal any abnormality in animals from the control group (data not shown). However, at light microscopy, the MTX22 livers revealed disperse regions of focal necrosis without changes in the organ architecture (Fig. 3). The hepatic tissue presented an apparent proliferation of kupffer cells, hepatocyte oedema in the periportal regions and enlargement of periportal spaces with cellular infiltration and collagen deposition (Fig. 3). In the same group, transmission electron microscopy confirmed the cellular oedema mainly located in the periportal region. Moreover, an increased density of lysosomes (Fig. 3) and mild steatosis affecting the majority of hepatocytes were observed. In general, the hepatocytes presented several nucleoli (more than 2–3 per cell) and abundant rough endoplasmic reticulum, without signs of mitochondria swelling. Frequent perisinusoidal cells containing lipid droplets, suggestive of stellate cells, as well as collagen fibres proliferation into the Disse spaces, and abundant hepatic and endothelial microvilli were also observed (Fig. 3).

In the MTX48 group, the periportal cellular oedema apparently decreased when compared with the MTX22 group, although with an enlargement of periportal spaces and a more evident fibrotic area. A higher number of areas containing cellular infiltration with apparent mild disorganization of the lobular structure were seen (Fig. 3). In general, the transmission electron microscopy revealed a high content of lysosomes in hepatocytes, abundant Kupffer and stellate cells, as well as a huge proliferation of collagen fibres into the Disse spaces.

© 2013 Nordic Pharmacological Society. Published by John Wiley & Sons Ltd

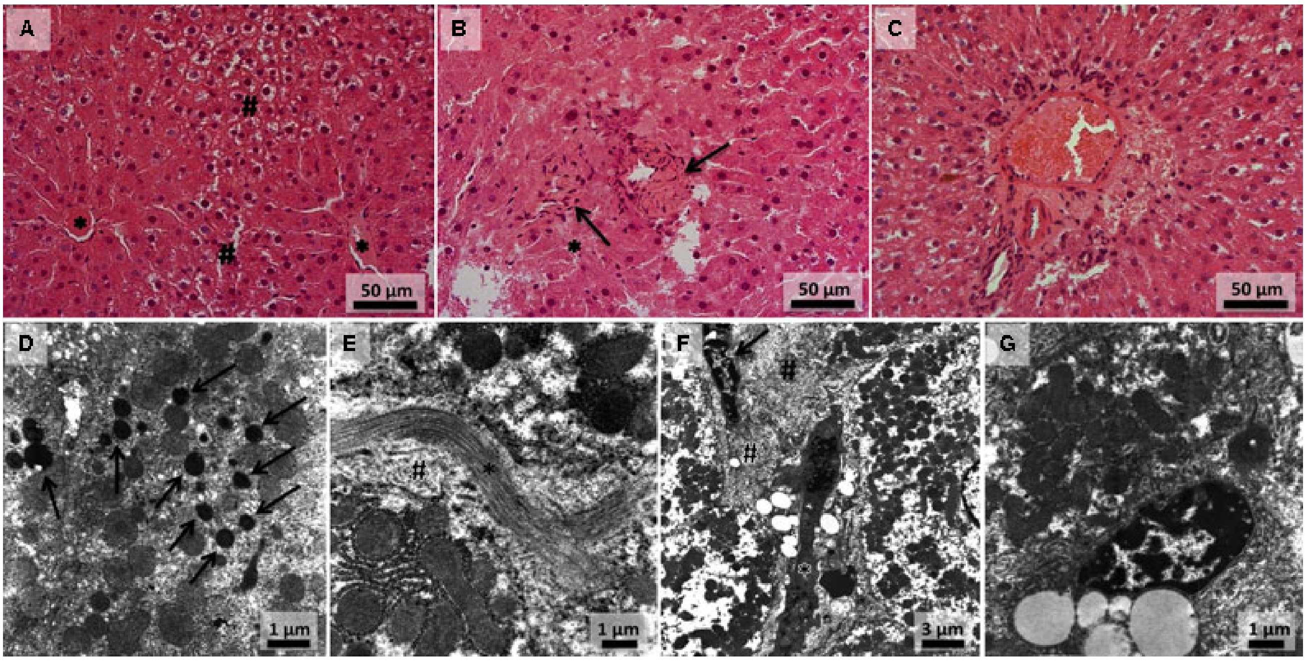

Fig. 3. Light (A, B and C) and electron micrographs (D, E, F and G) of liver sections illustrating the structural and ultrastructure alterations observed in MTX treated animals. In (A) (from MTX22 group), two central veins (*) surrounded by hepatocytes displaying a normal morphology are seen; however, at the periphery of the lobule, the presence of swollen hepatocytes is notorious (#); (B) (from MTX48) depicts a necrotic area (*) infiltrated by fibroblasts like cells with deposition of connective tissue (arrows); (C) (from MTX48 group) displays a portal area with enlargement of periportal space, which is invaded by connective tissue and infiltrated by fibroblasts like cells and leucocytes; (D) (from MTX22 group) depicts a great amount of lysosomes within a hepatocyte (arrows), with mitochondria presenting a normal morphology without signals of swelling; In (E) (from MTX22 group), the presence of collagen fibres (*) in the Disse space as well as an area of high density of hepatocyte microvilli are shown (#); (F) (from MTX22 group) shows two adjacent swollen hepatocytes, containing mitochondria with normal morphology (at left and right sides), separated by a space occupied by abundant microvilli (#) with a Kupffer cell near by (arrow); at the centre, a stellate like cell (*) with several lipid droplets; In (G) (from the MTX48 group), a stellate cell is depicted.

Changes in the hepatic macro- and microscopic architecture were not accompanied by significant alterations in the hepatic relative mass (data not shown).

MTX-induced hepatic alterations in the protein levels, glutathione status and ATP levels.

The hepatic protein levels were significantly decreased in the MTX22 group (54.1 ± 3.5 mg/g) when compared to control (107.3 ± 28.6 mg/g). The values observed in the MTX48 group (165.5 ± 91.8 mg/g) suggest a recovery of hepatic proteins, being similar to control values (Fig. 4). Moreover, as shown in Fig. 5, late significant increases were observed in the hepatic GSHt levels (47.3 ± 11.0 nmol/mg in the MTX48 group *versus* 26.3 ± 7.6 nmol/mg and 25.4 ± 3.6 nmol/mg in the control and MTX22 groups, respectively). This increase in GSHt corresponds to the late increase in the GSH (37.4 ± 8.5 nmol/mg in the MTX48 group compared with 22.9 ± 7.7 nmol/mg in the control and 19.5 ± 2.5 nmol/mg in the MTX22 group), and a great increase in the GSSG levels in the MTX48 group (4.9 ± 1.3 nmol/mg *versus* 1.7 ± 0.3 nmol/mg in the control and 2.9 ± 1.1 nmol/mg in the MTX22 group). Regarding hepatic ATP levels, a significant decrease in the MTX48 group (5.2 ± 1.5 nmol/mg) compared with control (10.1 ± 1.5 nmol/mg) or MTX22 (9.0 ± 1.5 nmol/mg) groups was seen (Fig. 6).

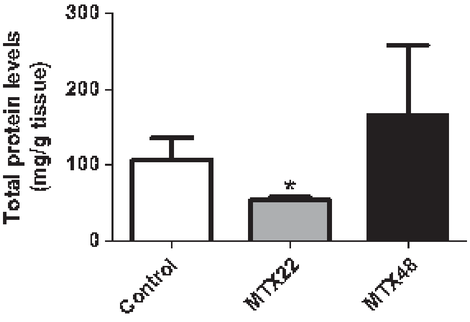

Fig. 4. Hepatic protein levels of the animals treated with MTX (three cycles of 2.5 mg/kg) and control group. Results are presented as means ± standard deviation. Statistical analysis was performed using Kruskal Wallis test (ANOVA on ranks) followed by the Student Newman Keuls *post hoc* test (*$p < 0.05$ *versus* control).

Discussion

This work aimed to investigate the potential hepatotoxicity and haematotoxicity of MTX using a multiple dose *in vivo* model. To evaluate whether the toxic effects were also cumulative and long-lasting, as it happens in some cardiac events, two time-points were selected: 2 and 28 days after the last administration of MTX. The choice of two different time-points represented by the MTX22 and MTX48 groups is

© 2013 Nordic Pharmacological Society. Published by John Wiley & Sons Ltd

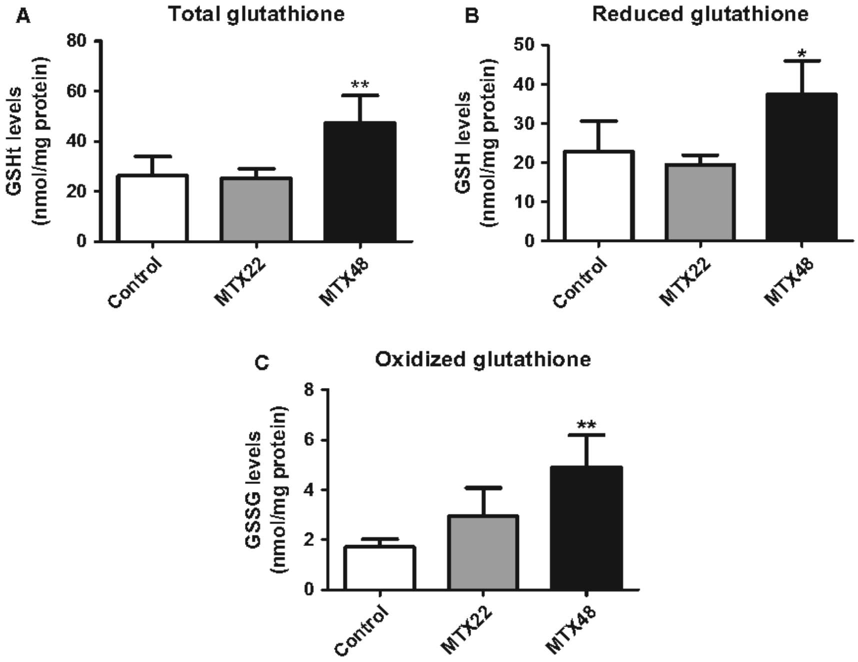

Fig. 5. Hepatic (A) GSHt, (B) GSH and (C) GSSG levels of the animals treated with MTX and control group. Results are presented as means ± standard deviation. Statistical analysis was performed using the Kruskal–Wallis test (ANOVA on ranks) followed by the Student Newman Keuls *post hoc* test (*$p < 0.05$ *versus* control).

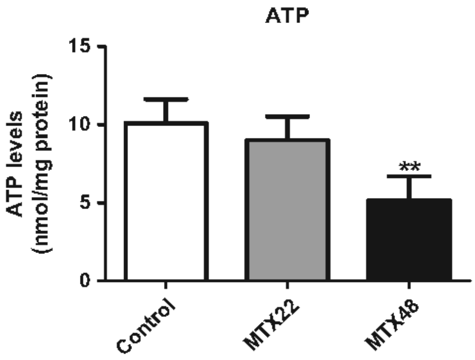

Fig. 6. Hepatic ATP levels of the animals treated with MTX and control group. Results are presented as means ± standard deviation. Statistical analysis was performed using the Kruskal–Wallis test (ANOVA on ranks) followed by the Student Newman Keuls *post hoc* test (*$p < 0.05$ *versus* control).

important to evaluate acute/adaptive and transient/ultimate effects of the liver or haematological function, because they present high turnover and plasticity [13].

We observed hepatotoxicity and haematological toxic effects after MTX administration to rats, as demonstrated by the macro- and microscopic changes in the hepatic architecture (Figs 2 and 3), and by several haematological alterations (Table 1). The reduction in hepatic protein levels in the MTX22 group, the late increases in the GSHt hepatic levels, demonstrated by an increase in GSH and GSSG contents, and late decreases in the hepatic ATP values in the MTX48 group showed mechanistic responses of hepatic tissue after MTX administration (Figs 4 6, respectively).

The MTX-induced haematological toxic effects were demonstrated by an early bone marrow depression on MTX22 group (Table 1) followed by signals of haematopoiesis recovery, observed in the MTX48 group. Indeed, MTX22 presented a reduction in WBCs, RBCs and reticulocytes, associated with an increase in non-conjugated bilirubin that was followed, at MTX48, by a recovery of WBCs and RBCs. The return to basal values of RBCs at MTX48 was probably due to a significant increase in reticulocytes, leading to macrocytosis and anisocytosis, as shown by the significant increase in the RDW and in MCV. Additionally, increased levels of plasma iron suggest an increase in iron absorption to overcome the initial reduction in RBCs. These results are in accordance with what has been observed in human beings and justify the importance of monitoring haematological parameters during MTX chemotherapy [1]. In fact, the MTX-induced myelosuppression manifests mostly as leukopaenia, thus being the main dose-limiting effect that occurs shortly after MTX treatment [18]. Also, in human beings, after administration of MTX (38 mg/m^2), the WBC counting returned to normal values within 7 days [18]. However, patients treated with higher dose regimens tend to present an even faster blood count recovery [1]. The presence of micronucleus in MTX22 blood smears (Fig. 1) was constant in all animals from this treated group, suggesting a genotoxic potential for MTX. Altogether, these data elucidate the rational for continued blood cell counts after MTX-therapy cessation due to the risk of MTX-associated secondary acute leukaemia [2]. As for other topoisomerase II inhibitors, there are only limited data on the MTX genotoxicity using microbial conventional assays [10]. However, it is well known that

© 2013 Nordic Pharmacological Society. Published by John Wiley & Sons Ltd

MTX causes single and double breaks in the DNA [1,3] and also affects the cell cycle at various stages [3,19].

As stated before, MTX is an immunosuppressive drug that promotes apoptosis in antigen-presenting cells and reduces the levels of all types of immune cells [2,20]. Accordingly, we observed a transient decrease in the plasma IgG levels in the MTX22 rats (Table 1). Another study assessing the human safety of MTX, rituximab, ifosfamide and etoposide combined therapy demonstrated significant decrease in the IgG levels in patients treated for non-Hodgkin's lymphoma [21]. The IgG is synthesized by blood cells and corresponds to about 80% of total immunoglobulin [22]. Thus, the significant decreases in IgG levels in the MTX22 group may correlate with the observed decreases in the plasma total protein levels observed in this group. The levels of the main plasma protein albumin remained constant in the MTX-treated groups (data not shown).

The MTX-induced hepatotoxicity was clearly demonstrated by the macroscopic changes observed in the MTX-treated livers (Fig. 2). Signals of hepatic injury were found in the earlier time-point (MTX22 group), notably by changes in plasma-related liver parameters, in the hepatic macro- and microscopic changes (Fig. 3) and by alterations in biochemical hepatic values (Fig. 4). These data suggest hepatic dysfunction, demonstrated by the decrease in plasma enzyme levels, protein turn-over and higher free cholesterol. The impairment of hepatic function in both treated groups is also shown by decreases in the plasma triglycerides, which are mainly synthesized by the hepatocytes (Table 1). Furthermore, the increase in the plasma cholesterol levels in the MTX22 group is consistent with the mild steatosis observed by structural analysis, which can be related to the decreased hepatic synthesis of lipoproteins. The diminished hepatic protein synthesis was demonstrated by lower protein hepatic levels (MTX22), and lower levels of plasma biochemical parameters such as ALT, alkaline phosphatase and transferrin in both MTX-treated groups. In fact, in human beings, the acute hepatotoxicity of MTX manifests as transient increases in serum bilirubin levels and in the activity of liver enzymes [10]. However, decreases in the hepatic synthesis of these enzymes are considered a result of (sub)chronic hepatotoxicity observed with other xenobiotics [23 26]. Possibly due to the marked decrease in protein turnover, MTX22 hepatocytes show large nucleoli and abundant rough endoplasmic reticulum, as a compensation mechanism to attempt restoring hepatic synthesis diminished by the action of the drug. The apparent recover of the hepatic total protein levels (Fig. 4) on MTX48 compared with MTX22 does not mean total functional gain, considering the changes in MTX48 hepatic ATP, glutathione and plasma protein levels.

Moreover, increases in the unconjugated bilirubin in both treated groups are suggestive of impaired conjugation with glucuronides. Subclinical unconjugated hyperbilirubinaemia is related to antituberculosis therapy, and it is attributed to the inhibition of the bile salt exporter pumps [26]. Microscopic hepatic evaluations (Fig. 3) demonstrated a huge proliferation in the Kupffer cells, leucocyte infiltration and collagen deposition, which are indicative of an inflammatory process. Indeed, it might be related to the notorious increases observed in the plasma C4 complement levels because this component is synthesized by Kupffer cells [27]. The hepatic microscopic changes were more notorious at a later time-point (MTX48 group). As already mentioned, MTX and naphthoquinoxaline (an active metabolite) are retained in the hepatic tissue [5,28], and the continued hepatic exposure may result in hepatic injury. Recently, we described some significant changes related to cardiotoxicity in the MTX22 group (decreased levels of CK, CK-MB, increased cardiac relative mass and adaptive increase in the mitochondrial complexes IV and V). However, it was demonstrated that the cardiac energetic damage was established at a later time-point (increased levels of plasma lactate and cardiac relative mass, decrease in the mitochondrial complex V activity with consequent depletion of cardiac ATP levels) [6]. One hypothesis for the MTX-induced hepatotoxicity is that it was secondary to the concomitant MTX-induced cardiotoxicity. However, microscopic data do not support the theory that the classic late cardiotoxicity of MTX [6] may contribute to promote a secondary hepatic lesion [8] considering the absence of significant centrilobular damage or dilatation of centrilobular sinusoids by blood congestion. In another study, the hepatic histophatological results of mice treated with MTX (15 mg/kg) demonstrated intense hydropic vacuolization of the cytoplasm, necrosis areas, picnosis and nuclear lysis not recovered until 5 days after the single dose administration [9]. Accordingly, in the present study, the MTX-induced hepatic damage continued until the end of the evaluations.

Oxidative stress seems to assume a more important role in the MTX hepatotoxicity when compared to the oxidative damage observed in the MTX-related cardiomyopathy [6,7]. Increases in the hepatic levels of GSHt were observed in the MTX48 group. As shown in Fig. 5, this increase is related to a slight (but significant) increase in the GSH hepatic levels and GSSG levels. Increases in the GSH might be interpreted as an attempt to enhance the antioxidant content to respond to injury, while increased levels of GSSG are a clear sign of oxidative stress. It is known that Kupffer cells, which were abundantly present in the MTX48 livers, are a source of reactive oxygen and nitrogen species [29]. The link between oxidative stress and the MTX-induced hepatic damage was already suggested in a study with mice, where the administration of MTX (15 mg/kg) caused increases in the lipid peroxidation, decreases in the antioxidant enzymes (superoxide dismutase, catalase and glutathione peroxidase) and depletion of the hepatic retinol and GSH content [9]. Moreover, the incubation of MTX (100 μM) with HepG2 cells for 6 hr was enough to promote the decrease in the GSH levels [30]. The apparent contradiction between our results (increased in the GSH hepatic levels) and the previously reported data (decreases in the GSH content) may be explained by the differences in the experimental design or models. Both referred studies assessed the GSH levels 3, 4 and 5 days after MTX administration [9] or 6 hr after high MTX concentration incubation [30]. In the present study, significant changes in the glutathione sta-

© 2013 Nordic Pharmacological Society. Published by John Wiley & Sons Ltd

tus were seen only at the last evaluated time-point, 28 days after the last dose administration. Hence, the organism is subjected to compensatory/adaptive effects favoured by the elapsed time between the last MTX administration and rat euthanasia.

To the best of our knowledge, it is the first time that late hepatic energetic imbalance is associated with MTX-induced hepatotoxicity. The decrease in the hepatic ATP levels observed in the MTX48 group (Fig. 6) occurred 28 days after the last MTX administration. One can speculate about this result. Decreases in the ATP hepatic levels are observed in the human non-alcoholic steatohepatitis [31], and are associated with covalent binding of drugs with intracellular proteins [32]. As already stated, MTX and its toxic known metabolite accumulates in the liver tissue [5,28] and its long-lasting effects can be attributed to MTX persistence in the cells and its strong affinity for cellular macromolecules and membranes [33]. Additionally, the ATP decreases can be related to mitochondrial disruption. In other models related to myocytes, the MTX-induced decreases in the ATP levels have already been described [6,7,34]. In these models, the observed cardiac energetic depletion was already attributed to the mitochondrial toxicity induced by MTX, affecting the ATP synthesis through perturbations in the mitochondrial membrane potential and late inhibition of ATP synthase activity *in vitro* and *in vivo* [6,7]. Moreover, in a work by Shipp *et al.* [34], the MTX-metabolite naphthoquinoxaline also disrupted ATP homeostasis in neonatal rat heart cells. Although, in the present study, mitochondrial morphologic changes in the hepatic tissue were not observed, one cannot exclude the existence of functional mitochondrial disturbances.

In summary, this study allowed to better understand the long-term effect of MTX treatment. Moreover, the intrinsic hepatotoxic potential of chemotherapy is of great concern because an altered hepatic function might decrease the cancer therapy effectiveness and/or increase toxic adverse effects [13]. In this study, we described a severe hepatotoxicity. We did not find hepatic changes suggestive of heart failure and the location of the histological findings in the periportal region seem to reinforce the direct hepatotoxic potential of MTX. After 28 days of the last MTX cycle, hepatic tissue remained with reduced levels of glutathione and ATP, which are essential for the hepatic function.

Acknowledgements

This work was supported by the Fundação para a Ciência e Tecnologia (FCT) - project (EXPL/DTP-FTO/0290/2012) - QREN initiative with EU/FEDER financing through COMPETE - Operational Programme for Competitiveness Factors. The work was also supported by FCT within the framework of Strategic Projects for Scientific Research Units of R&D (project PEst-C/EQB/LA0006/2011). LGR, VMC and RJD-O thank FCT for their PhD grant (SFRH/BD/63473/2009) and Post-doc grants (SFRH/BPD/63746/2009) and (SFRH/BPD/36865/2007), respectively. MDA thanks Capes Foundation (Brazil) for his PhD Grant (BEX 0593/10-9).

References

1 Seiter K. Toxicity of the topoisomerase II inhibitors. Expert Opin Drug Saf 2005;**4**:219–34.

2 Neuhaus O, Kieseier BC, Hartung H-P. Therapeutic role of mitoxantrone in multiple sclerosis. Pharmacol Ther 2006;**109**:198–209.

3 Ehninger G, Schuler U, Proksch B, Zeller KP, Blanz J. Pharmacokinetics and metabolism of mitoxantrone. A review. Clin Pharmacokinet 1990;**18**:365–80.

4 Wang J-S, Zhu H-J, Markowitz JS, Donovan JL, Yuan H-J, Devane CL. Antipsychotic drugs inhibit the function of breast cancer resistance protein. Basic Clin Pharmacol Toxicol 2008;**103**:336–41.

5 Rossato L, Costa V, de Pinho P, Freitas V, Viloune L, Bastos M *et al.* The metabolic profile of mitoxantrone and its relation with mitoxantrone-induced cardiotoxicity. Arch Toxicol 2013;**87**:1809–20.

6 Rossato LG, Costa VM, Dallegrave E, Arbo M, Silva R, Ferreira R *et al.* Mitochondrial cumulative damage induced by mitoxantrone: late onset cardiac energetic impairment. Cardiovasc Toxicol 2013; In Press. DOI: 10.1007/s12012-013-9230-2.

7 Rossato LG, Costa VM, Villas-Boas V, de Lourdes Bastos M, Rolo A, Palmeira C *et al.* Therapeutic concentrations of mitoxantrone elicit energetic imbalance in H9c2 cells as an earlier effect. Cardiovasc Toxicol 2013; In Press. DOI: 10.1007/s12012-013-9224-0.

8 Saner FH, Heuer M, Meyer M, Canbay A, Sotiropoulos GC, Radtke A *et al.* When the heart kills the liver: acute liver failure in congestive heart failure. Eur J Med Res 2009;**14**:541–6.

9 Llesuy SF, Arnaiz SL. Hepatotoxicity of mitoxantrone and doxorubicin. Toxicology 1990;**63**:187–98.

10 IARC Mitoxantrone. IARC Monographs, 2011; 289–315.

11 Mewes K, Blanz J, Ehninger G, Gebhardt R, Zeller KP. Cytochrome P-450-induced cytotoxicity of mitoxantrone by formation of electrophilic intermediates. Cancer Res 1993;**53**:5135–42.

12 Juntti-Patinen L, Kuitunen T, Pere P, Neuvonen PJ. Drug-related visits to a district hospital emergency room. Basic Clin Pharmacol Toxicol 2006;**98**:212–7.

13 King PD, Perry MC. Hepatotoxicity of chemotherapy. Oncologist 2001;**6**:162–76.

14 International Committee for Standardization in Haematology. ICSH reference method for staining of blood and bone marrow films by azure B and eosin Y (Romanowsky stain). Br J Haematol 1984;**54**:707–10.

15 Pontes H, Duarte JA, de Pinho PG, Soares ME, Fernandes E, Dinis-Oliveira RJ *et al.* Chronic exposure to ethanol exacerbates MDMA-induced hyperthermia and exposes liver to severe MDMA-induced toxicity in CD1 mice. Toxicology 2008;**252**:64–71.

16 Rossato LG, Costa VM, de Pinho PG, Carvalho F, Bastos ML, Remião F. Structural isomerization of synephrine influences its uptake and ensuing glutathione depletion in rat-isolated cardiomyocytes. Arch Toxicol Springer 2011;**85**:929–39.

17 Barbosa DJ, Capela JP, Oliveira JM, Silva R, Ferreira LM, Siopa F *et al.* Pro-oxidant effects of Ecstasy and its metabolites in mouse brain synaptosomes. Br J Pharmacol 2012;**165**:1017–33.

18 Alberts DS, Surwit EA, Peng Y, McCloskey T, Rivest R, Graham V *et al.* Phase I clinical and pharmacokinetic intraperitoneal administration study of mitoxantrone given to patients by intraperitoneal administration. Cancer Res 1988;**48**:5874–7.

19 Khan SN, Lai SK, Kumar P, Khan AU. Effect of mitoxantrone on proliferation dynamics and cell cycle progression. Biosci Rep 2010;**30**:375–81.

20 Neuhaus O, Wiendl H, Kieseier BC, Archelos JJ, Hemmer B, Stüve O *et al.* Multiple sclerosis: mitoxantrone promotes differential effects on immunocompetent cells in vitro. J Neuroimmunol 2005;**168**:128–37.

21 Joyce RM. A phase I-II study of rituximab, ifosfamide, mitoxantrone and etoposide (R-IME) for B cell non-Hodgkin's lymphoma prior to and after high-dose chemotherapy and autologous stem cell transplantation (HDC-ASCT). Ann Oncol 2003;**14**:i21–7.

22 Lehrer SB, Reish R, Fernandes J, Gaudry P, Dai G, Reese G. Enhancement of murine IgE antibody detection by IgG removal. J Immunol Meth 2004;**284**:1–6.

23 Solter P, Liu Z, Guzman R. Decreased hepatic ALT synthesis is an outcome of subchronic microcystin-LR toxicity. Toxicol App Pharmacol 2000;**164**:216–20.

24 Karinch A, Martin J, Vary T. Acute and chronic ethanol consumption differentially impact pathways limiting hepatic protein synthesis. Am J Physiol Endocrinol Metab 2008;**295**:E3–9.

25 Gonzalez MC, Sutherland E, Simon FR. Regulation of hepatic transport of bile salts: effect of protein synthesis inhibition on excretion of bile salts and their binding to liver surface membrane fraction. J Clin Invest 1979;**63**:684–94.

26 Saukkonen JJ, Cohn DL, Jasmer RM, Schenker S, Jereb JA, Nolan CM *et al.* An official ATS statement: hepatotoxicity of antituberculosis therapy. Am Respir Crit Care Med 2006;**174**:935–52.

27 Miura N, Prentice HL, Schneider PM, Perlmutter DH. Synthesis and regulation of the two human complement C4 genes in stable transfected mouse fibroblasts. J Biol Chem 1987;**262**:7298–305.

28 Batra VK, Morrison JA, Woodward DL, Siverd NS, Yacobi A. Pharmacokinetics of mitoxantrone in man and laboratory animals. Drug Metab Rev 1986;**17**:311–29.

29 Jaeschke H, Gores GJ, Cederbaum AI, Hinson JA, Pessayre D, Lemasters JJ. Mechanisms of hepatotoxicity. Toxicol Sci 2002;**65**: 166–76.

30 Duthie SJ, Grant MH. The role of reductive and oxidative metabolism in the toxicity of mitoxantrone, adriamycin and menadione in human liver derived Hep G2 hepatoma cells. Br J Cancer 1989;**60**: 566–71.

31 Cortez-Pinto H, Chatham J, Chacko VP, Arnold C, Rashid A, Diehl AM. Alterations in liver ATP homeostasis in human nonalcoholic steatohepatitis: a pilot study. JAMA 1999;**282**: 1659–64.

32 Mehta N, Ozick L, Gbadehan E, Sharma S, Tavalera F, Rice T. Drug-induced hepatotoxicity. Medscape reference. 2012 [cited 1BC Dec 13]. Available from: http://emedicine.medscape.com/article/169814-overview

33 Feofanov A, Sharonov S, Fleury F, Kudelina I, Nabiev I. Quantitative confocal spectral imaging analysis of mitoxantrone within living K562 cells: intracellular accumulation and distribution of monomers, aggregates, naphtoquinoxaline metabolite, and drug-target complexes. Biophys J 1997;**73**:3328–36.

34 Shipp NG, Dorr RT, Alberts DS, Dawson BV, Hendrix M. Characterization of experimental mitoxantrone cardiotoxicity and its partial inhibition by ICRF-187 in cultured neonatal rat heart cells. Cancer Res 1993;**53**:550–6.

© 2013 Nordic Pharmacological Society. Published by John Wiley & Sons Ltd

PART III

Discussion and Conclusions

The major findings of this thesis were the elucidation of the mechanisms involved in the MTX-induced cardiotoxicity, mainly regarding its metabolism and energetic status changes. The metabolic profile of MTX after incubation with rat hepatic S9 fractions was described and MTX and the MTX-naphtoquinoxaline metabolite were found in extracts of heart and liver of male Wistar rats previously injected (24h before, i.p.) with MTX. The presence of MTX metabolites increased the MTX cytotoxicity in a cardiomyoblast *in vitro* model (H9c2) and, in the same model, the cell damage was partially prevented by the inhibition of the CYP450 metabolism and specifically of the CYP2E1 isoenzyme metabolism, highlighting the relevance of MTX metabolism to its cardiotoxicity. Our results also suggest an important mitochondrial toxicity evidenced both *in vitro* and *in vivo*, which is characterized by an energetic gap observed by decreases in the ATP levels and disturbances in the mitochondrial complexes. Noteworthy, at the late time point (96h) the onset of an oxidative stress phenomenon at the *in vitro* model was observed at the same incubation period that the energetic injury was more dramatic. Moreover, by using an *in vivo* model we observed the occurrence of an intense MTX-mediated hepatotoxicity and hematological disturbances. All these aspects are discussed below.

The *in vitro* and *in vivo* models, doses/concentrations, and time of incubation/exposition used were adapted to study the MTX-induced cardiotoxicity. For the present work, it could be highlighted the fact that the results are originated from *in vitro* and *in vivo* studies performed in parallel with coordinated goals, generating complementary data regarding the advantages of each approach and trying to surpass their limitations. Emphasis is given to the mechanistic pathways identified by the *in vitro* studies and pharmacokinetics and biochemical studies by *in vivo* studies.

IV.1. Metabolic profile of MTX: *in vitro* and *in vivo* studies

In studies undertaken in the Manuscript I, the metabolism of MTX was simulated *in vitro* by using hepatic S9 fractions isolated from adult rats, supplemented with NADPH (1mM) and GSH (4mM). After a 4h incubation with MTX (100µM), the MTX content was 35% lower than at time 0; five chromatographic peaks were identified as MTX related products, namely the naphtoquinoxaline metabolite, an acetoxy ester derivative (never described before in this model), two MTX GSH conjugates and a MTX monocarboxylic acid derivative (trace amounts) (Figure 5) (Manuscript I).

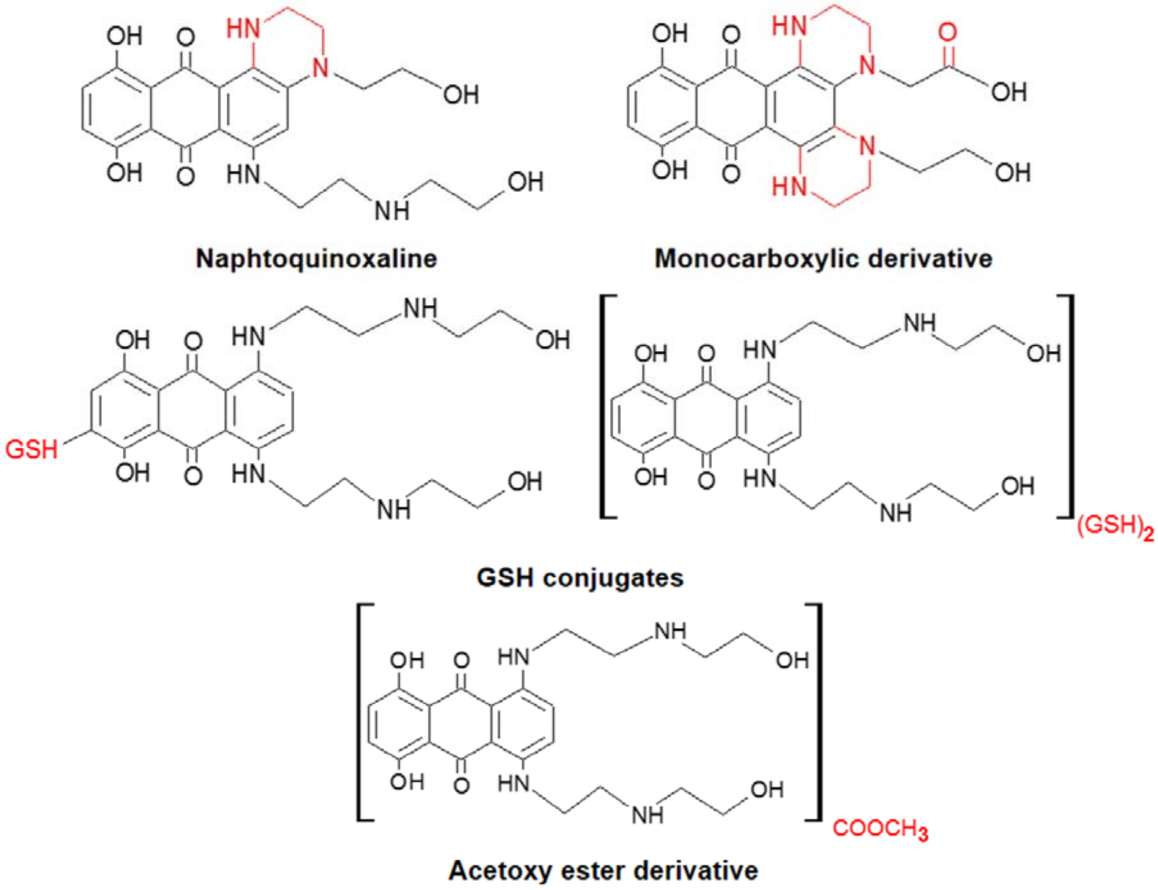

Figure 5: Proposed chemical structure of the metabolites corresponding to the five chromatographic peaks obtained by LC/DAD-ESI/MS analysis. Compounds were obtained after 4h incubation of MTX (100µM) with hepatic S9 fractions isolated from adult male rats pre-treated with phenobarbital (0.2% in drinking water for one week prior isolation). Hepatic S9 fractions (4mg/ml) were supplemented with NADPH (1mM) and GSH (4mM).

The UV-VIS spectrum of the MTX obtained products showed that they retained the tricyclic planar chromophore group, suggesting that all compounds could have pharmacological interest, namely the ability to form covalent complexes with DNA (21). However, the only metabolite ever reported as bioactive is the naphtoquinoxaline metabolite (Figure 2 and Figure 5) (27,30,37,44). In fact, this metabolite was already described as the product of MTX metabolism through heme containing enzymes systems, CYP450, and peroxidases, and as an excretion product in the urine of humans and many laboratory animals (27,30) (Table 2).

A novel compound was described as a MTX metabolic product (Manuscript I) (Figure 5) with a –$COOCH_3$ group introduced in the MTX molecule. The pathways involved in the metabolite formation remain unclear, but we suggested that the acetoxy derivative can result from an N-oxygenation in the aromatic amine, followed by an acetylation. In fact, in primary and secondary aromatic amines, N-oxygenation by CYP450 usually results in the formation of arylhydroxylamines, which can be converted by N-acetyltransferases (present in S9 fractions), functioning as O-acetyltransferases, to acetoxy esters (124). Another structural possibility for this compound is the introduction of the –CH_2COOH group in the MTX molecule instead of the –$COOCH_3$, which is also compatible with the MS spectrum; however, those metabolic routes are unlikely.

MTX-derived GSH conjugates are known as one of the detoxifying products of MTX (27,32) (Table 2). The methodology employed in our study does not allow a conclusion about the site of GSH conjugation. Two hypotheses were considered regarding the GSH conjugation site, namely in the diaminobenzene and in the dihydroxybenzene part of MTX molecule. Initially, Blanz and co-workers described both GSH conjugates on the diaminophenyl part using ^{13}C-NMR and ^{1}H-NMR techniques. ^{13}C-NMR data showed that regarding the two carbon resonances of MTX attributed to C6/C7 and C2/C3, one suffered a downfield shift, indicating a symmetrical substitution of two hydrogen atoms by sulfur-containing groups. However, the location of the conjugation site remained unclear because the chemical shifts of these carbons were nearly equivalent. Thus, the ^{1}H-NMR data suggested that the conjugation was at C6/C7 because the resonance typical for the protons at C6/C7 disappeared (27). However, in a subsequent investigation applying two-dimensional ^{1}H-^{13}C-heteronuclear multiple-bond connectivity NMR and within the same group of authors, it became apparent that the S-atom of GSH was bound to C2 (37). Thus, it was concluded that, while the intramolecular attack of the nucleophilic side chain N-atom on the oxidized MTX takes place at position C6, leading to the naphtoquinoxaline metabolite, the corresponding reaction with external nucleophiles, such as GSH, occurs at the dihydroxybenzene part (Figure 6) (37).

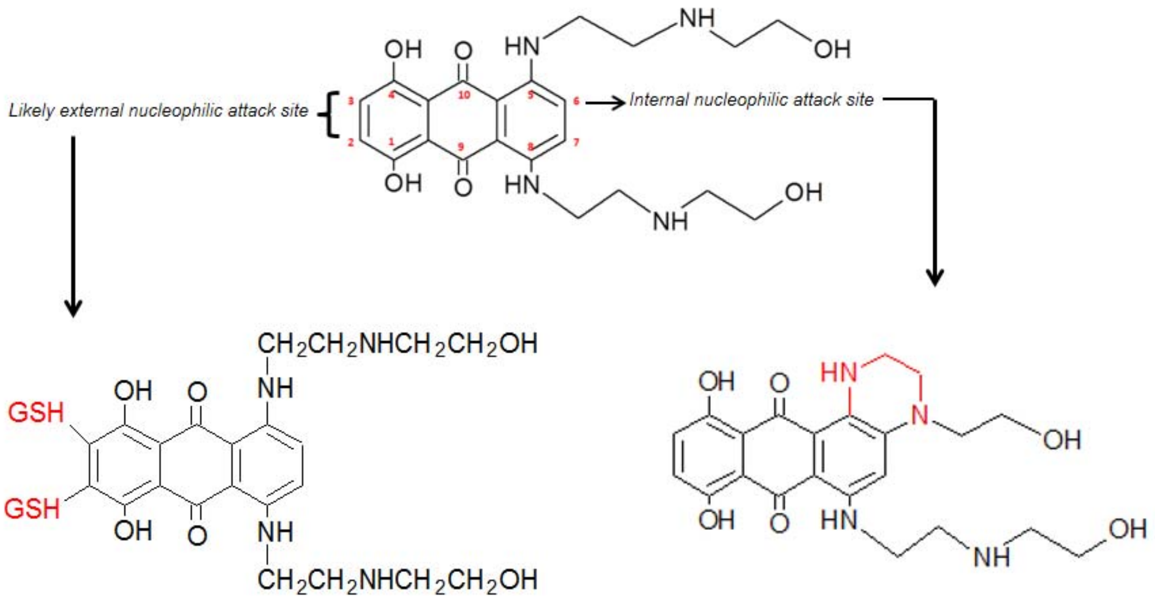
Likely external nucleophilic attack site
Internal nucleophilic attack site
OH
O
HN
NH
OH
1
2
3
4
5
6
7
8
9
10
GSH
GSH
CH2CH2NHCH2CH2OH
HN
N

Figure 6: Chemical representation of nucleophilic attack sites in the MTX molecule. The position 6 of MTX is the site of the intramolecular attack of the nucleophilic side chain resulting in the formation of the naphtoquinoxaline metabolite. The external nucleophilic attack is favored at position 2 and 3 of MTX molecule.

Given the trace amounts of MTX monocarboxylic acid derivative, little information regarding its MS spectrum characteristics was obtained. However, recently, a compound with the same molecular ion mass was associated with oxidative metabolism of MTX, MTX-derivative dicyclicmonocarboxylic acid (30). Thus, we suggested that the trace metabolite found in our experimental conditions has the structure of the dicyclicmonocarboxylic acid derivative shown in the Figure 5. Its pharmacological effect was not tested, although, we can speculatively say that this compound is a reasonable candidate to elicit antitumor effect given its ionisability (30). MTX monocarboxylic acid derivative was already detected in rat metabolism in very low and variable levels and its formation was related to CYP450-catalyzed reactions (27,30,31). To the best of our knowledge, the formation of the monocarboxylic acid derivative from the napthoquinoxaline structure (as proposed here) was only related to peroxidase-catalyzed reactions (30). Nonetheless, CYP450 and peroxidase enzyme systems, despite differing in the reaction mechanisms, apparently can generate identical reaction products (30).

In order to evaluate the *in vivo* MTX and napthoquinoxaline metabolite presence in the liver (the main metabolic organ) and heart (the main toxicity target of MTX), extracts of both organs were analyzed after excision from rats treated with MTX (7.5mg/kg, i.p.) 24h before the euthanasia.

In liver extracts of animals treated with MTX, it was possible to observe the presence of MTX and seven additional peaks when compared to the control livers; hence, they were assigned as MTX metabolites (Manuscript I). All the compounds absorb radiation in the VIS region (between 500 and 700nm), suggesting that the chromophore group remained intact. Due to the huge background present in the chromatograms, only MTX and naphtoquinoxaline metabolite, the most pharmacological relevant compound, were identified through UV-VIS spectrum characteristics and by the MS fragmentation. Although the UV-VIS spectrum does not provide an accurate identification of the compounds as does the MS fragmentation, an interesting discovery showed that all the compounds present in the liver extract of MTX-treated rats possessed a UV-VIS spectrum profile similar to those metabolites proposed in the above mentioned *in vitro* study, using hepatic S9 fractions. The two first peaks assigned as MTX metabolites in the liver chromatogram presented a maximum absorbance in the visible region set at 619nm and 673nm, agreeing with the UV-VIS spectrum of the MTX-GSH conjugate. The next metabolite peak had the same absorbance profile in the visible region of the dicyclicnaphtoquinoxaline monocarboxylic acid derivative, namely 610nm and 658nm. The three remaining compounds had a UV-VIS spectrum with absorbance maximum at 610 nm and 661nm, which are the absorbance maximum peaks of the novel metabolite (acetoxy ester) and MTX. These data suggest that *in vivo* MTX metabolites found in the hepatic tissue are, at least, chemically similar to those produced *in vitro*.

In the heart extracts of the animals treated with MTX, only MTX and the naphtoquinoxaline metabolite were found in trace amounts. Both compounds were identified through analysis of their DAD spectrum properties and MS fragmentation (Manuscript I).

The presence of MTX in heart and liver of MTX treated rats herein shown is in accordance with the current literature that states the broad tissue distribution profile of MTX (26,104). It is known that MTX is retained in these organs even one month after a single dose treatment (12mg/m^2) in humans (1,26). However, this is the first time that the presence of the naphtoquinoxaline metabolite in liver and heart was described in an animal model. The detection of the naphtoquinoxaline metabolite in the liver and heart suggests that this metabolite also has the potential to be retained in highly perfused organs. Nonetheless, for how long this compound is found in these tissues remains unknown. We only evaluated the end-point of 24h after MTX treatment, which is a short period to evaluate MTX tissue retention profile. Even so, it might account to MTX toxicity observed in these organs, such as those observed in the studies performed within this thesis (discussed below).

IV.2. Influence of MTX metabolism on its (cardio)toxicity

According to the results presented in the Manuscript I, metabolites of MTX are more cytotoxic than MTX in the H9c2 cells, suggesting the relevance of MTX metabolism to its cardiotoxicity. In fact, in the study described in the Methods section we have treatment groups with the extracts of the previous incubations of the supplemented S9 fractions with 100μM MTX at time 0 (non-metabolized MTX) and after 4h (containing 35% less MTX than at time 0 plus the proposed metabolites presented in the Figure 5). Furthermore, the experimental protocol included a matrix group that did not contain MTX. Analyses of the extracts were performed through LC/DAD-ESI/MS, prior to the incubations with H9c2 cells, to guarantee the identity and content of each extract. Results revealed that even with less amounts of MTX, the presence of the metabolites significantly increased the cell's cytotoxicity, evaluated through the reduction of MTT assay after a 24h period of incubation, when compared to the non-metabolized MTX group.

The complex metabolic extract containing all *in vitro* formed metabolites (Figure 5) is more cytotoxic than MTX without previous metabolism. However, the individual contribution of each byproduct was not determined and, as already referred, the majority of the proposed metabolites have unknown toxicity profiles. In fact, considering the five proposed metabolites, the only that has known toxicological relevance is the naphtoquinoxaline (34,37,125). Regarding naphtoquinoxaline-induced cardiac damage, Shipp and co-workers described, in 1993, a depletion of ATP levels to 67.3±6.3% of control after 72h of previous 3h naphtoquinoxaline (39μM) incubation in cultured neonatal rat cardiomyocytes. In the same study and using the same incubation conditions and cell model, MTX at 3.9μM, caused a depletion in the ATP levels of about 55.1±3.9% of control (125). These results demonstrate that, in the tested conditions, MTX has a greater effect on ATP levels than its metabolite since a significant lower concentration of MTX (10 fold) was used to obtain similar energetic effects. However, in our study, even considering that we did not quantified the naphtoquinoxaline levels present in the MTX+metabolites group, its concentration is certainly lower than MTX, since it was formed from MTX (100μM) incubation with supplemented S9 fractions. Obviously, this treatment group contains other MTX metabolites besides naphtoquinoxaline, which may account for the enhancement of the toxic effects even with about 35% less MTX (since MTX was biotransformed) when compared to MTX alone group. In fact, the enhanced cytotoxicity of MTX after the inhibition of epoxide hydrolase has been already described, suggesting that MTX is oxidized by the CYP450 oxidase mixed function to an epoxide (33). Epoxides are quite reactive, but none of such toxic metabolites were detected in our study; of notice epoxide hydrolase induction may occur by previous phenobarbital administration to the rat.

Additionally, it is important to refer that in the study performed by Shipp and co-workers the cells were incubated for only 3h, washed, the medium was replaced, and ATP levels were evaluated after 72h showing that the initial exposure to the metabolite or MTX was sufficient to elicit a toxic response. In contrast, in the study presented in this thesis, the incubation period was longer and continuous (24h) and the cytotoxicity was measured by MTT reduction assay. In both studies the energetic depletion was evident. Differences in the response magnitude might be related to the cell model used since Shipp used cultured neonatal rat cardiomyocytes.

Another great contribution of our work was to highlight the *in locu* bioactivation of MTX mediated through CYP450 and namely CYP2E1 as a contributor to MTX cytotoxicity. For the first time, the partial reversion of MTX-induced cytotoxic effects by co-incubation with CYP450 metabolism inhibitors, and in particular of CYP2E1 inhibitor, was evidenced in a cardiomyoblast model. It is important to consider the relevance of the extra-hepatic metabolism to MTX-induced organ toxicity regarding that this drug accumulates in many organs (26). In the manuscript I, we demonstrated the presence of both MTX and naphtoquinoxaline metabolite in the liver and in the heart tissue of MTX treated rats. The toxic metabolites can be produced in the liver and carried to other organs and/or be formed *in locu*. The heart is an organ that express both CYP450 enzymes and NADPH cytochrome reductase (33). Noteworthy, CYP2E1 is markedly abundant in the heart when compared to other isoenzymes of that family (126), and we showed that it contributes to MTX cytotoxicity since by the inhibition of this isoenzyme the observed cytotoxicity was partially prevented (Manuscript I).

Despite the significant protection obtained with CYP450 and CYP2E1 inhibitors, MTP (0.5mM) and DAS (150µM) respectively, the damage was only partially counteracted. This partial protection may be related to the direct toxic effect of MTX or the involvement of other enzymes present in the H9c2 cells that can promote the bioactivation of MTX. Additionally, the co-incubation of these inhibitors with MTX (100nM and 1µM) did not prevent the increase in the caspase-3 activity shown in the absence of metabolism inhibitors, favoring the participation of other metabolites or of MTX-itself to this effect (Manuscript II). Thus, these results suggest that CYP inhibition and the metabolites generated by it were not associated to apoptosis.

In accordance with our results, in a previous study performed by co-incubating HepG2 cells with MTP (0.5mM) and MTX (5µM) for 4h the decrease in the cell growth was prevented when quantified 48h after removing these compounds, and compared to MTX incubation in the absence of MTP (33). Conversely, co-incubation of MTP (0.5mM) with MTX (10 and 200µM) for 4h partially prevented the cytotoxicity of MTX, evaluated through the LDH leakage assay, in the MCF7 human breast cancer cells subjected to CYP450 induced metabolism. Furthermore, in the same model, MTP (0.5mM) co-incubated with a lower concentration of MTX (10µM) for 4h counteracted the GSH depletion observed in the absence of the CYP450 inhibitor (36). The partial counteraction by MTP in the reduction of GSH levels might be related to the decreased need of GSH to detoxify the MTX toxic metabolites by conjugation, since the formation of those intermediary species is inhibited by MTP. Another possibility is that the inhibition of CYP450 leads to the formation of less reactive species resulting of the electron leakage of the CYP450 reaction by itself, thus consuming less GSH. At high MTX concentration (200µM), although the membrane cellular integrity was preserved by MTP (0.5mM) co-incubation, CYP450 inhibition did not alter the intracellular GSH levels reduced by MTX incubation (36). Noteworthy, full protection of MTX-induced cytotoxicity was observed with the simultaneous incubation of MTP (1mM) and MTX at high concentrations (200 to 400µM) in two different hepatic cell models, namely hepatocytes isolated from male adult rats and HepG2 cells incubated for 4 and 9h (37). The prevention of MTX-induced cytotoxicity with MTP obtained by Mewes and co-workers (37) was superior of those demonstrated by us and by the work of Li and co-workers (36). However, it is important to refer that we cannot directly compare different endpoints, cell models, MTX and MTP concentrations. In fact, the concentration of MTP employed by Mewes and co-workers (1mM) was twice the one used by us and Li and co-workers (0.5mM) and our incubation period was longer (96h) with lower MTX concentrations. Moreover, the full *vs.* partial protection observed can be related to the differences in the parameters evaluated to measure the cell damage. Mewes and co-workers quantified the ultimate cell viability loss through the LDH leakage assay and we used the MTT reduction assay in our protective studies with metabolism inhibitors. At least in the H9c2 cell model, the MTT reduction assay demonstrated to be more sensitive to detect MTX cytotoxicity than LDH leakage test, as demonstrated by the time and response curves using the same MTX concentration range and incubation periods in the H9c2 cells (Manuscript II). This result could be explained by the nature of both cytotoxicity assays: the MTT reduction test is related to the cell ability to metabolize formazan crystals. The MTT metabolization is mostly catalyzed by mitochondrial dehydrogenases, thus the reduction of MTT is commonly considered as a mitochondrial viability index (106). On the other hand, LDH leakage assay is associated to membrane disruption and consequent loss of cellular integrity (127). Hence, LDH leakage assay usually measures irreversible damage while changes in the MTT reduction assay, as well as alterations in the antioxidant defenses, commonly manifest themselves earlier. Thus, it can explain the MTP-induced full protection observed in the LDH leakage assay and the absence of a protective effect considering the GSH levels observed by Li and co-workers with MTX high concentration (200µM) (36).

IV.2.1. Cytoxicity as a consequence of metabolic activation

Traditionally, it is believed that the mechanisms of MTX cardiotoxicity involve the oxidative activation of its quinone group, leading to reactive species generation (36,37). Indeed, it was demonstrated that the incubation of MTX (1.60µM) with H9c2 cells elicits late increases in the peroxides production after a 16h incubation (128). However, the knowledge that the one-electron reduction potential of MTX does not favor the formation of a semi-quinone radical brought up questions concerning whether the MTX redox cycling has a primary role in MTX cardiotoxicity (35,59,129). Some authors defend that, instead of causing oxidative stress, MTX elicits antioxidant effects (1,29) since the inhibition of lipid peroxidation after MTX incubation was observed in many *in vitro* models, such as heart sarcosomes isolated from rabbit, mitochondria isolated from rabbit, and in liver microsomes isolated from rabbit (29,75). Notwithstanding the contradictory results, the interest in the assessment of the MTX effects among (anti)oxidative pathways still persists because MTX does not seem to be innocuous to the cellular antioxidant defenses.

The enzymatic pathway of MTX oxidation has a strong influence in the extent and nature of all formed metabolites (30). For a long time, it was discussed whether MTX undergoes one- or two-electron reduction since this issue will be connected to the magnitude of oxidative stress formed as consequence of MTX bioactivation (32,33,35,130). The one-electron reduction yields reactive semi-quinone radicals and is promoted by reductases (e.g. flavin NADPH cytochrome reductases) and peroxidases such as myeloperoxidase (30,33,38) (Figure 7). The generated semi-quinones enter in deleterious redox cycling with oxygen, forming many reactive oxygen species and, consequently, oxidative stress, in a process similar to what is described for doxorubicin (33,35). The two-electron reduction is mediated by CYP450 mixed function oxidases and NADPH quinone acceptor oxidoreductase (also known as DT-diaphorase) and forms hydroquinones, which are more stable products (32,33,35,130) (Figure 7). Commonly, hydroquinones are rapidly eliminated from the cell, but sometimes, in the presence of oxygen, they enter in a redox cycle due to auto-oxidation to semiquinones and quinones, also generating superoxide radical anion, as represented in the Figure 7 (36).

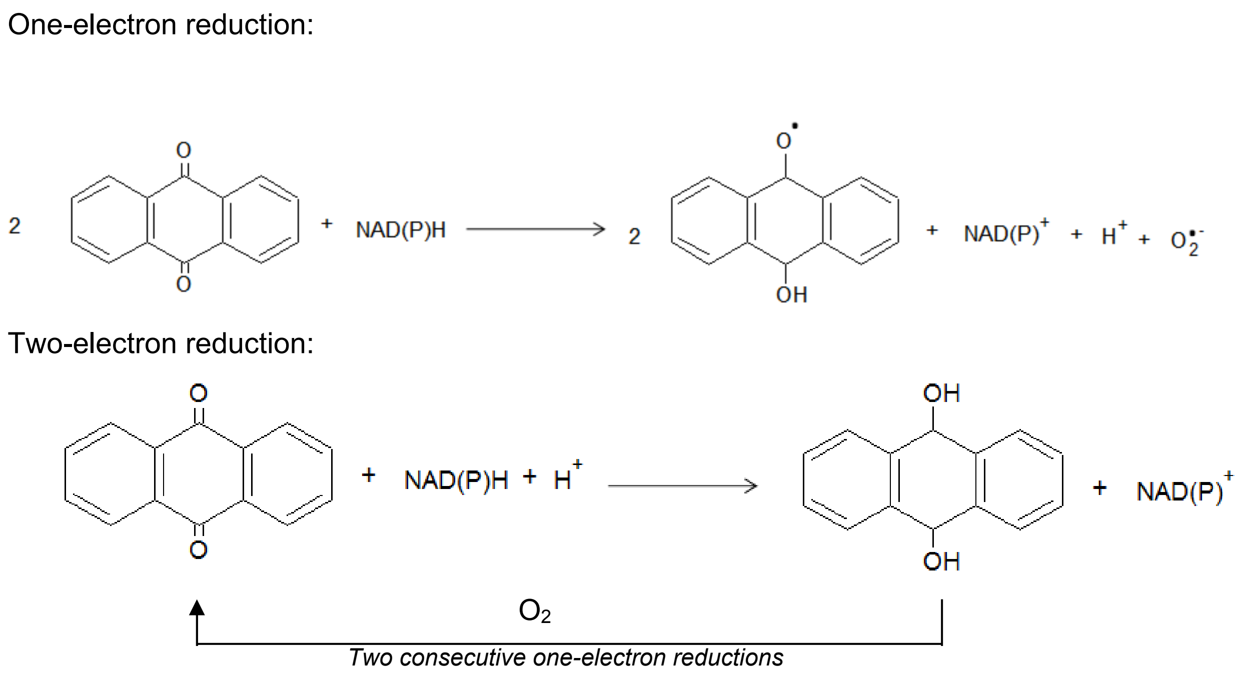

Figure 7: Schematic representation of one-electron and two-electron reduction of anthraquinones. The one-electron reduction involves the formation of semi-quinone radicals that can enter into redox cycling. Two-electron reduction generates hydroquinones, which can be detoxified or suffer auto-oxidation (two consecutive one-electron reductions). Adapted from (36,130).

Regarding MTX metabolism, the two-electron reduction is considered the preferential pathway, as evidenced by the prevention of the MTX bioactivation with CYP450-mediated metabolism inhibition (33,36,37), which was also observed by us (Manuscript I). One product of the two-electron reduction is the naphtoquinoxaline metabolite. However, studies demonstrate that MTX can also be metabolized by peroxidases in two steps of one-electron reductions to naphtoquinoxaline metabolite, which may contribute to the great effectiveness of MTX in the treatment of solid tumors containing high peroxidase secretion capacity (30,34,38). Thus, soluble peroxidase/hydrogen peroxide systems present in the extracellular spaces of solid tumors, such as lymphoma, breast, and prostate cancer can oxidize MTX and the consequent acidic oxidation products may accumulate in the neutral intra-cellular compartments, binding to cell targets and increasing MTX cytotoxicity (30).

The naphtoquinoxaline metabolite formation has been reported through the action of CYP450s, DT-diaphorase, NADPH cytochrome reductases, and peroxidases, however it is plausible that the naphtoquinoxaline detected in urine samples of MTX patients is primary derived from CYP450 oxidation, since it is the main oxidoreductive pathway (30). The formation of naphtoquinoxaline involves the abstraction of two electrons. Thus, when suffering one-electron reduction, the naphtoquinoxaline formation might be due to two consecutive one-electron abstractions, the second one removed via enzyme interaction with MTX radicals or from enzyme-independent radical disprotonation process (30). Moreover, as already mentioned, the reduction of MTX by flavin-reductases is not easy due to its low one-electron reduction potential (35). Additionally, oxidation by peroxidases is strongly dependent on hydrogen peroxide availability (30). The availability of NADPH is also crucial, as shown in a study using isolated human liver NADPH CYP450 reductase, since the reductive activation of MTX was demonstrated only in the presence of high amounts of NADPH (500μM) (28). While incubation of MTX (100μM) in the presence of isolated NADPH-cytochrome reductase increased the rate of NADPH oxidation about 20 fold, using a more complex system such as rabbit hepatic microsomes, MTX incubation did not stimulate the basal oxidation of NADPH (29), corroborating the difficulty of MTX undergoing one-electron reduction in non-isolated enzyme systems.

In order to evaluate the role of the metabolic enzymes in MTX-induced cytotoxicity, Li and co-workers did a study in 1995 using the MCF7 cell model and cells were pre-treated with 1,2-benzanthracene (25μM) for three days. Pre-treatment with 1,2-benzanthrecene induced by 64- and 1.6-fold the activities of CYP450 and DT-diaphorase, respectively. An increase of MTX-induced cytotoxicity, evaluated through the LDH leakage assay, was related to a decrease in the GSH and protein contents after pre-treatment with 1,2-benzanthrecene. Even in the cells that had a high increase in CYP450 activity, the co-incubation of MTX (10μM) with the CYP450 inhibitor MTP (0.5mM) for 4h prevented the GSH depletion and reduced the LDH leakage, when comparing to the results observed in the absence of MTP (MTX concentrations of 10μM and 200μM). Moreover, co-incubation of MTX and dicoumarol (an inhibitor of DT-diaphorase) (30μM) for 4h prevented the MTX deleterious effects upon GSH levels in all the MTX treated groups (10, 100, and 200μM), in the protein content in 100 and 200μM MTX, and in the LDH leakage assay only in the lower MTX concentration tested (10μM). These results show the importance of the two-electron reduction in MTX bioactivation and its involvement in MTX cytotoxicity and impairment of oxidative stress defenses. In the same cell model, pre-treatment with dexamethasone (1μM) elicited a small but significant increase in the NADPH cytochrome c reductase activity. This increased activity of NADPH cytochrome c reductase had no effect on MTX-induced cytotoxicity, evidencing, once more, that the one-electron reduction does not seem to be relevant for MTX cytotoxicity (36). However, in a study using HepG2 cells by Duthie and co-workers in 1989, no protective effect in GSH levels was observed by the incubation of MTX (100μM) with dicoumarol (30μM) (33). Moreover, dicoumarol potentiated the cytotoxicity observed with MTX, evaluated by the LDH leakage assay (33). These results contradict the results demonstrated by Li and co-workers (36), probably due to the use of different cell models with dissimilar metabolic competence (HepG2 cells *vs.* MCF7 cells).

IV.2.2. MTX-induced oxidative stress and its (cardio)toxicity

Oxidative stress appears to be an important component to the toxicity mechanisms of several xenobiotics, which contain or can be biotransformed into a quinone (124,131). Actually, oxidative stress is commonly referred as a key factor for the intrinsic cardiotoxicity elicited by catecholamines (118,132) and the cardiotoxic effects of antineoplastic agents such as doxorubicin and daunorubicin (58,133,134). Since the cardiotoxicity of MTX is clinically similar to that observed with doxorubicin, it was believed that these drugs also shared the mechanisms involved in the late cardiac disease (102). Hence, the possibility that oxidative stress exerts a leading role in the MTX-induced cardiotoxicity has been considered and largely investigated (49,125,129,130,135).

The cardiac tissue is particularly susceptible to oxidative stress when compared to other organs due to its limited antioxidant defenses (136). Cardiac GSH levels and antioxidant enzymes, namely catalase, superoxide dismutase, and glutathione peroxidase are less abundant in the cardiac tissue than in the liver (137,138). Even so, paradoxically, the heart generates higher levels of hydrogen peroxide than other organs (139) and it may contribute to its vulnerability to drug-induced oxidative imbalance. It is known that there is a significant positive correlation between the metabolism of most quinone(di)imines and the generation of superoxide anion radical, which makes the heart a target to drugs containing these chemical structures, such as MTX (124,130,131). Another feature that aggravates the consequences of drug-induced cardiotoxicity is the modest regenerative ability of the heart. Nowadays, it is known that cardiac cells present a limited capacity for myocardial regeneration, although it is commonly insufficient to restore normal heart function after cardiac injury (140).

Besides the above oxidative stress thesis for MTX-induced cardiotoxicity, the results compiled in Manuscript II and the glutathione status evaluated in MTX treated heart presented in the Manuscript III are consistent with the old thesis of Butler and co-workers that MTX metabolism is expected to produce few, if any, reactive species (130). The controversy of these results will be discussed in the following paragraphs in order to clarify the different perspectives and studies related with the formation of reactive species, lipid peroxidation, GSH content, and the use of antioxidants as NAC or of iron chelators.

Low levels of reactive species formation were observed with some quinone(di)imines, such as indophenol, N,N-dimethylindolaniline, 2,3’6-trichloroindophenol trifluoracetate, and N,N'-dichloro-2-chloro-1,4-benzoquinonediimine, and apparently, MTX. These compounds undergo rapid metabolism, forming little or no detectable reactive species (131). Moreover, as already referred, the oxidoreductive reactions involved in the MTX metabolism favor the formation of hydroquinones instead of semi-quinones (33,36,37). Hence, there is a minor formation of reactive species directly associated with this metabolism in comparison with those generated by quinone/semi-quinone redox cycling (130). Even so, the auto-oxidation of hydroquinones can also lead to some reactive species generation (36). The studies conducted in the H9c2 cells (Manuscript II) suggested that the oxidative stress might not be the primary cause of the MTX cytotoxicity, since the evaluation of several markers of oxidative stress showed that they remained largely unchanged.

Regarding lipid peroxidation, we did not observe any significant changes in the malondialdehyde levels after incubation with MTX (100nM and 1μM) in H9c2 cells at any time point tested (24, 48, or 96h) in comparison with control levels (Manuscript II). This finding is in accordance with the results obtained in heart homogenates from MTX treated mice (15mg/kg, i.p.) evaluated two and five days after MTX single dose (59). Surprisingly, MTX *in vitro* was already associated with the inhibition of lipid peroxidation. In fact, in liver microsomes, heart sarcosomes, and mitochondria isolated from rabbit incubated with MTX (50, 100, and 200μM), the rate of lipid peroxidation was significant lower than that observed in controls (29,75). Moreover, besides inhibiting the endogenous lipid peroxidation, it has been demonstrated that MTX incubation at micro molar levels inhibited doxorubicin induced lipid peroxidation, ferric ion- and ADP ferric ion-mediated lipid peroxidation (29). The mechanisms involved in these inhibitory effects on lipid peroxidation remain mainly unknown: it has been suggested, however, that MTX can modify oxidative homeostasis. Data suggest that MTX-inhibition of lipid peroxidation is not related to the lower formation of superoxide radical anion since the inhibition of doxorubicin-induced microsomal superoxide generation is only reached with higher MTX concentrations than those required to inhibit the lipid peroxidation (29,75). Furthermore, MTX weakly complexes iron, which is involved in the initiation/propagation of lipid peroxidation (75). Hence, authors suggest that the MTX-inhibition of lipid peroxidation occurs at a mechanistic step subsequent to the enzymatic generation of superoxide and cannot be attributed to any of MTX iron chelation abilities (75).

Alterations in the oxidative stress parameters, namely increase in the reactive species and decrease in the GSH intracellular levels, were found only in the last time-point evaluated in the H9c2 cell model. In fact, after 96h incubation with MTX, both working concentrations (100nM and 1μM) caused a significant increase in the reactive species (Manuscript II), evidencing that this effect is a late event, since it did not occur in any of earlier time points tested (1h to 10h incubation). The modest potential to generate reactive species in short incubation periods was also demonstrated in MCF7 S9 fractions, where a very low superoxide anion generation was observed after 30min incubation with MTX (100µM) and no hydroxyl radical or semiquinone formation was detected after incubation with MTX (even with the high concentration of 400µM) (35,129). Incubation of MTX (100µM) in the presence of NADPH-cytochrome reductase increased superoxide and hydrogen peroxide generation about 20-fold, however this was considered a slight increase when compared to structural analogues. Furthermore, using more complex systems such as rabbit hepatic microsomes, MTX incubation did not stimulate any detectable superoxide formation (29), suggesting that this pro-oxidant potential is only reached with isolated enzymes. Nevertheless, in the H9c2 cells after a 16h incubation with MTX (1.60µM), peroxide production increased (128). In the results presented in the Manuscript II, we detected increases in reactive species generation after 96h of MTX incubation (100nM and 1µM). These results corroborate the suggested hypothesis that the oxidative imbalance eventually associated with MTX is secondary to another initial toxic mechanism. Considering *in vivo* studies, mice treated with a single dose of MTX (15mg/kg, i.p.) did not present any cardiac significant changes in the hydroperoxide-initiated chemiluminescence, after two to five days (59).

After 96h incubation with MTX at the lower working concentration (100nM), a slight but significant decline in the GSHt and GSH levels was observed (Manuscript II), without any change in the GSSG levels. One hypothesis that could explain this finding is that the GSSG formed can be extruded by multidrug resistance proteins for the extracellular medium, since the GSSG efflux is a cellular response aiming to protect the cells from oxidative stress (108,141). Another possibility is that GSH levels are diminished due to conjugation with either MTX or its metabolites. The later hypothesis should be regarded as plausible, since the conjugation of MTX metabolites with GSH is described as one of the main detoxifying pathway of MTX (36).

In our study, decrease of intracellular GSH content was not observed for 1µM of MTX, even considering that similar levels of reactive species were generated when compared to MTX 100nM group, at 96h incubation (Manuscript II). One possible explanation is that GSH levels already recovered at 96h of 1µM MTX incubation by GSH synthesis. Another hypothesis is that MTX elicited a concentration biphasic decrease in the GSHt *in vitro*. The biphasic effect of MTX upon GSHt levels was already demonstrated in another cardiac cell model (HL-1 cells), where after 24h, the incubation of MTX (1µM) increased the GSHt levels compared to control cells and the higher concentration (10µM) did not affect GSHt levels in the same incubation conditions (142). At a longer incubation period (48h), while the values of intracellular GSHt levels remained similar to control with the lower MTX concentration of 1µM, at 10µM MTX incubation elicited a significant decrease in the GSHt levels (142). Regarding *in vivo* results obtained in the scope of Manuscript III, no significant changes were observed in the cardiac glutathione levels (GSHt, GSH, and GSSG) in none of the treated animals (MTX22 or MTX48). Conversely, cardiac GSH levels were not affected by MTX treatment (15mg/kg, i.p.), in mice that suffered euthanasia 2-5 days after MTX administration (59) and cardiac GSH content, glutathione peroxidase, catalase and superoxide dismutase activities were not altered in female BALB/c mice weekly treated with MTX (0.2mg/kg, i.p.) over 12 weeks and suffered euthanasia one week after the last treatment (50).

The use of NAC (1mM) failed to prevent the cytotoxicity elicited by MTX (100nM and 1µM) after 96h incubation with H9c2 cells (Manuscript II), evaluated through the MTT reduction assay. NAC is a powerful scavenger of reactive species and it improves the GSH synthesis (143). Because of these properties, NAC has been shown to be effective in protecting cells when oxidative stress conditions are imperative (113,114,127). However, the only cytotoxic parameter evaluated by using this protective study was the reduction of MTT evaluated only at 96h. Thus, it should not be excluded that NAC might ameliorate the oxidative stress altered parameters, such as late reactive species generation or GSH decrease in the MTX 100nM group (143). Even so, in case that protection occurred, it was not enough to prevent cellular damage, again suggesting that oxidative stress does not occupy a leading role in the MTX-mediated cytotoxicity.

Contradictory results exist regarding the protective effects elicited by ICRF-187, an iron chelator, in the MTX-induced toxic effects. The aim of using ICRF-187 is to block the iron-stimulated free radical formation via Fenton reaction (144). In MTX-treated isolated neonatal rat cardiomyocytes, the incubation with ICRF-187 (50µg/ml) elicited a partial cytoprotection when continuous incubated 3h before, during, and 72h after previous MTX (2µg/ml) 3h incubation, as evaluated through the ATP measurement. However, regarding 3h co-incubation of MTX and ICRF-187 (without ICRF-187 pre-treatment or post treatment but using the same concentrations), this regimen was not effective in protecting the cells against MTX-induced cell damage on ATP levels (125). Thus, the cellular protection was probably dependent on the time of ICRF-187 incubation. Moreover, ICRF-187 administered 5min before MTX, (at doses 20 times higher than MTX dose) delayed the MTX-induced death on CD-1 mice receiving MTX (twice weekly, at doses 2mg/kg and 4mg/kg, treated on weeks one, two, and five and suffered euthanasia on the week seven) (125), corroborating the cardioprotective effect shown *in vitro* (125). Despite the cardioprotection demonstrated *in vitro* and *in vivo,* ICRF-187 did not affect the MTX antitumor action in the L1210 cell line (a mouse leukemia cell model) and in a DBA/2J mice bearing P-388 leukemia (125), which suggested that the mechanisms involved in the

MTX-antitumor action and MTX-induced cardiotoxicity are diverse. In contrast with the good results obtained by Shipp and co-workers, female BALB/c mice weekly treated with ICRF-187 (12.5mg/kg, 30min prior to MTX) and MTX (0.2mg/kg) over 12 weeks, suffered euthanasia one week after the last treatment, did not present significant changes in the cardiac parameters evaluated (morphological changes evaluated through light and electron microscopy) compared to mice that did not receive ICRF-187 (50). The mismatched results may arise from differences in MTX doses and regimen administration, namely the duration of treatment. Even so, the partial protective effects of ICRF-187 *in vitro* and *in vivo* suggest that divalent metal ions, such as iron, can be partially involved in the MTX-cardiotoxicity (125), not necessarily through iron-mediated oxidative stress. Moreover, we cannot exclude the possibility that the partial protection observed is due to another intracellular mechanism of ICRF-187, which is not yet elucidated.

Despite the majority of negative results in cardiac models, oxidative stress seems to assume a more pronounced role in other target organs such as the liver. The MTX-induced hepatic damage evidenced in the study presented in the Manuscript IV, for example, was associated with increases in the hepatic levels of GSHt observed in the MTX48 group. This increase was related to a slight (but significant) increase in the GSH hepatic levels and to a notorious increase in the GSSG levels. Increases in GSH might be interpreted as an attempt to enhance the antioxidant content in order to counteract the inflicted injury, while increased levels of GSSG are related with oxidative stress. It is known that Kupffer cells, which were abundantly present in the MTX48 livers (Manuscript IV), are a source of reactive species (145). The link between oxidative stress and the MTX-induced hepatic damage was already suggested in a study with mice, where a single administration of MTX (15mg/kg) caused increases in the hepatic lipid peroxidation, decreases in the antioxidant enzymes activities (superoxide dismutase, catalase, and glutathione peroxidase), and depletion of hepatic retinol and GSH levels (49). Moreover, the incubation of MTX (100μM) with HepG2 cells for 6h was enough to promote the decrease in the GSH levels (33). The apparent contradiction between our results (increase in the GSH hepatic levels) and the previously reported data (decreases in the GSH content) may be explained by the differences in the experimental design and model. The quoted studies assess *in vivo* the liver GSH levels three, four, and five days after MTX administration (49) or 6h after high concentration incubation of cells with MTX (33). In the present study, the significant changes in the glutathione status were a late event, only observed 28 days after the last cycle of a cumulative dose administration regimen. Hence, the organism is probably subjected to compensatory effects, in order to counteract the increase in the hepatic GSSG levels and this adaptive phenomenon is favored by the long time between last MTX administration and rat euthanasia. Another evidence of MTX-potential oxidative stress on the liver, in particular in human liver microsomes incubated in anaerobic conditions with MTX (50µM), is the increased formation of reactive species detected through electron spin resonance analysis (135).

We hypothesize that the different propensity to oxidative stress in different tissues might be related to organ metabolic competence. The enzymatic availability in the liver is much higher than in the heart. Therefore it is possible that in other systems with a smaller amount of enzymes available, such as heart, the oxidative stress is not a primary cause of damage, because MTX one reduction potential is very low (527± 5 mV) (35). In contrast, in an enzymatic abundant environment, the extent of MTX suffering oxidative activation (and, therefore, producing reactive intermediates) is higher, and despite the preference for two-electron reduction pathway, a minor extent (but higher than in another organs enzymatically poorer) might undergo to one-electron reduction.

IV.3. Calcium regulation, mitochondrial membrane potential and cell death

The role of calcium on cell physiology goes from cell signaling to cell death (146). Normally, intracellular calcium levels are tightly regulated between the range of 10-100nM by ionic channels and transporters, energy-dependent pumps, and organelles that uptake and buffer this ion (147–149) (Figure 9). The first calcium barrier is the plasma membrane, which mediates the calcium influx by ligand-gated and voltage-channels in order to maintain a large calcium gradient across the membrane (149). The endoplasmic reticulum is the largest reservoir of calcium in cardiomyocytes, having concentrations that can reach the milimolar levels (148,149). Furthermore, mitochondria perform the function of buffering intracellular calcium. The influx of calcium into the mitochondrial matrix is dependent on the membrane electrochemical potential, which is maintained by mitochondrial respiration, and by a low resting intra- mitochondrial calcium concentration, which is maintained primarily by the mitochondrial sodium/calcium exchanger (146).

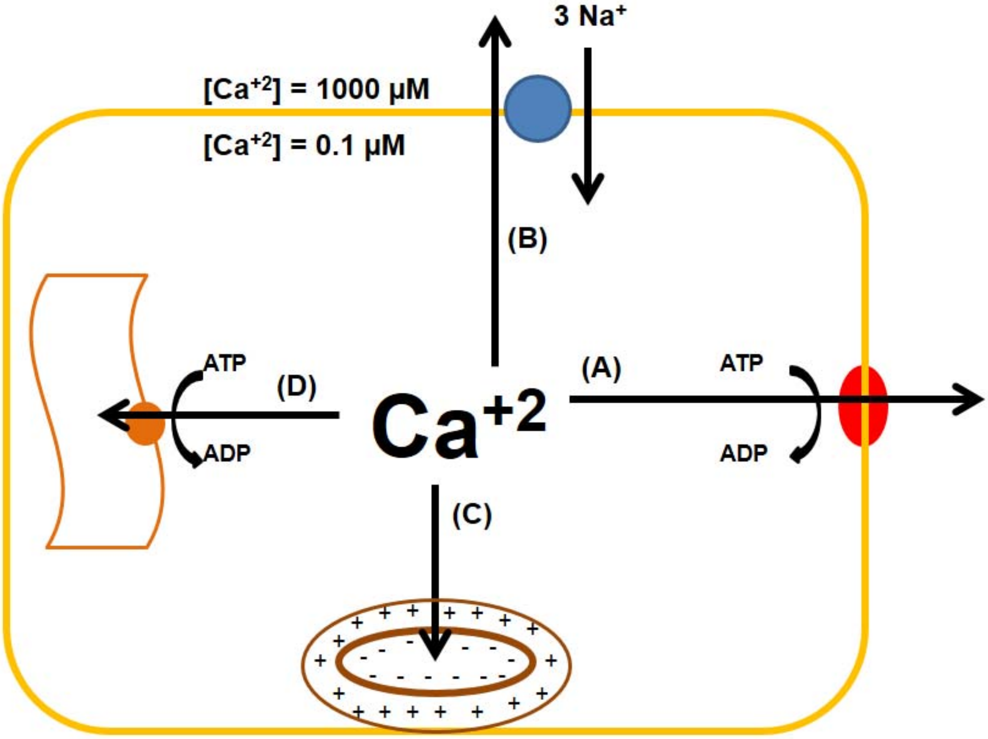

Figure 8: Mechanisms of elimination and maintenance of calcium cytosolic levels. (A) Calcium ATPase-mediated pumping into the extracellular space, (B) ion-gradient driven transport into the extracellular space by the sodium/calcium exchanger, (C) ion-gradient driven transport into mitochondria by calcium uniporter, and (D) ATPase-mediated transport into the endoplasmic reticulum. Adapted from (148).

Intracellular calcium levels rise when calcium flux into the cell is increased, following the energetic impairment and/or in conditions that modify the release or uptake of calcium from the endoplasmic reticulum and/or mitochondria (147). As a consequence, elevated intracellular calcium levels may activate hydrolytic enzymes, such as phospholipases, endonucleases, and proteases, resulting in the modification of the permeability of the membranes and degradation of intracellular structures (146–148). Moreover, calcium overload may elicit the depletion of energy reserves, the dysfunction in microfilaments and the generation of reactive species (148). Hence, the calcium hypothesis is based on the observation that pathological increases in the intracellular calcium lead to degenerative events that can be avoided if those increases are prevented (146).

A sustained increase in the intracellular calcium precede cellular pre-lethal and lethal changes (147). It is known that calcium overload can trigger both cell death forms: necrosis and apoptosis (146). The cell death mechanisms are discussed in more detail below, but calcium increases have an important role on caspase activation and consequent apoptosis (149).

In the *in vitro* study presented in the Manuscript II, MTX incubation with H9c2 cells led to increased calcium intracellular levels with concomitant increase in the mitochondrial membrane potential. A close relationship between the mitochondrial membrane potential and calcium intracellular levels is well known, since the regulation of calcium mitochondrial levels is mediated through the calcium uniporter using the mitochondrial membrane potential as driving force (148,150). The retention of mitochondrial membrane potential during calcium increase favors mitochondrial calcium uptake and overload, resulting in cell death, normally by apoptosis (149). The mitochondrial calcium overload secondary to a cytoplasmic calcium overload may trigger the mitochondrial permeability transition pore (MPT) (149). Although a low conductance state of the pore is reversible, sustained transitions dissipate the mitochondrial membrane potential, impairing ATP synthesis, leading to the release of cytochrome c and, consequently, initiation of apoptosis (148,149,151). The increase in mitochondrial membrane potential is observed in pathological conditions, such as ischemic cardiomyocytes during reperfusion. In ischemic conditions, cardiac mitochondria are energized and permit calcium uptake and mitochondrial damage. During reperfusion, the mitochondrial membrane potential increases in order to allow the respiration, lethally damaging other organelles by cytosolic increases of calcium (149). Other examples of increased mitochondrial membrane potential occurred in mitochondrial vascular endothelial cells subjected to pulsatile shear stress (152), and physiologically during pre-implantation stages of human and mouse embryo development, in response of metabolic demand (153). The hyperpolarization of mitochondrial membrane potential sometimes can precede the mitochondrial collapse and, consequently, cell death (154).

The chronology of the calcium impairment-induced lesion also can be opposite, e.g., a direct lesion in the mitochondria or injuries affecting the energetic metabolism can affect calcium regulation since the cellular mechanisms involved in calcium handling are ATP dependent. Thus, at low energetic levels, calcium pumping activity decreases, resulting in cytosolic calcium increase (149) ultimately driving the cell to the “no return point”, leading to cell death (147). In our work, we observed an important energetic depletion caused by MTX *in vitro* and *in vivo* and signs of mitochondrial toxicity. However, it was not yet possible to conclude if the calcium overload is a cause or a consequence of that mitochondrial lesion.

In contrast to our present work, a study of Kluza and co-workers in 2004, also with the H9c2 cells and using similar MTX concentrations and incubation periods (1.60μM for 24h), showed a decrease in the mitochondrial membrane potential (128). In fact, in our study, 24h incubation with 100nM and 1μM MTX caused an increase and no alteration in the mitochondrial membrane potential, respectively. Considering that we used the same cell model and similar MTX concentrations, it is possible that a slight increment in MTX concentration (1.60μM instead of 1μM) is enough to promote a different cellular response, namely the loss of the mitochondrial membrane potential. Also in the study performed by Kluza and co-workers, the MTX concentration of 1.60μM was defined as the mean lethal concentration (LC_{50}) at 24h incubation, evaluated through the trypan blue exclusion test. In our cytotoxicity studies the LD_{50} at 24h was about between 10 and 50μM (in the LDH leakage assay) and 5 and 10μM (in the MTT reduction test). The discrepancy between our results and those presented by Kluza and co-workers might be explained through the nature of the cytotoxicity tests used (trypan blue exclusion assay *vs.* LDH leakage assay and MTT reduction test). Moreover, in the protocol performed by Kluza, they employed a trypsinization step before the trypan blue exclusion assay, which may have contributed to the apparent higher cytotoxic effects observed since the cells were already fragile due to the previous incubation with MTX. Furthermore, another data that could help to understand these differences is the working number of passages of H9c2 cells, however, this information was not available in the manuscript by Kluza. Notwithstanding, in the same study, the 24h incubation of MTX (1.60μM) with MTLn3 mammary adenocarcinoma cells caused a significant decrease in the aggregation of JC-1 probe, which the authors attribute to an increase in the mitochondrial mass (128). It could be an adaptive phenomenon, since mitochondria play a significant role in the calcium-dependent cell signaling by acting as a buffer of cytosolic calcium excess (98,146,155).

IV.4. MTX-induced cell death

Cell death is a normal phenomenon occurring during developmental stages and also in adult life, allowing the cells' turnover (147). Typically, cell death can be divided in two modes: necrosis, generally seen as an uncontrolled process, and apoptosis, a programmed manner of cell death (148). Additionally, there is cell-death by autophagy, which is characterized by the sequestration of cytoplasmic material within autophagosomes prior to degradation and occurs without chromatin condensation but with massive autophagic vacuolization of the cytoplasm (156).

During early stages of necrosis, cell can present alterations in compartment volume, e.g. swelling and rupture of endoplasmic reticulum or mitochondria, cytoplasmic blebbing, chromatin condensation, and eventually, cell membrane disruption (147,157). Based on the morphologic features of necrosis, it has been considered as an unregulated or accidental fate (158). Recently, however, this view is under debate and it is considered that some types of necrotic death may be regulated (158). Thus, a new concept emerged: the necroptosis or aponecrosis, a cell-death process that shares the morphologic features of necrosis but is highly regulated, like apoptosis (159).

Apoptosis occurs during development, aging, and even to allow the normal cell renewal, functioning as a homeostatic control of cell population (157). Morphologically, comparing to necrosis, the apoptotic cells typically shrink rather than swell, the nuclear chromatin condensation is more pronounced (pyknosis), and the cytoplasmic blebs usually contain organelles such as mitochondria (147). Afterwards, when the nuclear and cytoplasmic content are condensed, it breaks into membrane-bound fragments named apoptotic bodies that are phagocytized (148).

Cells can trigger apoptotic death through different pathways that are linked and can mutually influence each other (157). Additionally to the intrinsic and extrinsic pathways, there is an additional caspase dependent pathway that involves T-cell mediated cytotoxicity and perforin-granzyme-dependent killing of the cell (Figure 8). Caspases are cysteine proteases, mostly located in the cytoplasm in their inactive forms (procaspases). When caspases are activated, they cleave structural proteins, especially in specific aspartate residues sites (148) (Figure 8).

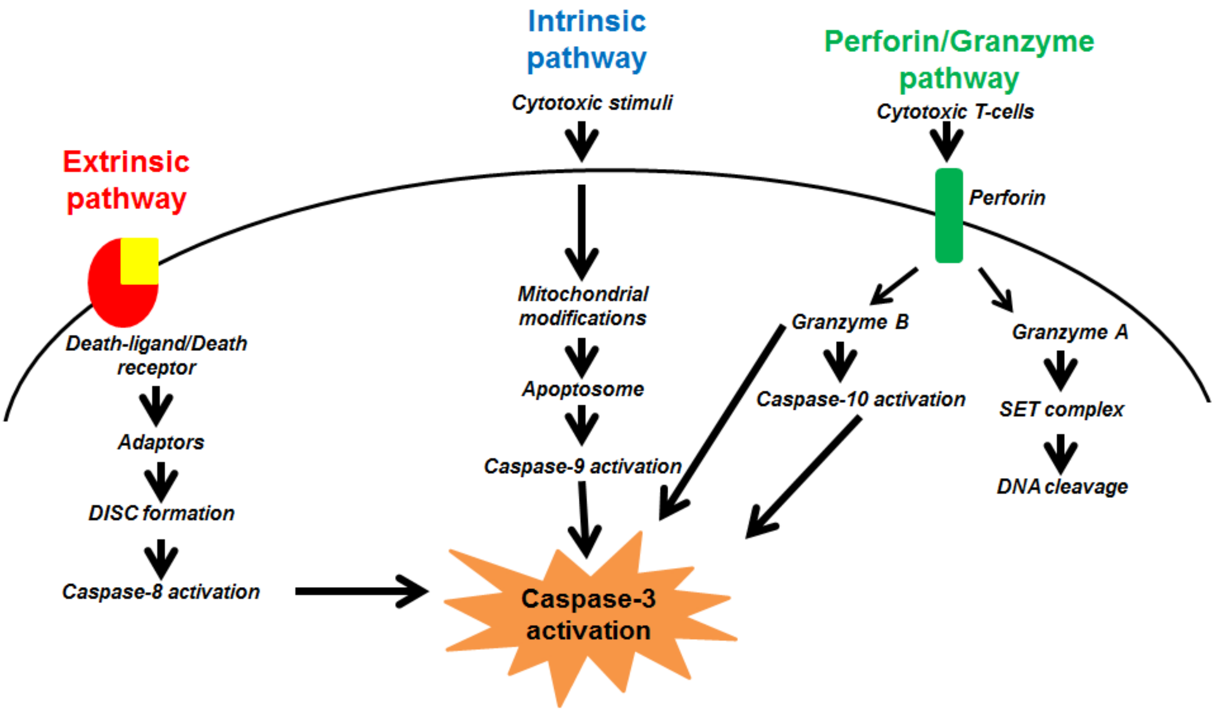
Intrinsic pathway
Cytotoxic stimuli
Perforin/Granzyme pathway
Cytotoxic T-cells
Extrinsic pathway
Perforin
Mitochondrial modifications
Granzyme B
Granzyme A
Death-ligand/Death receptor
Apoptosome
Caspase-10 activation
SET complex
Adaptors
Caspase-9 activation
DNA cleavage
DISC formation
Caspase-8 activation
Caspase-3 activation

Figure 9: Schematic representation of the energetic-dependent cascade of events leading to diverse apoptotic pathways. Each pathway activates its own procaspase, which will converge to caspase-3 activation (with the exception of granzyme A via that is caspase-independent). Caspase-3 activation results in other procaspases activation (procaspase 6 and 7) and, finally, leads to morphological and biochemical features of apoptosis. Adapted from (148,157).

The intrinsic pathway involves mitochondria and is independent of receptor-mediated stimuli (148,157) (Figure 8). The cytotoxic stimuli provoke changes in the inner mitochondrial membrane that results in the opening of MPT. It induces loss of the mitochondrial transmembrane potential and release of pro-apoptotic proteins, such as cytochrome c, Smac/DIABLO, and HtrA2/Omi into cytosol, which, consequently, activate the caspase-dependent mitochondrial pathway (157) (Figure 8). Caspase-9 is activated through the formation of the apoptosome, which consists in seven heterodimers of apoptotic protease activating factor-1 (Apaf-1), joined with cytochrome *c* that form a symmetrical “wheel”, which binds to procaspase-9 and promotes its activation (160). Thus, caspase-3 is sequentially activated by caspase-9 (148).

The extrinsic pathway is related to cell surface death receptors (158). The ligands bind to their respective cell death receptor, normally members of the tumor necrosis factor receptor gene family (157). Subsequently, a trimerization of the receptor and the recruitment of adapter molecules and procaspases to the cytoplasmic tail of the receptor occur (148). Then, the death-inducing signaling complex (DISC) is formed and results in the auto-catalytic activation of caspase-8, subsequently triggering to execution phase of apoptosis, also with caspase 3 activation (157).

The perforin-granzyme-dependent pathway involves immunocytotoxicity mediated through T-cells that exert their cytotoxic effects on tumor cells and virus-infected cells via the secretion of perforin (a transmembrane pore-forming molecule) and release of cytoplasmic granules (granzymes) through the pore and into the target cell (157,161). As shown in the Figure 8, the granzyme B activates caspase-10, while granzyme A induces apoptosis through caspase independent pathways (157).

Caspase-3 is seen as a key executioner to apoptosis, considering that the extrinsic and intrinsic pathways converge to its activation (107). In fact, execution caspases (caspase-3, caspase-6, and caspase-7) activate cytoplasmic endonucleases and proteases that degrade nuclear material and nuclear/cytoskeletal proteins, ultimately leading to irreversible death of the cell (157,160).

Knowing the main cell death mechanisms, it is interesting to observe that the mechanisms underlying cell death induced by MTX are described as bimodal: apoptosis at lower concentrations and necrosis at higher concentrations (15). As already stated, in the present *in vitro* studies we used MTX working concentrations clinically relevant given the plasma and tissue levels of MTX (14,26). Noteworthy, we observed a time- and concentration- dependent cytotoxicity, being the effects more pronounced in the MTT reduction assay rather than in the LDH leakage assay (related to cell membrane disruption) in all time-points tested. At 24h incubation, only the high concentration of 50μM caused a loss of viability higher than 50% in the LDH leakage assay. Even after 96h incubation with MTX (100nM and 1μM), the majority of cells maintained their cellular membrane integrity, which means that we are not predominantly working in a necrotic field with those concentrations (Manuscript II). At higher concentrations, namely more than 5μM, the results in the LDH leakage assay start to be more expressive at 48 and 72h incubation (in the range of 50-60% of viability), being extensive at 96h MTX incubation (maintaining only about 25% of total cell viability). These data suggest that the MTX-induced damage into the cellular metabolic competence is prior to the loss of cellular membrane integrity.

Considering the death mechanisms, we showed that MTX (100nM and 1μM) elicited an increase in the caspase-3 activity after 24h incubation in H9c2 cells (Manuscript II). These results are in accordance with previously reported characteristic signals of apoptosis (appearance of hypoploid DNA content, cytoplasm and chromatin condensation) after 24h incubation in the H9c2 cells with MTX (1.60μM) (128). After 48h incubation of MTX (1.60μM) in H9c2 cells, features of late phase of apoptosis, such as nuclear disintegration and apoptotic bodies formation, can be observed (128). Recently, the evaluation of caspase-9, caspase-8, and caspase-3 activities after MTX incubation with the HL-1 cell model demonstrated that after 24h incubation, MTX (1µM and 10µM) promoted significant activity increases in all caspase subtypes tested (142). Thus, it was not possible to indicate one preferential pathway of MTX-induced apoptosis, suggesting that MTX can promote intrinsic- and extrinsic-mediated apoptosis. In the same study, after 48h incubation, no changes were observed in caspase 3, caspase-8, and caspase-9 activities compared to control cells (142), being in accordance with our pilot studies. When we evaluated the caspase-3 activity after longer incubation periods (48h and 96h) in H9c2 cells (*data not shown*), no significant differences were observed, suggesting that caspase cascade activation is an earlier effect.

Despite the partial protection towards MTX cytotoxicity (at 100nM and 1µM) after 96h with the co-incubation with the CYP450 inhibitor MTP (0.5mM) or with the CYP2E1 inhibitor DAS (150µM) (Manuscript I), the co-incubation with these metabolism inhibitors did not prevent the increase in the caspase-3 activity promoted by MTX incubation at 24h. Thus, the previous partial protection obtained with the metabolism inhibitors is not associated with apoptosis prevention.

IV.5. Energetic imbalance as a protagonist of MTX-induced cardiotoxicity

Besides the sustained rise in intracellular calcium levels, another critical biochemical disorder that may lead to cell death is ATP depletion. ATP is the major source of energy in the cardiac tissue (162,163). In fact, ATP plays a pivotal role in cellular maintenance, since it is utilized in biosynthetic reactions, incorporated into co-factors and nucleic acids, required for muscle contraction, cellular motility, cell division, vesicular transport, and even for the maintenance of ionic homeostasis and cell morphology (148). In healthy hearts, ATP levels are maintained constant. Despite studies regarding failing hearts have not reached a consensus, some reports found decreased levels of ATP in human failing hearts and that loss has been correlated with the degree of cardiac impairment (164,165).

Due to the importance of energy supply for the muscular function, there is another important muscle energetic reserve system: the phosphocreatine (PCr), which is present in the heart at twice the ATP cardiac concentration (162). The reaction catalyzed by the enzyme CK transfers the phosphoryl group from ATP to creatine, forming PCr (Figure 10) at a rate about ten times faster than the rate of ATP synthesis. There are 3 major CK enzyme subtypes identified: CK-MM is the principal form in skeletal muscle, CK-BB is the predominant form in the brain and the kidney, and CK-MB is the main subtype in the myocardium, although CK-MM is also found in the heart (162). PCr is considered an energetic source of rapid demand and when ATP use exceeds ATP supply, the use of PCr is a major pathway of energy (162). The total creatine pool is about 60 % lower in failing hearts, while CK levels are relatively abundant in this condition (163). Thus, a lower total creatine pool means that PCr must also be lower (163).

$$\boxed{\text{PCr+ ADP +H}^{+} \leftrightarrow \text{creatine + ATP}}$$

Figure 10: Schematic representation of PCr mobilization. PCr is an energetic reserve that, through CK catalyzed-reaction, produces creatine and ATP.

In the present work, decreased levels of ATP were observed in both *in vitro* myoblasts incubated with MTX and *ex vivo* in the heart from MTX-treated rats (Manuscripts II and III, respectively). In the H9c2 cells, the decrease in the ATP intracellular content was evident in all time points tested (24, 48, and 96h), in both MTX working concentrations (100nM and 1µM) and it preceded the declines in the ATP-synthase expression and activity (Manuscript II). In the *in vivo* study, significant decreases in cardiac ATP levels were only seen in the late endpoint (MTX48 group), demonstrating that this effect is a late response. Significant decreased levels of ATP were already demonstrated as a late event (72h after pre-incubation) in cultured neonatal rat cardiac cells pre-incubated with MTX (about 0.1µM - 10µM for 3h) (125). Failing human hearts have about 25-40% less ATP than healthy hearts and the heart in energetic starvation fails to support an increase in the workload (163,165). Thus, the length of time that the heart can survive with such ATP depletion still remains unclear (163), and speculatively could help to explain the two deaths observed in the MTX48 group (Manuscript III).

It has been described that the loss of ATP in the failing myocardium is a slow and progressive phenomenon, only detectable when the heart is in severe failure (163), which is in agreement with our *in vivo* results. The sequence of events in the establishment of a failing and energy starved heart are: the decrease in the PCr levels followed by the loss in the creatine levels and, ultimately, ATP depletion (163). Decreases in the plasma total CK activity and CK-MB levels were observed in the MTX22 group (Manuscript III) and may be interpreted as a hallmark of the development of the heart failure (136). However, signaling pathways involved in CK alterations remain to be elucidated (136). Even so, it has been reported a decreased CK activity in heart mitochondria isolated from MTX treated female rats (1mg/kg, twice a week, for four weeks), immediately after the first dose (166).

Moreover, in the same study, the creatine content of heart mitochondria was increased, evidencing the loss of mitochondrial membrane permeability (166).

Besides the ATP depletion observed in MTX48 hearts, plasma lactate levels were increased in this group in comparison with MTX22 and control levels (Manuscript III), which was accompanied by increases in the cardiac relative mass, suggesting a cardiac failure condition. Increased levels of plasma lactate are suggestive of lactic acidosis and occurs in response of tissue hypoxia, uncoupling of oxidative phosphorylation, generalized cachexia (due to increased anaerobic glycolysis in the skeletal muscle), congestive heart failure, and in situations where the hepatic clearance is compromised (which can also be the case regarding the hepatic damage described in Manuscript IV) (136,167). However, in failing hearts, the heart assumes the fetal pattern, switching the main substrate of energetic sources from fatty acids to glycolysis with a reduced oxidative metabolism (136,168), thus, more lactate is produced and lower levels of ATP is generated (136).

The glycolytic pathway and the tricarboxylic acid cycle usually give small contributions to the cardiac ATP content, being the major source of ATP the mitochondrial oxidative phosphorylation, which is usually enough to support the normal needs of the heart, even when the heart's demand is increased (162). The factors required by the mitochondria are usually obtained after β-oxidation of fatty acids in the mitochondria and peroxissomes. Thus, when ATP supply and demand are mismatched, it can indicate a defect in mitochondrial synthesis of ATP. For instance, in ischemic, hypoxic and cardiomyopathic hearts, the cell's ability to match ATP supply and demand is disrupted and the depletion of the cardiac energy pool is accompanied by a dysfunction on mitochondrial ATP turnover mechanisms (169).

IV.6. MTX-induced mitochondrial toxicity

In general, mitochondria perform central functions in the cardiac cell such as energy supply, regulation of reactive species formation, buffer cytosolic calcium, and regulation of apoptosis (155). Mitochondria have two membranes: the outer membrane is rich in cholesterol and is permeable to ions and solutes up to 14KDa while the inner membrane contains membrane proteins that transport selected ions and metabolites across the membrane. Additionally, the inner membrane delimits the matrix, where the mitochondrial DNA and soluble enzymes such as those from the tricarboxylic acids cycle and β-oxidation are found (170). The respiratory chain is located in the mitochondrial inner membrane and is responsible for ATP production through the oxidation of NADH and ubiquinol, which transfer electrons to the oxygen through the respiratory chain complexes.

There are five mitochondrial respiratory chain complexes: complex I (NADH:ubiquinone reductase), complex II (succinate:ubiquinone reductase), complex III (ubiquinol:cytochrome *c* reductase), complex IV (cytochrome c oxidase), and complex V (ATP synthase). Mitochondrial respiration promotes the proton ejection without charge compensation. Hence, the electrochemical gradient and free energy provided are enough to serve as motive force to the ATP synthesis (96,155).

Heart muscle is a highly oxidative tissue that produces more than 90% of its energy through mitochondrial respiration (136). Mitochondria occupy about 30% of cardiomyocyte space, suggesting its relevance for cardiac performance (136,162). Cardiac mitochondria have a large number of *cristae*, which is justified due to the high energetic demand and respiratory activity of the cardiac tissue (96). Considering that mitochondrial oxidative phosphorylation is the major source of ATP, mitochondrial dysfunction and consequent disruption of energy metabolism are associated to rapid depletion of cellular energy reserves (169).

It was already demonstrated that mitochondria is involved in doxorubicin-induced cardiomyopathy. After the doxorubicin acceptance of unpaired electrons from complex I of the mitochondrial electron transport chain, the resulting reactive species are stabilized by superoxide dismutase and by reacting with mitochondrial reducing equivalents such as GSH. As a consequence, GSH oxidation leads to the MPT opening and, subsequently, mitochondrial swelling, depolarization, loss of calcium regulation, and inhibition of mitochondrial bioenergetics (97).

The H9c2 cells incubation with MTX (100nM and 1μM) caused the late inhibition of ATP synthase expression and activity (Manuscript II), suggesting that MTX causes a direct inhibition of ATP synthesis. However, decreased levels of ATP were observed earlier than ATP synthase expression and activity inhibition (table 4), suggesting that other effects besides interference with ATP synthase are involved in intracellular ATP depletion. Considering that this cell model privileges the glycolytic pathway, another possible target of MTX is enzymes involved in glycolysis. Other possibilities are the lack of nucleotides (which was not investigated by us) or increased consumption of ATP by diverse biochemical mechanisms. The late (96h) inhibition of ATP synthase and expression induced by MTX, to the best of our knowledge, was described for the first time by our works. Additionally, in this cell model, the mitochondrial membrane potential was hyperpolarized after MTX (100nM and 1μM) incubation at 24, 48, and 96h. At 24h incubation with 1μM MTX neither the hyperpolarization of mitochondrial membrane potential nor the elevation of calcium intracellular levels were observed. In the other experimental conditions tested (48 and 96h), the mitochondrial membrane potential was elevated simultaneously with rise of intracellular calcium levels, which may difficult to assert which was the first event. Even so, the mitochondrial membrane potential may be elevated as an attempt to provide motive force to restore the energetic homeostasis that is altered given the early decreases in the ATP levels. At 96h incubation, the decreases in the ATP-synthase content and activity are accompanied by increases in the reactive species generation, suggesting a possible connection between events (Manuscript II). The chronology of the energetic imbalance observed in the H9c2 studies was summarized in the table 4.

Table 4: Diagram representing the chronogram of energetic/mitochondrial changes observed in the H9c2 cells after incubation with MTX. (yes = presence of the effect, n.o = not observed [absence of the effect], n.d= not determined). The results were obtained after comparison with control cells.

	MTX 100nM			MTX 1μM		
	24h	48h	96h	24h	48h	96h
Decreases in the intracellular ATP levels	yes	yes	yes	yes	yes	yes
Inhibition of ATP synthase expression	n.o	n.o	yes	n.o	n.o	yes
Inhibition of ATP synthase activity	n.d	n.d	yes	n.d	n.d	yes
Hyperpolarization of mitochondrial membrane potential	yes	yes	yes	n.o	yes	yes
Increases in the intracellular calcium levels	yes	yes	yes	n.o	yes	yes
Increases in the reactive species generation	n.d	n.d	yes	n.d	n.d	yes

Considering the suggested mitochondrial injury, *L*-carnitine was used to study the possible protection of MTX effects in the H9c2 cell model. First, the transport of fatty acids across mitochondrial membrane is only possible when these substrates are attached to carnitine (171), allowing their β-oxidation. Furthermore, *L*-carnitine improves the *trans*-esterification/excretion of acyl-CoA esters, the oxidation of α-ketoacids, and the removal of toxic acylcarnitine ester from the mitochondria (171,172). However, although *L*-carnitine (1mM) is considered a mitochondrial enhancer, under our experimental conditions it did not protect the H9c2 cells from the cytotoxicity induced by MTX incubation (96h), evaluated through the MTT reduction test. This lack of protection probably occurs because the MTX-induced cytotoxicity has a mitochondrial mechanism other than the ones targeted by *L*-carnitine. In fact, our results suggest that MTX causes important energetic crises, directly affecting ATP content and synthesis. Even so, in contrast to our data, protective effects of *L*-carnitine were observed in MTX treated mice: the administration of *L*-carnitine decreased the lethal toxicity of MTX (LD_{50} MTX alone=15.2mg/kg *vs.* LD_{50} MTX+*L*-carnitine 200mg/kg=21.8mg/kg) (173), which may indicate that *in vivo,* the enhancement of mitochondrial function elicited by *L*-carnitine may favor a better response to MTX. Nonetheless, regarding mice with solid Ehrlich tumor, the co-administration of *L*-carnitine did not present any potentiating effect on the antitumor efficacy of MTX considering the tumor growth rate or increased the survival of mice (174). In fact, the acetyl ester of carnitine (*L*-acetyl-carnitine) may impair the antineoplastic treatment since the combined therapy of MTX and acetyl-*L*-carnitine in mice with solid Ehrlich tumor showed a higher occurrence of metastases with broad dissemination to the kidneys, lung, heart, and mediastinum (175), greatly harming the clinical efficacy of MTX.

Trying to evaluate MTX-induced mitochondrial toxic effects *in vivo*, the cumulative mitochondrionopathy of MTX was studied using male adult Wistar rats (Manuscript III). Early and late toxic effects (two days *vs.* 28 days after reaching the MTX total cumulative dose - MTX22 and MTX48 groups, respectively) were evaluated in order to better understand the (mal)adaptive responses involved in MTX-induced cardiotoxicity (Manuscript III). The mitochondrial functional and morphological disturbances were demonstrated in both treated groups and were more pronounced in the late time point (Manuscript III). In the present study, the mitochondrial *cristae* were well defined and swelling was absent, thus, the mitochondrial morphologic changes were restricted to giant and collapsed mitochondria (Manuscript III). One hypothesis that could explain this finding is the MTX ability to intercalate into the DNA molecule causing single and double breaks and inhibiting DNA and RNA synthesis (22), compromising the mitochondrial turnover. Other changes in the mitochondria morphology were already reported after MTX administration. A chronic administration regimen of MTX (0.2mg/kg, weekly for 12 weeks, reaching a total cumulative dose of 2.4mg/kg) in female BALB/c mice caused late cardiac mitochondrial degenerative changes, such as mitochondrial swelling, partial clearing of the matrix, and the appearance of myelin figures (50). Moreover, comparative studies with MTX and doxorubicin demonstrated an increased mitochondrial toxicity potential of MTX compared to doxorubicin (102).

In our *in vivo* study, in both treated groups (MTX22 and MTX48) increased activity of the mitochondrial complex IV was observed. In the activity of complex V dissimilar results were shown in different groups: MTX22 had increased levels while in MTX48 the activity of complex V decreased (Manuscript III). The increases in the activity of the complex IV and V in MTX22 may result from an adaptation of mitochondria to provide more efficiently ATP in response to MTX toxic effects. Conversely, in the MTX22 group, no significant difference in the ATP cardiac content compared to control rats was observed, showing that, at this time point, the increased activity of the complexes appears to be sufficient to maintain ATP overall levels, although other mechanisms should not be neglected.

However, the increase in complex IV activity was not enough to support the ATP demand when accompanied by decreased mitochondrial complex V activity, as observed in the MTX48 group, as levels of cardiac ATP significantly decrease. A reduction in the electron transfer activity of state III and a concomitant uncoupling of oxidative phosphorylation were already observed in cardiac mitochondria isolated from MTX treated female rats (1mg/kg, twice a week, for four weeks reaching a cumulative dose of 8mg/kg) (166). Furthermore, cardiac mitochondria showed a reduction in the electron transfer and the respiratory chain activity, uncoupling of oxidative phosphorylation with consequent relevant drop in the Na^+/K^+ ATPase activity (166). It is also important to refer that besides the association of the ATP decreased levels and an inhibited ATP synthesis suggested by the late decreases in the activity of ATP synthase complex presented here, changes in the ATP levels in the failing myocardium can also be related to the loss of total tissue purines (165), which were not evaluated in our studies.

In contrast to the mitochondrial effects demonstrated *in vivo*, the incubation of MTX (10nM, 100nM, and 1μM) with cardiac mitochondria isolated from untreated rats did not cause any change in the mitochondrial functionality evaluated by the distribution of TPP^+ assay. In contrast, mitochondria isolated from two animals from the MTX48 group presented an increased lag phase, demonstrating a difficulty to repolarize and sustain the mitochondrial potential, which is consistent with an inhibition of ATP synthesis. As already referred, MTX metabolism exerts a pivotal role to the MTX-induced toxicity. Thus, one possibility is that the direct toxic effect mediated by MTX *in vitro* may be residual and insufficient to elicit significant alterations in this model without being biotransformed. Hence, differences in the metabolism rate might be behind the intersubject variability observed in the clinical evaluations of the treated animals presented in the present work (discussed further) and in the human MTX therapy.

IV.7. Types of cardiomyopathies

Diseases of the myocardium usually produce abnormalities in cardiac wall thickness and chamber size, and mechanical and/or electrical dysfunction, which are associated with significant morbidity and mortality (176). Cardiomyopathies are classified in three forms: restrictive, hypertrophic, and dilated (176,177) that will be described in the following paragraphs.

The restrictive cardiomyopathy is the less frequent and it is a disorder characterized by an impaired ventricular filling during diastole due to a less compliant ventricle without changes in the systolic function of the left ventricle (176).

The cardiac hypertrophy is classified in concentric hypertrophy or eccentric hypertrophy (162,177). In concentric hypertrophy, new contractile protein units are disposed in parallel resulting in cardiomyocyte enlargement, while in eccentric hypertrophy the assembly of new contractile protein units occurs in series, producing increases in the length of cardiomyocytes (162). Essentially, in affected individuals, a disproportionate thickening of the interventricular septum when compared with the free wall of the left ventricle occurs (176). Additionally, hypercontractile systolic function resulting in exaggerated pump function is accompanied by a poor relaxation of the heart resulting in diastolic dysfunction (177). The hypertrophy involves alteration of components of sarcomere and, histologically, a massive hypertrophy of the muscle fibers, mainly in the interventricular septum, acute interstitial fibrosis, and loss of muscle fiber organization are observed (176). Both hypertrophy and restrictive cardiomyopathies can cause heart failure due to the diastolic impairment while the mechanism involved in the heart failure related to dilated cardiomyopathy is mainly systolic dysfunction (176).

Dilated cardiomyopathy is the most prevalent cardiomyopathy and it is characterized by increased volume of cardiac chambers (176,177). Histologically, some hypertrophy can be seen, although, it is not as pronounced as in the hypertrophic cardiomyopathy. The most abundant microscopic feature of dilated cardiomyopathy is the abundant interstitial fibrosis without loss of organization in the muscle fibers (176). Moreover, it involves alterations in a wide variety of proteins, predominantly of the cytoskeleton, but also affecting the sarcomere, mitochondria, and nuclear envelope (176,177). Although hypertrophic and dilated cardiomyopathies have different morphologies and subcellular phenotypes, they share the same clinical complications, such as shortness of breath, easy fatigability, inability to tolerate physical exercise, fainting, light headedness, sweating at rest and in some cases, increased heart rate, enlargement of the liver, and sudden death (177).

Dilated cardiomyopathy is most commonly associated to anthracycline treatment, as evidenced by hystopathomorphological data (97), but sometimes children receiving drugs from this therapeutic class can develop restrictive cardiomyopathy (3,176). The cardiac damage shown in the histology performed in the present study was observed in both ventricular sides without differences, suggesting that both sides were equally affected. Considering cardiac abnormalities induced by MTX, in our studies, light microscopy of right and left cardiac ventricles from rats subjected to MTX treatment (MTX22 group) revealed dispersed cellular and interstitial edema, diffusion of inflammatory cells, and proliferation of connective tissue (Manuscript III). In the MTX48 group, dispersed areas of an intense proliferation of the connective tissue with abundant cellular infiltration, probably by fibroblasts, was observed. The sub-endocardial region was considered more affected compared to the sub-pericardial since the cellular edema and fibrosis were more pronounced in this region. The transmission electron microscopy of MTX22 and MTX48 hearts revealed edema of cardiomyocytes, lysossomal activation in the cardiomyocytes, and proliferation of connective tissue and fibroblasts, suggesting a chronic inflammatory process probably because of an adaptation/repairing process due to continuous cell death. Conversely, abundant collagen deposition in the interstitial space was observed in MTX48 group and the heart from these animals presented significant increase in heart relative mass. Interstitial reparative fibrosis typically occurs as a response to the loss of myocytes due to myocardial ischemia or senescence (178).

The increase in the cardiac relative mass was not accompanied by differences in the total cardiac protein levels. Thus, our results suggest that the increase of cardiac relative mass was related to water retaining instead of hypertrophy. Cellular edema was observed as an increase of the cellular perimeter. It can be distinguished from cardiac hypertrophy since hypertrophic cardiomyocytes present homogenous eosinophilic cytoplasm because of the close contact of myofibrils. In the cellular edema, however, it is observed the separation of myofibrils and increased amount of water within the cell. Thus, in this condition, the eosinophilic coloration of cytoplasm remains irregular (white areas and vacuoles between the myofibrils) (Figure 2, manuscript III). The accumulation of connective tissue in response to continuous cardiomyocyte death may also contribute to the increased cardiac relative mass, however, the method used to quantify protein does not detect collagen. These changes in the cardiac collagen network are seen in response of pressure/volume overload, after myocardial infarction (178), and, as already mentioned, in dilated cardiomyopathy (176).

Microscopic data from heart of MTX-treated rats evidenced the presence of digiform endothelial projections suggesting endothelial degeneration (Manuscript III). This finding was consistent in all MTX treated rats, in both right and left ventricles, and it was also seen in our previous pilot studies with higher doses (three cycles of 5 and 10mg/kg) in a dose-dependent manner (*data not shown*). Similar endothelial alterations were reported in intestinal epithelium and in human skeletal muscle capillaries after prolonged ischemia (179,180). Thus, it is possible that this microscopic observation may be related to cardiac hypoxia, which is in accordance with the signs of small caliber arteries obstruction seen in the histology (Manuscript III).

IV.8. Intersubject variability in the *in vivo* study

During the *in vivo* MTX treatment (Manuscripts III and IV), rats received three cycles of 2.5mg/kg MTX at days 0, 10, and 20, reaching the cumulative dose of 7.5mg/kg or 48mg/m^2 at the end of the third cycle. Clinical evaluations of rats showed great variability, especially in the MTX48 group after the third cycle of treatment. Also the clinical responses during the experiment were already heterogenous: on the day 22, two rats from the MTX22 group presented moderate piloerection. On the day 25, three animals from the group MTX48 showed intense signals of toxicity, namely slight dehydratation, cyanosis, and slight bleeding. The cyanosis seems to be a common observation related to MTX treatment considering that female rats previously treated with MTX (1mg/kg, twice a week, for four weeks) presented a blue coloration of the skin and tissues, color that was also observed in isolated mitochondria from the heart of these rats (166). In humans, discoloration of the nails was already associated to MTX therapy and it was related to early anemia (181). One of those clinically debilitated animals presented clinical recover, but the other two died on day 35, 15 days after the end of treatment. The death circumstances of those animals were not elucidated, but we speculate that it might be related with the cardiac ATP depletion or with a non-reverted myelossupression. Paradoxically, the two animals that complete the MTX48 group did not present any significant clinical observed change during all the experiment. Variations in the clinical responses were already associated to MTX treatment in humans, and it highlights that intersubject variation is crucial in the MTX toxic effects (26).

The variability of MTX effects was also suggested by the increases in the standard deviations in the % of relative body weight gain after the third cycle until the day 30 (Manuscript III). Animals treated with MTX showed a tendency to decrease the relative body weight gain compared to control group after the second cycle. These decreases were more evident and statistically significant after the third cycle until day 30 and were not accompanied by changes in food and water consumptions. This change is indicative of toxicity. MTX (6, 9, and 12mg/kg) treatment was already associated with a lower body mass gain in mice with Ehrlich tumor (175). Transient changes in the food and water consumption were individually observed in the animals that presented clinical toxic manifestations, namely decreases in the water consumption in rats presenting dehydration and fluctuations on food consumption in those animals presenting bleeding (*data not shown*).

IV.9. MTX-induced hepatotoxicity

The MTX sub-chronic treatment of rats induced an important hepatotoxicity. Firstly, the MTX-induced hepatic damage was clearly evidenced at necropsy by the macroscopic changes observed in the MTX treated livers (Manuscript IV). Excised livers presented mild edema (characterized by the beaded edge and brilliant aspect) and rigid consistency, being more severe in the MTX48 group than in the MTX22 group. Signals of the cumulative hepatic injury were also observed in both treated groups and were characterized by macro- and microscopic changes in the hepatic architecture, biochemical alterations, and decreases in the hepatic protein levels in the MTX22 group, late decreases in the hepatic ATP content and by the increases in the GSHt, GSH, and GSSG hepatic levels in MTX48 group.

Signals of the cumulative hepatic injury are observed in the earlier time point (MTX22 group), namely by changes in plasma parameters (decreases in the total plasma protein, ALT, alkaline phosphatase, triglycerides, and transferrin and increases in C4 complement, cholesterol, and iron levels) and decreases in the hepatic total protein levels. These data suggest a hepatic dysfunction, seen in lower plasma hepatic enzyme levels but higher free cholesterol as seen in other reports (182,183). This increase in the plasma cholesterol levels in the MTX22 group is consistent with the mild steatosis observed in the respective histology, which can be related to the decreased hepatic synthesis of lipoproteins (60). The impairment of hepatic functionality is also evidenced by early increases in the iron levels and decreases in plasma triglycerides in both treated groups, being the last molecules mainly synthesized by the hepatocytes.

The hepatic protein synthesis seems to be impaired in both treated groups as evidenced by the low levels of plasma biochemical parameters such as ALT, alkaline phosphatase, and transferrin (Manuscript IV). AST activity remained unchanged in both treated groups when compared to control levels. The lack of changes in AST activity might be related to its slower released pattern in comparison to ALT (175). For this reason and considering that ALT is primarily found in the liver, while AST is also distributed among other tissues such as heart, kidney, brain, and muscle, ALT is the standard biomarker of hepatotoxicity (184). In fact, as already mentioned, in humans, acute hepatotoxicity of MTX manifests as transient increases in the activity of both liver enzymes (9). In mice with Ehrlich tumor treated with MTX single dose (9 and 12mg/kg), AST activity increased when compared to control and ALT activity increased only with the higher dose of MTX after 14 days of MTX-treatment (175). Given the AST broad distribution, rises in its activity in the absence of concomitant ALT increases are frequently interpreted as indicative of abnormalities in tissues such as the heart (184). Thus, it is possible that the changes in the liver aminotransferases after MTX single doses observed in the study performed by Niang and co-workers are related to the classic MTX-cardiotoxicity. In that administration regimen, only the higher MTX dose might have elicited hepatotoxicity, considering the rises in ALT activity observed with this dose (175).

The lower plasma enzyme levels observed in Manuscript IV suggest that protein turnover is decreased. Moreover, decreases in the hepatic synthesis of these enzymes were considered an outcome to the (sub)chronic hepatotoxicity induced by others xenobiotics (60,183,185,186). Increases in the unconjugated bilirubin (observed indirectly, since it was shown by decreases in conjugated bilirubin and no significant changes in total bilirubin) in both treated groups are suggestive of impaired conjugation with glucuronides. Sub-clinical unconjugated hyperbilirubinemia is related to antituberculosis therapy, and it is attributed to the inhibition of the bile salt exporter pumps (187).

The apparent recovery of the hepatic total protein levels on MTX48 compared to MTX22 does not mean functionality gain, considering the alterations in MTX48 hepatic ATP and plasma protein levels. Indeed, instead of recovery, the hepatic lesion was more pronounced in the later time point (MTX48 group) as seen by liver histology. In rats, the liver is able to repair from hepatic injury in five to seven days (188). Even so, despite the adaptive/repair ability of the liver to react to a hepatic injury, this organ seems to be vulnerable to MTX toxic effects since that mice treated with MTX (15mg/kg) presented significant changes in the liver microscopic architecture that were not reverted until five days after the MTX-administration (49). In our study, histologic data did not revealed signals of a hepatic damage secondary to heart failure. As already stated, MTX and its toxic metabolite are retained in the hepatic tissue (Manuscript I) and the continued hepatic exposure might lead to prolonged hepatic injury. Furthermore, in the later time point, the classic late cardiotoxicity of MTX (which was described in the Manuscript III) may contribute to promote a secondary hepatic lesion (189).

Microscopic evaluations of liver showed a huge proliferation in the Kupffer cells, hepatic edema, and collagen proliferation, which are indicative of an inflammatory process. Indeed, that was corroborated by the significant increases in the plasma C4 complement levels since this component is synthesized by Kupffer cells (190). Previously, a single dose administration of MTX (15mg/kg) was enough to cause an intense hydropic vacuolization of the cytoplasm, necrosis areas, picnosis, and nuclear lysis in the hepatic tissue, observed five days after treatment (49).

As already discussed, the cumulative late MTX-induced hepatotoxicity was associated with oxidative stress as seen by significant increases in the hepatic levels of GSHt, GSH, and GSSG observed in the MTX48 group. Moreover, to the best of our knowledge, it was the first time that hepatic late energetic imbalance was associated to

MTX-induced hepatotoxicity. In the present study, the inhibition of the hepatic protein synthesis occurred prior to the decreases in the ATP content in the liver. This early effect might be related to the MTX ability to inhibit protein synthesis (2). The late decrease in the hepatic ATP levels was observed even 28 days after the last MTX administration. Decreases in the ATP hepatic levels are observed in the human nonalcoholic steatohepatitis (191) and are associated to covalent binding of drugs to intracellular proteins (192). Thus, once again these effects can be attributed to the ability of MTX and naphtoquinoxaline metabolite to accumulate in the liver (26). MTX persistence in the cells is related to its strong affinity for cellular macromolecules and membranes (35,44).

IV.10. MTX-induced hematotoxicity

In our *in vivo* study, the MTX-induced hematological toxic effects were evidenced by a notorious early bone marrow depression on MTX22 group, characterized by the significant decreases in red blood cell (RBC) count, HCT, and reticulocytes, as well as in WBC count, as compared to control. Additionally, an anemic condition was observed since Hb levels were significantly decreased. Besides being a signal of hepatic lesion, the increase in the plasma iron might be related to an increase in iron absorption to overcome the reduction in RBC. Increased of MPV and a marked bone marrow suppression were observed in the MTX22 group, as shown by the absence of circulating reticulocytes. Recovery signals of the hematopoiesis were observed in the MTX48 group, namely by increases in reticulocytes when compared to control. Additionally, increase of MCH and MCV levels were observed when compared with the control. The observed macrocytosis and anisocytosis are associated with increases in the reticulocytes count (Manuscript IV). The reduction in blood cells is probably mainly due to marrow suppression. Caution is needed in the interpretation of the cause of the anemia since disturbances in the iron metabolism (increases in the iron plasma levels and decreases in the transferrin levels) and increases in the non-conjugated bilirubin levels can represent confounding factors. It is important to take into account that, simultaneously to a hematologic disturbance, an impaired hepatic function has been established in our model. Despite of hemorrhagic clinical signals seen in some MTX-treated rats, no increase in the LDH plasma levels was observed.

As already mentioned, MTX is an immunosuppressive agent that acts by promoting apoptosis in antigen-presenting cells and reducing levels of all types of immune cells (15,24). Accordingly, the MTX administration caused transient decreases in plasma IgG levels in MTX22 rats. In another study that assessed the human safety of MTX, rituximab, ifosfamide, and etoposide combined therapy a significant decrease in the IgG levels in treated patients with non-Hodgkin's lymphoma was demonstrated (193). The IgG is synthesized by blood cells and corresponds to about 80% of total immunoglobulin (194). Thus, the huge decreases in IgG levels observed in the MTX22 group might be the cause of the decreases observed in the total plasma protein levels in this group since albumin levels are similar to control levels (*data not shown*). Additionally, the absence of significant differences in the plasma albumin levels might be related to its long turnover (195). Conversely, decreases in serum total protein levels without changes in the serum albumin levels were already described in MTX single dose (6, 9, or 12mg/kg) treatment in mice with Ehrlich tumor (175).

The presence of micronucleus in MTX22 blood smears was constant in all animals from this group, suggesting the genotoxicity capacity of MTX. This genotoxicity could underlie an ineffective hematopoiesis, supporting our hematologic data at MTX22 (bone marrow suppression). Accordingly, it is well known that MTX causes single and double breaks in the DNA (1,2) and also affects the cell cycle at various stages (1,22), with known mutagenicity ability.

The pancytopenia was not proven only because the PLT lineage is not depleted. The circulation time of PLT in healthy conditions is about seven to ten days (196). Thus, it is possible that, at the time points evaluated, the PLT count was already normalized in opposition to other lineages. Moreover, it is in accordance with the reports describing that thrombocytopenia is a mild, less common event in the MTX treatment (2). The MPV is increased in the MTX22 group and it no changes in the PDW were seen, demonstrating that the PLT population is homogeneously macrocytic. Despite the clinical use of this parameter is not yet well validated, studies demonstrate an association between enlarged MPV and cardiovascular risk because larger PLTs are hemostatically more active, leading to higher risk of myocardial infarction (196–198). Pro-inflammatory states frequently present PLT with higher volume because cytokines such as interleukines 3 and 6 can mediate the production of PLT with higher MPV and metabolic/enzymatically more actives (196).

The myelossupression observed in our work is in accordance to what is observed in humans and justifies the importance of monitoring hematological parameters during MTX chemotherapy (2). The MTX-induced myelosuppression manifests mostly as leukopenia, thus being its main dose-limiting effect (61). In humans, after the administration of high dose MTX (38mg/m^2, i.p.), the WBC counting returned to normal values within seven days (61). However, it is known that patients treated with higher dose regimens tend to present a faster blood count recovery (2). Additionally, blood cell counts should be continued after MTX-therapy cessation due to the risk of MTX-associated secondary acute leukemia (15).

In the present study using clinically relevant doses, RBC and WBC counts, which were depressed in the early time point, returned to normal values in the MTX48 (28 days after the MTX last cycle) (Manuscript IV).

IV.11. Conclusions and future perspectives

Four hallmarks are defined as contributing to the pathology of cardiac disease: a critical energy loss; a critical accumulation of cellular calcium; effects of reactive species formation; and injurious effects of the accumulation of long-chain acyl compounds (169). From these, we demonstrated the occurrence of marked energy depletion *in vitro* and *in vivo*, increased levels of intracellular calcium after MTX incubation in the H9c2 cells, increased generation of reactive species only at the longer incubation period of 96h with concomitant mitochondrial disturbance. The acyl compounds accumulation was not evaluated but the negative results in the protective studies with *L*-carnitine suggested that it did not exert a leading role in the MTX-mediated cytotoxicity.

MTX induces a relevant cumulative mitochondrionopathy characterized by the aberrant mitochondria found in the cardiac tissue after *in vivo* MTX treatment, the disturbances in the mitochondrial complexes and ATP synthesis, and perturbations in the mitochondrial membrane potential. MTX interference with the mitochondrial functionality and consequent energetic imbalance result in a dysfunctional heart since depleted of its energetic content, the cardiac performance is impaired. Hence, this thesis highlights the relevance of the MTX-induced mitochondrial toxicity to the cardiomyopathy related to the MTX therapy.

In the opposite of what is observed in the doxorubicin cardiomyopathy, the oxidative stress does not seem to occupy a central role in the MTX-mediated cardiac disease. The eventual MTX-related oxidative stress does not seem to be related to quinone activation, but secondary to energetic loss. Thus, the contribution of the metabolism to the cardiotoxicity seems to be more related to the reaction products (for an example, the naphtoquinoxaline metabolite, which was demonstrated to accumulates in liver and heart) than the sub-products (reactive species generation associated to quinone activation). Increased levels of reactive species formation were only observed in a late time point, secondary to another significant changes such as energetic depletion, intracellular calcium overload, and mitochondrial disturbances. Even so, studies demonstrating the inhibition of lipid peroxidation after MTX incubation (29) suggest that MTX may alter the antioxidant defenses in some extent and it is worth to be highlighted.

It was also demonstrated a relevant hepatotoxicity associated to MTX therapy in rats. After 28 days of the last MTX administration, the liver regeneration was limited and the hepatic tissue remained with altered levels of glutathione and ATP, which are essential for the hepatic function, namely protein synthesis and detoxifying process. Despite the direct hepatotoxic potential, cardiotoxic drugs such as MTX, can cause acute liver failure as a result of a primary congestive heart failure (189). In the case of congestive heart failure, the low cardiac output results in a reduced hepatic blood flow (189). However, in the histology of MTX-damaged livers, no signals suggestive of congestive heart failure-mediated hepatic lesion were observed. Thus, it is possible that MTX exerts a significant direct hepatotoxicity.

Considering MTX cardiomyopathy, our results demonstrate an abundant interstitial fibrosis without loss of organization in the muscle fibers and mitochondrial disorganization, suggestive of dilated cardiomyopathy. However, conclusive studies regarding the protein alterations after MTX therapy are required to confirm the cardiomyopathy type related to MTX treatment. The only protective agents that partially counteracted the cellular lesion caused by MTX incubation were metabolism inhibitors. However, despite the evidenced metabolic relevance to MTX-cardiomyopathy, bioactivation is also required for the MTX pharmacological effects. Hence, blocking MTX systemic metabolism is not a viable alternative since it would compromise the antineoplastic treatment. Even so, the studies presented within this thesis may open up ways to enhance MTX therapy.

Regarding future perspectives, the relation between MTX treatment and long-term hematotoxicity, which can result in the serious late secondary leukemia, needs to be better highlighted. Furthermore, understanding the MTX toxic effects among hematopoiesis are the first step to circumvent them and to increase the MTX tolerance and safety. Moreover, the intrinsic hepatotoxic potential of chemotherapy is of great concern because an altered hepatic function might compromise the therapy and/or increase toxic adverse effects (60). Given that relevance, more studies highlighting the mechanisms involved in the MTX-induced hepatotoxic potential are needed in order to improve therapy. Furthermore, the pharmacological and toxicological potential of the metabolites presented in the Manuscript I need to be highlighted. If they have a good pharmacological potential and a negligible toxicity, one possibility is to isolate, purify, and to explore these promising compounds in preclinical studies. However, it is important to point that, in the case of MTX derivatives, long term protocols to assess the toxicity are needed. Other future directions aim to define if the MTX pharmacological action is also dependent of MTX mitochondrial effects and to explore mitochondrial protective agents to counteract the MTX-induced mitochondrionopathy, minimizing cardiac side effects without affecting the MTX-pharmacological effectiveness.

PART IV

References

1. Ehninger G, Schuler U, Proksch B, Zeller KP, Blanz J. Pharmacokinetics and metabolism of mitoxantrone. A review. Clin Pharmacokinet. 1990;18(5):365–80.

2. Seiter K. Toxicity of the topoisomerase II inhibitors. Expert Opin Drug Saf. 2005;4(2):219–34.

3. Minotti G, Menna P, Salvatorelli E, Cairo G, Gianni L. Anthracyclines: molecular advances and pharmacologic developments in antitumor activity and cardiotoxicity. Pharmacol Rev. 2004;56(2):185–229.

4. Weiss R. The anthracyclines: will we ever find a better doxorubicin? Semin Oncol. 1992;19(6):670–86.

5. Johnson RK, Zee-Cheng RK, Lee WW, Acton EM, Henry DW, Cheng CC. Experimental antitumour activity of aminoanthraquinones. Cancer Treat Rep. 1979;63(3):425–39.

6. Cheng CC, Zee-Cheng RKY, Narayanan VL, Ing RB, Paul I KD. The collaborative development of a new family of antineoplastic drugs. Trends Pharmacol Sci. 1981;2:223–4.

7. Zee-Chung RKY, Cheng CC. Anthraquinone anticancer agents. Drugs Future. 1983;8:229–49.

8. Murdock CK, Child RG, Fabio PF, Angier RB, Wallace RE, Durr FE, et al. Antitumour Agents. I. 1,4-Bis-[(aminoalkyl)amino]-9,10- anthracenediones. J Med Chem. 1979;22(9):1024–30.

9. IARC, International Agency for Research on Cancer. Mitoxantrone. IARC Monographs. 2011 p. 289–315.

10. Moffat A, Osselton M, Widdop B, editors. Clarke's analysis of drugs and poisons in pharmaceutical, body fluids and postmortem material. 4th ed. London: Pharmaceutical Press; 2011.

11. Slordal L, Andersen A, Warren D. A sensitive and simple high-performance liquid chromatographic method for the determination of mitoxantrone in plasma. Ther Drug Monit. 1993;15(4):328–33.

12. Micromedex Healthcare series. Available from: www.micromedex.com [cited 2013 Apr 5].

13. Avasarala JR, Cross AH, Clifford DB, Singer BA, Siegel BA, Abbey EE. Rapid onset mitoxantrone-induced cardiotoxicity in secondary progressive multiple sclerosis. Mult Scler. 2003;9(1):59–62.

14. Canal P, Attal M, Chatelut E, Guichard S, Huguet F, Muller C, et al. Plasma and cellular pharmacokinetics of mitoxantrone in high-dose chemotherapeutic regimen for refractory lymphomas. Cancer Res. 1993;53(20):4850–4.

15. Neuhaus O, Kieseier BC, Hartung H-P. Therapeutic role of mitoxantrone in multiple sclerosis. Pharmacol Ther. 2006;109(1-2):198–209.

16. INFARMED. Resumo das características do medicamento: mitoxantrona. Available from: www.infarmed.pt [cited 2013 May 5].

17. Lorenzi TF. Patologia dos leucócitos. In: Manual de Hematologia: propedêutica e clínica. Rio de Janeiro: Guanabara Koogan; 2006. p. 295–493.

18. Hopfinger G, Busch R, Pflug N, Weit N, Westermann A, Fink A-M, et al. Sequential chemoimmunotherapy of fludarabine, mitoxantrone, and cyclophosphamide induction followed by alemtuzumab consolidation is effective in T-cell prolymphocytic leukemia. Cancer. 2013;119(12):2258–67.

19. Peak S, Tsao-Wei DD, Chamberlain MC. Mitoxantrone in secondary progressive multiple sclerosis: a review of toxicity in 41 patients. Therapy. 2007;4(1):55–8.

20. Namaka M, Turcotte D, Klowak M, Leong C, Grossberndt A, Le Dorze J, et al. Early mitoxantrone-induced cardiotoxicity detected in secondary progressive multiple sclerosis. Clin Med Insights Ther. 2011;3:449–58.

21. Hsin L-W, Wang H-P, Kao P-H, Lee O, Chen W-R, Chen H-W, et al. Synthesis, DNA binding, and cytotoxicity of 1,4-bis(2-amino-ethylamino)anthraquinone-amino acid conjugates. Bioorg Med Chem. 2008;16(2):1006–14.

22. Khan SN, Lai SK, Kumar P, Khan AU. Effect of mitoxantrone on proliferation dynamics and cell cycle progression. Biosci Rep. 2010;30(6):375–81.

23. Hajihassan Z, Rabbani-Chadegani A. Interaction of mitoxantrone, as an anticancer drug, with chromatin proteins, core histones and H1, in solution. Int J Biol Macromol. 2011;48(1):87–92.

24. Neuhaus O, Wiendl H, Kieseier BC, Archelos JJ, Hemmer B, Stüve O, et al. Multiple sclerosis: Mitoxantrone promotes differential effects on immunocompetent cells in vitro. J Neuroimmunol. 2005;168(1-2):128–37.

25. Burns S, Archer L, Chavis J, Tull C, Hensley LL, Drew PD. Mitoxantrone repression of astrocyte activation: Relevance to multiple sclerosis. Brain Res. 2012;14(1473):236–41.

26. Batra VK, Morrison JA, Woodward DL, Siverd NS, Yacobi A. Pharmacokinetics of mitoxantrone in man and laboratory animals. Drug Metab. Rev. 1986;17(3&4):311–29.

27. Blanz J, Mewes K, Ehninger G, Proksch B, Waidelich D, Greger B, et al. Evidence for oxidative activation of mitoxantrone in human, pig, and rat. Drug Metab Dispos. 1991;19(5):871–80.

28. Kostrzewa-Nowak D, Paine MJI, Korytowska A, Serwatka K, Piotrowska S, Wolf CR, et al. Bioreductive activation of mitoxantrone by NADPH cytochrome P-450

reductase. Implications for increasing its ability to inhibit the growth of sensitive and multidrug resistant leukaemia HL60 cells. Cancer Lett. 2007;245(1-2):252–62.

29. Novak RF, Kharasch ED. Mitoxantrone: propensity for free radical formation and lipid peroxidation - implications for cardiotoxicity. Invest New Drugs. 1985;3(2):95–9.

30. Brück TB, Brück DW. Oxidative metabolism of the anti-cancer agent mitoxantrone by horseradish, lacto-and lignin peroxidase. Biochimie. 2011;93(2):217–26.

31. Richard B, Fabre G, De Sousa G, Fabre I, Rahmani R, Cano JP. Interspecies variability in mitoxantrone metabolism using primary cultures of hepatocytes isolated from rat, rabbit and humans. Biochem Pharmacol. 1991;41(2):255–62.

32. Wolf C, Macpherson J, Smyth J. Evidence for the metabolism of mitozantrone by microsomal glutathione transferases and 3-methylcholanthrene-inducible glucoronosyl transferases. Biochem Pharmacol. 1986;35(9):1577–81.

33. Duthie SJ, Grant MH. The role of reductive and oxidative metabolism in the toxicity of mitoxantrone, adriamycin and menadione in human liver derived Hep G2 hepatoma cells. Br J Cancer. 1989;60(4):566–71.

34. Panousis C, Kettle a J, Phillips DR. Neutrophil-mediated activation of mitoxantrone to metabolites which form adducts with DNA. Cancer Lett. 1997;113(1-2):173–8.

35. Fisher GR, Patterson LH. Lack of involvement of reactive oxygen in the cytotoxicity of mitoxantrone, CI941 and ametantrone in MCF-7 cells: comparison with doxorubicin. Cancer Chemother Pharmacol. 1992;30(6):451–8.

36. Li SJ, Rodgers EH, Grant MH. The activity of xenobiotic enzymes and the cytotoxicity of mitoxantrone in MCF 7 human breast cancer cells treated with inducing agents. Chem Biol Interac. 1995;97(2):101–18.

37. Mewes K, Blanz J, Ehninger G, Gebhardt R, Zeller KP. Cytochrome P-450-induced cytotoxicity of mitoxantrone by formation of electrophilic intermediates. Cancer Res. 1993;53(21):5135–42.

38. Panousis C, Kettle A, DR Phillips. Myeloperoxidase oxidizes mitoxantrone to metabolites which bind covalently DNA and RNA. Anticancer Drug Des. 1995;10(8):593–605.

39. Haritova AM, Schrickx L, Lashev L, Fink-Gremmels J. ABC efflux transporters: P-GP, MRP2 and BCRP - the 3 dimension in kinetics not only for fluoroquinolones. Bulgarian Journal of Veterinary Medicine. 2006;9(4):223–42.

40. Xu C, Li CY, Kong AN. Induction of phase I, II, and III metabolism/transport by xenobiotics. Arch Pharm Res. 2005;28(3):249–68.

41. Kim IS, Kim HG, Kim DC, Eom HS, Kong SY, Shin HJ, et al. ABCG2 Q141K polymorphism is associated with chemotherapy-induced diarrhea in patients with

diffuse large B-cell lymphoma who received frontline rituximab plus cyclophosphamide/doxorubicin/vincristine/prednisone chemotherapy. Cancer Sci. 2008;99(12):2496–501.

42. Yang X, Morris ME. Pharmacokinetics and biliary excretion of mitoxantrone in rats. J Pharm Sci. 2010;99(5):2502–10.

43. Hsiao CJ, Li TK, Chan YL, Hsin LW, Liao CH, Lee CH, et al. WRC-213, an l-methionine-conjugated mitoxantrone derivative, displays anticancer activity with reduced cardiotoxicity and drug resistance: identification of topoisomerase II inhibition and apoptotic machinery in prostate cancers. Biochem Pharmacol. 2008;75(4):847–56.

44. Feofanov A, Sharonov S, Fleury F, Kudelina I, Nabiev I. Quantitative confocal spectral imaging analysis of mitoxantrone within living K562 cells: intracellular accumulation and distribution of monomers, aggregates, naphtoquinoxaline metabolite, and drug-target complexes. Biophys J. 1997;73(6):3328–36.

45. Chiccarelli FS, Morrison JA, Cosulich DB, Perkinson NA, Ridge DN, Sum FW, et al. Identification of human urinary mitoxantrone metabolites. Cancer Res. 1986;46(9):4858–61.

46. Kingwell E, Koch M, Leung B, Isserow S, Geddes J, Rieckmann P, et al. Cardiotoxicity and other adverse events associated with mitoxantrone treatment for MS. Neurology. 2010;74(22):1822–6.

47. Wiffen P, Mitchel M, Snelling M, Stoner N. Oxford handbook of clinical pharmacy. 2nd ed. Oxford Medicine; 2012.

48. Henderson B, Dougherty W, James V, Tilley L, Noble J. Safety assessment of a new anticancer compound, mitoxantrone, in beagle dogs: Comparison with doxorubicin. Cancer Treat Rep. 1982;66(5):1139–43.

49. Llesuy SF, Arnaiz SL. Hepatotoxicity of mitoxantrone and doxorubicin. Toxicology. 1990;63(2):187–98.

50. Alderton PM, Gross J, Green MD. Comparative study of doxorubicin, mitoxantrone, and epirubicin in combination with ICRF-187 (ADR-529) in a chronic cardiotoxicity animal model. Cancer Res. 1992;52(1):194–201.

51. Fox EJ. Management of worsening multiple sclerosis with mitoxantrone: a review. Clin Ther. 2006;28(4):461–74.

52. Nistri M, Perrini P, Di Lorenzo N, Cellerini M, Villari N, Mascalchi M. Early mitoxantrone-induced cardiotoxicity in secondary progressive multiple sclerosis. J Neurol Neurosurg Psychiatry. 2007;78(2):197–8.

53. Colombo A, Cardinale D. Using cardiac biomarkers and treating cardiotoxicity in cancer. Future Cardiol. 2013;9(1):105–18.

54. Darko W, Smith AL, King EL, Grethlein SJ. Mitoxantrone-induced cardiotoxicity. J Oncol Pharm Pr. 2001;7(1):47–8.

55. Wang G, Zhou X, Eschenhagen T, Korth M. Effects of mitoxantrone on action potential and membrane currents in isolated cardiac myocytes. Br J Pharmacol. 1999;127:321–30.

56. Montú MB, Arruda WO, de Oliveira MDSR, Ramina R. Mitoxantrone in secondarily progressive multiple sclerosis: a series of 18 patients. Arq Neuropsiquiatr. 2005;63(2-A):225–7.

57. Singhal B, Sheth G, Hundalani S, Menon S. Efficacy and safety of mitoxantrone, as an initial therapy, in multiple sclerosis: experience in an Indian tertiary care setting. Neurol India. 2009;57(4):418–23.

58. Menna P, Salvatorelli E, Minotti G. Cardiotoxicity of antitumor drugs. Chem Res Toxicol. 2008;21(5):978–89.

59. Arnaiz SL, Llesuy S. Oxidative stress in mouse heart by antitumoral drugs: a comparative study of doxorubicin and mitoxantrone. Toxicology. 1993;77(1-2):31–8.

60. King PD, Perry MC. Hepatotoxicity of chemotherapy. Oncologist. 2001;6(2):162–76.

61. Alberts DS, Surwit EA, Peng Y, Mccloskey T, Rivest R, Graham V, et al. Phase I clinical and pharmacokinetic intraperitoneal administration study of mitoxantrone given to patients by intraperitoneal administration. Cancer Res. 1988;48(20):5874–7.

62. Feldman E, Alberts D, Arlin Z. Phase I clinical and pharmacokinetic evaluation of high dose mitoxantrone in combination with cytarabine in patients with acute leukemia. J Clin Oncol. 1993;10(11):2002–9.

63. Constanzo FD, Sdrobolini A, Manzione L, Bilancia D, Acito L, Gasperon S, et al. Dose intensification of mitoxantrone in combination with paclitaxel in advanced breast cancer: a phase II study. Breast Cancer Res Treat. 1999;54(2):165–71.

64. Kimura K, Yoshikawa S, Yoshikawa H, Yamada K, Hirano M, Ikeda Y, et al. Phase II study of mitoxantrone in patients with acute leukemia. Gan To Kagaku Ryoho. 1986;13(8):2573–80.

65. Felix CA, Blaine W, Germano G, Christos P, Raffini L, Nigro L, et al. Translocation mechanism in secondary leukemias following topoisomerase II poisons. Haematol Rep. 2006;2(15):30–3.

66. Chacon E, Bond J, Lemasters J. Evaluation of in vitro cytotoxicity modeling. In: Cardiovascular Toxicology. London: Taylor & Francis; 2001. p. 59–78.

67. Acosta D, Chacon E, Ramos K. Cardiovascular toxicology. In: Cardiovascular Toxicology. New York Raven Press; 1992. p. 3–17.

68. Ramos K, Acosta D. Application of in vitro modelo systems to the study of cardiovascular toxicity. In: In Vitro Toxicology. New York Raven Press; 1994. p. 221–30.

69. Jia L, Liu X. The conduct of drug metabolism studies considered good practice (II): in vitro experiments. Curr Drug Metab. 2007;8(8):822–9.

70. Yoshihara S, Makishima M, Suzuki N, Ohta S. Metabolic activation of bisphenol A by rat liver S9 fraction. Toxicol Sci. 2001;62(2):221–7.

71. Brandon EFA, Raap CD, Meijerman I, Beijnen JH, Schellens JHM. An update on in vitro test methods in human hepatic drug biotransformation research: pros and cons. Toxicol Appl Pharmacol. 2003;189(3):233–46.

72. Buchinger S, Campen E, Helmers E, Morosow V, Krefft M, Reifferscheid G. Development of a freeze-drying protocol for the long-term storage of S9-fraction at ambient temperatures. Cryobiology. 2009;58(2):139–44.

73. Morffi J, Rodeiro I, Hernandez S, Gonzalez L, Herrera J, Espinosa-Aguirre J. Antimutagenic properties of mangifera indica L. stem bark extract and evaluation of its effects on hepatic CYP1A1. Plant Foods Hum Nutr. 2012;67(3):223–8.

74. Chandrasekaran C V, Sundarajan K, Gupta A, Srikanth HS, Edwin J, Agarwal A. Evaluation of genotoxic potential of standardized extract of Glycyrrhiza glabra (GutGard). Regul Toxicol Pharmacol. 2011;61(3):373–80.

75. Kharasch ED, Novak RF. Inhibitory effects of anthracenedione antineoplastic agents on hepatic and cardiac lipid peroxidation. J Pharmacol Exp Ther. 1983;226(2):500–6.

76. Tavoloni N, Jones M, Berk P. Dose-related effects of phenobarbital on hepatic microsomal enzymes. Proc Soc Exp Biol Med. 1983;174(1):20–7.

77. Allen DD, Caviedes R, Cárdenas AM, Shimahara T, Segura-Aguilar J, Caviedes PA. Cell lines as in vitro models for drug screening and toxicity studies. Drug Dev Ind Pharm. 2005;31(8):757–68.

78. Hescheler J, Meyer R, Plant S, Krautwurst D, Rosenthal W, Schultz G. Morphological, biochemical, and electrophysiological characterization of a clonal cell (H9c2) line from rat heart. Circ Res. 1991;69(6):1476–86.

79. Kimes BW, Brandt BL. Properties of a clonal muscle from rat heart. Exp Cell Res. 1976;98(2):367–81.

80. Spido K, Marban E. L-type calcium channels, potassium channels, and novel nonspecific cation channels in a clonal muscle cell line derived from embryonic rat ventricle. Circ Res. 1991;69(6):1487–1499.

81. ATCC. ATCC Product information sheet. Cultures. 2010. p. 1–2.

82. Dangel V, Giray J, Ratge D, Wisser H. Regulation of beta-adrenoceptor density and mRNA levels in the rat heart cell-line H9c2. Biochem J. 1996;317(Pt 3):925–31.

83. Yamamoto M, Satoshi O, Naoki O, Carsten S, Yoshihiro I. Dowregulation of caveolin expression by cAMP signal. Life Sci. 1999;64(15):1349–57.

84. Fujita T, Toya Y, Iwatsubo K, Onda T, Kimura K, Umemura S, et al. Accumulation of molecules involved in alpha1-adrenergic signal within caveolae: caveolin expression and the development of cardiac hypertrophy. Cardiovasc Res. 2001;51(4):709–16.

85. Watkins SJ, Borthwick GM, Arthur HM. The H9C2 cell line and primary neonatal cardiomyocyte cells show similar hypertrophic responses in vitro. In Vitro Cell Dev Biol Anim. 2011;47(2):125–31.

86. Pereira SL, Ramalho-Santos J, Branco AF, Sardão VA, Oliveira PJ, Carvalho RA. Metabolic remodeling during H9c2 myoblast differentiation: relevance for in vitro toxicity studies. Cardiovasc Toxicol. 2011;11(2):180–90.

87. Meischl C, Buermans H, Hazes T, Zuidwijk M, Musters R, Boer C, et al. H9c2 cardiomyoblasts produce thyroid hormone. Am J Physiol Cell Physiol. 2008;294(5):C1227–C1233.

88. Girard B, Ouafik L, Boudouresque F. Characterization and regulation of peptidylglycine alpha-amidating monooxygenase (PAM) expression in H9c2 cardiac myoblasts. Cell Tissue Res. 1999;298(3):489–97.

89. Zordoky BNM, El-Kadi AOS. H9c2 cell line is a valuable in vitro model to study the drug metabolizing enzymes in the heart. J Pharmacol Toxicol Methods. 2007;56(3):317–22.

90. Zhang PL, Lun M, Teng J, Huang J, Blasick TM, Yin L, et al. Preinduced molecular chaperones in the endoplasmic reticulum protect cardiomyocytes from lethal injury. Ann Clin Lab Sci. 2004;34(4):449–57.

91. Park E, Park K. Gene expression profiles of cultured rat cardiomyocytes (H9C2 cells) in response to arsenic trioxide at subcytotoxic level and oxidative stress. J Health Sci. 2006;52(5):512–21.

92. Bernuzzi F, Recalcati S, Alberghini A, Cairo G. Reactive oxygen species-independent apoptosis in doxorubicin-treated H9c2 cardiomyocytes: role for heme oxygenase-1 down-modulation. Chem Biol Interact. 2009;177(1):12–20.

93. Diogo CV, Félix L, Vilela S, Burgeiro A, Barbosa IA, Carvalho MJM, et al. Mitochondrial toxicity of the phyotochemicals daphnetoxin and daphnoretin-relevance for possible anti-cancer application. Toxicol In Vitro. 2009;23(5):772–9.

94. Smith J, Matus I, Beard D, Green A. Differential expression of cardiac mitochondrial proteins. Proteomics. 2008;8(3):446–62.

95. Padrão AI, Ferreira RMP, Vitorino R, Alves RMP, Neuparth MJ, Duarte JA, et al. OXPHOS susceptibility to oxidative modifications: the role of heart mitochondrial subcellular location. Biochim Biophys Acta. 2011;1807(9):1106–13.

96. Santos DJSL. Stresse oxidativo mitocondrial associado a patologias: acção protectora de fármacos [Tese]. Coimbra: Universidade de Coimbra; 2002. p. 185.

97. Wallace KB. Doxorubicin-induced cardiac mitochondrionopathy. Pharmacol Toxicol. 2003;93(3):105–15.

98. Wallace K. Adriamycin-induced interference with cardiac mitochondrial calcium homeostasis. Cardiovasc Toxicol. 2007;7(2):101–7.

99. Zhou S, Starkov A, Froberg MK, Leino RL, Wallace KB. Cumulative and irreversible cardiac mitochondrial dysfunction induced by doxorubicin. Cancer Res. 2001;61:771–7.

100. Iannaccone P, Jacob H. Rats! Dis Model Mech. 2009;2(5-6):206–10.

101. Johnson M, Gad S. The rat. In: Gad S, editor. Animal Models in Toxicology. Taylor & Francis; 2006. p. 147–276.

102. Zbinden G, Beilstein AK. Comparison of cardiotoxicity of two anthracenediones and doxorubicin in rats. Toxicol Lett. 1982;11(3-4):289–97.

103. Bolaman Z, Cicek C, Kadikoylu G, Barutca S, Serter M, Yenisey C, et al. The protective effects of amifostine on adriamycin-induced acute cardiotoxicity in rats. Tohoku J Exp Med. 2005;207(4):249–53.

104. An G, Morris ME. HPLC analysis of mitoxantrone in mouse plasma and tissues: application in a pharmacokinetic study. J Pharm Biomed Anal. 2010;51(3):750–3.

105. Rossato L, Costa V, de Pinho P, Freitas V, Viloune L, Bastos M, et al. The metabolic profile of mitoxantrone and its relation with mitoxantrone-induced cardiotoxicity. Arch. Toxicol. 2013;87(10):1808–20.

106. Silva R, Carmo H, Dinis-Oliveira R, Cordeiro-da-Silva A, Lima SC, Carvalho F, et al. In vitro study of P-glycoprotein induction as an antidotal pathway to prevent cytotoxicity in Caco-2 cells. Arch Toxicol. 2011;85(4):315–26.

107. Mirkes PE, Little SA. Cytochrome c release from mitochondria of early postimplantation murine embryos exposed to 4-hydroperoxycyclophosphamide, heat shock, and staurosporine. Toxicol App Pharmacol. 2000;162(3):197–206.

108. Costa VM, Silva R, Ferreira R, Amado F, Carvalho F, Bastos ML, et al. Adrenaline in pro-oxidant conditions elicits intracellular survival pathways in isolated rat cardiomyocytes. Toxicology. 2009;257(1-2):70–9.

109. Angeloni C, Spencer JPE, Leoncini E, Biagi PL, Hrelia S. Role of quercetin and its in vivo metabolites in protecting H9c2 cells against oxidative stress. Biochimie. 2007;89(1):73–82.

110. Uemura K, Adachi-Akahane S, Shintani-Ishida K, Yoshida K. Carbon monoxide protects cardiomyogenic cells against ischemic death through L-type Ca2+ channel inhibition. Biochem Biophys Res Commun. 2005;334(2):661–8.

111. Crow JP. Dichlorodihydrofluorescein and dihydrorhodamine 123 are sensitive indicators of peroxynitrite in vitro: implications for intracellular measurement of reactive nitrogen and oxygen species. Nitric Oxide. 1997;1(2):145–57.

112. Ichikawa T, Li J, Meyer CJ, Janicki JS, Hannink M, Cui T. Dihydro-CDDO-trifluoroethyl amide (dh404), a novel Nrf2 activator, suppresses oxidative stress in cardiomyocytes. PLoS One. 2009;4(12):e8391.

113. Barbosa DJ, Capela JP, Oliveira JM, Silva R, Ferreira LM, Siopa F, et al. Pro-oxidant effects of Ecstasy and its metabolites in mouse brain synaptosomes. Br J Pharmacol. 2012;165(4b):1017–33.

114. Rossato LG, Costa VM, de Pinho PG, Carvalho F, Bastos ML, Remião F. Structural isomerization of synephrine influences its uptake and ensuing glutathione depletion in rat-isolated cardiomyocytes. Arch Toxicol. 2011;85(8):929–39.

115. Grotto D, Valentini J, Boeira S, Paniz C, Maria LS, Vicentini J, et al. Importance of the lipid peroxidation biomarkers and methodological aspects for malondialdehyde quantification. Quim Nov. 2009;32(1):169–74.

116. Grotto D, Santa Maria LD, Boeira S, Valentini J, Charão MF, Moro AM, et al. Rapid quantification of malondialdehyde in plasma by high performance liquid chromatography-visible detection. J Pharm Biomed Anal. 2007;43(2):619–24.

117. Grotto D, Valentini J, Boeira S, Paniz C, Maria LS, Vicentini J, et al. Avaliação da estabilidade do marcador plasmático do estresse oxidativo malondialdeído. Quim Nov. 2008;31(2):275–9.

118. Costa VM, Silva R, Ferreira LM, Branco PS, Carvalho F, Bastos ML, et al. Oxidation process of adrenaline in freshly isolated rat cardiomyocytes: formation of adrenochrome, quinoproteins, and GSH adduct. Chem Res Toxicol. 2007;20(8):1183–91.

119. Duarte FV, Simões AM, Teodoro JS, Rolo AP, Palmeira CM. Exposure to dibenzofuran affects lung mitochondrial function in vitro. Toxicol Mech Methods. 2011;21(8):571–6.

120. Rolo AP, Oliveira PJ, Moreno AJ, Palmeira CM. Bile acids affect liver mitochondrial bioenergetics: possible relevance for cholestasis therapy. Toxicol Sci. 2000;57(1):177–85.

121. Pontes H, Duarte JA, de Pinho PG, Soares ME, Fernandes E, Dinis-Oliveira RJ, et al. Chronic exposure to ethanol exacerbates MDMA-induced hyperthermia and exposes liver to severe MDMA-induced toxicity in CD1 mice. Toxicology. 2008;252(1-3):64–71.

122. ICSH, International Committee for Standardization in Haematology. ICSH reference method for staining of blood and bone marrow films by azure B and eosin Y (Romanowsky stain). Br J Haematol. 1984;707–10.

123. Lowry OH, Rosebrough NJ, Farr AL, Randall RJ. Protein measurment with the Folin phenol reagent. J Biol Chem. 1951;193:265–72.

124. Parkinson A, Ogilvie BW. Biotransformation of xenobiotics. In: Klaassen C, editor. Casarett Doull's Toxicology - the basic science of poisons. 7th ed. McGraw-Hill; 2008. p. 1331.

125. Shipp NG, Dorr RT, Alberts DS, Dawson B V, Hendrix M. Characterization of experimental mitoxantrone cardiotoxicity and its partial inhibition by ICRF-187 in cultured neonatal rat heart cells. Cancer Res. 1993;53(3):550–6.

126. Michaud V, Frappier M, Dumas MC, Turgeon J. Metabolic activity and mRNA levels of human cardiac CYP450s involved in drug metabolism. PLoS One. 2010;5(12):e15666.

127. Capela JP, Fernandes E, Remião F, Bastos ML, Meisel A, Carvalho F. Ecstasy induces apoptosis via 5-HT(2A)-receptor stimulation in cortical neurons. Neurotoxicology. 2007;28(4):868–75.

128. Kluza J, Marchetti P, Gallego MA, Lancel S, Fournier C, Loyens A, et al. Mitochondrial proliferation during apoptosis induced by anticancer agents: effects of doxorubicin and mitoxantrone on cancer and cardiac cells. Oncogene. 2004;23(42):7018–30.

129. Fisher GR, Patterson LH, Gutierrez PL. A comparison of free radical formation by quinone anti- tumour agents in MCF-7 cells and the role of NAD(P)H (quinone-acceptor) oxidoreductase (DT-diaphorase). Chem Biol Interact. 1993;88:137–53.

130. Butler J, Hoey BM. Are reduced quinones necessarily involved in the antitumour activity of quinone drugs? Br J Cancer. 1987;8:53–9.

131. Powis G, Hodnett EM, Santone KS, See KL, Melder DC. Role of metabolism and oxidation-reduction cycling in the cytotoxicity of antitumor quinoneimines and quinonediimines. Cancer Res. 1987;47:2363–70.

132. Costa VM, Silva R, Tavares LC, Vitorino R, Amado F, Carvalho F, et al. Adrenaline and reactive oxygen species elicit proteome and energetic metabolism modifications in freshly isolated rat cardiomyocytes. Toxicology. 2009;260(1-3):84–96.

133. Chen Y, Jungsuwadee P, Vore M, Butterfield A, Clair DKS. Collateral damage in cancer chemotherapy: oxidative stress in nontargeted tissues. Mol Interv. 2007;7(3):147–56.

134. Zhou S, Palmeira CM, Wallace KB. Doxorubicin-induced persistent oxidative stress to cardiac myocytes. Toxicol Lett. 2001;121(3):151–7.

135. Basra J, Wolf CR, Brown JR, Patterson LH. Evidence for human liver mediated-free radical formation by doxorubicin and mitozantrone. Anti-cancer Drug Des. 1985;45–52.

136. Ventura-Clapier R, Garnier A, Veksler V. Energy metabolism in heart failure. J Physiol. 2004;555(Pt 1):1–13.

137. Doroshow JH, Locker GY, Myers CE. Enzymatic defenses of the mouse heart against reactive oxygen metabolites: alterations produced by doxorubicin. J Clin Invest. 1980;65(1):128–35.

138. Thayer WS. Adriamycin stimulated superoxide dismutase formation in submitochondrial particles. Chem Biol Interact. 1977;19(3):265–78.

139. Costa VM. Role of catecholamines and reactive oxygen species in the mechanism of oxidative stress-induced heart disease: in vitro studies using freshly isolated cardiomyocytes [Thesis]. Porto: Universidade do Porto; 2009. p. 319.

140. Mercola M, Ruiz-Lozano P, Schneider MD. Cardiac muscle regeneration: lessons from development. Genes Dev. 2011;25(4):299–309.

141. Rossato LG, Costa VM, Limberger RP, Bastos MDL, Remião F. Synephrine: from trace concentrations to massive consumption in weight-loss. Food Chem Toxicol. 2011;49(1):8–16.

142. Costa VM, Capela JP, Bastos ML, Duarte JA, Remião F, Carvalho F. Pharmacological concentrations of mitoxantrone are able to activate caspases and dually modify glutathione pathways in HL-1 cardiomyocytes. Br J Pharmacol. 2011;10(3):C052.

143. Shi R, Huang CC, Aronstam RS, Ercal N, Martin A, Huang Y-W. N-acetylcysteine amide decreases oxidative stress but not cell death induced by doxorubicin in H9c2 cardiomyocytes. BMC Pharmacol. 2009;9(7):1–9.

144. Carvalho RA, Sousa RPB, Cadete VJJ, Lopaschuk GD, Palmeira CMM, Bjork JA, et al. Metabolic remodeling associated with subchronic doxorubicin cardiomyopathy. Toxicology. 2010;270(2-3):92–8.

145. Jaeschke H, Gores GJ, Cederbaum AI, Hinson JA, Pessayre D, Lemasters JJ. Mechanisms of hepatotoxicity. Toxicol Sci. 2002;65(2):166–76.

146. Duchen MR. Mitochondria and calcium: from cell signalling to cell death. J Physiol. 2000;529(Pt 1):57–68.

147. Trump BF, Berezesky IK. Calcium-mediated cell injury and cell death. FASEB J. 1995;9(2):219–28.

148. Gregus Z. Mechanisms of toxicity. In: Klaassen C, editor. Casarett Doull's Toxicology - the basic science of poisons. 7th ed. McGraw-Hill; 2008. p. 1331.

149. Dong Z, Saikumar P, Weinberg JM, Venkatachalam MA. Calcium in cell injury and death. Annu Rev Pathol. 2006;1:405–34.

150. Brookes PS, Yoon Y, Robotham JL, Anders MW, Sheu SS. Calcium, ATP, and ROS: a mitochondrial love-hate triangle. Am J Physiol Cell Physiol. 2004;287(4):C817–33.

151. Berridge MJ, Lipp P, Bootman MD. The versatility and universality of calcium signalling. Nat Rev Mol Cell Biol. 2000;1(1):11–21.

152. Li R, Beebe T, Cui J, Rouhanizadeh M, Ai L, Wang P, et al. Pulsatile shear stress increased mitochondrial membrane potential: implication of Mn-SOD. Biochem Biophys Res Commun. 2009;388(2):406–12.

153. Acton BM, Jurisicova A, Jurisica I, Casper RF. Alterations in mitochondrial membrane potential during preimplantation stages of mouse and human embryo development. Mol Hum Reprod. 2004;10(1):23–32.

154. Paglin S, Lee NY, Nakar C, Fitzgerald M, Plotkin J, Deuel B, et al. Rapamycin-sensitive pathway regulates mitochondrial membrane potential, autophagy, and survival in irradiated MCF-7 cells. Cancer Res. 2005;65(23):11061–70.

155. Wallace DC, Fan W, Procaccio V. Mitochondrial energetics and therapeutics. Annu Rev Pathol. 2010;5:297–348.

156. Kroemer G, Galluzzi L, Vandenabeele P, Abrams J, Alnemri E, Baehrecke E, et al. Classification of cell death: recommendations of the Nommenclature Committee on Cell Death 2009. Cell Death Differ. 2009;16(1):3–11.

157. Elmore S. Apoptosis: a review of programmed cell death. Toxicol Pathol. 2007;35(4):495–516.

158. Kung G, Konstantinidis K, Kitsis RN. Programmed necrosis, not apoptosis, in the heart. Circ. Res. 2011;108(8):1017–36.

159. Günther C, Neumann H, Neurath MF, Becker C. Apoptosis, necrosis and necroptosis: cell death regulation in the intestinal epithelium. Gut. 2013;62(7):1062–71.

160. Soustiel JF, Larisch S. Mitochondrial damage: a target for new therapeutic horizons. Neurotherapeutics. 2010;7(1):13–21.

161. Chattopadhyay PK, Betts MR, Price DA, Gostick E, Horton H, Roederer M, et al. The cytolytic enzymes granyzme A, granzyme B, and perforin: expression patterns,

cell distribution, and their relationship to cell maturity and bright CD57 expression. J Leukoc Biol. 2009;85(1):88–97.

162. Kang J. Toxic responses of the heart and vascular system. In: Klaassen C, editor. Casarett Doull's Toxicol. - the basic science of poisons. 2008. p. 1331.

163. Ingwall JS, Weiss RG. Is the failing heart energy starved? On using chemical energy to support cardiac function. Circ Res. 2004;95(2):135–45.

164. Shen W, Asai K, Uechi M, Mathier MA, Shannon RP, Vatner SF, et al. Progressive loss of myocardial ATP due to a loss of total purines during the development of heart failure in dogs: a compensatory role for the parallel loss of creatine. Circulation. 1999;100(20):2113–8.

165. Dzeja PP, Redfield MM, Burnett JC, Terzic A. Failing energetics in failing hearts. Curr Cardiol Rep. 2000;2(3):212–7.

166. Bachmann E, Weber E, Zbinden G. Effect of mitoxantrone and doxorubicin on energy metabolism of the rat heart. Cancer Treat Rep. 1987;71:361–6.

167. Luft FC. Lactic acidosis update for critical care clinicians. J Am Soc Nephrol. 2001;12(1):S15–9.

168. Kolwicz SC, Tian R. Glucose metabolism and cardiac hypertrophy. Cardiovasc Res. 2011;90(2):194–201.

169. Sinatra ST. Metabolic cardiology: the missing link in cardiovascular disease. Altern Ther Health Med. 2009;15(2):48–50.

170. Wallace KB, Starkov AA. Mitochondrial targets of drug toxicity. Annu Rev Pharmacol Toxicol. 2000;40:353–88.

171. Hoang BX, Graeme Shaw D, Pham P, Levine S. Restoration of cellular energetic balance with L-carnitine in the neuro-bioenergetic approach for cancer prevention and treatment. Med Hypotheses. 2007;69(2):262–72.

172. Mijares A, López JR. L-carnitine prevents increase in diastolic [Ca2+] induced by doxorubicin in cardiac cells. Eur J Pharmacol. 2001;425(2):117–20.

173. Niang M, Tomšík P, Mělka M, Stoklasová A, Cerman J, Šišpera L. Effect of L-carnitine against acute mitoxantrone toxicity in mice. Cent Eur J Biol. 2008;3(3):268–72.

174. Niang M, Melka M, Stoklasová A, Cerman J, Tomsík P. Evaluation of the antineoplastic activity of mitoxantrone-L-carnitine combination therapy on an experimental solid form of ehrlich tumour in mice. Pharmacol Res. 2006;54(6):447–51.

175. Niang M, Soukup T, Zivný P, Tomšík P, Bukač J, Rezáčová M, et al. Biochemical and pharmacological effects of mitoxantrone and acetyl-L-carnitine in mice with a solid form of Ehrlich tumour. Chemotherapy. 2011;57(1):35–42.

176. Robins I, Stanley L. Pathologic basis of disease. 8th ed. Saunders Elsevier; 2010.

177. Towbin JA, Bowles NE. The failing heart. Nature. 2002;415(6868):227–33.

178. Piuhola J. Regulation of cardiac responses to increased load: role of endothelin-1, angiotensin II, and collagen XV [Thesis]. Oulu: University of Oulu; 2002.

179. Hammersen F, Hammersen E. The ultrastructure of microvascular endothelial cell reactions to various stimuli. Prog Appl Microcirc. 1984;6:91–108.

180. Kelly D, Anthony A, Piasecki C, Lewin J, Pounder RE, Wakefield AJ. Endothelial changes precede mucosal ulceration induced by indomethacin: an experimental study in the rat. Aliment Pharmacol Ther. 2000;14(4):489–96.

181. Seminara P, Franchi F, Codacci-Pisanelli G, Aronne T, Abdolrahimzadeh S. Discoloration of the nails and early anemia after mitoxantrone, folinic acid and 5-fluorouracil. Med Onc Tumor Pharmacother. 1990;7(4):291–2.

182. Tamasawa N, Tamasawa A, Takebe K. Higher levels of plasma cholesterol sulfate in patients with liver cirrhosis and hypercholesterolemia. Lipids. 1993;28(9):883–6.

183. Gonzalez MC, Sutherland E, Simon FR. Regulation of hepatic transport of bile salts: effect of protein synthesis inhibition on excretion of bile salts and their binding to liver surface membrane fraction. J Clin Invest. 1979;63(4):684–94.

184. Singh A, Bhat TK, Sharma OP. Clinical biochemistry of hepatotoxicity. J Clin. Toxicol. 2011;(s4):1–19.

185. Solter P, Liu Z, Guzman R. Decreased hepatic ALT synthesis is an outcome of subchronic microcystin-LR toxicity. Toxicol App Pharmacol. 2000;164(2):216–20.

186. Karinch AM, Martin JH, Vary TC. Acute and chronic ethanol consumption differentially impact pathways limiting hepatic protein synthesis. Am J Physiol Endocrinol Metab. 2008;295(1):E3–E9.

187. Saukkonen JJ, Cohn DL, Jasmer RM, Schenker S, Jereb JA, Nolan CM, et al. An official ATS statement: hepatotoxicity of antituberculosis therapy. Am J Respir Crit Care Med. 2006;174(8):935–52.

188. Guyton AC, Hall JE. Tratado de fisiologia médica. 11th ed. Saunders Elsevier; 2006. p. 1115.

189. Saner FH, Heuer M, Meyer M, Canbay A, Sotiropoulos GC, Radtke A, et al. When the heart kills the liver: acute liver failure in congestive heart failure. Eur J Med Res. 2009;14:541–6.

190. Miura N, Prentice HL, Schneider PM, Perlmutter DH. Synthesis and regulation of the two human complement C4 genes in stable transfected mouse fibroblasts. J Biol Chem. 1987;262(15):7298–305.

191. Cortez-Pinto H, Chatham J, Chacko VP, Arnold C, Rashid A, Diehl AM. Alterations in liver ATP homeostasis in human nonalcoholic steatohepatitis: a pilot study. JAMA. 1999;282(17):1659–64.

192. Mehta N, Ozick LA, Gbadehan E, Sharma S, Tavalera F, Rice T. Drug-induced hepatotoxicity. Medscape Reference. Available from: http://emedicine.medscape.com/article/169814-overview [cited 2012 Dec 13].

193. Joyce RM, Regan M, Ottaway J, Umiel T, Tetreault JC, Levine J, et al. A phase I-II study of rituximab, ifosfamide, mitoxantrone and etoposide (R-IME) for B cell non-Hodgkin’s lymphoma prior to and after high-dose chemotherapy and autologous stem cell transplantation (HDC-ASCT). Ann Oncol. 2003;14(1):i21–i27.

194. Lehrer SB, Reish R, Fernandes J, Gaudry P, Dai G, Reese G. Enhancement of murine IgE antibody detection by IgG removal. J Immunol Methods. 2004;284(1-2):1–6.

195. Dufour DR, Lott JA, Nolte FS, Gretch DR, Koff RS, Seeff LB. Diagnosis and monitoring of hepatic injury. I. Performance characteristics of laboratory tests. Clin Chem. 2000;46(12):2027–49.

196. Maluf CB. Valores de referência dos parâmetros de volume plaquetário: estudo longitudinal de saúde do adulto - Minas Gerais (ELSA-MG) [Thesis]. Belo Horizonte: Universidade Federal de Minas Gerais; 2011.

197. Alkhouri N, Kistangari G, Campbell C, Lopez R, Zein NN, Feldestein AE. Mean platelet volume as a marker of increased cardiovascular risk in patients with nonalcoholic steatohepatitis. Hepatology. 2012;55(1):1–331.

198. Khandekar MM, Khurana AS, Deshmukh SD, Kakrani AL, Katdare AD, Inamdar AK. Platelet volume indices in patients with coronary artery disease and acute myocardial infarction: an Indian scenario. J Clin Pathol. 2006;59(2):146–9.